論文 / 著書情報
Article / Book Information

題目(和文)	
Title(English)	Three-dimensional airborne ultrasonic position and velocity measurement based on echolocation
著者(和文)	THONG-UNNATEE
Author(English)	Natee Thongun
出典(和文)	学位:博士(工学), 学位授与機関:東京工業大学, 報告番号:甲第10039号, 授与年月日:2015年12月31日, 学位の種別:課程博士, 審査員:黒澤 実,山口 雅浩,杉野 暢彦,田原 麻梨江,蜂屋 弘之
Citation(English)	Degree:Doctor (Engineering), Conferring organization: Tokyo Institute of Technology, Report number:甲第10039号, Conferred date:2015/12/31, Degree Type:Course doctor, Examiner:,,,,
学位種別(和文)	博士論文
Type(English)	Doctoral Thesis

Three-dimensional airborne ultrasonic position and velocity measurement based on echolocation

Thesis submitted
for the
Degree of Doctor of Philosophy

Department of Information Processing
Interdisciplinary Graduate School of Science and Engineering
Tokyo Institute of Technology, Japan

NATEE THONG-UN

Advisor: Professor. Minoru Kurosawa

2015

Contents

1

Introduction

1.1 Background

Robots in the United States have been practically introduced into many industries since the mid-20^{th}century. There are industrial robots more than 1,000,000 units around the word in various fields, for examples, a production line in factories, home robots, and underwater [1]. Nowadays, the researches and the developments of the next-generation robots such as micro robots, service robots, and personal robots have been developed rapidly with the various objectives and applications. A micro robot used in a narrow space, in which an operator does not enter, is performed [2]. A service robot supports the rescue activities in nursing assistances and disaster sites [3]. A personal robot, the ASIMO or the AIBO, is widely contributed in the living environment because it is capable of performing communication with human beings [4-5]. The realization of these next-generation personal robots in accordance with the surrounding situation for performing autonomous movement and human intellectual activity by the determination is required. The technology of autonomous robots using sensors for measuring the spatial information and the actuators for controlling their performance is interesting. The key point of developments in autonomous robots requires high accuracy, high resolution, small size and low cost. Therefore, the robot study of high-performance key components moving toward the practical use has been actively carried out.

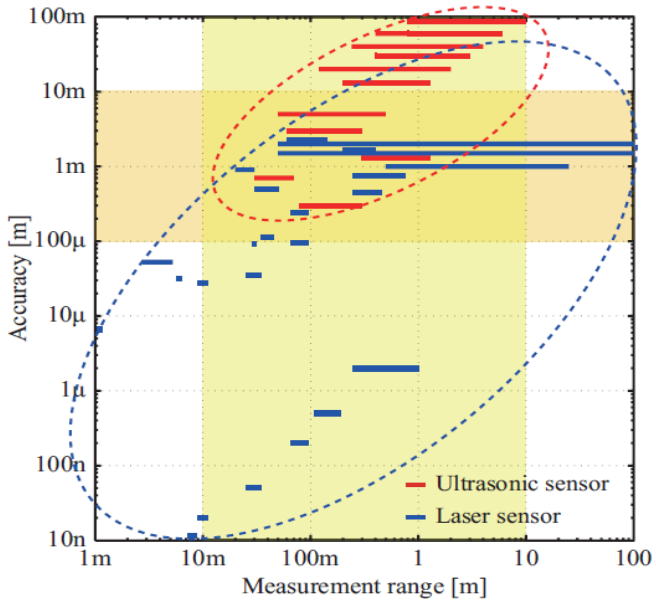

Figure 1.1 Measurement range and accuracy using laser sensor and ultrasonic sensor.[6]

1.2 Spatial information measurements in autonomous mobile robot

Spatial information is a type of key components required by autonomous robots to achieve their own objectives, for examples, the presence or absence of obstacles, distance measurement, velocity measurement, and localization. The laser sensor, the high speed camera, the millimeter-wave sensor, and the ultrasonic sensor are typically utilized for these quantities.

1.2.1 Distance measurement

In a case of the distance measurement, the laser in markets today has the measurement rage and the measurement precision when compared with the ultrasonic sensor, shown in Figure 1.1. The distance measurement of the target in the vicinity of the autonomous mobile robot is in the range from a few centimeters up to several meters, and the accuracy of measurement about 100 μm-10 mm is given. To understand advantages and disadvantages of laser sensors, information of the laser for the distance measurement is briefly explained. First, the confocal laser method provides the irradiated laser passing

through the objective lens to the focal point on the surface of the object. It can measure distance with a very high accuracy 10 nm -2 μm of the range measurement 1 mm-10 mm but there is a narrow range. Second, the triangulation principle [7], the laser beam is projected from the instrument and is reflected from a target surface to a collection lens. This lens is typically located adjacent to the laser emitter. The lens focuses an image of the spot on a linear array camera (CMOS array). The camera views the measurement range from an angle at the center of the measurement range, depending on the particular model. The position of the spot image on the pixels of the camera is then processed to determine the distance to the target. The camera integrates the light falling on it, so longer exposure times allow greater sensitivity to weak reflections. The beam is viewed from one side so that the apparent location of the spot changes with the distance to the target. This instrument can carry out the distance measurement with a high accuracy measurement 10 m-1 mm of the range measurement 1mm-1 m. This method can provide a wider range of the distance measurement when relatively compared with the confocal measurement method. Third, the laser sensor can measure the distance by the phase difference reflected from the target. It can measure distance with accuracy 1 mm-2 mm of the range measurement 10 cm-100 m. It is possible to carry out the distance measurement on a very wide range. Since the propagation speed of the laser in air is very fast to measure the distance, it is difficult to measure the short distance (a few centimeters) in the laser sensor by phase difference method. Thus, the laser sensor can be concluded that it has the sufficiently high precision and the wide rage in the distance measurement; however, it is difficult to measure the distance reflected from the target such as liquid, glass, and mirror surface.

The image measurement by high-speed camera can measure the distance from the change in position of the target reflected in the camera image. However, the image measurement by high-speed camera requires extensive measuring equipment and complicated image processing [8]. It is not appropriate for spatial information measurement of autonomous mobile robot.

Mitsubishi Electric Corporation has developed a millimeter-wave radar for automotive application. Monolithic microwave integrated circuits (MMICs), developed specifically for this application by Mitsubishi Electric, are used for the radio-frequency (RF) module to obtain outstanding radar performance [9]. This millimeter-wave radar incorporates a signal-processing unit in the radar head, resulting in a more compact, lightweight radar system that is easy to install on vehicles. The method of measuring the distance from radar to a target vehicle depends on the type of radar system employed. Millimeter-wave radar systems for automotive application include pulse

radar, frequency-modulated continuous-wave (FM-CW) radar and spread spectrum radar. The radar transmits a frequency modulated millimeter-wave signal, and the signal reflected by a target is received by the radar. By mixing the received and transmitted signals, the system obtains a beat signal having a frequency. This beat signal features a time delay due to the distance from the radar to the target. This technology can measure distance with accuracy 1 m of the range measurement 0 m-120 m. However, it has very low accuracy and not appropriate at a total distance less than 5 meters due to high cost when used in autonomous robots.

Ultrasound, which has slow propagation in air when compared with the laser, is easily reflected by the surface of the structure. The distance measurement using the ultrasonic sensor can be determined by the time difference of the echoes reflected from the target. This is called Pulse-echo method. When a high frequency pulse of ultrasound is used for determination of the distance measurement, accuracy obtained is approximately 0.2-1 mm. Although it is possible to achieve the distance measurement with high range resolution, but the distance is limited to the 1 m below the measurement range under the influence of ultrasonic attenuation and noise. However, if we use a low frequency burst wave instead of a high frequency pulse, the measurement range can be improved up to 10 m, and accuracy is approximately 1 cm-10 cm. The distance resolution is reduced to be 1 cm. To improve the distance resolution and signal to noise ratio (SNR), a pulse compression, which is widely used in the field of radar and communication by the pulse echo method, is performed. A duration time between a received signal and a transmitted signal as a reference signal in the pulse-echo method by the pulse compression is computed using a cross correlation method. However, the computational cost of the cross - correlation method is greatly increased. Next, similar to the laser, a phase shift method of a continuous ultrasonic wave observes the phase difference between the transmitted and received signals. The phase difference is directly proportional to the distance measurement.

1.2.2 Velocity measurement

Recently, the relative velocity measurement of autonomous robots can be performed by many technologies, for examples, laser and ultrasound. First, when the laser is reflected from a moving object, the change of the laser frequency due to the Doppler effect is proportional to the relative velocity measurement to the moving object. A laser Doppler method for measuring the Doppler velocity of the moving object from the Doppler shift provides very high accuracy [10]. The velocity range of the laser

sensor is about 30 m/s; however, the laser sensor is high cost and large size. A low cost and small size laser sensor with a wide range (100 m/s) exists but it is low accuracy [11].

There are several methods for measuring the velocity measurement by ultrasound, such as continuous wave Doppler method, pulse Doppler method, and speckle method. In the continuous wave method, when the ultrasonic wave is reflected from a moving object, the change of the ultrasonic frequency due to the Doppler effect is proportional to the relative velocity measurement to the moving object. In the pulse Doppler method, a transmitted ultrasonic pulse, which is modulated by a sine wave or M-sequence code, can measure the Doppler velocity of the object from the Doppler shift in the frequency of the echo reflected from the moving object. Next, if the transmitted ultrasonic waves are reflected by the somewhat rough surface, a punctate pattern called speckle can be seen in the echo. The ultrasound speckle method is to measure the velocity of the object from the speckle pattern.

The velocity measurement using ultrasonic wave can also be used in medical ultrasound applications, such as blood flow measurements. It is interesting that this method has been not used much in autonomous mobile robots. When realization in light weighted devices is expected, the ultrasound method, which is relatively compared with the laser method, is low cost and small size. Nevertheless, the limitation is low resolution in the range measurement and high - computational - cost time due to signal processing.

1.3 Purposes

In general, ultrasonic distance measurement, which uses an ultrasonic system, is a relatively flexible approach for environmental recognition in robotic systems. Ultrasonic distance measurements can be determined simply by using the time-of-flight (TOF) method, which is a measurement of the time for sound waves to travel between the sound source and the object, multiplied by the sound velocity. TOF can typically be computed by performing a cross-correlation between the transmitted and received signals. As a result, TOF is a measurement of the maximum peak during a sample time. Chirp signals are an ingenious method of handling a practical problem in ultrasonic distance measurement because they give the accuracy and resolution of TOF measurements. A linear-period-modulated (LPM) signal, which is a type of chirp signal, has a period that is swept linearly with time and, is presented. This signal allows the cross-correlation function to determine the TOF via the Doppler effect. Resolution and signal

processing costs for measuring the distance and the velocity using ultrasound system are in a trade-off relationship. Thus, a low-calculation-cost method of ultrasonic measurement by pulse compression comprising two cycles of LPM signals and Doppler-shift compensation has been proposed [12-13]. Accordingly, to achieve fast signal processing, this paper has applied such a method. Ultrasonic distance and velocity measurements have already been accomplished by using one microphone [14]. In the case of an ultrasonic two-dimensional system, a solution for two-dimensional position and velocity measurements by exploiting two microphones has also been proposed [15].

Nevertheless, the development of position and velocity measurement under ultrasonic system is far from complete. This dissertation presents ultrasonic three-dimensional position and velocity measurements using a simple algorithm to provide fast signal processing, which is accomplished via one-bit signal processing. The proposed systems are simply designed to support low cost devices. Additionally, to support real-application, FPGA has been used to achieve the parallel computation.

1.4 Organization

This dissertation is organized to nine chapters. Chapter 2 can serve as a review and a summary of traditional one, two, and three dimensional position and velocity measurement techniques using ultrasonic technology. Chapter 3 is then covered on a basis of 1 - bit Delta - Sigma ($\Delta\Sigma$) modulated signal, an implementation on acoustical devices and a field programmable gate array (FPGA) involving with this dissertation. Chapter 4 expresses a principle of Doppler-shift, Doppler velocity estimation using LPM signals, and reflections from different-shape objects. Chapter 5 proposes an ultrasonic position and velocity measurement by an iterative method. Chapter 6 presents an ultrasonic position and velocity measurement by a Direction of - Arrival method. Chapter 7 explains an ultrasonic position and velocity measurement by a linear algebra method. Chapter 8 introduces performance evaluation, testing, and comparisons in different types of noise. Chapter 10 is conclusions of this dissertation.

2

Ultrasonic position and velocity measurement

2.1 Traditional distance measurement techniques

2.1.1 Pulse echo method

The pulse- echo method is one of the typical ultrasound distance measurement techniques. This method determines an ultrasonic waves time of flight (TOF) [16]. The TOF is the interval from the transmission of an ultrasonic pulse to the reception of an echo reflected from a target. The targets distance is estimated from the product of the TOF and the propagation velocity of an ultrasonic wave. TOF is:

$$TOF = \frac{2d}{v_0}, \tag{2.1}$$

where d is a distance and v_0 is sound propagation. The reflection model $f(t)$ can be represented in a form of TOF as follows:

$$f(t) = \delta(t - TOF), \tag{2.2}$$

Assume that the transmitted signal $h(i)$, which has a length of N samples, is sent to the target, and the received signal $x(t)$ is then obtained, show as Figure 2.1. The echo can be defined by convolution between the transmitted signal and the reflection model in Equation (2.3).

$$x(t) = h(i) \otimes f(t)$$

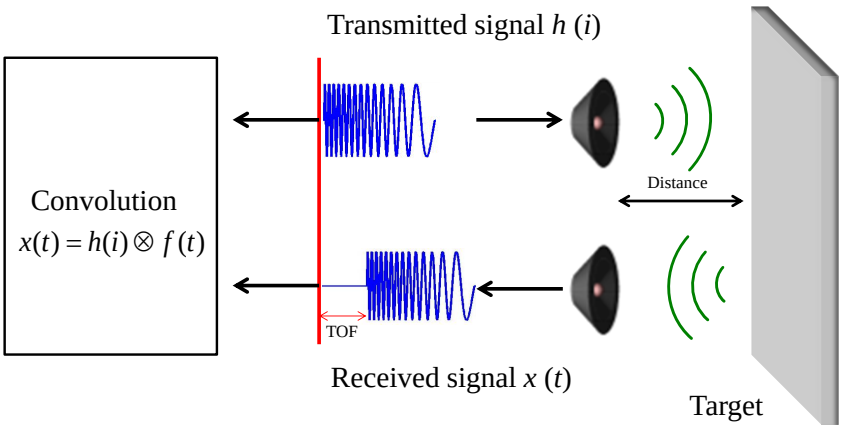

Figure 2.1 Transmitted and received signals of the pulse echo method.

$$x(t) = \sum_{i=0}^{N-1} h(i) f(t-i) \tag{2.3}$$

Otherwise, the reflection model $f(t)$ can be computed from the transmitted signal $h(i)$ and the received signal $x(t)$ using deconvolution. The higher-range-resolution application is often seen for a relatively short distance such as in the field of medical applications. To satisfy such a problem, the transmitted signal $h(i)$ with a short wave length (2-3 cycles) is used, and TOF computation by using the pulse echo method can accomplish a high time resolution. However, when attenuation in environment is large, ultrasonic energy of the transmitted signal $h(i)$ is also small due to the short wave length. If the signal is susceptible to the effects of noise, this deflect happened is a narrow measurement range.

2.1.2 Phase difference method

A principle of phase difference method is the phase measurement of the echo reflected from the ultrasonic continuous wave. The distance is determined from the phase difference between the transmitted signal and the received signal. In conventional phase

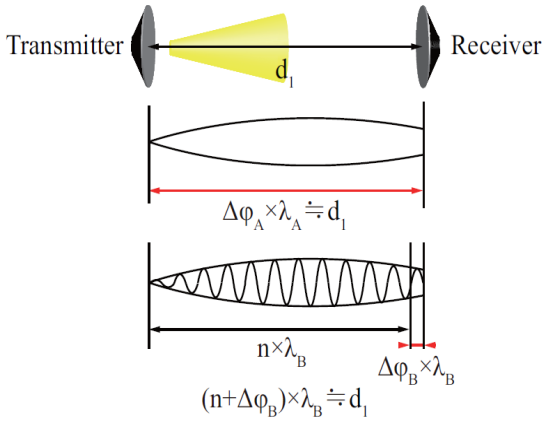

Figure 2.2 Measurement principle of the phase difference method of multiple phase difference method.[6]

difference method, range resolution is determined by the wavelength resolution and the transmission signal of the measured phase difference. To improve the distance resolution of the phase difference method, multiple phase difference method for performing multiple modulated transmission signals has been proposed [17-18]. In the multiple phase difference method, the measurement of the distance d_1 from $\varphi_A \mathrm{x} \lambda_A$ by using the phase difference φ_A of the measured wavelength λ_A is shown in Figure 2.2. Measuring the distance d_1 with a high resolution is expressed by $(n + \delta\varphi_B) \cdot \lambda_B$ using phase difference φ_B of the wavelength λ_B. We can obtain n from the measurement of d_1. However, since the phase difference method is the measurement accuracy depends on the echo of the SNR, it is sensitive to noise. In the case the moving target, phase and the wavelength of the echo becomes difficult to accurately measure the distance due to the Doppler effect.

2.1.3 Cross-correlation method

The cross-correlation method is to correlate between the received signal and the reference signal [19 -20]. In a case of frequency domain, we can express a relationship of the received signal $X(\omega)$, the transmitted signal $H(\omega)$, and the reflection model $F(\omega)$

shown as follows:

$$\begin{aligned} X(\omega) &= \sum_{t=0}^{M-1} x(t)\exp^{-j\omega t} \\ &= \sum_{t=0}^{M-1}\left[\sum_{i=0}^{N-1} h(i)f(t-i)\right]\exp^{-j\omega t} \\ &= \sum_{t=0}^{M-1}\left[\sum_{i=0}^{N-1} h(i)f(t-i)\right]\exp^{-j\omega(t-i)}\exp^{-j\omega i} \\ &= \left[\sum_{i=0}^{N-1} h(i)\exp^{-j\omega i}\right]\left[\sum_{t=0}^{M-1} f(t-i)\exp^{-j\omega(t-i)}\right] \\ &= H(\omega)F(\omega). \end{aligned} \tag{2.4}$$

Easily speaking from Equations (2.3) and (2.4), a convolution of time domain can be expressed as a product of frequency domain. If $H(\omega) \neq 0$, $F(\omega) = X(\omega)\ /\ H(\omega)$. Inverse Fourier transform of $F(\omega)$ is:

$$\begin{aligned} f(t) &= \frac{1}{N}\sum_{i=0}^{N-1} F(\omega_i)\exp^{j\omega_i t} \\ &= \frac{1}{N}\sum_{i=0}^{N-1} \frac{X(\omega_i)}{H(\omega_i)}\exp^{j\omega_i t}. \end{aligned} \tag{2.5}$$

However, expression in influence of noise contained in the received signal $x(t)$ in Equation (2.4) are not stable. Cross correlation between Fourier transform of the transmitted signal $H(\omega)$ and the received signal $X(\omega)$ is shown in Equation (2.6):

$$\begin{aligned} C(\omega) &= F(\omega)H^*(\omega) \\ &= X(\omega)H(\omega)H^*(\omega), \end{aligned} \tag{2.6}$$

where $H^*(\omega)$ is match filter. $H(\omega)H^*(\omega)$ is the Fourier transform of the autocorrelation function of the reference signal. Fourier transform of the cross-correlation function is called the cross spectrum $C(\omega)$. Inverse Fourier transform of the cross spectrum, which is convolution between the complex conjugate transmitted signal $h^*(i)$ and the received

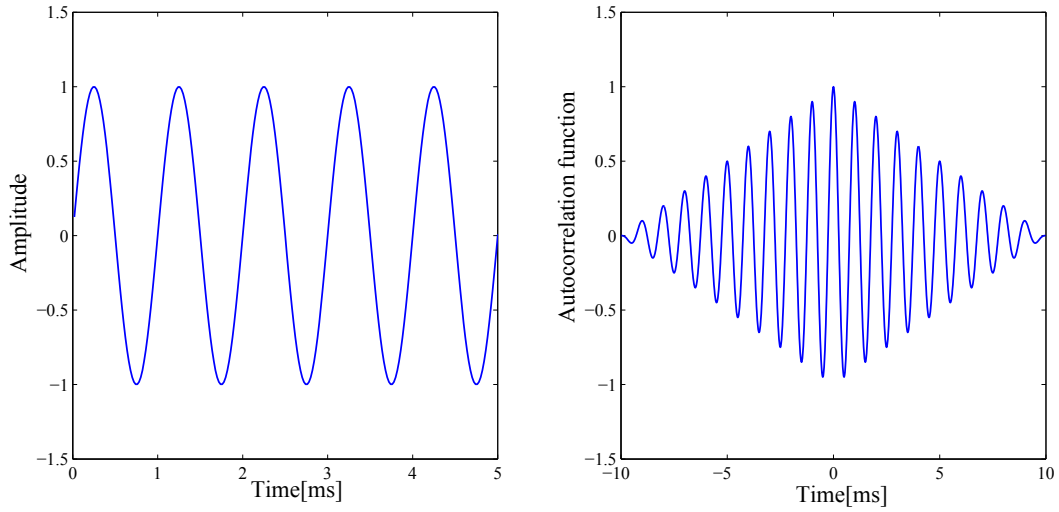

Figure 2.3 A sinusoidal signal of 1 kHz and the autocorrelation function.

signal $x(t)$, is shown as follows:

$$\begin{aligned} c(t) &= \sum_{i=0}^{N-1} h^*(i)x(t-i) \\ &= \sum_{i=0}^{N-1} h(N-i)x(t-i). \end{aligned} \tag{2.7}$$

Moreover, the cross-correlation function in Equation (2.6) can be seen in a form of convolution between autocorrelation of the transmitted signal and the reflection model. The advantage of the cross-correlation method can improve the SNR of the received signal included by white noise. Therefore, the cross-correlation method has properties to improve the time resolution of the TOF. A chirp signal, which indicates the change in instantaneous frequency with time, using the cross-correlation method for TOF computation has been proposed [21-22]. The cross-correlation method for transmitting a pseudo- random code in ultrasonic wave code modulation, such as M-sequence codes and Gold sequence used for spectrum spread in the field of wireless communications has been proposed [23-24].

A sinusoidal signal with 1 kHz and its own autocorrelation is shown as Figure 2.3. The sinusoidal signal as shown in Figure 2.3 does not have a sharp peak in the autocorrelation function. A chirp signal, linearly varying frequency from 0 kHz to 5

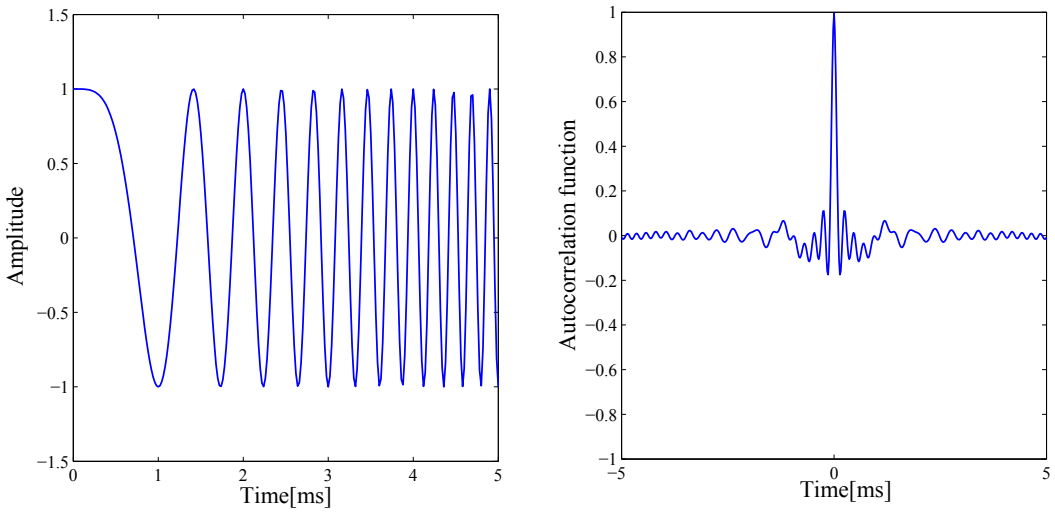

Figure 2.4 A chirp signal varying the frequency 0 kHz to 5 kHz and the autocorrelation function.

kHz, and the autocorrelation is shown as Figure 2.4. The M-sequence code is a pseudo -random code. A binary with the longest period is generated from a Linear Feedback Shift Register (LFSR). n-order of M sequence code is a binary code having a period of 2n -1 samples generated from n-bit LFSR. 15 -order M-sequence code is the transmitted signal and the autocorrelation function, pictured in Figure 2.5.There is a sharp peak in the autocorrelation function of all Figures. Therefore, in all the presented signals, TOF can be identified in a peak of the cross-correlation function.

The cross-correlation method as described above can improve the time resolution of TOF, when SNR is quite low, by performing a cross-correlation between the received signal and the reference signal. However, the cross-correlation process significantly requires to the signal processing cost of the digital circuit including a large number of product and sum operations.

2.1.4 Phase transform method

In the cross-correlation method, it is noticed that there are the side lobes near the cross-correlation peak. A method to make the sharper peak is to whiten the cross-correlation function using a weighting function. It is so-called a generalized cross-correlation technique. The generalized cross-correlation processor can be simply demonstrated in a block diagram of Figure 2.6. The phase transform is typically the generalized cross-

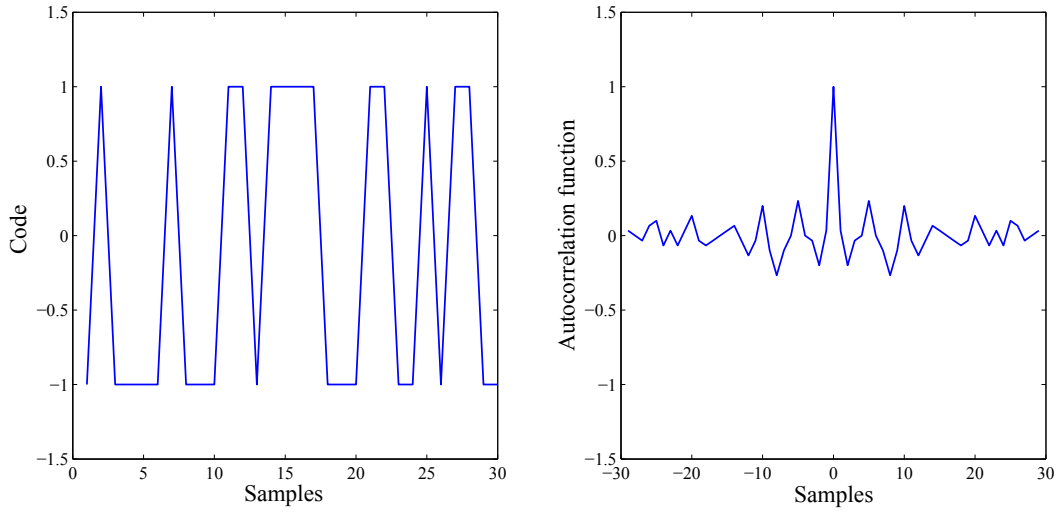

Figure 2.5 30 samples of 15-order M-sequence code and its autocorrelation function.

correlation step which has obtained considerable attention due to its ability to decrease the side lobes causing spreading of the peak in the cross-correlation function [25]. This method is shown mathematically by Equation (2.8):

$$r(t) = \frac{1}{N}\sum_{i=0}^{N-1} C(\omega_i)\Psi(\omega_i)\exp^{j\omega_i t}, \text{and}\Psi = \frac{1}{|C(\omega_i)|}, \tag{2.8}$$

where $C(\omega_i)$ is the cross-spectrum between the transmitted signal and the received signal and $\Psi(\omega_i)$ is the weighting function. According to (2.8), only the phase information is preserved after the cross spectrum is divided by its magnitude. Ideally (there is no additive noise), this processor approaches a delta centered at the correct delay.

A sinusoidal signal with 1 kHz and the generalized autocorrelation function is shown as Figure 2.7. A chirp signal, linearly varying frequency from 0 kHz to 5 kHz, and the generalized autocorrelation function is shown as Figure 2.8. 15-order M-sequence code is the transmitted signal and the generalized autocorrelation function, pictured in Figure 2.9. Obviously, when relatively compared with the cross-correlation method, the generalized cross-correlation method can concentrate only the peak and smooth the side lobes. Although this method has a remarkable ability to sharpen the peak for TOF measurement, it is weak to very low SNR. Moreover, it significantly requires the complicated process because Fourier transform and inverse Fourier transform are performed. The generalized cross-correlation method thus requires a huge of accumulations and

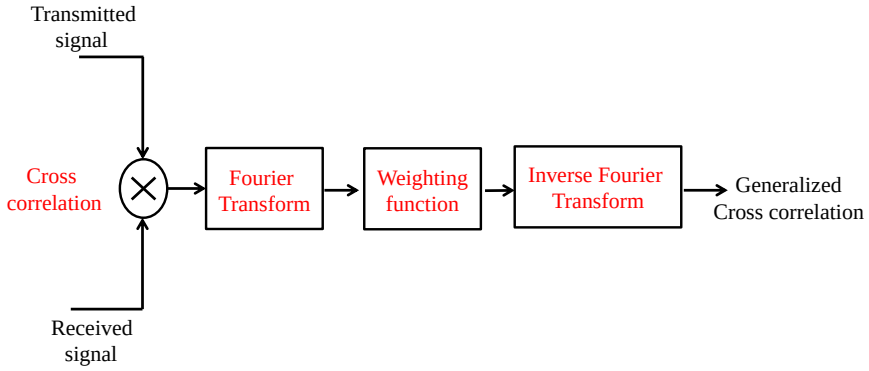

Figure 2.6 Generalized cross-correlation processor.

summations.

2.1.5 Maximum likelihood method

The maximum likelihood method, which is identically defined as the Hannan and Thomson [26], is another significant idea of the generalized cross correlation category since it provides the maximum likelihood solution for TOF problem. The accuracy of time-delay estimation can be improved using the maximum likelihood weighting function $\Phi(\omega)$ to attenuate into the correlator in spectral region. The maximum likelihood estimator can provide comparatively simplicity of implementation and optimality under appropriate situation. The maximum likelihood method of TOF estimation for uncorrelated Gaussian signal and noise condition i.e. no reverberation is asymptotically unbiased and efficient in the limit of long observation duration [27]. This method can be mathematically expressed by Equation (2.9):

$$m(t) = \frac{1}{N} \sum_{i=0}^{N-1} C(\omega_i)\Phi(\omega_i)\exp^{j\omega_i t}, \tag{2.9}$$

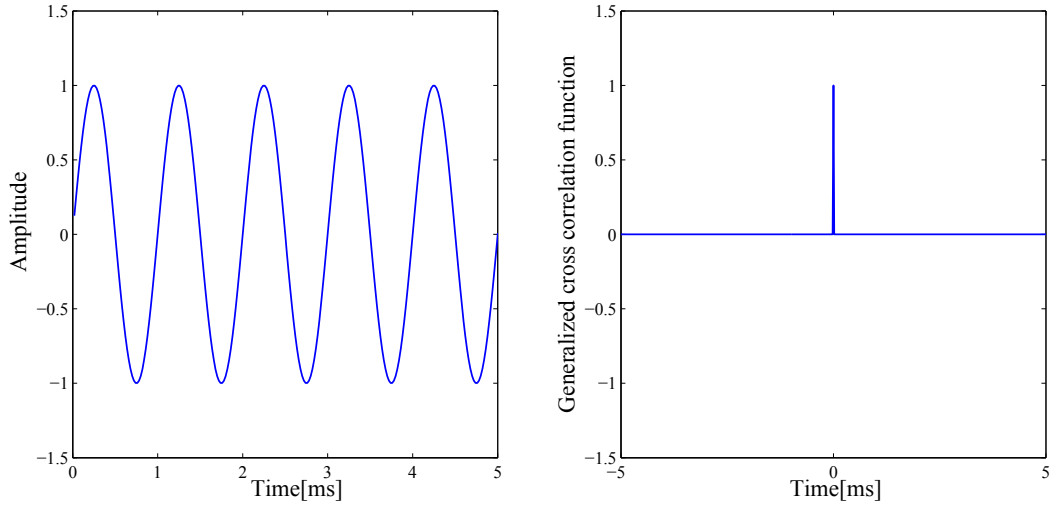

Figure 2.7 A sinusoidal signal of 1 kHz and the generalized cross-correlation function.

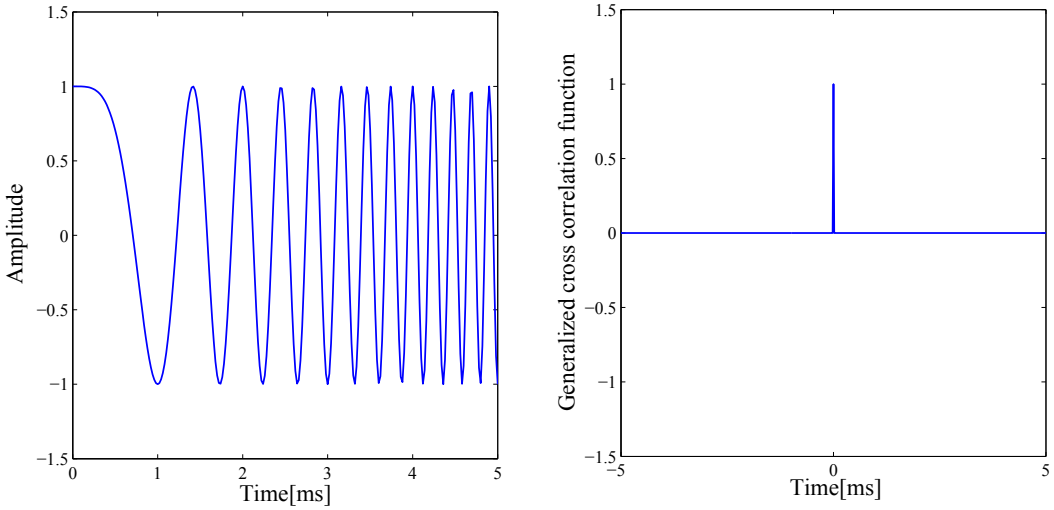

Figure 2.8 A chirp signal varying the frequency 0 kHz to 5 kHz and the cross-correlation function.

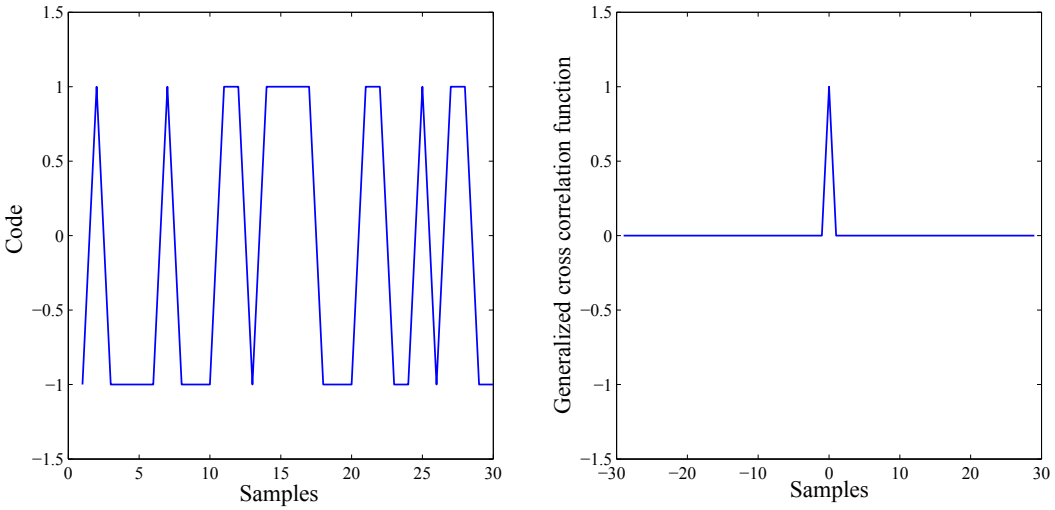

Figure 2.9 30 samples of 15-order M-sequence code and the generalized cross-correlation function.

$$\Phi(\omega_i) = \frac{1}{|C(\omega_i)|} \frac{|\Upsilon(\omega_i)|^2}{1 - |\Upsilon(\omega_i)|^2}$$
$$|\Upsilon(\omega_i)|^2 = \frac{|C(\omega_i)|^2}{A_{11}(\omega_i) A_{22}(\omega_i)}.$$

$|\Upsilon(\omega_i)|^2$ is the magnitude coherency squared, $\Phi(\omega_i)$ is the maximum likelihood weighting function. $A_{11}(\omega_i)$ is the autocorrelation of the transmitted signal, $A_{22}(\omega_i)$ is the autocorrelation of the received signal, and $C(\omega_i)$ is the cross correlation. The maximum likelihood consists of the fundamental term $\Upsilon^2/(1-\Upsilon^2)$. Accordingly, the better weight is put on frequency bands providing near-unity coherence. M, frequency bands appearing in the coherence near zero are deemphasizing [26]. The maximum likelihood processor can develop the cross-spectral phase from estimation when the variance of the estimated phase error is white noise.

When we carefully look back to Equation (2.9), the magnitude coherency squared is one from the autocorrelation function. The maximum likelihood weighting function becomes infinity, and then the maximum likelihood correlation cannot be computed. If we want to notice the maximum likelihood correlation of autocorrelation, the maximum likelihood weighting function has to be relaxed by adding a tiny noise to make the signal

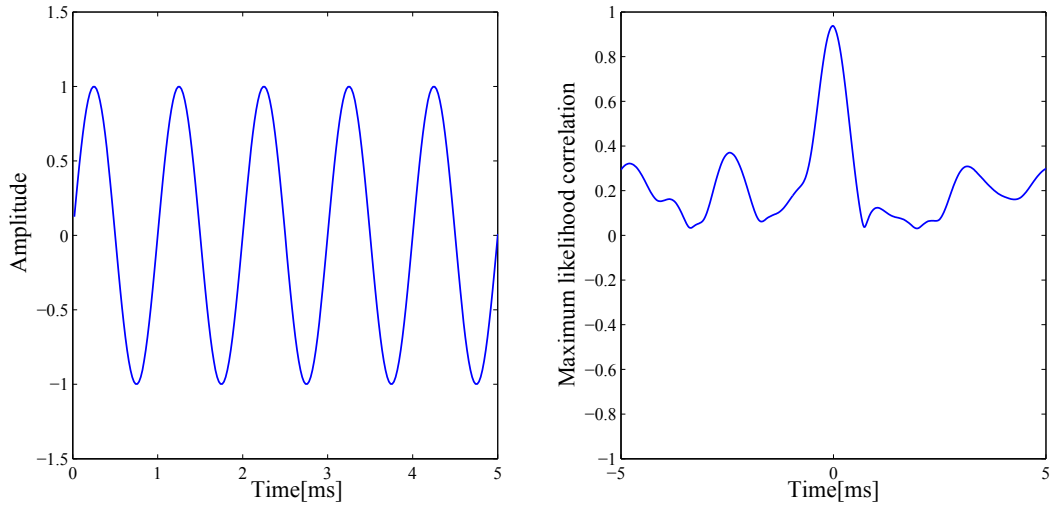

Figure 2.10 A sinusoidal signal of 1 kHz and the maximum likelihood cross-correlation function.

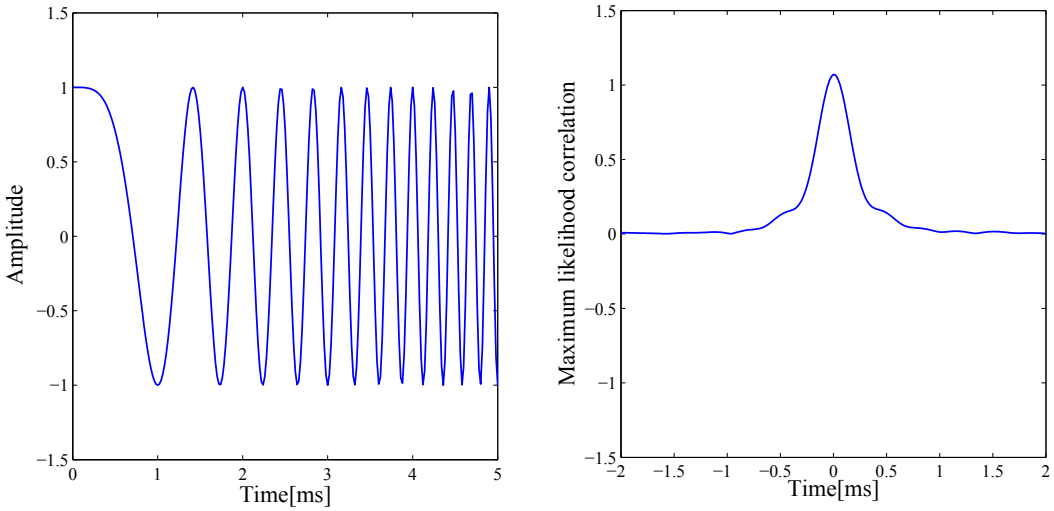

Figure 2.11 A chirp signal varying the frequency 0 kHz to 5 kHz and the maximum likelihood cross-correlation function.

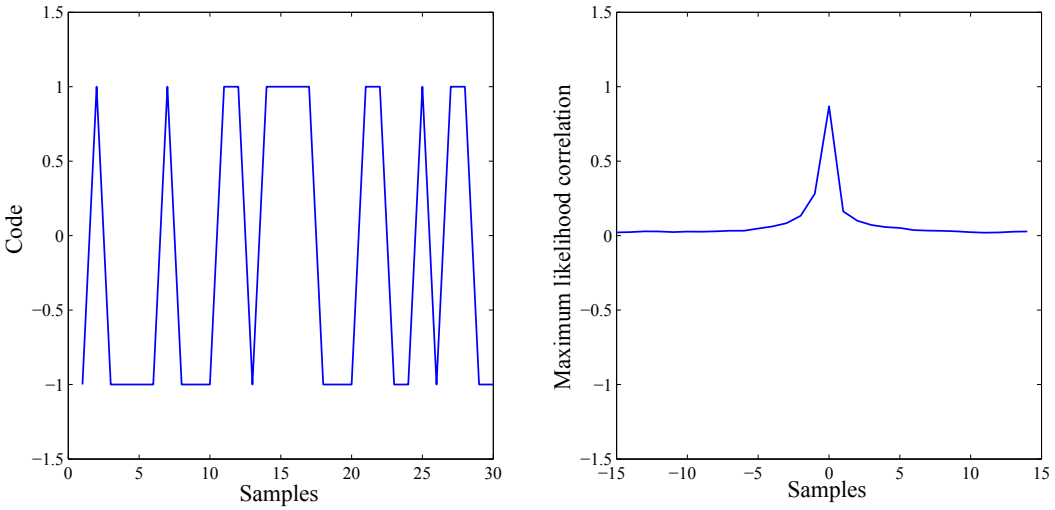

Figure 2.12 30 samples of 15-order M-sequence code and the maximum likelihood cross-correlation function.

very high SNR for the pseudo autocorrelation. A sinusoidal signal with 1 kHz and the maximum likelihood correlation is shown as Figure 2.10. A chirp signal, linearly varying frequency from 0 kHz to 5 kHz, and the maximum likelihood correlation is shown as Figure 2.11. 15-order M-sequence code is the transmitted signal and the maximum likelihood correlation, pictured in Figure 2.12. Although the maximum likelihood method has a remarkable ability to sharpen the peak for TOF measurement, but it is still sensitive to very low SNR. Moreover, it significantly requires the complicated process because a few numbers of Fourier transform and inverse Fourier transform are performed. The maximum likelihood correlation thus uses a huge of accumulations and summations.

In both the generalized cross correlation and the maximum likelihood correlation, the spectrum of the weighting function cannot be obtained from infinite observations, so only estimation can be computed. Finite time measurement causes a certain variance of the estimated cross-power spectrum , which may affect the accuracy of TOF [28-29]. It leads to a large error when the actual observation interval is short. On the other hands, the assumption of long observation interval is inconsistent with other prevailing conditions, such as assumptions of stationary process and constant delay will only be satisfied over a limited time interval.

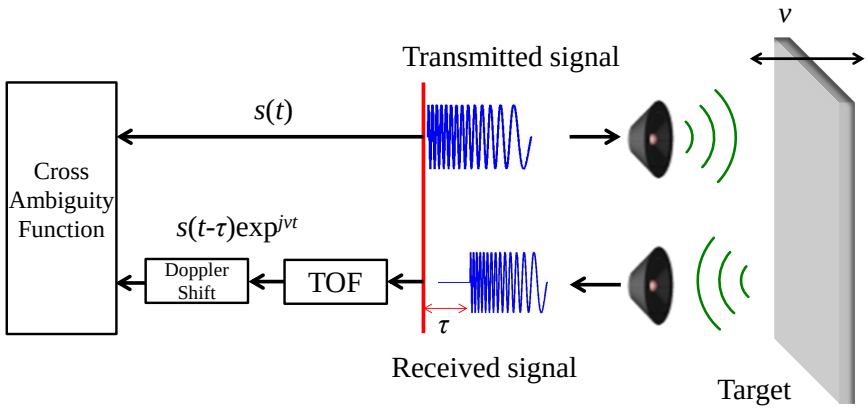

Figure 2.13 Coarse process of computing the cross ambiguity function.

2.1.6 Cross ambiguity method

As known in the previous methods, we can measure TOF by obtaining the echo reflected from a target. A distance is then computed by multiplying TOF with sound velocity but we do not know information of velocity. The cross-ambiguity function method is applied to detect the stationary and moving targets in various target detection scenarios [30]. The contour plots of the cross-ambiguity function are computed as a function of delay and Doppler frequency shift. In Figure 2.13, the received signal, including the time delay and the frequency offset, is $s(t-\tau)\exp^{jvt}$, where τ is TOF and v represents Doppler shift, with respect to the transmitted signal $s(t)$. The cross ambiguity function can be viewed as Fourier transform of lag products and given by [31]:

$$A(\tau, v) = \sum_{i=0}^{N-1} h(i)x^*(i+\tau)\exp^{\frac{j2\pi vn}{f_s}}, \tag{2.10}$$

Where $h(i)$ is the transmitted signal $x(i)$ is the received signal and f_s is a sampling frequency. Though Equation (2.10) is mathematically correct, the ambiguity function, which is computed using Equation (2.10) is a brute force method where no data reduction is performed. It may be advantageous in some applications [31]. In Figure

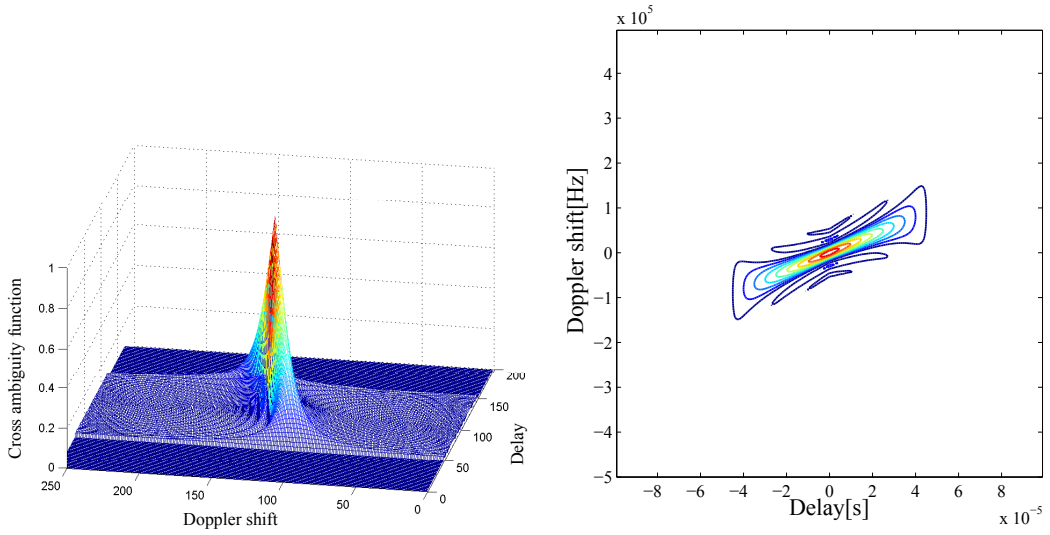

Figure 2.14 Cross ambiguity function of a chirp signal.

2.14, a delay and a Doppler shift of a chirp signal are computed by means of the cross ambiguity function. A peak can be located on both the delay axis and the Doppler shift axis. Cross ambiguity function, which is often used in the radar technology, consists of huge iterations of multiplications and accumulations, and requires high- cost digital signal processing. Therefore, real-time distance measurements by the cross-correlation method are difficult because of the limited computational ability in autonomous mobile robots.

2.1.7 Threshold detection method

The easiest method for the TOF measurement is to check the arrival of the ultrasonic wave using a trigger when the ultrasonic sensor exceeds evaluated threshold. The predetermined-wave type can be considered as a single frequency signal, or an impulse signal. In general, tone-bursts several cycles of a single-frequency signal play an important role for the transmitted ultrasonic wave. Moreover, this method is usually windowed to optimized spectral content. It is thus leaded into applications requiring narrow-bandwidth transducers.

The advantages of threshold detection method are that it does not need complicated calculations at all and can be achieved with a simple circuit. Therefore, low-cost single-frequency narrow-band ultrasonic transducers can be implemented because of economy reason. However, although a simple form is given for thresholding system,

three significant problems exist: low sampling frequency, low SNR, and inherent bias [32].

2.2 Conventional velocity measurement

2.2.1 Continuous wave Doppler method and pulsed Doppler method

The continuous wave Doppler method and the pulsed Doppler method, which is a typical ultrasonic velocity measurement technique with a constant frequency, measure the frequency of the echo reflected from a target. If the target is moving, the Doppler effect is generated by the velocity of the target. The Doppler shift frequency of the echo comes from the relative velocity between the target and the transmitter. This method can determine the relative velocity of the moving object by measuring the Doppler shift frequency of the echo. In this technique, the Doppler shift frequency is performed using the signal processing of quadrature detection, shown in Figure 2.15. The echo, which is obtained by the ultrasonic receiver, is blended with the reference signal and the quadrature signal as follows in Equation (2.11) and Equation (2.12), and low pass filters are operated to obtain the Doppler shift frequency as follows in Equation (2.13) and (2.14).

$$\begin{aligned} s(t) &= A\cos\Big((\omega_0+\omega_d)t\Big)\sin(\omega_0 t) \\ &= A\sin\Big((2\omega_0+\omega_d)t\Big) - A\sin(2\omega_d t) \end{aligned} \tag{2.11}$$

$$\begin{aligned} c(t) &= A\cos\Big((\omega_0+\omega_d)t\Big)\cos(\omega_0 t) \\ &= A\cos\Big((2\omega_0+\omega_d)t\Big) - A\cos(2\omega_d t) \end{aligned} \tag{2.12}$$

$$\begin{aligned} s_f(t) &= lowpass(s(t)) \\ &= -A\sin(\omega_d t) \end{aligned} \tag{2.13}$$

$$\begin{aligned} c_f(t) &= lowpass(c(t)) \\ &= A\cos(\omega_d t) \end{aligned} \tag{2.14}$$

The method of frequency analysis to determine the Doppler shift frequency ω_d from the cos function is to obtain the sin function from the quadrature detection. To do so, there are several methods such as instantaneous frequency method, Discrete Fourier transform method, and variable time window function method. They are available depending on the applications. Therefore, Doppler shift frequency measurement for the autonomous mobile robot is not suitable for the robot measuring system.

Discrete Fourier transform method, which is obtained from the quadrature detection, is a method of estimating Doppler shift frequency ω_d from the frequency spectrum. This technique is relatively fast. It has been used in blood flow measurement with multiple velocity components. There also needs to determine the sign of the relative speed prior to Fourier transform. Frequency resolution of this approach is determined by the time T to perform the Fourier transform as shown in Equation (2.15), where N is the number of samples, f_s is the sampling time.

$$\Delta f_s = \frac{1}{N t_s} = \frac{1}{T} \tag{2.15}$$

In general, autonomous mobile, compared with the surrounding environment, can move with the velocity about $\pm$ 5 m/s. It is relatively slow. When an ultrasonic wave with 40 kHz and resolution of discrete Fourier transform with 10 Hz are transmitted continuously, we can obtain a velocity resolution of 0.1 m/s in a continuous wave Doppler method. However, discrete Fourier transform is a method requiring large computational cost and circuit scale. It is hard to say that this technique is suitable for signal processing of the dynamic type robot.

Instantaneous frequency method, obtained from the quadrature detection of the sin function, can estimate the Doppler shift frequency ω_d by calculating the phase difference from four samples of adjacent time of the cos function [33]. This approach does not need to determine the sign of the relative velocity, and computational cost required is less than the discrete Fourier transform method. This method can compute the Doppler shift frequency ω_d as Equations (2.16)-(2.18).

$$\tan(\omega_d t) = \frac{s_f(\omega_d t)}{c_f(\omega_d t)} \tag{2.16}$$

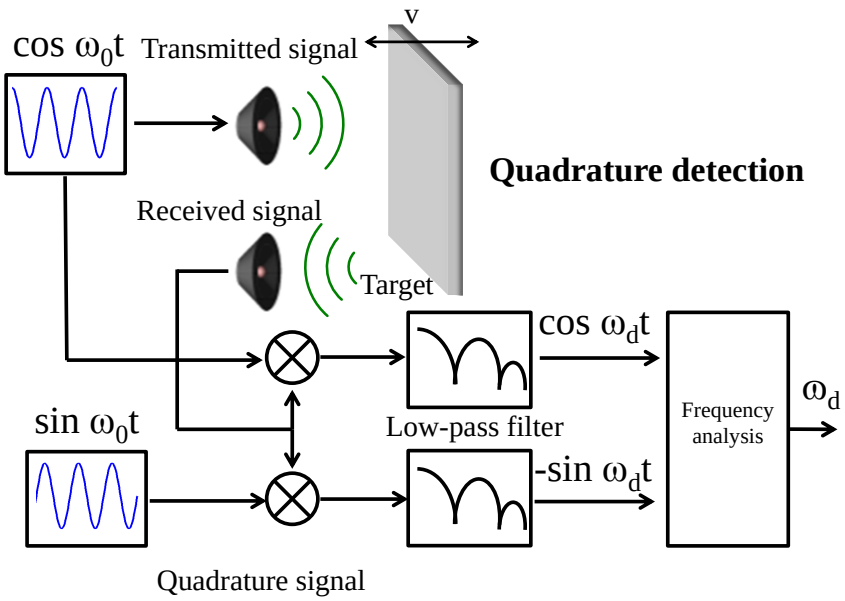

Figure 2.15 Signal processing for quadrature detection in the continuous wave Doppler method and the pulse Doppler method.

$$\tan(\omega_d(t-\Delta t)) = \frac{s_f(\omega_d(t-\Delta t))}{c_f(\omega_d(t-\Delta t))} \tag{2.17}$$

$$\omega_d = \frac{1}{\Delta T}\tan^{-1}\frac{s_f(t)c_f(t-\Delta t) - c_f(t)s_f(t-\Delta t)}{s_f(t)s_f(t-\Delta t) + c_f(t)c_f(t-\Delta t)} \tag{2.18}$$

If we carefully deem Equations (2.16)-(2.18) to identify velocity measurement, they require various complicated processes. It is quite comparative slow for autonomous robots.

2.2.2 Speckle method

Ultrasound speckle method to measure the velocity using speckle pattern is seen in the echoes, which is reflected from somewhat rough surface [34]. Zero-crossing method of the received signal containing the echo envelope detection is used in a velocity measurement by ultrasonic speckle method [35]-[37]. Since the zero crossing number of the results obtained is proportional to the velocity of the object, we can measure the velocity of the moving object directly. However, the coefficient of the zero-crossing number is

directly proportional to the speed and the distance. It varies greatly depending on the angle. In addition, since the speckle pattern changes depending on the surface shape of the target, it is not suitable for measuring the speed of the autonomous mobile robot.

2.2.3 Velocity measurement technique from the signal length of the echo

In the continuous wave Doppler method and the pulse Doppler method, they are necessary to transmit the constant frequency of the ultrasonic wave. It is not possible to simultaneously measure the cross-correlation method for transmitting ultrasonic chirp wave. Furthermore, in order to measure the Doppler velocity of the target from the frequency of the echo, Complex arithmetic processing are required extensive arithmetic circuits. Frequency of echo by the Doppler effect to Doppler shift is shown in Equation (2.19). v_d is the Doppler velocity of the object , v_0 is the propagation velocity of ultrasonic waves in air. Similarly signal period and signal length is also expressed in Equation (2.20), and the Doppler shift can be computed in Equation (2.21), where p_0 is the period of the transmit signal, l_0 is a signal length. p_d is the period of Doppler shift signal, and l_d is the Doppler shift length.

$$\omega_d = \omega_0 \frac{v_0 + v_d}{v_0} \tag{2.19}$$

$$p_d = p_0 \frac{v_0}{v_0 + v_d} \tag{2.20}$$

$$l_d = l_0 \frac{v_0}{v_0 + v_d} \tag{2.21}$$

The Doppler velocity of the object is described above. It is understood that it can be measured from the signal length of the echo. Signal length of echo, which is transmitted by a chirp signal, can be estimated by cross-correlation method. It is relatively simple signal processing method. We can improve the velocity resolution of Doppler velocity by increasing the time resolution of the signal length of the measured echo.

2.3 Position and velocity measurement techniques for two dimensions

The purpose of a planar mobile robot is defined by its lateral (x, y) and angular (ϕ) position. In absolute position, both lateral and angular positions are measured relatively

to pre-defined objects A typical methods for absolute positioning are triangulation, trilateration, GPSs etc. A method for measuring the relative position and orientation between two mobile robots using a dual binaural ultrasonic sensor system is proposed [38]. Each robot is equipped with a ultrasound transmitter that sends signals to two receivers, which are mounted on the other robot.

An ultrasonic-based localization using ultrasonic sensors built on the poles serve as receivers and the mobile robot serves as a transmitter, and all ultrasonic sensors integrated with their Zig-Bee modules is proposed [39]. By the sequential ultrasonic signal transmission between the robot and the poles, the ultrasonic sensors on the poles can then measure the TOF without interference to calculate the distance between the receiver and transmitter ends. According to an established two-dimensional coordinate model, position of the robot can be obtained based on the distance measurements.

A two-dimensional position measuring method based on the principle of ultrasonic position measurement by phase difference and its applications to human interface is proposed [40]. It is computed with the phase difference between the waves received by two pairs of sensors. By attaching a transmitter to an adequate device, various kinds of motor actions of a computer user are available to screen pointing by the device, which allows the user various pointing styles such as mouse-like one and pen-like one.

A method to extract multiple acoustic landmarks for the indoor navigation of a mobile robot is described [41]. The environment is modeled by specular vertical walls. An ultrasonic sensor mounted on the mobile robot scans around the surrounding walls and detects multiple echo pulses. On the horizontal plane at the height of the ultrasonic sensor from the floor, the two-dimensional environment is described by the distance as a function of angle in the scan. Due to the specularity of the walls, the distance function has a manageable number of retroreflective parts that can be used as landmarks. By virtue of the constancy of the relative positions between the ultrasonic sensor and the walls in scanning, the echo pulses reflected from a certain reflection points (RP) have the same time-of-flight in the ultrasonic scan data.

Developing a blind robot which focuses on the study of continuous and discrete 2D mapping is proposed [42]. Ultrasonic sensors are used to sense the obstacles while the robot is moving. User is also allowed to vary the speed of robot and move forward and backward with the robot. There is a two-dimensional memory map program to track the robot position and obstacles detected by proximity sensor on the robot. The program written is able to control the robot by displaying the two-dimensional map that plots the location of the robot and obstacles, displaying coordinates of the robot, control turning of robot at various degrees and move or stop the robot.

A calibration model including probability directional diagram of the sensor, probability estimation of the sensor measurements is proposed [43]. An interface, which enables an external microprocessor system to read correctly the information from a POLAROID ultrasonic ranging system, is presented as well. In accordance with the accomplished, an implementation of the developed means in mobile robot map building is described.

An idea for position and velocity measurements for a moving object with the echolocation technique under the ultrasonic system is presented [15]. The moving-object location is based on the TOF. Cross correlation, low-calculation-cost Doppler-shift compensation, plays an important role in the TOF determination. The velocity of the moving object is determined from the peak interval and peak form in the cross-correlation function. Linear-period-modulated (LPM) ultrasonic waves are employed to support the influence of the Doppler effect.

2.4 Position and velocity measurement techniques for three dimensions

A method describing a laboratory prototype capable of measuring the position of a four-legged walking robot using a combination of electromagnetic and ultrasonic wanes produced by a spark-generator, avoiding any physical link between the root and the environment is proposed [44]. The 3D position is obtained from range data that can be estimated from the travel time of the acoustical wave from the sparking point to three static receivers. The track-data obtained by the position meter is used to know the dynamic behavior of the robot and to study the improvement introduced by the use of inclinometers.

A localization system for wireless sensor network based on ultrasonic TOF measurements is presented [45]. The participants send out ultrasonic pulses while a central localization unit measures the Time-Difference-of-Arrival (TDOA) between four ultrasonic sensors to compute the Angle-of-Arrival (AOA). The radio frequency transceiver of the sensor nodes enables distance measurements using TDOA in addition. This technique requires several filter stages including Kalman-filtering minimize the number of outliers and fluctuations of the calculated distance and angles.

The main sources of error in an ultrasonic 3D position measurement system including shadowing of some of the receivers, air turbulence and the effect of the wind are described [46]. This method is suggested which improves precision and robustness, by taking advantage of the redundancy in the number of measurements and the use of a

modified trimmed median (MTM) filter.

A simple low-cost 2D and 3D positioning system for mobile robots is proposed [47]. The system makes use of both ultrasound and radio frequency signals to achieve positional accuracies. This system integrates the positioning system into the simulation tools Player/Stage, in order to combine simulated robots with real robots in a hybrid embodied simulation.

A work presents the development of a 3-Dimensional Positioning Acquisition System, proposed for applications in real-time processing [48]. The system is based on ultrasound sensors that present reasonable compromise between cost and flexibility. The signals from the sensors are processed in real-time and a position within a limited space can be obtained with a resolution of tenths of millimeters.

A system can simultaneously identify the 3D position and the velocity of a moving object. This system uses a method called Extended Phase Accordance Method [49], which can precisely provide the distance between an ultrasonic microphone and a moving transmitter by rapidly estimating the frequency shift of the transmitted signal. However, this method is not enough to be used for real-time applications due to a high-computational-cost time.

2.5 Summary

Many methods involving with the ultrasonic system for autonomous mobile robots are described above. The most important points for enabling autonomous mobile robots real-time signal processing are low computational time, reliability and low cost. Although the most of proposed ultrasonic systems can provide high accuracy of the position measurement, they may use the complex devices, which require a long computational time and a high price. In addition, they have only the ability of measuring the position without the knowledge of the velocity measurement. A system capable of concurrently measuring the 3D position and the velocity measurements is proposed. This method, in which an ultrasonic transmitter is a moving target, can be applied in a special work. Nevertheless, the development of simultaneously measuring the 3D position and the velocity under echolocation system with low computational cost is far from complete.

One-bit stream signal processing is well known as a digital decoder of Super Audio CD (SACD) with Direct Stream Digital (DSD) Technology. This processing allows SACD to achieve high audio quality that is better than any other digital or analog technology [50]. The third chapter will explain in more details of low-computation-cost

cross correlation using one-bit technology. This signal processing plays a vital role in dissertation.

3

Delta-sigma modulation and cross-correlation using one-bit signal processing

3.1 Need for oversampling and Delta-Sigma modulation

Nowadays, digital signal processing is the most powerful method in dealing with several signal processing problems because digital circuits are robust. They can be designed and performed effectively in small structures to obtain very complicated, accurate, fast systems. The development of the speed and density inside digital integrated circuits is required. This makes researches of digital signal processing (DSP) growing up in every year to predominately satisfy in almost areas of communication and consumer products. In general, analog signals are original information, which can be observed from surrounding, in the physical world. To perform them in the digital world, data conversion methods are necessary to transform analog signal to digital signal. According to the speed and capability of DSP cores increases, signal processing methods must require the speed and accuracy of the converters associated with them.

Data converters can be classified into two categories due to sampling rate: Nyquist-rate and oversampling. The Nyquist rate is the simplest basis of converters by directly corresponding a one-to-one transformation between the input and output samples. Each sample from input is processed without the knowledge of the earlier samples. It makes this converter no memory. The sampling rate f_s of Nyquist rate can be as low as Nyquists criterion requires at least twice of the bandwidth f_B of the input signal. In many applications such as digital audio [50-52], they require higher resolution than an

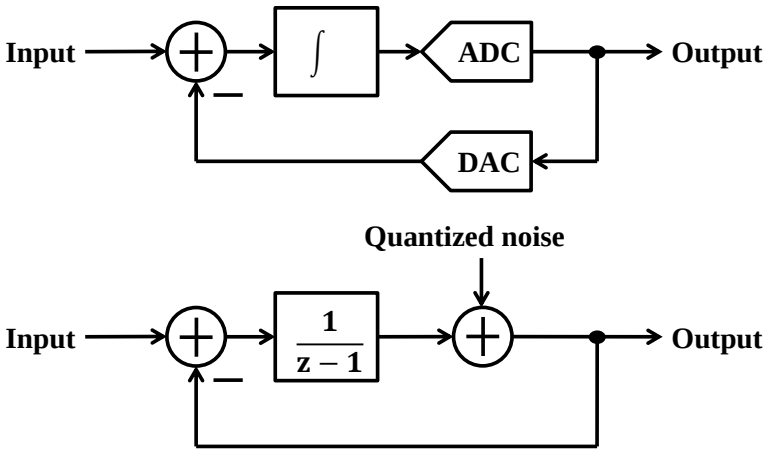

Figure 3.1 A delta-sigma modulator and its linear z-domain model.

usual case. The only Nyquist-rate converters capable of such accuracy are the integrating or counting ones. These, however, require at least $2N$ clock periods to convert a single sample, and hence they are too slow for most signal-processing applications. Oversampling data converters can achieve higher resolution at high conversion speeds by relying on a trade-off. They use sampling rates much higher than the Nyquist rate by a factor between 8 and 512 [53], and generate each output utilizing all preceding input values. Accordingly, the converter incorporates memory elements in its structure. This property destroys the one-to-one relation between input and output samples. Now only a comparison of the complete input and output waveforms can be used to evaluate the converts accuracy, either in the time or in the frequency domain.

The name delta modulator is derived from the face that the output is based on the difference between a sample of the input and a predicted value of that sample. In general, the loop filter may be a higher-order circuit, which generates a more accurate prediction of the input sample. This type of modulator is sometimes called a predictive encoder. The advantage of this structure is that for oversampled signals the difference of inputs is much smaller than only input itself, on average, and hence larger input signals can be allowed. Hence, the basic structure of Figure 3.1 comes to be called

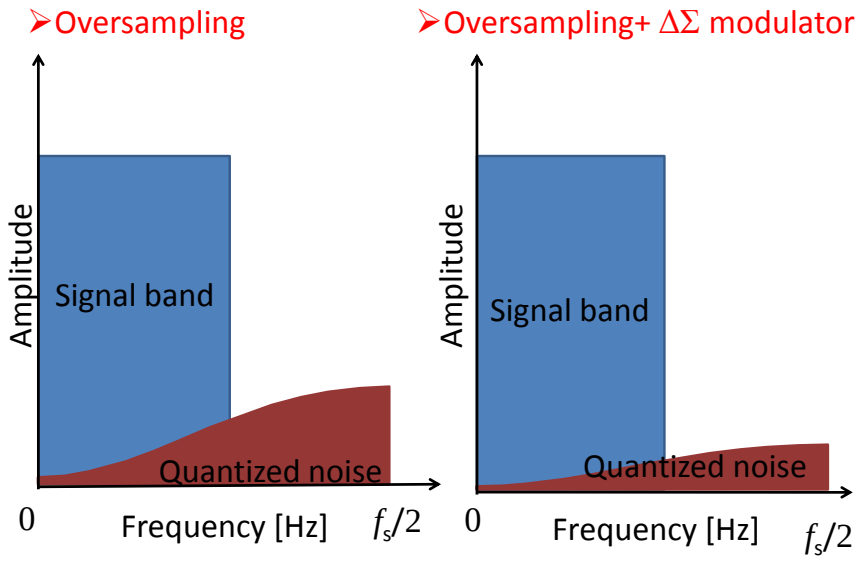

Figure 3.2 Quantized noise distribution by modulation.

a Delta-Sigma $\Delta\Sigma$ modulator. Quantized noise, which is the instinct of Analog to Digital conversion (ADC), can be relatively reduced inside the signal band by $\Delta\Sigma$ modulation shown in Fig. 3.2. The order of $\Delta\Sigma$ modulator simply means the number of the loop filters to be applied during the feedback of the quantization error. The order number can change the noise shaping characteristics or the quantized noise distribution. Although $\Delta\Sigma$ modulation is a technique that is also used in a multi- bit ADC converter, it can convert a digital signal to be a bit stream signal by additionally using a digital comparator.

In general, it is said that the minimum sampling frequency is at least twice of signal bandwidth by the sampling theorem of Nyquist. The oversampling technique has sufficiently higher frequency than the Nyquist frequency. Quantized noise caused by the quantization is the DC component signal during conversion. If the oversampling frequency is performed sufficiently, we can decrease quantized noise inside the signal band according to Figure 3.3. Therefore, by combining the oversampling technique and $\Delta\Sigma$ modulation, even in 1 or 2 bits of quantization, a high quantization resolution in the low frequency band is obtained.

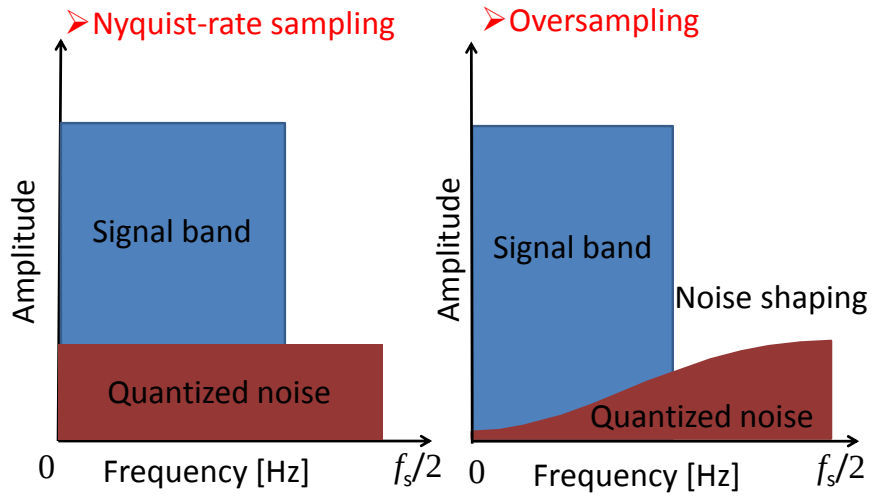

Figure 3.3 The quantized noise distribution by oversampling

3.2 ΔΣ modulators

In a ΔΣ modulator, the noise shaping characteristic is tuned following to the order of the loop. In general, 1 and 2 orders of ΔΣ modulator can guarantee stability of loops, whenever increasing the order to be 3 or higher order ΔΣ modulator, the output of the integrator is endlessly increased. The quantizer of the ΔΣ modulator becomes unstable (overload). To design higher-order ΔΣ modulator, it is necessary to set the weighting coefficient and the feedback coefficients of the input to obtain a proper loop gain. To design higher-order ΔΣ modulator, it is necessary to set the weighting coefficient and the feedback coefficients of the input to obtain a proper loop gain.

3.2.1 First order ΔΣ modulator

Figure 3.4 is a block diagram of first-order ΔΣ modulator. In first-order ΔΣ modulator, a quantized noise generated during one-bit quantizer is to improve noise shaping. Input (X), output (Y) signals, and the quantized noise (N_q) of the first-order ΔΣ modulator

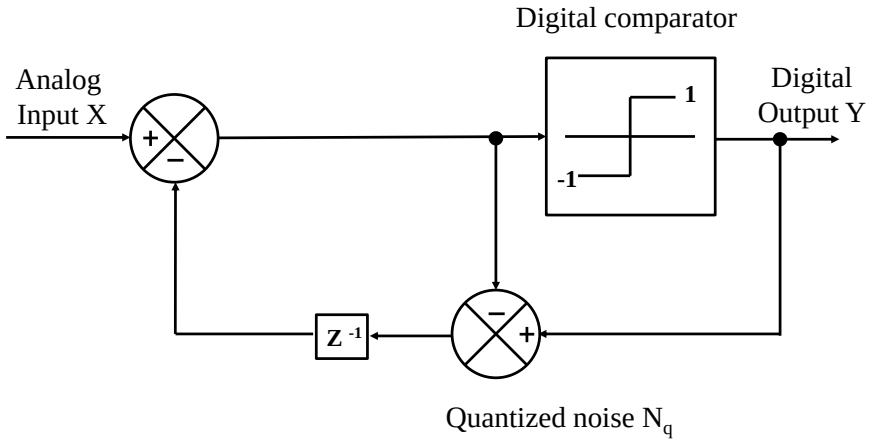

Figure 3.4 Block diagram of first-order ΔΣ modulator.

can be expressed by Equation 3.1.

$$Y = X + (1 - Z^{-1})N_q. \tag{3.1}$$

The characteristics of the one -bit ΔΣ modulated signal obtained from the first-order ΔΣ modulator are generated using MATLAB computer simulation. An oversampling frequency in this simulation is 12.5 MHz. Figure 3.5 is a comparison of 1 kHz sine wave with a reconstruction of the first-order ΔΣ modulator. The frequency spectrum of the one -bit ΔΣ modulated signal obtained from first ΔΣ modulator using 200,002 samples is pictured in Figure 3.6. Quantized noise of one-bit ΔΣ modulated signal from Figure 3.6 can be seen that it is concentrated in the high frequency band. Figure 3.7 is a block diagram of first-order ΔΣ modulator.

3.2.2 Second order ΔΣ modulator

In second-order ΔΣ modulator, a quantized noise generated during one-bit quantizer is to improve noise shaping. Input (X), output (Y) signals, and the quantized noise (Nq) of the second-order ΔΣ

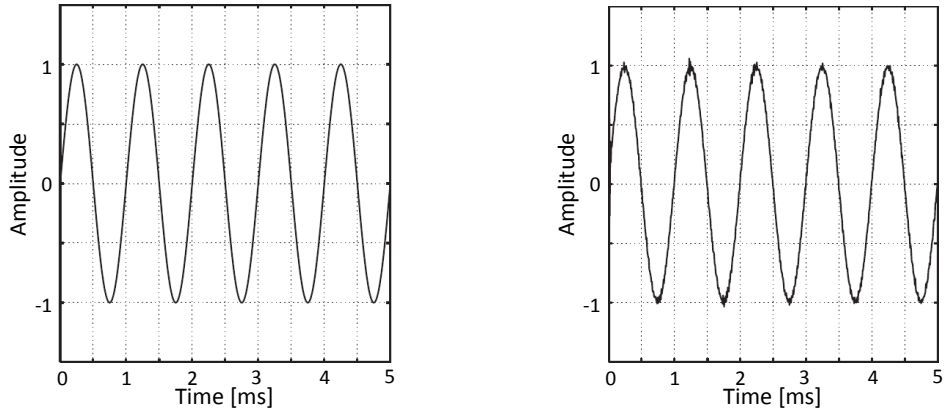

Figure 3.5 1 kHz sine wave of input signal and reconstruction from first order ΔΣ modulator.

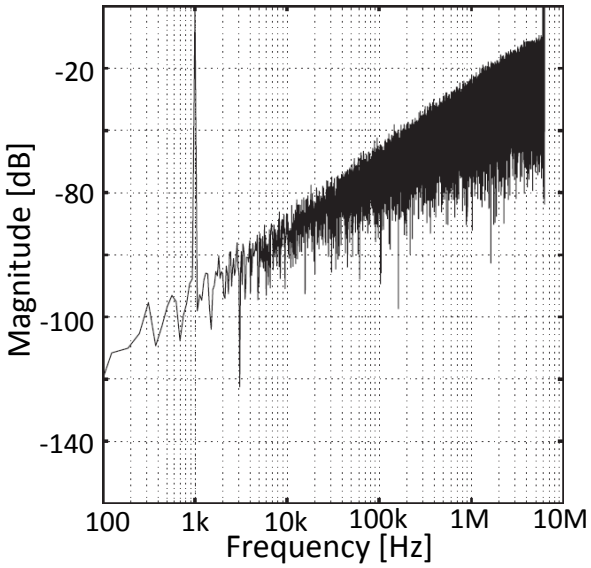

Figure 3.6 The frequency spectrum of the one -bit ΔΣ modulated signal obtained from first order ΔΣ modulator.

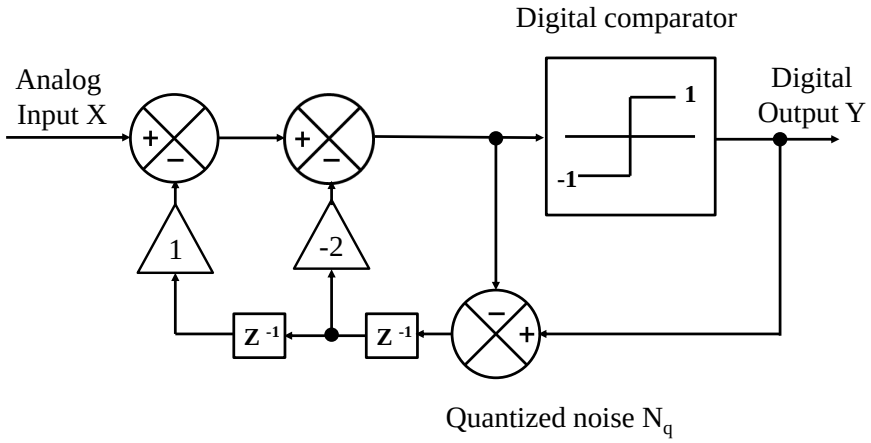

Figure 3.7 Block diagram of second-order ΔΣ modulator.

$$Y = X + (1 - Z^{-1})^2 N_q. \tag{3.2}$$

modulator can be expressed by Equation 3.2. The characteristics of the one-bit ΔΣ modulated signal obtained from the second-order ΔΣ modulator are generated using MATLAB computer simulation. An oversampling frequency in this simulation is 12.5 MHz. Figure 3.8 is a comparison of 1 kHz sine wave with a reconstruction of the second-order ΔΣ modulator. The frequency spectrum of the one -bit ΔΣ modulated signal obtained from second-order ΔΣ modulator using 200,002 samples is pictured in Figure 3.9. Quantized noise of one-bit ΔΣ modulated signal from Figure 3.9 can be seen that it is concentrated in the high frequency band.

3.2.3 7-order ΔΣ modulator (AD7720)

In this dissertation, 7-order ΔΣ modulator using AD7720 of Analog Device is performed in experiments [54]. AD7720 is performed converting the analog signal to a high speed one-bit stream. The original signal can be reconstructed with an appropriate digital filter. 12.5 MHz master clock frequency and 0 V to 2.5 V input range are required. In Figure 3.10, a sine wave with frequency 1 kHz and amplitude 1 V, which is generated

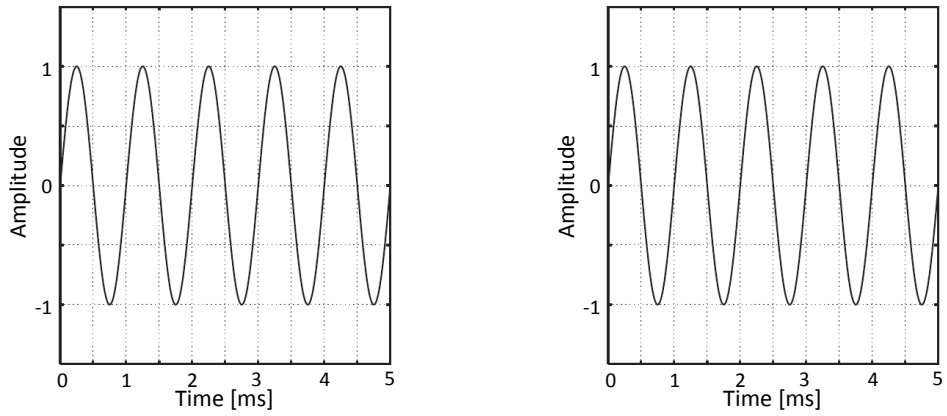

Figure 3.8 1 kHz sine wave of input signal and reconstruction from second order ΔΣ modulator.

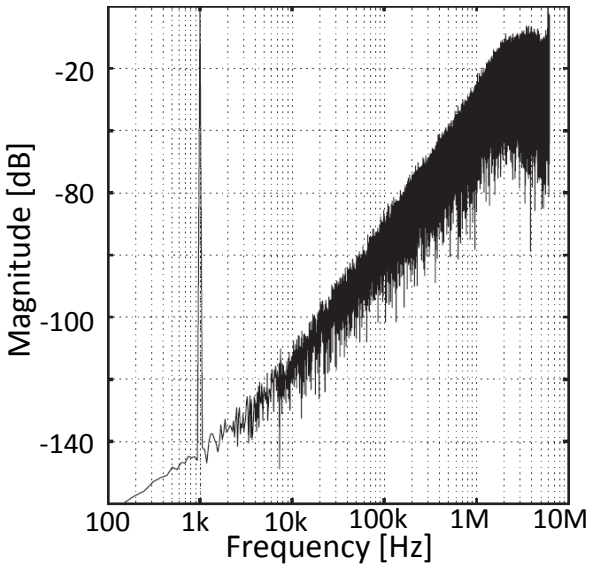

Figure 3.9 The frequency spectrum of the one -bit ΔΣ modulated signal obtained from second order ΔΣ modulator.

by a function generator, is used to perform the one -bit ΔΣ modulation signal obtained from AD7720. Input signal shown in Figure 3.11 is incorporated into the computer as an 8 -bit digital signal using an oscilloscope. A sampling frequency of AD7720 is 12.5 MHz. The frequency spectrum of the one -bit ΔΣ modulated signal obtained from AD7720 is 200002 samples. The frequency spectrum of the one -bit ΔΣ modulated signal obtained from AD7720 is shown in Figure 3.12.

A block diagram of the 7 -order ΔΣ modulator consists of a cascade structure of the resonator having an input and distributed feedback (CRFB structure) is shown in Figure 3.13. MATLAB program computer supporting Delta-Sigma toolbox can compute the coefficient parameter of 7-order ΔΣ modulator. We can model 7-order ΔΣ modulation structure to realize AD7720 characteristics [55]. AD7720 containing the ΔΣ modulation including seven digital filters changes the analog signal into the bit stream with very high resolution. The analog signal is continuously switched using a capacitor at twice the sampling rate of the master clock. This type provides the bit stream at a data rate equal to master clock with 12.5 MHz. In addition, an AD7720 board organized in this thesis for supporting 4 channels of one-bit signal converter was made to perform bit stream, as shown in Figure 3.10.

3.3 Signal to noise ratio of one-bit ΔΣ signal

In general, we can improve the SNR of the digital signal of conventional multi-bit signal by increasing the bit number of quantization. On the other hand, the SNR in one-bit ΔΣ modulation signal can be increased by a digital low-pass filter to decrease the quantized noise in the high frequency band. Therefore, enabling the high sampling frequency to reduce the quantized noise of the cut-off frequency below the low pass filter can improve the SNR of one-bit signal processing.

3.3.1 Multi-bit signal

Quantized noise in the multi-bit signals can be determined by the bit number of quantization. Assume that the minimum step of N bits is set Δ; therefore, the full scale of multi-bit signal is $(2N-1)\Delta$. The effective power (S) of the multi-bit signal obtained by converting the sine wave of full scale is given by the following Equation 3.3.

$$S = \frac{\left((2^N - 1)\Delta\right)^2}{2} \tag{3.3}$$

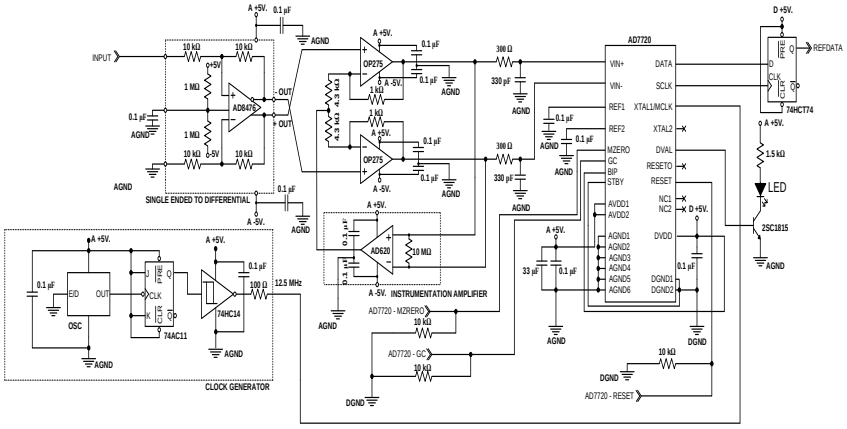

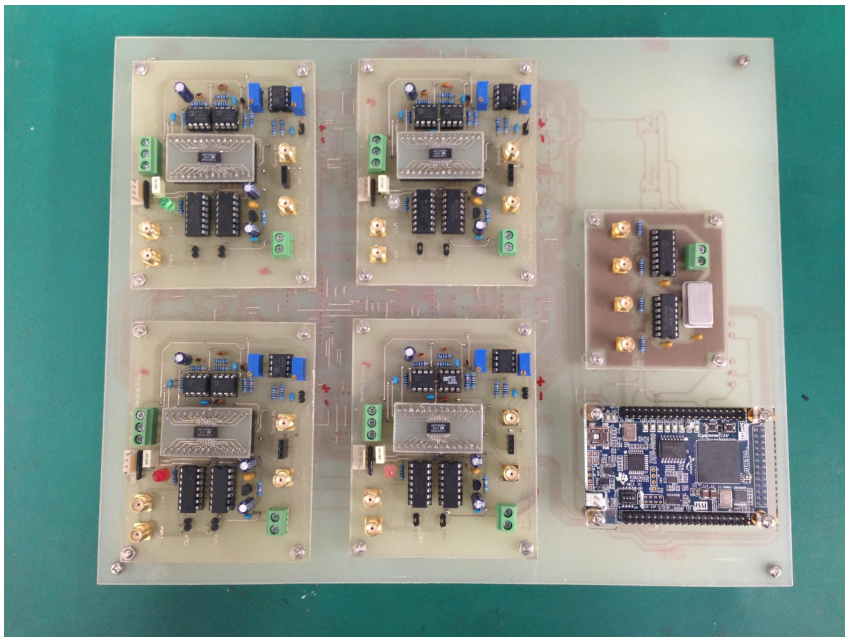

Figure 3.10 Four channels of an AD7720 board for one-bit signal conversion.

Quantized noise (N_q) in the multi-bit signal obtained by converting the sine wave of full scale can be formed as a value in the range of $\pm\frac{\Delta}{2}$. Quantized noise (N_q) in the

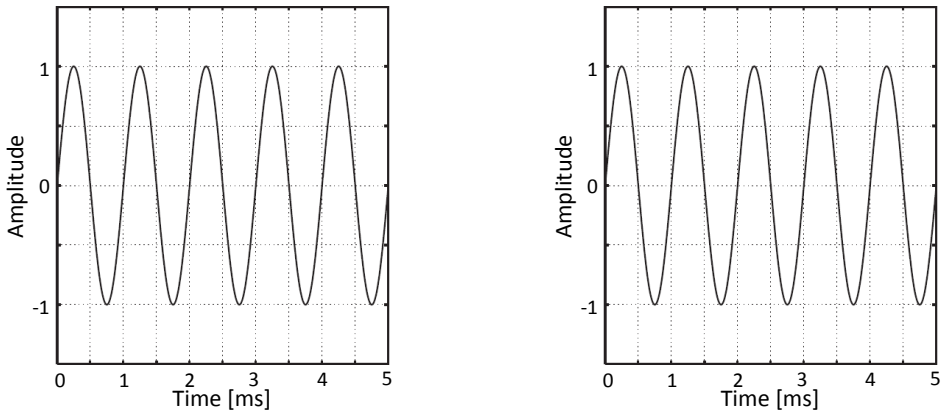

Figure 3.11 1 kHz sine wave of input signal generated a function generator and reconstruction from 7 order ΔΣ modulator (AD7720).

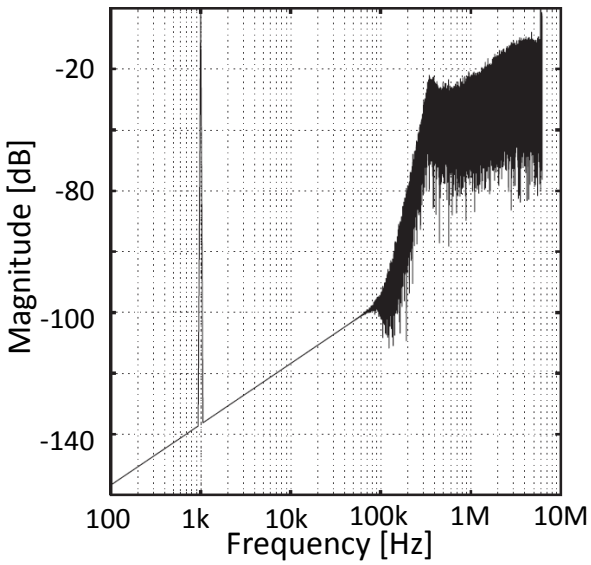

Figure 3.12 The frequency spectrum of the one -bit ΔΣ modulated signal obtained from AD7720

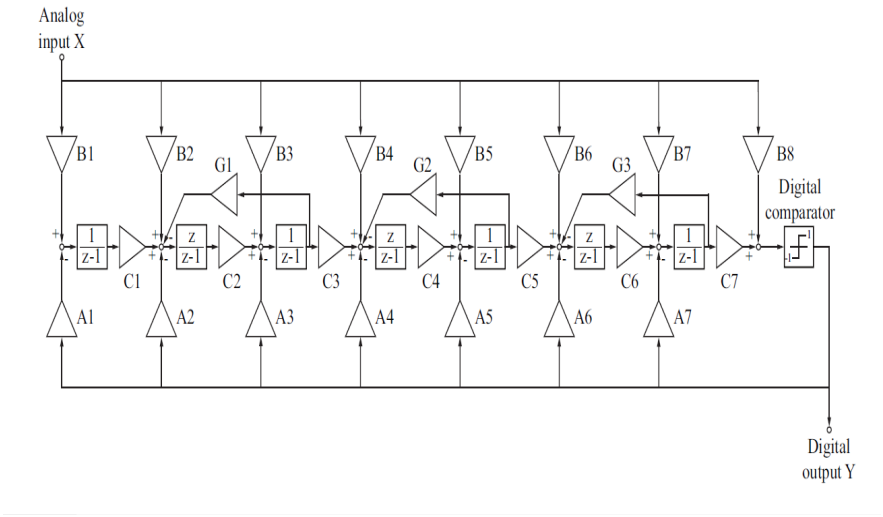

Figure 3.13 Block diagram of the 7 -order ΔΣ modulator containing CRFB structure[6].

multi-bit signal obtained by converting the sine wave of full scale can be formed as a value in the range of $\pm\frac{\Delta}{2}$. Assuming that noise is white; the quantized noise is uniformly distributed in the range of $\pm\frac{\Delta}{2}$. Effective power (N_0) quantized noise is given as follows:

$$\begin{aligned} N_0 &= \frac{1}{\Delta}\int_{-\frac{\Delta}{2}}^{+\frac{\Delta}{2}} N_q^2 dN_q \\ &= \frac{\Delta^2}{12}. \end{aligned} \tag{3.4}$$

SNR of the multi-bit signal with N bits by converting the sine wave of full scale from Equation (3.4) is expressed as follows:

$$\begin{aligned} SNR &= 10\log_{10}\left(\frac{S}{N_0}\right) \\ &= 6.02N + 1.76[\text{dB}]. \end{aligned} \tag{3.5}$$

If the sampling frequency of the multi-bit is f_s, the band width of the quantized noise

is contained in the frequency band within the range of $0 \leq \frac{f_s}{2}$. The higher sampling frequency, the lower quantized noise in the signal band becomes. This is a method to improve SNR in the multi-signal. Oversampling ratio (OSR) indicating the ratio of the Nyquist frequency f_s (sampling frequency) and the input frequency f_{in} is :

$$OSR = \frac{f_s}{2f_{in}}. \tag{3.6}$$

The effective power (N_{OSR}) of the quantized noise in the signal band by oversampling can be explained in the form of OSR as follows Equation (3.7).

$$\begin{aligned} N_{OSR} &= \frac{N_0}{OSR} \\ &= \frac{\Delta^2}{12OSR} \end{aligned} \tag{3.7}$$

The oversampling method, when converting the sine wave of full scale N bits, can improve the SNR of the multi-bit signal.

$$SNR = 6.02N + 1.76 + 10\log_{10}OSR[\text{dB}]. \tag{3.8}$$

Assume that OSR is twice, SNR improved is equal to 3dB (0.5 bits). It means that OSR is sufficiently high, SNR becomes higher even though the quantized-bit number is small. However, in the coarse quantized-bit number (1 or 2 bits), it is not practical to provide the sufficient SNR while a sampling frequency (GHz) is performed.

3.3.2 First-order $\Delta\Sigma$ modulation signal

The noise shaping of first-order $\Delta\Sigma$ modulator consisting of the quantized noise (N_q) and the delay signal term ($1-z^{-1}$) is shown in Equation (3.1). If we assign $z = \exp(\frac{2jf}{fs})$, gain frequency characteristic of the quantized noise (N_q) is given by the following expression in Equation (3.9).

$$g_{\Delta\Sigma 1} = 2\sin(\frac{\pi f}{f_s}). \tag{3.9}$$

Frequency characteristics of the effective power of the quantized noise inside first-order

ΔΣ modulation can be defined as

$$\begin{aligned} N_{\Delta\Sigma 1}(f) &= g^2_{\Delta\Sigma 2}(f)\frac{2N_0}{f_s} \\ &= \frac{8}{3}\sin^4(\frac{\pi f}{f_s})\frac{\Delta^2}{f_s}. \end{aligned} \tag{3.10}$$

If the sampling frequency is high enough (oversampling), we can approximate $\sin(\frac{\pi f}{f_s}) \approxeq (\frac{\pi f}{f_s})$. Effective power ($N_{\Delta\Sigma 1}$) of quantized noise after passing through the low- pass filter under a cut-off frequency (f_c) can be expressed as Equation (3.11).

$$\begin{aligned} N_{\Delta\Sigma 1}(f) &= \int_0^{f_c} N_{\Delta\Sigma 1}(f)df \\ &= \int_0^{f_c} \frac{2\pi^2}{3}\frac{f^2}{f_s^3}\Delta^2 df = \frac{2\pi^2}{9}\frac{f_c^3}{f_s^3}\Delta^2 \end{aligned} \tag{3.11}$$

In addition, effective power ($N_{\Delta\Sigma 1}$) of quantized noise after passing through the low-pass filter can be expressed in a term of OSR as well.

$$N_{\Delta\Sigma 1}(f) = \frac{\pi^2}{36}OSR^{-3}\Delta^2 \tag{3.12}$$

Thus, the SNR of first-order ΔΣ modulation signals with N bits can be expressed as the following Equation (3.13).

$$\begin{aligned} SNR &= 10\log_{10}(\frac{S}{N_{\Delta\Sigma 1}}) \\ &= 10\log_{10}\left(\frac{9}{2\pi^2}(2^N-1)^2 OSR^3\right) \end{aligned} \tag{3.13}$$

Simply speaking, assume that the number of quantization bits ($N = 1$), SNR of the one-bit ΔΣ modulated signal from Equation (3.13) can be expressed as the following Equation (3.14).

$$\begin{aligned} SNR &= 10\log_{10}\left(\frac{9}{2\pi^2}OSR^3\right) \\ &= 30\log_{10}OSR - 3.14[\text{dB}] \end{aligned} \tag{3.14}$$

The first-order ΔΣ modulator as described above, SNR of the one -bit ΔΣ modulated signal in the signal band used is relatively increased when compared with the multi-bit signal in Equation (3.8).

3.3.3 Second-order ΔΣ modulation signal

The noise shaping of second-order ΔΣ modulator consisting of the quantized noise (N_q) and the delay signal term $(1 - z^{-1})^2$ is shown in Equation (3.2). If we assign $z = \exp(\frac{2jf}{fs})$, gain frequency characteristic of the quantized noise (N_q) is given by the following expression in Equation (3.15).

$$g_{\Delta\Sigma 2} = 4\sin(\frac{\pi f}{f_s}). \tag{3.15}$$

Frequency characteristics of the effective power of the quantized noise inside first-order ΔΣ modulation can be defined as

$$\begin{aligned} N_{\Delta\Sigma 2}(f) &= g^2_{\Delta\Sigma 2}(f)\frac{2N_0}{f_s} \\ &= \frac{2}{3}\sin^2(\frac{\pi f}{f_s})\frac{\Delta^2}{f_s}. \end{aligned} \tag{3.16}$$

If the sampling frequency is high enough (oversampling), we can approximate $\sin(\frac{\pi f}{f_s}) \approxeq (\frac{\pi f}{f_s})$. Effective power ($N_{\Delta\Sigma 2}$) of quantized noise after passing through the low- pass filter under a cut-off frequency (f_c) can be expressed as Equation (3.17).

$$\begin{aligned} N_{\Delta\Sigma 2}(f) &= \int_0^{f_c} N_{\Delta\Sigma 2}(f)df \\ &= \int_0^{f_c} \frac{8\pi^2}{3}\frac{f^4}{f_s^5}\Delta^2 df \\ &= \frac{8\pi^2}{15}\frac{f_c^5}{f_s^5}\Delta^2 \end{aligned} \tag{3.17}$$

In addition, effective power ($N_{\Delta\Sigma 2}$) of quantized noise after passing through the low-pass filter can be expressed in a term of OSR as well.

$$N_{\Delta\Sigma 2}(f) = \frac{\pi^2}{60}OSR^{-5}\Delta^2 \tag{3.18}$$

Thus, the SNR of second-order ΔΣ modulation signals with N bits can be expressed

as the following Equation (3.19).

$$\begin{aligned} SNR &= 10\log_{10}(\frac{S}{N_{\Delta\Sigma 2}}) \\ &= 10\log_{10}\left(\frac{15}{2\pi^4}(2^N-1)^2 OSR^5\right) \end{aligned} \tag{3.19}$$

Simply speaking, assume that the number of quantization bits ($N = 1$), SNR of the one-bit $\Delta\Sigma$ modulated signal from Equation (3.19) can be expressed as the following Equation (3.20).

$$\begin{aligned} SNR &= 10\log_{10}\left(\frac{15}{2\pi^4}OSR^5\right) \\ &= 50\log_{10}OSR - 11.14[\text{dB}] \end{aligned} \tag{3.20}$$

The second-order $\Delta\Sigma$ modulator as described above, SNR of the one -bit $\Delta\Sigma$ modulated signal in the signal band used is relatively increased when compared with the first-order $\Delta\Sigma$ modulator in Equation (3.14).

Figure 3.14 shows the SNR comparison between second-order $\Delta\Sigma$ modulated signal, one-order $\Delta\Sigma$ modulated signal, and multi-bit signal from Equations (3.20), (3.14), and (3.8), respectively.

3.4 Cross correlation based on one-bit signal propessing

One-bit $\Delta\Sigma$ modulation signal can take advantage in areas of A/D conversion and digital audio communication. Faster than multi-bit signal, one-bit signal conversion requires high-speed sampling of circuit. Therefore, the $\Delta\Sigma$ A/D converter converts the analog input into one-bit signal with high speed and high resolution. In the field of digital audio, the audio signal, which is converted into one-bit $\Delta\Sigma$ modulated signal, is called Super Audio CD (SACD). This technology records the audio signal at a high frequency (2.8224 MHz). In SACD, using 24-bit digital filters, it is possible to obtain an acoustic signal at 192 kHz. It can achieve higher sound quality than the recorded music CD.

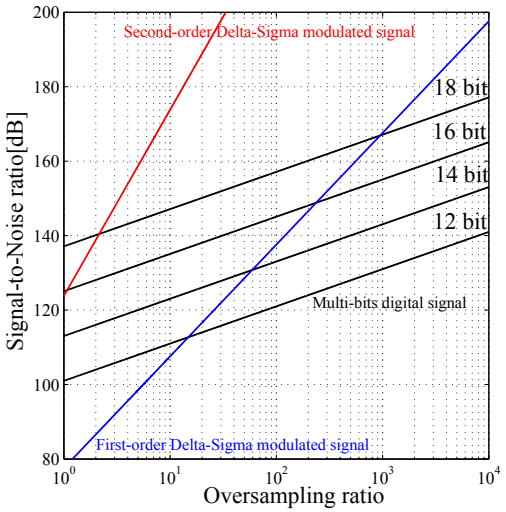

Figure 3.14 SNR of multi-bit signal and a one-bit $\Delta\Sigma$ modulation signal.

3.4.1 Recursive cross-correlation function

Firstly, we assume that a chirp signal is the main part of the transmitted signal. Computational cost of the cross correlation between the received signal converted one-bit $\Delta\Sigma$ Modulated signal and the reference signal (transmitted signal) changed to one-bit digital signal is performed. l is the signal length of chirp and f_s is the sampling frequency of the $\Delta\Sigma$ modulator. In each sampling clock, one-bit signals from both received signal and transmitted signal is in a process of multiplication and accumulation. Cross-correlation function of one-bit signal from each other can reduce the computational cost as compared with the computational cost of the cross- correlation between the conventional multi-bit signal [56]. However, in order to actually increase the sampling frequency of the $\Delta\Sigma$ modulator by oversampling, a number of operations is increased proportionally. It cannot be said that computational cost is reduced much. In general, the cross-correlation function using the one-bit signal with each other can be expressed by Equation (3.21).

$$c_1(t) = \sum_{i=0}^{N-1} h_1(N-i)x_1(t-i) \tag{3.21}$$

Next, the difference during each clock of the cross-correlation function between the

one-bit signals can be computed by Equation (3.22).

$$c_1(t) - c_1(t-1) = \sum_{i=0}^{N-1} h_1(N-i)x_1(t-i) - \sum_{i=0}^{N-1} h_1(N-i)x_1(t-i-1) \tag{3.22}$$

We can reform Equation (3.22):

$$\begin{aligned} c_1(t) - c_1(t-1) &= h_1(N)x_1(t) - h_1(1)x_1(t-N) \\ &\quad + \sum_{i=0}^{N-1} h_1(N-i) - h_1(N-i+1)x_1(t-i). \end{aligned} \tag{3.23}$$

Assume that $h_1(i)$ is a chirp signal in which the frequency is swept from 50 kHz to 30 kHz during a period time (5 ms). Since the reference signal $h_1(i)$ is the chirp signal converted into one-bit digital signal comparator, $h_1(1)$ is always 1 and $h_1(N)$ is always -1. The zero-cross point Z_i of the reference $h_1(i)$ is set to 399. $h_1(N-i) - h_1(N-i-1)$ can be expressed by the Equation (3.24) using a natural number (m).

$$c_1(t) - c_1(t-1) \begin{cases} = 2, \cdots N - i = Z_{2m-1} \\ = -2, \cdots N - i = Z_{2m} \\ = 0, \cdots N - i \neq Z_i \end{cases} \tag{3.24}$$

Difference per clock of the cross correlation function can be obtained by subtraction during 401 samples of one-bit signal as follows:

$$\begin{aligned} c_1(t) - c_1(t-1) &= -x_1(t) - x_1(t-N) \\ &\quad + 2x_1(t-N-Z_1) - 2x_1(t-N-Z_2) + \cdots + 2x_1(t-N+Z_{399}) \end{aligned} \tag{3.25}$$

The cross-correlation function $c_1(t)$ can be shown in a general form of the zero-cross

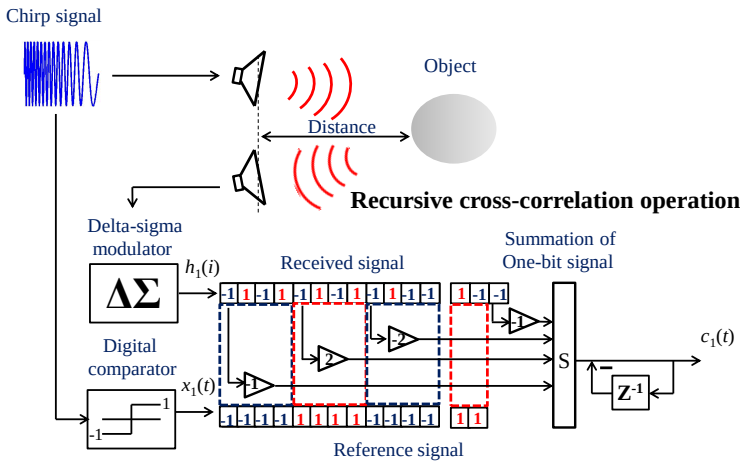

Figure 3.15 Configuration of one-bit signal processing to perform a recursive cross-correlation function.

points.

$$\begin{aligned} c_1(t) &= c_t(t-1) - x_1(t) - x_1(t-N) \\ &\quad + 2\Big\{ x_1(t-N-Z_1) - x_1(t-N-Z_2) + \cdots + x_1(t-N+Z_{399}) \Big\} \end{aligned} \tag{3.26}$$

The computational cost of the recursive cross-correlation process for one-bit signal is operated under 401 samples. The recursive cross-correlation function using one-bit signal [57] can be shown in Figure 3.15.

3.4.2 Implementation of recursive cross-correlation on FPGA

A field programmable gate array (FPGA) is a programmable semiconductor device, which has complex connections inside its own structure. Many basic logics or combinational logics are embedded on FPGA by means of computer programming to perform the proper functions, for examples, decoders and timers. Moreover, the memory blocks, which is made up of simple flip flop elements, is included in FPGAs for special func-

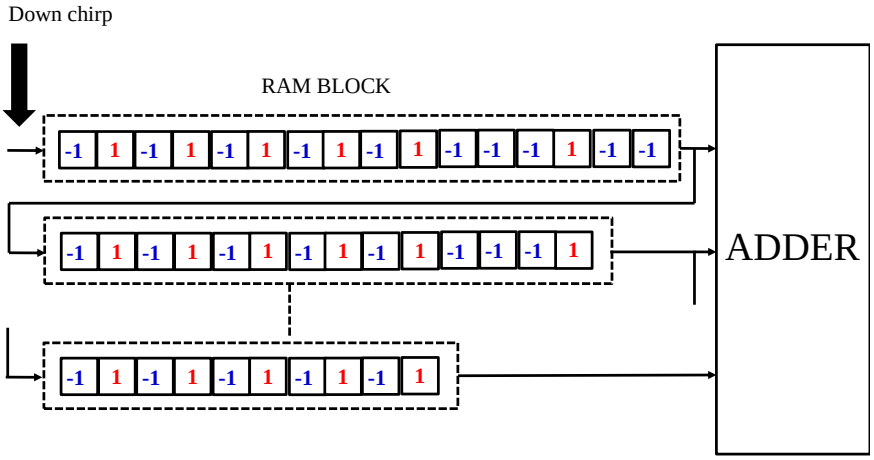

Figure 3.16 Register implementation of one-bit stream using a RAM.

tions. To measure ultrasonic position and velocity in low computational time, the recursive cross-correlation implementation in a FPGA is performed. FPGA used is Altera Cyclone V GX installed in Starter Kit Board, which is a robust hardware platform, lowest cost and low power requirement. The Cyclone V Starter Kit development board includes hardware such as Arduino Header, on-board USB Blaster, audio and video capabilities and much more [58].

As discussed in the previous section, employing a recursive cross-correlation function by one -bit signal for a low computational cost is in this study. By using the zero-crossing point of the reference signal, the cross-correlation computation is derived from the difference between the current input and the earlier input. To satisfy this operation, a shift register in the FPGA should have to have the twice of the signal length. The bit stream of the $\Delta\Sigma$ modulator is set 1 (high level) and -1 (low level). Since the master-clock frequency of the $\Delta\Sigma$ modulator to is 12.5 MHz and the signal length of the reference signal is a 3.274 ms, so the shift register requires 40,926 logic elements (LEs) per a channel for the recursive cross correlation. The proposed three dimensional ultrasonic position and velocity measurement employs, at the most, four ultrasonic receivers. Total logic elements for four channels are thus 163704 logic elements. Due to

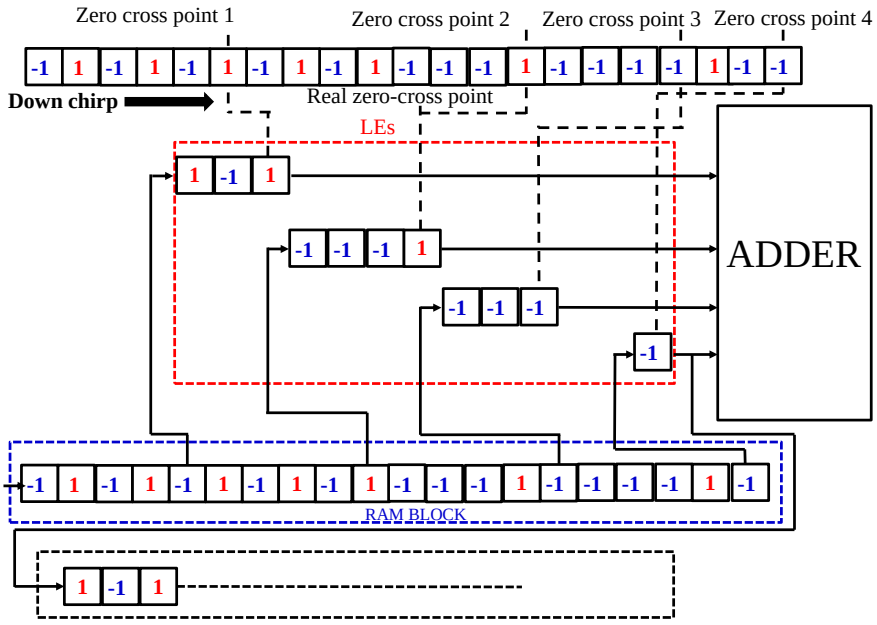

Figure 3.17 Register implementation of one-bit stream using a RAM (2).

the large size of circuit scale more than 100,000 LEs, a computational-cost problem is happened. Since Cyclone V having 4884 Kbits embedded memory of RAM is presented, this implementation is practically enough for four channels. Linear period modulated (LPM) signal (the reference signal), which is one of chirp signals, is swept from 50 μs to 20 μs in the signal length 3.274 ms when sampled signals at a sampling frequency of 12.5 MHz have total 199 zeros-cross points. We can separate the shift register to perform the zero cross point of the reference signal using RAM blocks as shown in Figure 3.16. Because the number of RAM blocks embedded on cyclone V is 66 blocks but 199 zero-cross points are required. It is impossible to actually implement. The zero-cross points should be improved by multiple combinations from reducing the number of RAM blocks into a single RAM block. However, when mounting the shift register using the RAM, we can generate a plurality of one shift register at the same RAM-blocks length. It is found that there is a restriction that is not possible to generate a plurality of shift registers at different lengths. LPM signal used in this study are getting shorter interval of the zero-cross point because of the down-chirp sweeping. Therefore, the multiple zero-cross points into a single RAM block is devised as shown in Figure 3.17. Since the reference signal used is known, the position of the zero-cross points can be calculated

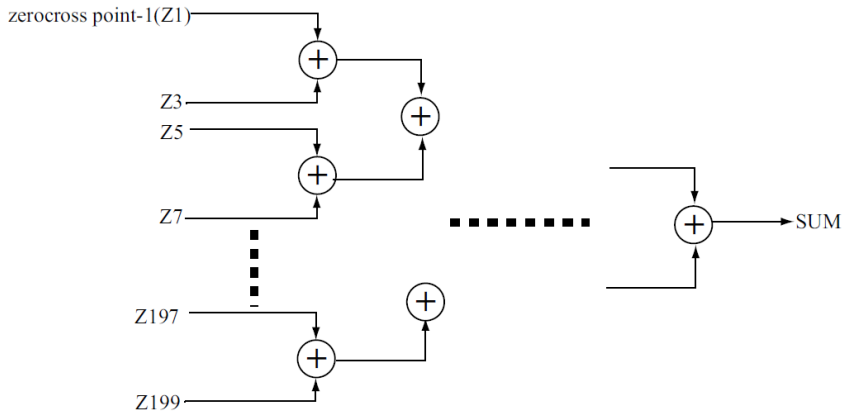

Figure 3.18 A tree type of summations from the zero-cross points.

beforehand. The interval from the sum of the zero-cross point is divided to four units. Because the shift registers are the same length, it can be collectively mounted on one of the RAM blocks. The value retrieved from the shift register which is generated in the RAM will be taken out at a time earlier than the actual zero cross point. To make the shift register by using the logic Elements for the timing error compensation, timing is adjusted to zero cross point. The four zero-cross point consumes 50 RAM blocks. The value of the odd-numbered zero-cross points are added by using a tree of adders shown in Figure 3.18. Similarly, a process of the odd-numbered zero-cross points is performed in the same manner. The total value of the odd-numbered zero- cross point is 99 summations, and the total value of the even-numbered zero- cross points is 98 summations.

3.5 Summary

One-bit $\Delta\Sigma$ modulation signal rather than a multi-bit signal sampled by means of over-sampling can obtain a high SNR. The cross-correlation using one-bit $\Delta\Sigma$ modulated signal processing is compared with the cross correlation of multibit digital signal. This

technique can be performed to reduce the circuit scale. To support a real-time application, FPGA cyclone V is useful to calculate recursive cross correlation of one-bit signals.

4

Ultrasonic linear period modulated signal and devices

4.1 Cross-correlation function of the LPM signal

In the ultrasonic position measurement using a cross-correlation method, if the target object is moving, frequency and signal length of the echo is changed due to the Doppler effect. Because of the influence of Doppler shift, the position measurement using a linear frequency modulated (LFM) signal is quite difficult to obtain the cross-correlation function. Based on the cross-correlation method, two ultrasonic linear-period-modulated (LPM) signals used for transmission is proposed to concurrently measure the position and Doppler velocity of a moving object.

4.1.1 Cross-correlation function of the LPM signal

LPM signal, of which a signal period varies linearly with respect to time, is a type of chirp signals. LPM signal can be defined by the expression of an angular frequency (ω_p) by integrating an initial time (T_0), a period of chirp width (ΔT), and a signal length (l_0) as follows:

$$\begin{aligned} \omega_p &= 2\pi \frac{1}{T_0 + \frac{\Delta T}{l_0} t} \\ &= 2\pi \frac{\frac{1}{\Delta T} l_0}{t + \frac{T_0}{\Delta T} l} \end{aligned} \tag{4.1}$$

We can express a phase (θ_p) of LPM signal as Equation (4.2).

$$\omega_p = 2\pi \frac{1}{\Delta T} l_0 \ln(t + \frac{T_0}{\Delta T} l_0) \tag{4.2}$$

Thus, LPM signal can be obtained from Equation (4.3).

$$s_{\mathrm{LPM}}(t) = \sin(2\pi \frac{1}{\Delta T} l_0 \ln(t + \frac{T_0}{\Delta T} l_0) - 2\pi \frac{1}{\Delta T} l_0 \ln(\frac{T_0}{\Delta T})) \tag{4.3}$$

LPM signal with varying a period from 20 μs to 50 μs at a signal length 3.274 ms can be generated by MATLAB computer simulation. The autocorrelation function and the frequency spectrum of LPM signal can be also computed using MATLAB when amplitude of LPM signal is 1 and the sampling frequency is 12.5 MHz. The autocorrelation function of the LPM signal is determined by the following Equation (4.4).

$$c(t) = \sum_{i=1}^{N} s_{\mathrm{LPM}}(N-i) s_{\mathrm{LPM}}(t-i) \tag{4.4}$$

The autocorrelation and the frequency spectrum of LPM signal are Figures 4.1. and 4.2, respectively. The maximum value of the autocorrelation function is normalized to 1 and full scale of the frequency spectrum is a sine wave with the amplitude of 1. Sharp peak of LPM signal in the autocorrelation function $c(t)$ is same as LFM signal. The frequency spectrums amplitude of the LPM signal decreases when the frequency becomes higher in the chirp bandwidth. The high frequency, which is out of the chirp bandwidth and gradually moving toward the higher frequency band, is reduced. Spread of the frequency spectrum from discrete Fourier transform is the spectral leakage that occurs when performing frequency analysis. It is not actually the frequency spectrum outside the band of LPM signal. In Figure 4.3, the amplitude of LPM signal is inversely proportional to the frequency and the amplitude becomes zero outside the band of the chirp signal. This is the frequency spectrum of the ideal LPM signal. Moreover, the LPM signal can be obtained from Fourier transform in Equation (4.5). $E_i(x) = \int \frac{\exp(x)}{x} df$ is called the exponential integral. It is the indefinite integral and cannot be expressed by elementary functions.

$$s_{\mathrm{LPM}}(t) = \int_{-\frac{1}{T_0}}^{-\frac{1}{T_0+\Delta T}} (-\frac{1}{f}) \exp(-j2\pi ft) df + \int_{\frac{1}{T_0}}^{\frac{1}{T_0+\Delta T}} (\frac{1}{f}) \exp(-j2\pi ft) df \tag{4.5}$$

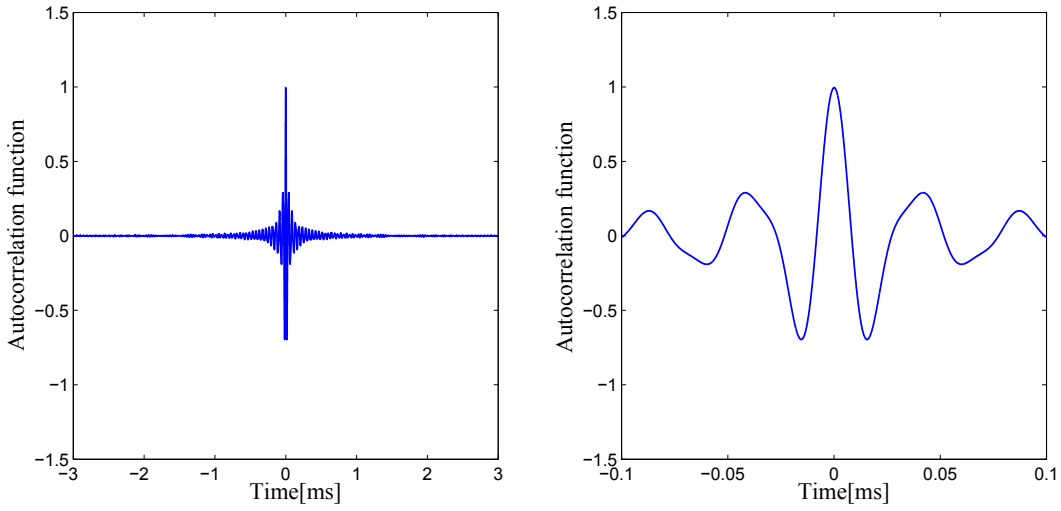

Figure 4.1 The autocorrelation function $c(t)$ of the LPM signal from 20 μs to 50 μs at signal length 3.274 ms and enlarged view of the vicinity of t=0.

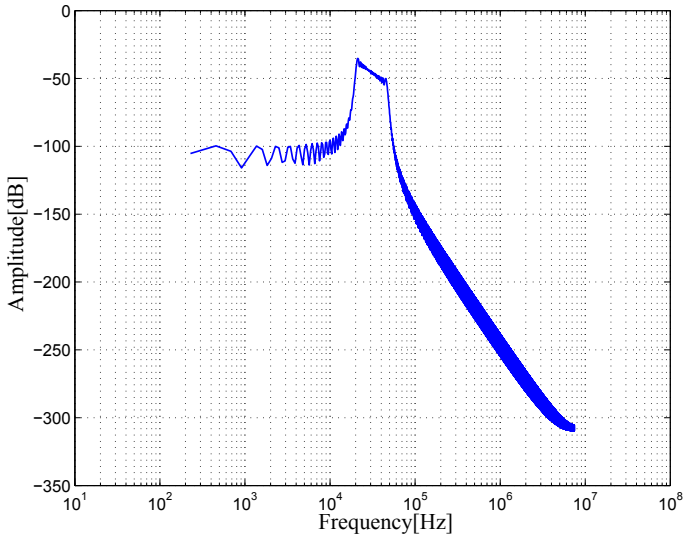

Figure 4.2 Frequency spectrum of the LPM signal when length is 3.274 ms and the period is changed from 20 μs to 50 μs.

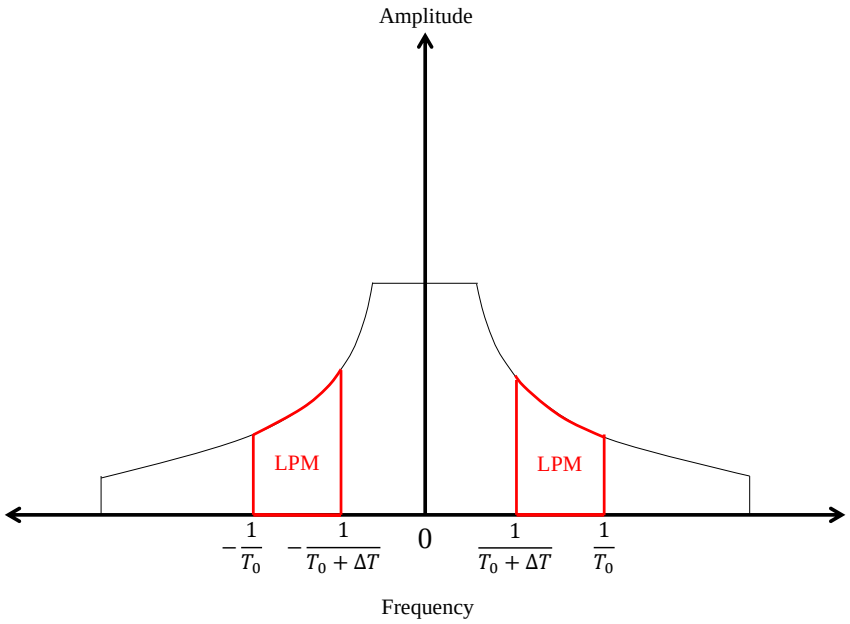

Figure 4.3 Frequency spectrum of the ideal LPM signal.

4.1.2 LFM signal and LPM signal

Previously, LPM signal, which was considered a chirp wave, has been described for the cross-correlation function. In the case of LFM signal, if the target is a moving object, LFM signal, which is modulated due to the Doppler effect, cannot correlate completely. To satisfy this phenomenon, LPM signal has been introduced [59-62]. Figures 4.4 and 4.5 show the change in frequency and period for time of LFM signal and LPM signal. LFM signal is varying a frequency from 50 kHz to 20 kHz at a signal length 4 ms. LPM signal is varying a period from 20 μs to 50 μs at a signal length 4 ms. LPM signal is a linear variation as shown in Figure 4.6 when Doppler shift of the echo is performed. When scrutinizing in Figure 4.6, LFM signal cannot take a correlation between the transmitted signal and the received echo. On the other hands, LPM signal cycle changes linearly with respect to a time and it can correlate together between the transmitted signal and the Doppler shifted LPM signal as shown in Figure 4.6. The cross-correlation function in the case of a moving object is also modulated due to the Doppler effect. The cross-correlation function of the Doppler-shift echo can be evaluated mathematically using MATLAB computer simulation, as shown in Figure 4.7. In the simulation, assume that LFM signal as a transmitted signal has the frequency

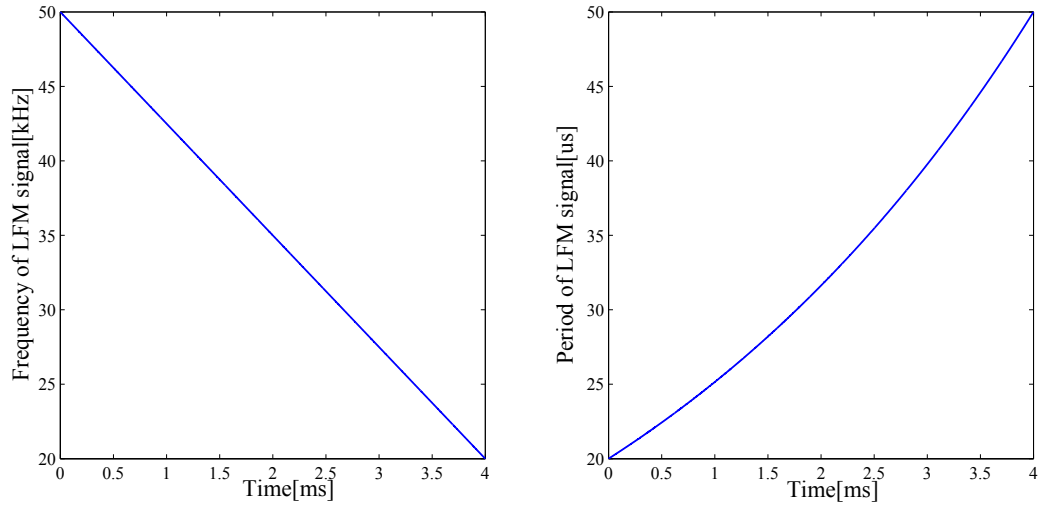

Figure 4.4 LFM signal varying from 50 kHz to 20 kHz at signal length 4 ms.

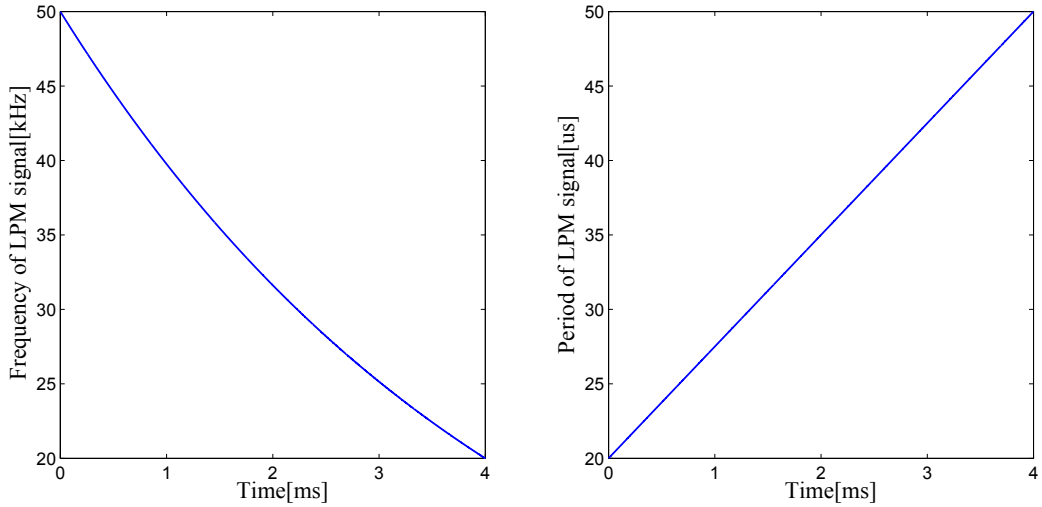

Figure 4.5 LPM signal varying from 20 μs to 50 μs at signal length 4 ms.

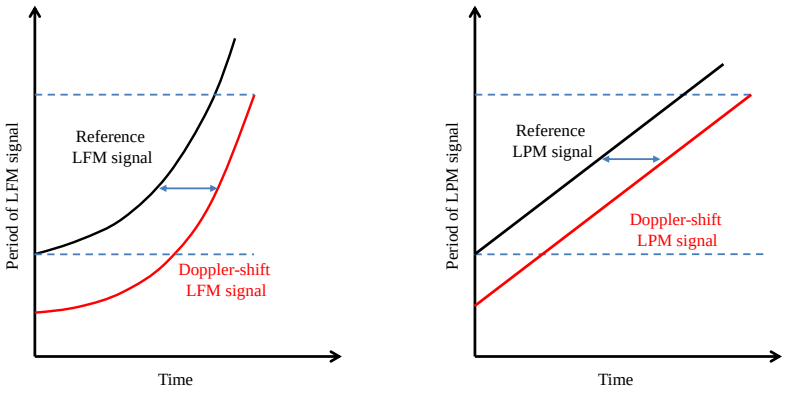

Figure 4.6 Period change and Doppler shift of both LFM signal and LPM signal.

swept from 20 kHz to 50 kHz at a signal length 3.429 ms. LPM signal is varied from 20 μs to 50 μs at 3.274 ms. The propagation speed of the ultrasonic wave is approximately 346.7 m/s at temperature 20^o. The sampling rate in simulation process is 12.5 MHz. The velocity of the moving object is 10 m/s.

4.1.3 Doppler- shift compensation of time-of-flight

The TOF of a pair of LPM signals is generally estimated from the maximum peak time in the cross-correlation function. However, considering the case of a moving object, the Doppler effect on the wave form of the modulated cross-correlation function is caused by the phase shift of the received LPM signal, as illustrated in Figure 4.8. The maximum peak value in the modulated cross-correlation function does not show the TOF of the received LPM signal. Therefore, the peak time in the envelope of the cross-correlation function t_e is obtained to estimate the TOF of the received LPM signal. To identify the TOF due to the cross-correlation, the peak time in the envelope of the cross-correlation function can still be compensated by the maximum peak P_{max} and the minimum peak P_{min} , the time at the maximum t_{max}, the minimum t_{min}, and the Doppler velocity measurements. The Doppler velocity measurements are required to

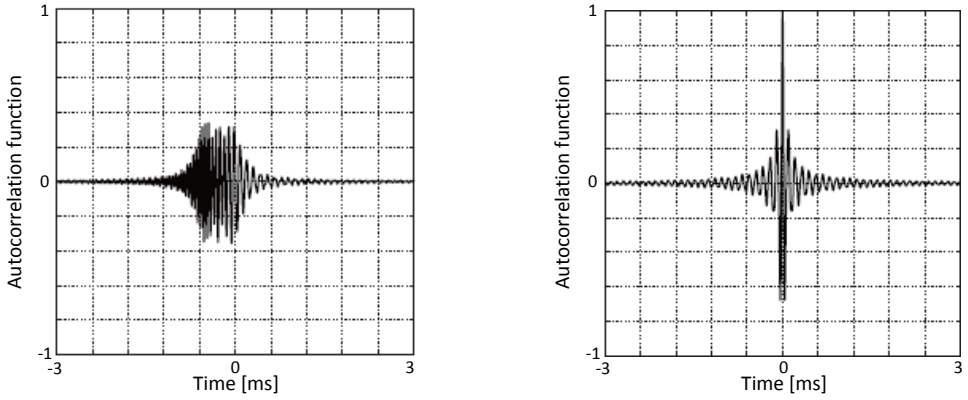

Figure 4.7 The autocorrelation function $c(t)$ of the Doppler shift LPM signal (left) and LFM signal (right) when Doppler velocity 10 m/s.

adjust the length of the modulated LPM signal to account for Doppler effects. The cross-correlation function between the pair of Doppler shift LPM signals and the single reference LPM signal in Figure 4.9 has two peaks. Thus, the interval containing the first maximum peak and the one containing the second maximum peak in the modulated cross-correlation function displays the Doppler shift length of the single LPM signal. The Doppler-shift length of the reference LPM signal is expressed as:

$$\Delta T = \frac{v - v_d}{v + v_d} l_0 \tag{4.6}$$

where ΔT is the Doppler-shift length of the received LPM signal, l_0 is the length of the reference LPM signal, v_d is the Doppler velocity, and v is the propagation velocity of an ultrasonic wave in the air. The original LPM signal is defined as Equation (4.3). In [63], the compensated peak time can be estimated from the maximum and minimum peak times and the Doppler velocity coefficient ξ. For a Doppler velocity $v\left(\exp(\frac{\Delta T}{l_0}m) - 1\right) < v_d < v\left(\exp(\frac{\Delta T}{l_0}m + 1) - 1\right)$

$$\xi = \left| -\frac{2l_0}{\Delta T} ln\left(\frac{v - v_d}{v + v_d}\right) - (2m + 1) \right|, \tag{4.7}$$

$$t_e = \xi t_{max} + (1 - \xi) t_{min} \tag{4.8}$$

where t_e is the compensated peak time and m is any integer. The TOF of the received

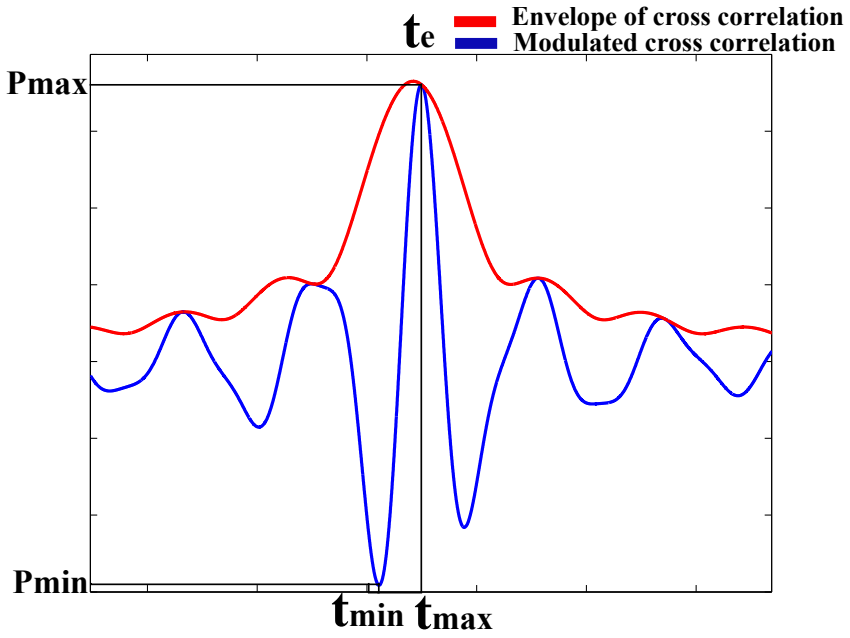

Figure 4.8 Modulated cross-correlation envelope of the LPM signal.

LPM signal is estimated as

$$TOF = t_e - \frac{v_d}{v + v_d}\frac{T_0 l_0}{\Delta T} \tag{4.9}$$

4.2 Ultrasonic transmitters (loudspeaker)

In this section, an ultrasonic transmitter, a loudspeaker, generating ultrasound wave to a target, plays an important role. In general, the loudspeaker for converting electrical signals into sound waves is an electromagnetic device. There are two types of loudspeakers. First, the vibrating-surface type, well known as the diaphragm, generates sound wave directly to any obstacle. Second, it is so called a horn, which is interposed between the air and the diaphragm. Both types can be technically called direct-radiator loudspeakers. In this dissertation, we select to utilize the vibrating-surface type because of its principle advantages: small size, low cost, and a satisfactory response over a comparatively wide frequency range. The direct-radiator type is useful in most home radio and in small public-address systems. However, the principle advantages of the direct-radiator type are low efficiency, narrow directivity at high fre-

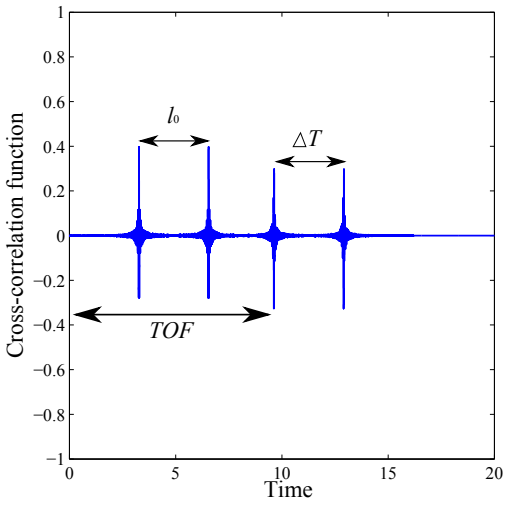

Figure 4.9 The cross-correlation function between the pair of Doppler shift LPM signals and the single reference LPM signal.

quencies, irregular response curve at high frequencies [64]. This is a very important point in the loudspeaker selection because the object in front of the loudspeaker has to be in a position that sound beam of the loudspeaker can radiate. In order fully to specify a sound source, we need to know its directivity characteristics at all frequencies of interest. Sound-beam radiation is somewhat necessary to study in the design of three dimensional ultrasonic position measurement.

4.2.1 Sound radiation by a disc

Assume that a plane-disc surface with radius ρ on which every point vibrate in phase with the same frequency ω and with normal velocity of amplitude V_0.The sound beam of waves distributed is symmetrical about the y-axis. To measure the potential at any point, it is sufficient only one point P at a displacement r from the disc center 0 and with its radius vector 0P making an angle θ with y-axis as Figure 4.10. Velocity potential ϕ produced in the point P, and integrated over the entire vibrating surface is defined as shown in Equation (4.10).

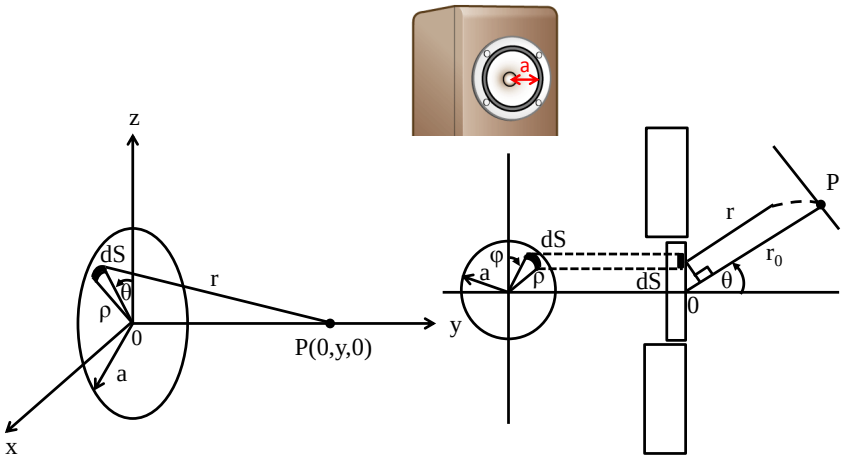

Figure 4.10 A uniform velocity with amplitude u_0 at P on y-axis and sound pressure distribution

$$\begin{aligned}\phi &= \frac{V_0}{2\pi}\iint_S \frac{\exp(-jkr)}{r}d\mathrm{S} \\ &= \frac{V_0 a^2}{2y}\exp(-jky)\end{aligned} \tag{4.10}$$

where k is a phase fix $k = 2\pi/\lambda$ and λ is sound length. A sound pressure at point P can be computed as Equation (4.11).

$$\begin{aligned}p_P &= j\omega\rho\phi \\ &= j\omega\rho\frac{V_0 a^2}{2y}\exp(-jky)\end{aligned} \tag{4.11}$$

At a surface element $dS = \rho d\rho d\varphi$, a distance r and air density ρ from the point P is $r \cong r_0 - \rho\cos\varphi\sin\theta$ when $r_0 \gg a$. It is also possible to approximate $r \cong r_0$ except for the phase term in the calculation of the integral equation 4.10. Therefore, the velocity

potential of the point P is:

$$\phi_{(\theta)} = \frac{u_0 \exp(-jkr_0)}{2\pi r_0} \int_0^a \int_0^{2\pi} \exp(jk\rho \cos\varphi \sin\theta)\rho d\rho d\varphi \tag{4.12}$$

The velocity of the point P in the first order Bessel function J_1 is:

$$\phi_{(\theta)} = \frac{u_0 \exp(-jkr_0)}{2\pi r_0} \pi a^2 \frac{2J_1(ka\sin\theta)}{ka\sin\theta} \tag{4.13}$$

In addition, if the velocity potential is on the central axis, it is equal to Equation (4.14).

$$\phi_{(0)} = \frac{u_0 \exp(-jkr_0)}{2\pi r_0} \tag{4.14}$$

From Equation (4.11), a sound pressure at θ can be expressed as follows:

$$p_{(\theta)} = j\omega\rho \frac{u_0 \exp(-jkr_0)}{2\pi r_0} \pi a^2 \frac{2J_1(ka\sin\theta)}{ka\sin\theta} \tag{4.15}$$

Directivity index and directivity factor $D_{(\theta)}$ can be computed in Equation (4.16).

$$D_{(\theta)} = \left| \frac{\phi_{(\theta)}}{\phi_{(0)}} \right| = \left| \frac{2J_1(ka\sin\theta)}{ka\sin\theta} \right| \tag{4.16}$$

An example of sound pressures is given in Figure 4.11, and directivity of radiation by a disc is shown in Figure 4.12. If we fix a constant radius of the circular plate and vary higher frequencies, sound-pressure directivity becomes narrower. Sound pressure directivity can be improved by enlarging the circular plate but a trade-off is the big size of devices.

4.2.2 Sound radiation by a rectangular plane

In this dissertation, a loudspeaker is assumed as a sound source, which radiates sound directly into the air. The loudspeaker that we use is Pioneer model PT-R4, which is the direct-radiator type. It is often used in a small public address system. The principle advantages of the direct-radiator type are small size, low cost, and a satisfactory response over comparatively wide frequency range. However, the main disadvantages of this type are low efficiency, narrow directivity pattern at high frequencies, and frequently irregular response at high frequencies. In order fully to specify our loudspeaker, we need to know its intensity levels of sound at all frequencies of interest. The loudspeaker of Pioneer model PT-R4 has a rectangular plane surface source. It is featured in Figure

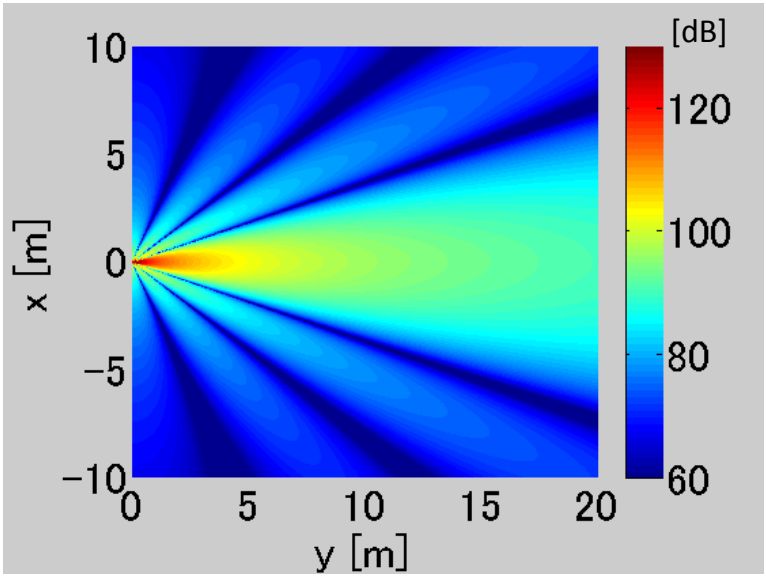

Figure 4.11 Sound pressure at $a = 0.003$ m, $f = 20$ kHz, and $u_0 = 0.2$ m/s.

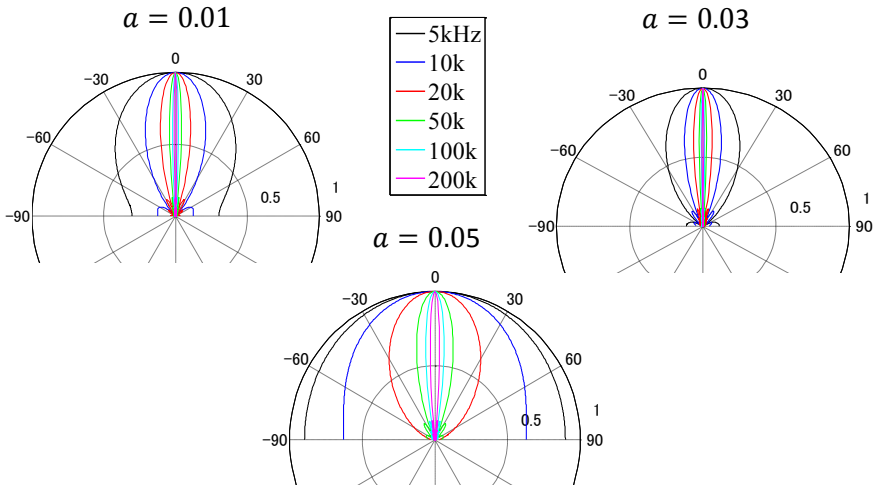

Figure 4.12 Directivity of radiation by a disc at various frequencies.

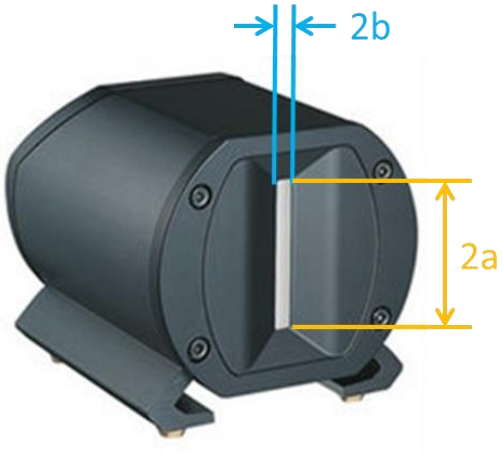

Figure 4.13 Pioneer PT-R4 loudspeaker used in three-dimensional ultrasonic position measurement.

4.13. Consider a rectangular plane with hight $2a$ and width $2b$ on which all points vibrate in phase with the same frequency ω. The method developed as a part of this chapter describes the field for the loudspeaker that can be divided in to small rectangular elements. If dS is each small element on a diaphragm as in Fig. 4.14 and has a center at $(x_n; z_n)$, this rectangular plane is assumed, at an original point, with a uniform normal velocity of amplitude u_n. The total potential for particle velocity ϕ_n at some point P proportional to the area dS of the small element and to the amplitude u_n at this area is given by the *Rayleigh integral* [65].

$$\phi_n(r,t) = u_n \exp(j\omega t) \int_S \frac{\exp(-jkr)}{2\pi r} dS, \tag{4.17}$$

where r is the distance of the element dS to the point P, and k is the wave number. According to the relation Equation (4.17), it is implied that acoustic waves generated by a real source must be diverge, so that the sound pressure p_n decreases with the distance from the sound source. Hence, the sound pressure can be defined as

$$\begin{aligned} p_n &= \rho \frac{\partial \phi_n}{\partial t} \\ &= j\omega\rho u_n \exp(j\omega t) \int_S \frac{\exp(-jkr)}{2\pi r} dS, \end{aligned} \tag{4.18}$$

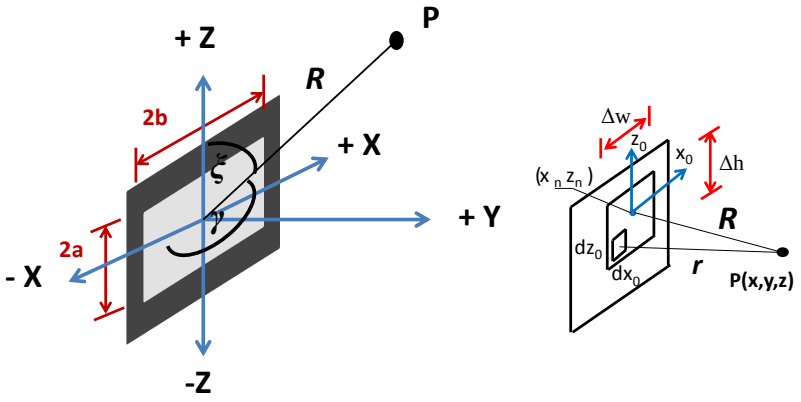

Figure 4.14 Sound radiation by rectangular surface source.

where ρ is the density of the air at rest. Consider the Equation (4.18), if we are interested on only the directivity of the sound pressure, ignore t-domain, the total pressure p_T at a point P in the field is the pressure contributed from each element.

$$p_T = j\omega\rho \sum_{n=1}^{N} u_n \int_{\Delta A} \frac{\exp(-jkr)}{2\pi r} dA, \tag{4.19}$$

where N is the number of elements of size $\Delta A = \Delta h \mathrm{x} \Delta w$. Consider the equation (4.19), the sound field computation for rectangular sources has been demonstrated in [66] as

$$p_T = \frac{j\omega\rho\Delta A}{2\pi R} \sum_{n=1}^{N} u_n \mathrm{sinc}\frac{k(x-x_n)\Delta w}{2R} \mathrm{sinc}\frac{k(z-z_n)\Delta h}{2R} \tag{4.20}$$

The two assumptions used to support Equation (4.20) are that $\frac{kx_0^2}{2R} + \frac{ky_0^2}{2R}$ is small compared to π and $r \cong R$ in all elements. Thus, the total sound pressure due to an area of rectangular plane $2a\mathrm{x}2b$ in Figure 4.14, symmetrical about the +Y axis, can be defined in a function of the angle of evaluation ξ and the azimuth angle γ at a center

of plane.

$$p_T = \frac{j\omega\rho u_T}{2\pi R} 4ab\text{sinc}(ka\cos\xi)\text{sinc}(kb\cos\gamma) \tag{4.21}$$

where $\Delta A = 4ab$ and . Also, the sound pressure at any point on the +Y axis is given with $\xi = 90^o$ and $\gamma = 90^o$.

$$p_0 = \frac{j\omega\rho u_T}{2\pi R} 4ab \tag{4.22}$$

A number is computed at each frequency that tells the degree of directivity without the necessity for showing the entire directivity pattern. This number is the directivity index $D_{\xi,\gamma}$ [64].

$$D_{\xi,\gamma}(\text{dB}) = 10\log_{10}|p_T| \tag{4.23}$$

thus, on the Z-Y plane

$$D_{Z-Y}(\text{dB}) = 10\log_{10}\left|\frac{j\omega\rho u_T}{2\pi R} 4ab\text{sinc}(ka\cos\xi)\right| \tag{4.24}$$

thus, on the X-Y plane

$$D_{X-Y}(\text{dB}) = 10\log_{10}\left|\frac{j\omega\rho u_T}{2\pi R} 4ab\text{sinc}(b\cos\gamma)\right| \tag{4.25}$$

Figures 4.15 and 4.16 show the directivity intensity of the loudspeaker, Pioneer model PT-R4,using MATLAB computer simulation, for the rectangular plane with a= 25 mm. and b = 3 mm. In this condition, the frequency ω is 20 kHz - 50 kHz, the density of the air is 1.20 kg/m^3, the amplitude of vibration on the plane is 2 μm, and the wave number k is ω/v_0 with the speed of the sound propagation v_0 = 345 m/s. In Figures 4.15 and 4.16, this analysis can tell us how much radiation ability of the loudspeaker is sufficient for detecting the object. The loudspeaker, at the normal position, can detect the object, on Z - Y plane, at approximately 20^o and, on X - Y plane, at 180^o about +Y axis. Since we use a pulse compression sweeping the frequency 50 kHz down to 20 kHz, so that expanding the area of vertical detection, this system is designed to scan the object position by moving the loudspeaker position up and down along to Z axis. It is noted that sound beam at frequency 20 kHz is wider that at frequency 50 kHz but sound pressure at 50 kHz is more powerful. In Figure 4.17, sound directivity is illustrated as Figure 4.17. The sizes of rectangular plates are effective directly to generate the sound directivity.

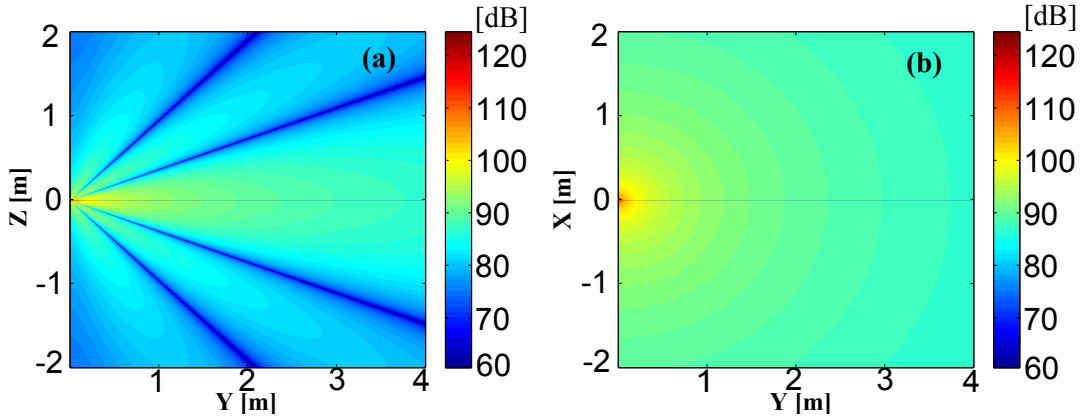

Figure 4.15 The directivity beam of loudspeaker (a) sound intensity on Z - Y plane (b) sound intensity on X - Y plane at 20 kHz.

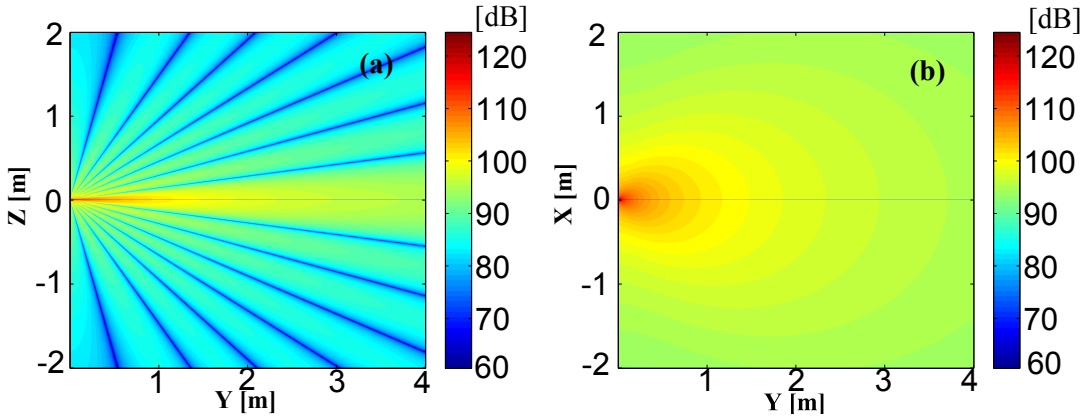

Figure 4.16 The directivity beam of loudspeaker (a) sound intensity on Z - Y plane (b) sound intensity on X - Y plane at 50 kHz.

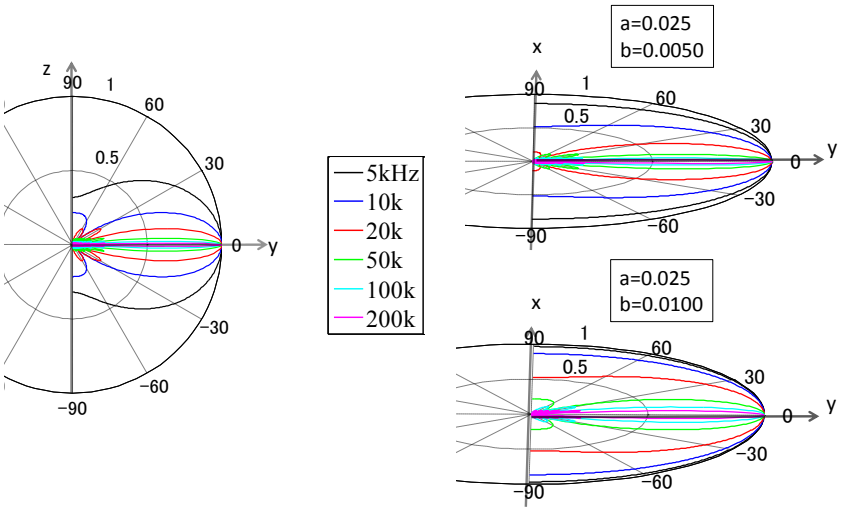

Figure 4.17 Directivity of radiation by a rectangular plate at various frequencies.

4.2.3 Sound radiation of PT-R4 loudspeaker from measurement

In previous chapter, we use MATLAB computer programming to analyze intensity of sound pressure. To realize the actual sound radiation, it is necessary to measure sound amplitude on ground at various positions. PT-R4 pioneer loudspeaker is brought to generate ultrasound propagation. LPM ultrasonic wave was produced by this loudspeaker, in which frequencies were swept from 50 kHz down to 20 kHz at a signal length 3.274 ms. A method of sound radiation estimation is that a ultrasound receiver was set on various positions in front of the loudspeaker, and ultrasound wave was then recorded by oscilloscope. An area used for sound detection was separated as a small area 5x5 cm^2. The total area is the width 60 cm, the high 60 cm, and the depth 100 cm. Sound radiation on X-Y plane from measurement is shown as Figure 4.18. Sound radiation on Z-Y plane from measurement is pictured as Figure 4.19. The experiment results can confirm that the sound beam on X-Y plane is approximately $\pm 50^o$ and that on Z-Y plane is $\pm 20^o$. These areas of both planes are the field of object-position detection in the sound radiation. In addition, we can improve ability of measurement, enabling the critical point, by moving the speaker's position.

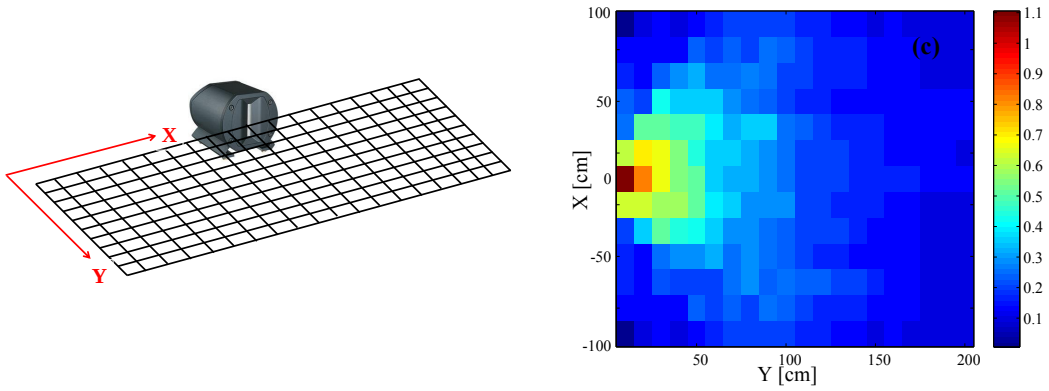

Figure 4.18 Sound radiation from measurement on X-Y plane.

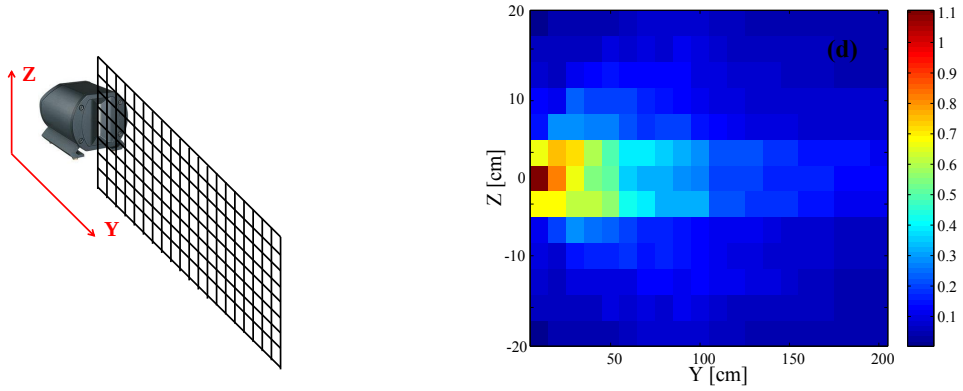

Figure 4.19 Sound radiation from measurement on Z-Y plane.

4.3 Ultrasonic receivers (microphone)

Acoustic receivers are electromagnetic transducers for transforming acoustic energy to electric energy. In general, a standard acoustic receiver for performing accuracy measurements has a very high price. It is important limitation of developing measurements that require using more sensors. This device is also weak to environment because it is designed for the controlled room in calibration. It must be taken care to avoid the damage. It is not convenient in setting up in the outdoor or robust applications. Therefore, an acoustic receiver, that has low cost, small size, reliability and quite strong to environment, is required. This topic is discussion for providing significant information of microphone selection. We need low-cost microphone and it can be performed for

three-dimensional ultrasonic position measurement. In previous works, B&K and ACO microphones were candidate; however, they are not appropriate when the number of microphone is required more. Thus, Knowles microphone can serve as an ultrasonic receiver for this task.

In this section, comparison between B&K microphone, ACO microphone, and Knowles microphone was presented in each other. A sound source used in experiment was PT-R4 Pioneer speaker. It was forced to transmit an LPM ultrasonic wave, swept from 50 kHz down to 20 kHz in a period time 3.27 ms. The microphone was located side by side with the speaker, and an object for measurement is a rectangular Aluminum flat plate, 17x25 cm^2. The object was in front of the speaker on a direct line with a few distances, 0.7, 1, and 1.4 m. Echoes were recorded on an oscilloscope after that TOF is obtained to compute the distance using Equation 4.26, where v_0 is the velocity of sound propagation d_0 is a distance between the speaker and the microphone. The amplitude of the input signal was expanded to 30 V_{p-p} and the distance between the speaker and the microphone was approximately 17 cm. A bubble-plastic insulator for direct ultrasonic-beam protection of the sound source was placed to absorb a transmitted ultrasonic wave. Temperature, humidity, and sound propagation under this environment were 25.3 degree, 27.9 % and 345 m/s, respectively.

$$d = \frac{\sqrt{(TOFv_0)^2 + d_0^2}}{2} \tag{4.26}$$

4.3.1 B&K microphone

B&K is the high standard for precision measurement microphone in the area of acoustics and vibration. In general, B&K microphone is an omnidirectional microphone used for calibration in control room monitors or studio room. Studio microphone design is not used only a logical evolutionary step but its improvement has been at a perfect time involving with the state-of-the-art of the recording technology with improved analogue techniques. Undoubtedly, B&K series omnidirectional microphones can serve many applications such as vocals, acoustic piano, percussion, string instruments, and drums [68]. They are accurate with an excellent dynamic range and colourless transient response. They can be said that they are the best choice of recording hardware. The reflected echoes at various distances recorded on the oscilloscope are shown as Figure 4.20. Next, these echoes from various distances were correlated with a reference signal by cross-correlation function for TOF computation. Cross-correlation function can be depicted in Figure 4.21. In Figure 4.21, the direct echo from the speaker is relatively

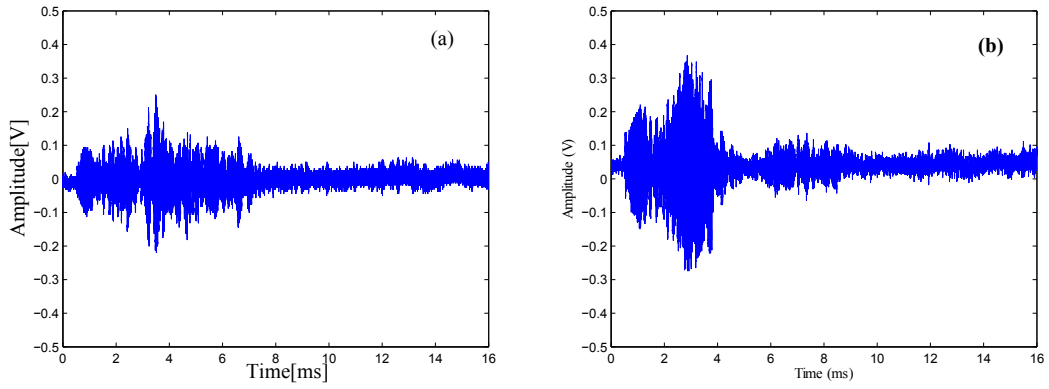

Figure 4.20 Echo measurements using B&K microphone at various distances (a) 0.7 m (b) 1 m.

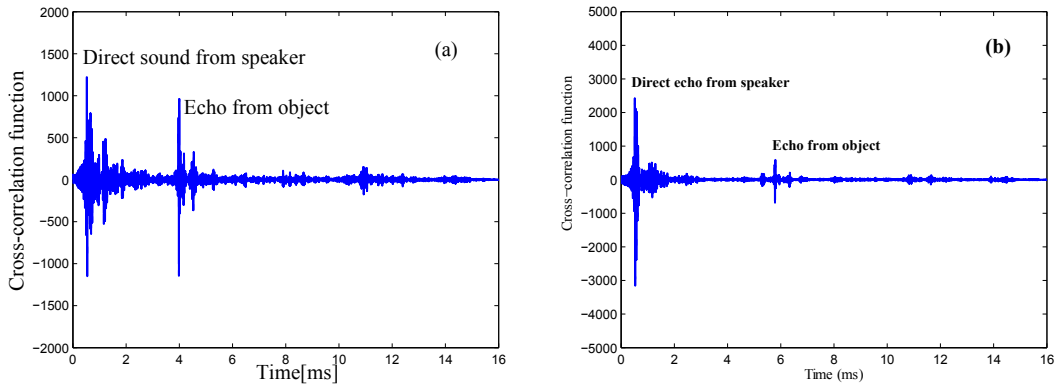

Figure 4.21 Cross-correlation function from B&K microphone at various distances (a) 0.7 m (b) 1 m.

small when compared with that from the object.

4.3.2 ACO microphone

ACO Co, Ltd was established as a sound measuring instrument manufacture and amassed an extensive performance record through its accumulation of research and development in cooperation with user companies, and research institutes at universities [69]. ACO microphone including preamplifier can measure with highly accurate resolution, enabling connection with several analyzers. ACO microphone is used for measurements of sound pressure with high resolution over wide frequency range. Wide

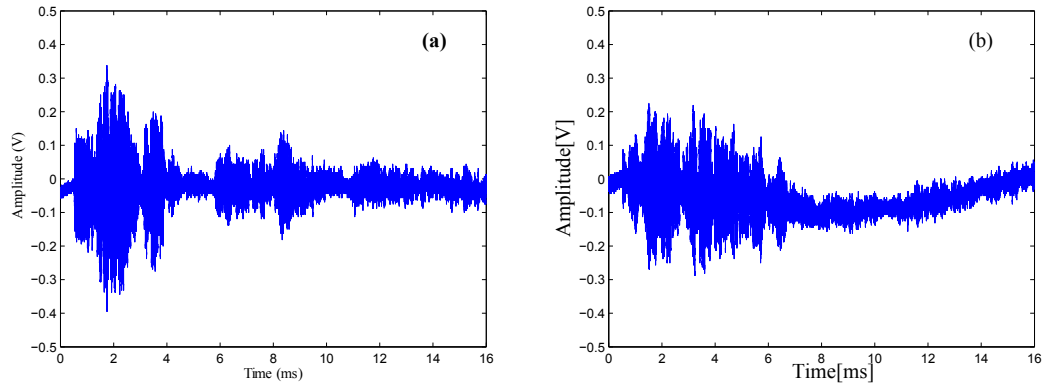

Figure 4.22 Echo measurements using ACO microphone at various distances (a) 1 m (b) 0.7 m.

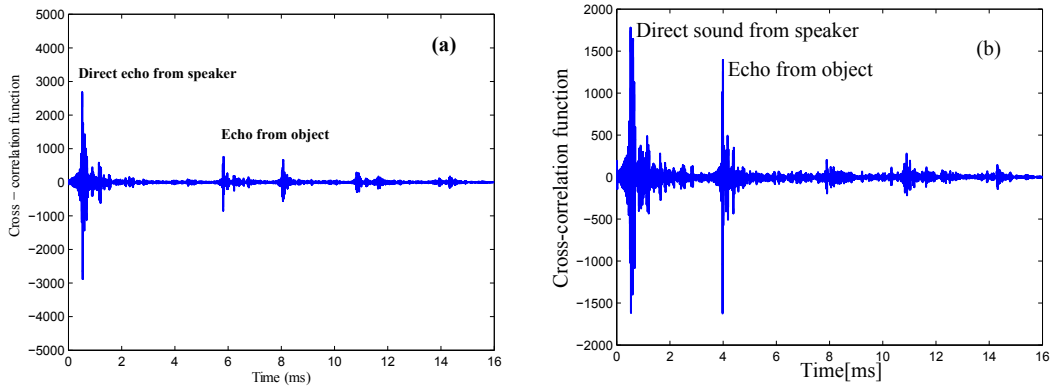

Figure 4.23 Cross-correlation function from ACO microphone at various distances (a) 1 m (b) 0.7 m.

range can measure from low-frequency to ultrasonic frequency (1 Hz 200 kHz), and measurement of high sound pressure level up to 170 dB is possible. The reflected echoes of ACO microphone at a few displacements recorded on the oscilloscope are shown as Figure 4.22. Echoes from various distances were correlated with a reference signal by cross-correlation function for TOF computation. Cross-correlation function can be depicted in Figure 4.23. In Figure 4.23, the direct echo from the speaker is relatively small when compared with that from the object.

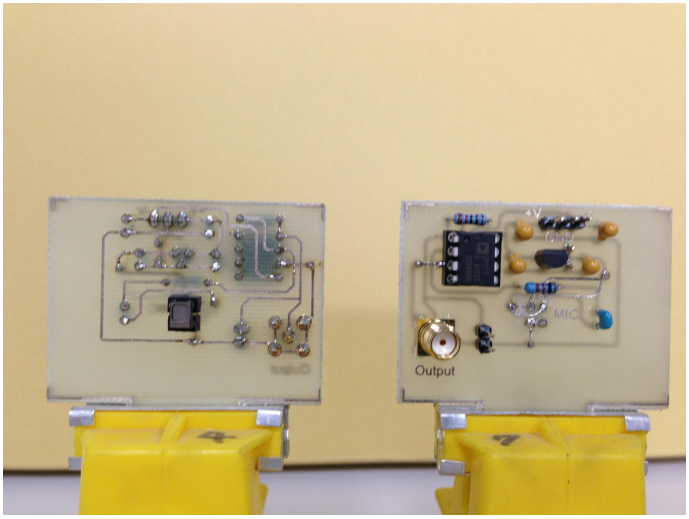

Figure 4.24 Proposed acoustical-receiver boards used to perform the echo measurement.

4.3.3 Knowles microphone

In previous microphones, they can be obtained to sense the echo for the TOF measurement using cross-correlation method. Although high sensitivity and resolution is given, they still have high price. The development of the system, enabling three-dimensional position measurement, requires more microphones. It is not possible to perform low-cost-application. The silicon MEMS microphones based on a device for hand-held telecommunication instruments developed by the Knowles company (model SPM024UD5) is fascinating. This model has sufficient sensitivity to detect sound pressure omnidirectionally [70]. Frequencies are allowed to pass through it from 10 to 100 kHz. A silicon microphone is embedded on a signal processing board containing a low pass frequency circuit with 60 kHz frequency cutoff and a preamplifier with 20 decibel (dB). Sensitivity achieves a minimum level of -47 dB at a humidity not over 70 R.H. The hand-held telecommunication device was embedded in a signal processing board, as shown in Figure 4.24. The reflected echoes of the proposed acoustical-receiver boards at a few displacements recorded on the oscilloscope are shown as Figure 4.25. Echoes from various distances were correlated with a reference signal by cross-correlation function for TOF computation. Cross-correlation function can be depicted in Figure 4.26. In Figure 4.26, the direct echo from the speaker is relatively small when compared with that from the object. In addition, in Figure 4.27, a frequency-distortion check of the

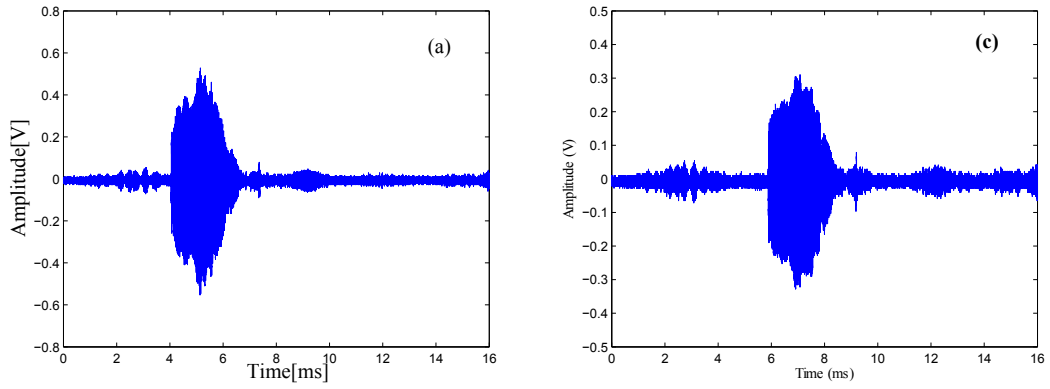

Figure 4.25 Echo measurements using ACO microphone at various distances (a) 0.7 m (c) 1 m.

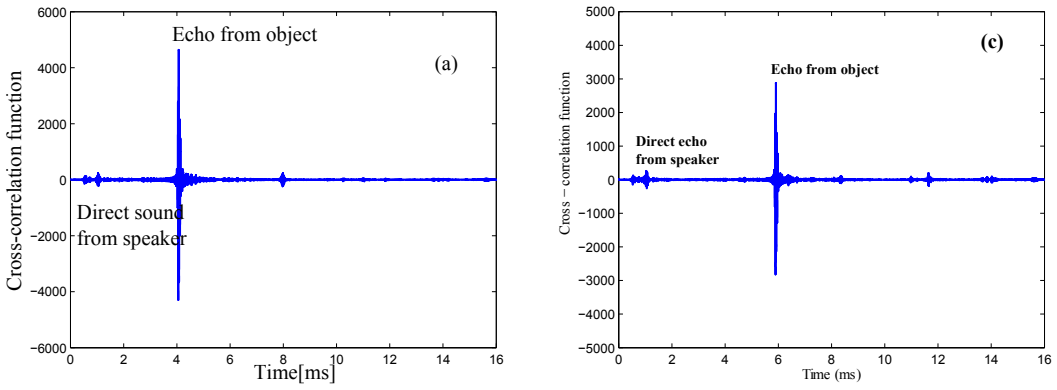

Figure 4.26 Cross-correlation function from proposed acoustical-receiver boards at various distances (a) 0.7 m (c) 1 m.

LPM signal at frequencies of 50 kHz to 20 kHz is shown. The results show that the transducer can agree with the original signal.

4.3.4 Distance measurement from each microphone

After the TOF was obtained using three types of microphones, the distance measurement was computed by plugging TOF in Equation 4.26. Next, repeatability of the distance measurements was 50 times of using cross-correlation function for TOF estimation. Repeatability of 0.7 meters distance measurement is depicted in Figure 4.28. Repeatability of 1 meters distance measurement is depicted in Figure 4.29.

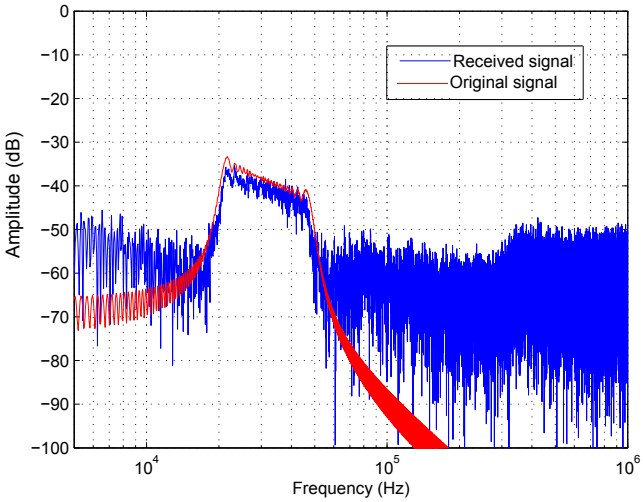

Figure 4.27 Frequency analysis of an LPM pulse compression signal from 50 kHz to 20 kHz measured by a Knowles Acoustic model silicon microphone embedded on the proposed board.

4.4 Reflection at a fluid-solid interface for echolocation

In general, echolocation for robots navigation is an issue involving with the study of sound propagation in medium and the reflection of target. The sound waves generated by the vibrating diaphragm of a loudspeaker can move through air, water and solids as longitudinal waves and also as transverse waves in solids. Amplitude of sound propagation is dependent on attenuation as a function of distance through the compressible medium, and attenuation in air is typically constant at 22.1 dB/m. Reflection is a change in direction of a wavefront at an interface between two different media to return from an origin that sound is generated. Consider a sound pressure wave in a fluid (air) incident on a plane fluid-solid boundary (air to object), as shown in Figure 4.30. To satisfy the interface boundary situations, this incident P-wave (compression wave) generates both transmitted P-wave and S-wave (shear wave), and this condition is called mode conversion. Next, we assume that the plane of incidence is considered as the x-y plane. Now, in our study (air to stainless steel interface), we consider the behavior of reflected and transmitted waves from the definition of Snells law. There are two critical angles present in the solid medium because speed wave in stainless steel (5790 m/s) is much more than that in air (345.1 m/s). The transmitted P and S - waves become an inhomogeneous wave. These waves do not affect to the reflected

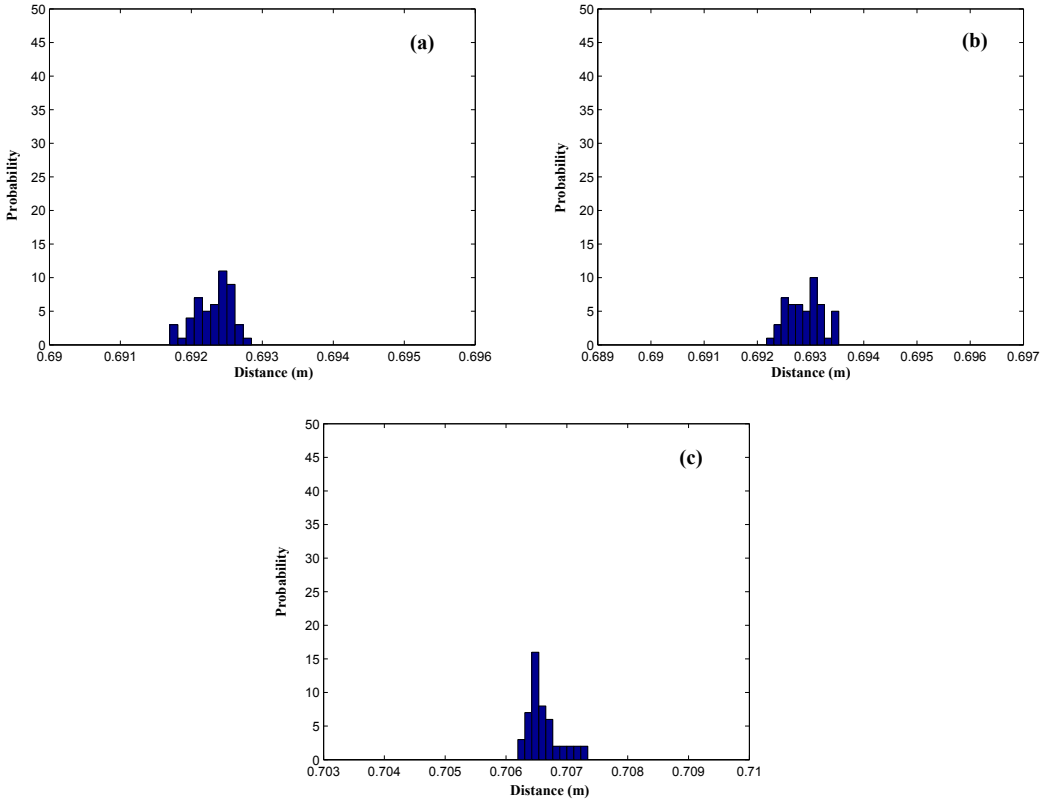

Figure 4.28 Probability function of 0.7 meters distance (a) ACO microphone (b) B&K microphone (c) Knowles microphone

echo sensed by microphones. ABAQUS, finite element analysis, was used to study the intensity of reflections from different surfaces when air and stainless steel densities of interface boundary were assumed as 7890 and 0.0012 kg/m3, respectively. The simulation results shown in Figure 4.31 summarize the intensity of reflections generated by rectangular, circular, and triangular objects. The sound source was located as a small color point opposite to the object position. Wavefront is observed that the reflection of the rectangular surface, as illustrated in Figure 4.31 (a), is the strongest intensity when relatively compared with other shapes. The reflection of the triangular surface in Figure 4.31 (c) has dispersion moving toward other directions compared with before incidence. It is difficult for navigation-based echolocation because the received echo at microphones is very low SNR. For the circular shape in Figure 4.31 (b), although some wavefront of the echo can be reflected to the same direction that a sound source generates but it is lower intensity than the rectangular shape. Therefore, the reflection

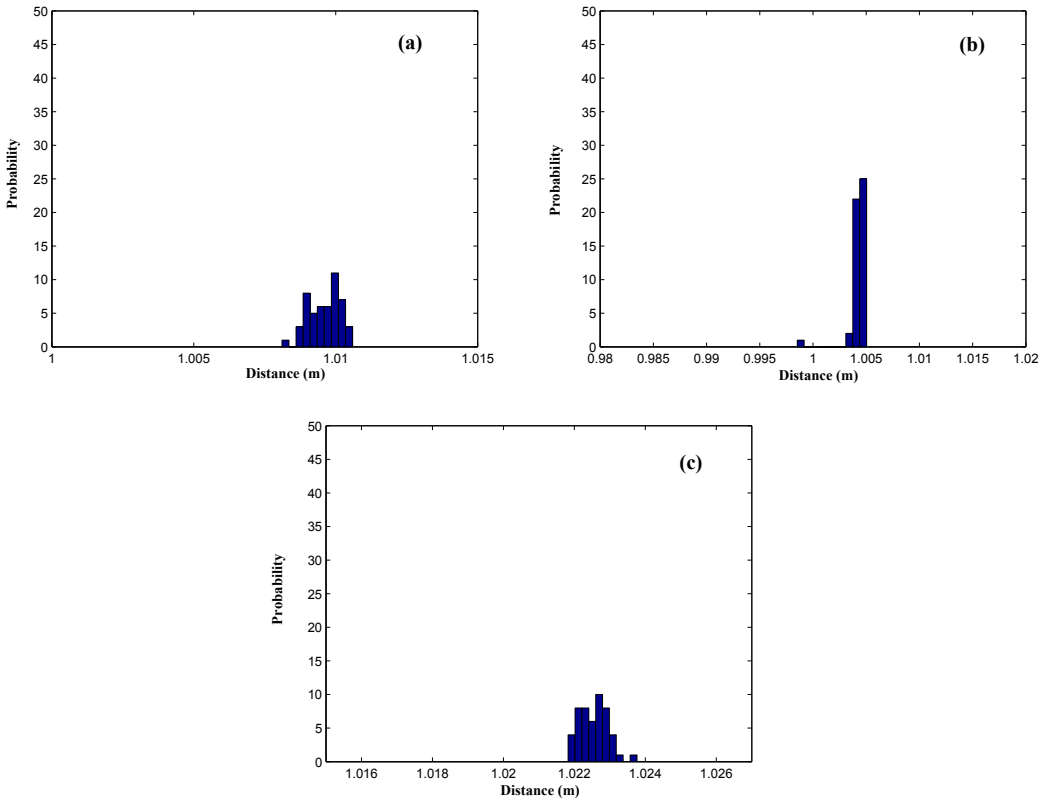

Figure 4.29 Probability function of 1 meters distance (a) ACO microphone (b) B&K microphone (c) Knowles microphone

of the spherical object as a target of the system-based echolocation is possible to be used for the study.

4.5 Summary

LPM ultrasonic wave, a period of which is linearly swept with time, was proposed for Doppler-effect compensation. This wave is directly generated by means of PT-R4 pioneer speaker from a sound source to a target. The loudspeaker of Pioneer model PT-R4 has a rectangular plane surface source. It can radiate ultrasonic wave from area X to +X and from area Z to +Z when the object appears in front of the loudspeaker in the +Y area. Moreover, a low-cost silicon MEMS microphone based on a development for hand-held telecommunication instruments is presented. It can extremely reduce the cost more than 100 times when relatively compared with the previous microphone of

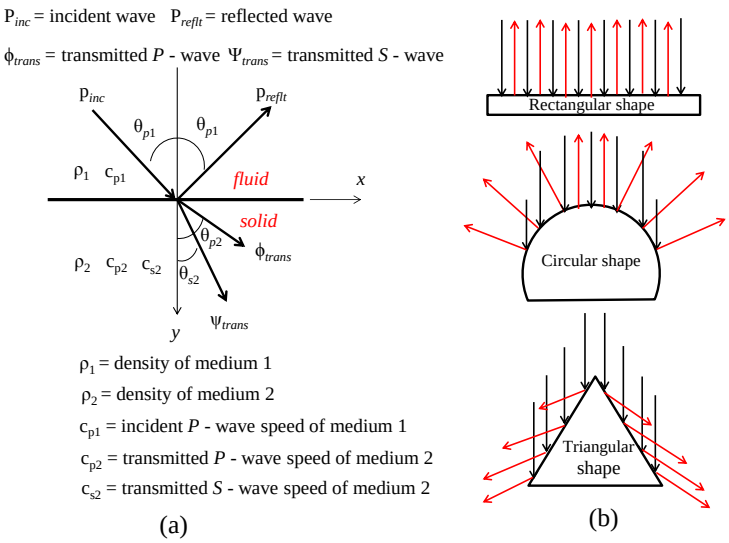

Figure 4.30 A plane wave traveling across a planar surface (a) reflection of a plane pressure wave incident on a fluid-solid interface. (b) reflection of different surfaces

B&K and ACO.

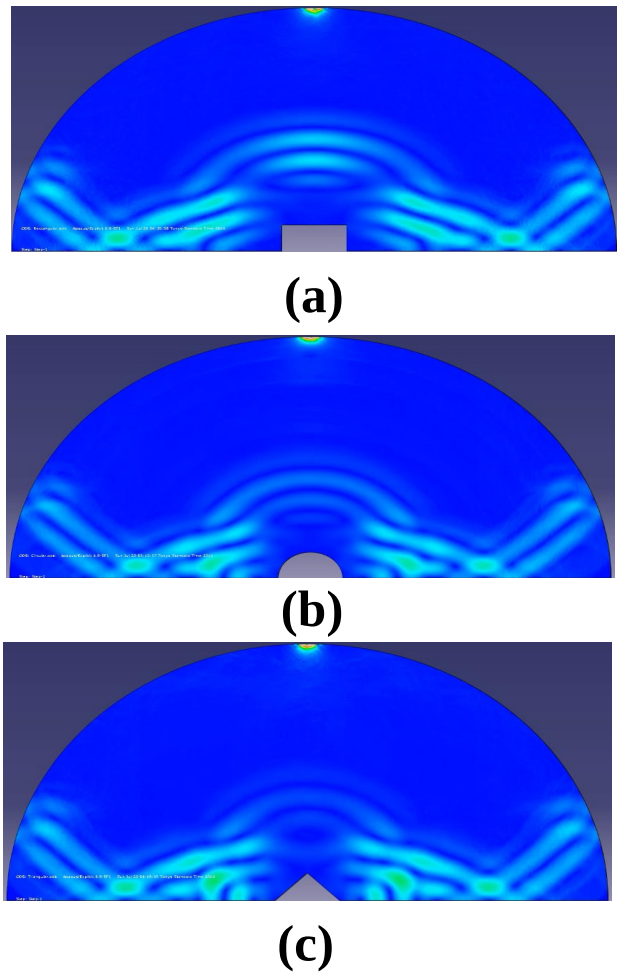

Figure 4.31 Comparison of reflected wavefront (a) rectangular shape (b) circular shape (c) triangular shape

5

Ultrasonic position and velocity measurement by an iterative method (First method)

5.1 Position measurement using an iterative method

In this chapter, a three dimensional airborne ultrasonic position system is presented using one sound source and the three ultrasonic receivers. A position is directly computed by TOF measurement. Space, in which the object appears, is assumed that an object is in X-Y-Z axes. Each axis is perpendicular in each other, and each microphone is set on these axes one by one whereas the speaker position is replaced on an original point. When we make relation between TOFs and distances from an original point into a target and return to microphone, a condition of relation can be seen in a nonlinear form. It is more difficult and complicated if we try to reform from nonlinear into linear. To satisfy this problem, a simple iterative method can achieve this gold. The previous research based on the iterative method, involving with position estimation, has been presented [71]. The well-known iterative method, relied on Taylor-series expansion, is Newton-Raphson estimation [72]. Newton-Raphson method uses only the first two terms of Taylor-series expansion. However, this solution is in situation of estimation, not an exact answer. It might have delay time for routines and not convergence; moreover, an initial value for starting is required. To protect a guess, a method for keeping the initial point is also defined.

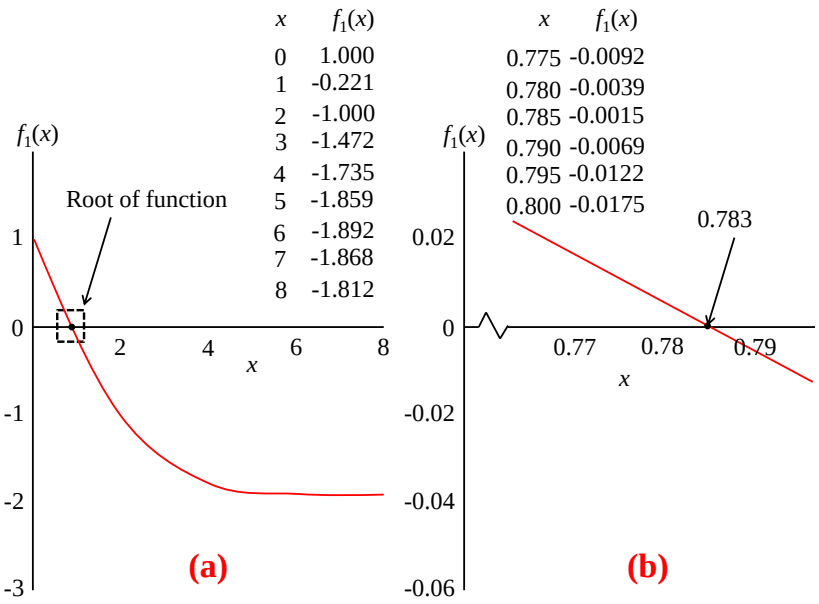

Figure 5.1 Plotting function $f_1(x)$of graphical method from various x values.

5.1.1 Iterative methods

Fundamental problems in science and engineering, often seen for analysis, are to solve roots of general equations. For example, assume that if there is a function $f(x)$, we then want to find out any value of x, enabling $f(x)$ equal to zero. It is not difficult task because we have ever seen it many times, especially in the primary school. In general, the function $f(x)$ is always in polynomial equations such as $f(x) = ax^2 + bx + c = 0$. Roots of such an equation are $x = \frac{-b \pm \sqrt{b^2-4ac}}{2a}$ when a, b, and c are the constant values. Indeed, functions $f(x)$ in science and engineering are not always in a simple polynomial form, for examples, a problem appearing in a transcendental function $f(x) = \cosh x \cos x + 1 = 0$. x value of this function is not easy to solve if we do not understand a correct procedure of solution. In this chapter, steps of correctly computing x value by means of 1) graphical method, 2) bisection method 3) false-position method, 4) one-point iterative method, and finally 5) Newton-Raphson method.

Solving an unknown value x, which is roots of equations $f(x)$, by graphical method is the simplest solution of iterative methods. The concept of graphical method is to study variations of the interested functions, and these functions are then plotted using a graph. Assume that we want to solve an engineering problem, having the function

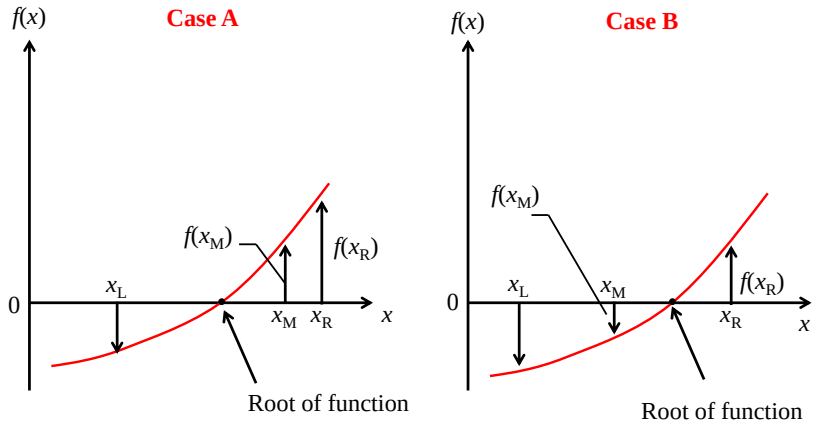

Figure 5.2 Bisection method for solving $f(x) = 0$.

$f_1(x) = \exp^{-x/4}(2 - x) - 1 = 0$. We can plot $f_1(x)$ as Figure 5.1. In Figure 5.1 (a), it is noted that $f_1(x)$ has a zero cross point at approximately $0.75 < x < 0.80$ and then we can plot $f_1(x)$ again from this range shown as Figure 5.1 (b). Considering Figure 5.1 (b), root of function $f_1(x)$ is obtained more accurate. It is roughly about 0.783. This result can be estimated by plotting and computation. Graphical method may be appropriate with a few problems, which do not require high accuracy of results, because it provides the simple solution. We can create a programing to deal with such a problem by a short source code. Although graphical method is quite easy, it takes long-time computation and lacks precision. Next, other iteration methods capable of achieving higher accuracy and simple are discussed.

Bisection method is different from graphical method in that function $f(x)$ always has opposite sign when any x values are more and less than a root of function $f(x)$ as shown in Figure 5.2. It is noticed that the answer is approximately $x = 0.783$; moreover, $f(x)$ is positive when $x < 0.783$ and $f(x)$ is negative when $x > 0.783$. In general, the variation characteristic of function $f(x)$ is in ether from a small value to a big value or from a big value to a small value. In Figure 5.2, this picture depicts variations of function $f(x)$ from a negative value of function $f(x)$ at $x = x_L$ to a positive value

of function $f(x)$ at $x = x_R$. Easily speaking, a root of function $f(x)$ is between x_L and x_R, and $f(x_L)$ and $f(x_R)$ are always opposite sign in each other. Computing a root of function $f(x)$ by bisection method is to compress a gap between x_L and x_R as narrowest as possible. In each step, we can assign the gap between x_L and x_R from their own function $f(x_L)$ and $f(x_R)$ when these functions have to always have opposite signs. Routines can be explained as:

*Step*1: Find x_M from x_L and x_R as follows

$$x_M = \frac{x_L + x_R}{2} \tag{5.1}$$

Function of x_M is computed. It is probably two cases that are case A (positive value) and case B (negative value) as shown in Figure 5.2.

*Step*2: Multiply between $f(x_M)$ and $f(x_R)$ if $f(x_M)f(x_R) > 0$ means $x_L <$ root $< x_M$. and $f(x_M)f(x_R) < 0$ means $x_M <$ root $< x_R$.

*Step*3: Adjust x_L or x_R again to be narrower range between these values. If a result from *step*2 is case A, set x_R equal to x_M; otherwise, if a result from *step*2 is case B, set x_L equal to x_M.

*Step*4: Check a convergence criterion as follows:

$$|f(x_M)| < \epsilon \tag{5.2}$$

ϵ is tolerance for stopping loop. If a result of Equation (5.2) is not satisfied, return to *step*1 again.

False-position method has the main concept similar to bisection method as said in the previous iterative method whereas false-position method can provide higher efficiency of convergence since functions of x_L and x_R are concerned with computation. It can be explained by Figure 5.3. The key idea of false-position method is that $f(x_L)$ and $f(x_R)$ at x_L and x_R, respectively, are connected together by a dashed line. It is called false-position method because the dash line cuts off X-axis at x_1, and this point has a deviation far away from a root of equations. Equations of false-position method can be realized as follows:

$$\begin{aligned} tan\beta &= tan\theta \\ \frac{f(x_R)}{x_R - x_1} &= \frac{f(x_L)}{x_L - x_1} \end{aligned} \tag{5.3}$$

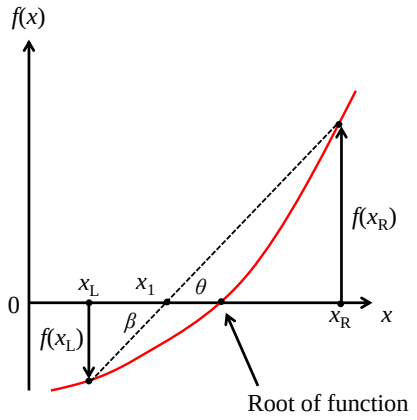

Figure 5.3 False-position method for finding out a root.

Therefore, x_1 can be computed by Equation (5.4).

$$x_1 = \frac{x_L f(x_R) - x_R f(x_L)}{f(x_R) - f(x_L)} \tag{5.4}$$

Steps of false-position method can conclude as

*Step*1: Find x_1 from x_L and x_R by Equation (5.4) x_1 is probably two cases that are $f(x_1) > 0$ and $f(x_1) < 0$.

*Step*2: Multiply between $f(x_1)$ and $f(x_R)$ if $f(x_1)f(x_R) < 0$ means $x1 <$ root $< x_R$. and $f(x_1)f(x_R) > 0$ means $x_L <$ root $< x_1$.

*Step*3: Adjust x_L or x_R again to be narrower range between these values.
If a result from step 2 is $f(x_1)f(x_R) < 0$, set x_L equal to x_1. If a result from step 2 is $f(x_1)f(x_R) > 0$, set x_R equal to x_1.

*Step*4: Check a convergence criterion as follows:

$$|f(x_1)| < \epsilon \tag{5.5}$$

ϵ is tolerance for stopping loop. If a result of Equation (5.5) is not satisfied, return to

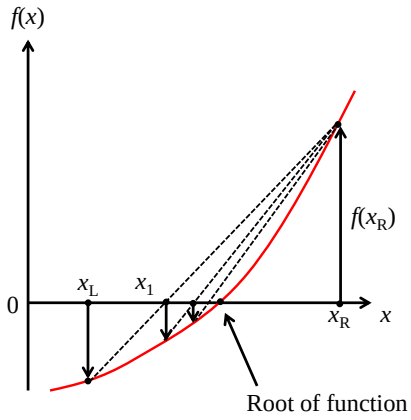

Figure 5.4 Convergence of finding out a root in false-position method.

step 1 again. When relatively compared with bisection method, false-position method can provide faster convergence because x_L and x_R are used directly. It can be explained by Figure 5.4. However, this method is necessary to require two initial points for starting routines. It is not convenient in practical problems in science and engineering. In the next method, the iterative methods requiring only an initial point is studied. We can call them open method since we do not worry about assigning a left value and a right value. A well-known method with only an initial guessed point for dealing with engineering problems[74-75] is Newton-Raphson method.

Newton-Raphson method is an open method using only one initial point to quickly achieve a final result. This property makes Newton-Raphson famous for a large-size analysis. Newton-Raphson method is an iterative method based on Taylor-series expansion; therefore, we should understand what Taylor series are before studying Newton-Raphson method. Taylor series, which is one type of series, is utilized to define a function at any x parameter from both the function at an initial point x_0 and derivatives of the function at various orders. Although Taylor series consists of infinite terms,

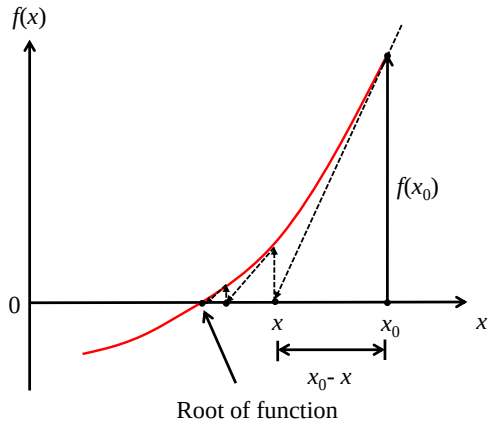

Figure 5.5 Convergence using Newton-Raphson method.

it can be realized simply by using only one term.

$$f(x) \cong f(x_0) \tag{5.6}$$

We can call it zero-order approximation. The function at x and x_0 will be equivalent if this function is only constant whereas considering other functions is not constant, they will correct approximately if x and x_0 get closer. We can use the first two terms of Taylor series for function estimation.

$$f(x) \cong f(x_0) + (x - x_0)\frac{df(x_0)}{dx} \tag{5.7}$$

We call Equation (5.7) the first-order approximation. Similarly, the quadratic function of Taylor series containing the first three terms is:

$$f(x) \cong f(x_0) + (x - x_0)\frac{df(x_0)}{dx} + \frac{(x - x_0)^2}{2!}\frac{d^2 f(x_0)}{dx^2}. \tag{5.8}$$

Therefore, in general functions, which are complicated and not expressed in polynomials, we can replace Taylor series with infinite terms instead of these functions.

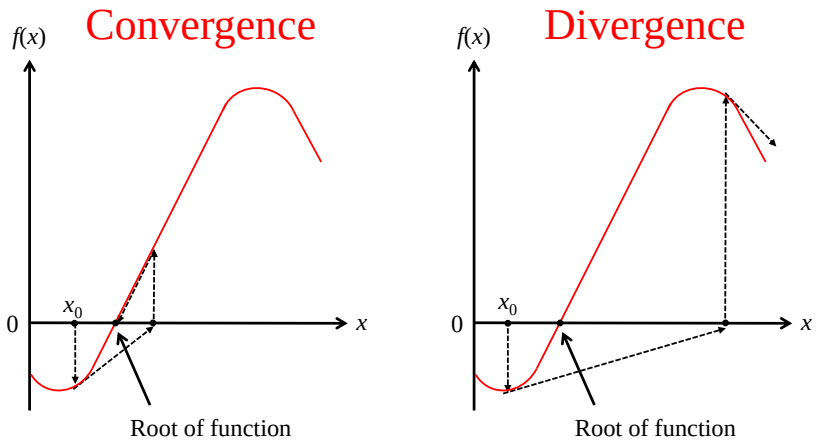

Figure 5.6 Convergence and divergence of Newton-Raphson method.

$$f(x) \cong f(x_0) + (x - x_0)\frac{df(x_0)}{dx} + \frac{(x - x_0)^2}{2!}\frac{d^2 f(x_0)}{dx^2} + \frac{(x - x_0)^n}{n!}\frac{d^n f(x_0)}{dx^n}. \tag{5.9}$$

Basic conception in Taylor series used in Newton-Raphson method for solving $f(x) = 0$ with the first two terms as Equation (5.7) can be expressed as

$$\begin{aligned} f(x) &= f(x_0) + (x - x_0)\frac{df(x_0)}{dx} = 0 \\ x - x_0 &= -\frac{f(x_0)}{\frac{df(x_0)}{dx}} \end{aligned} \tag{5.10}$$

The first step of Newton-Raphson method is the initial- point designation (x_0) as shown in Figure 5.5. Next, $f(x)$ and $df(x)/dx$, which are computed and plugged in Equation (5.10), result in a new position getting close up a root of the function $f(x)$. After that iteration for a new x will make x convergence into the root. Nevertheless, convergence of results might not be guaranteed because of the function characteristic and setting up an initial value x_0 as well. Convergence and divergence of functions can be pictured

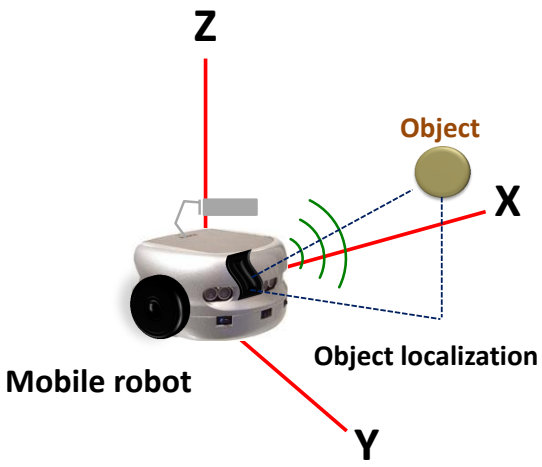

Figure 5.7 Mobile robot for searching out an object.

in Figure 5.6. We can simply conclude steps of Newton-Raphson method as follows:

*Step*1 : Compute function and derivative of an old value to a new value.

$$\Delta x_{k+1} = -\frac{f(x_k)}{\frac{df(x_k)}{dx}} \tag{5.11}$$

where k and $k+1$ are iteration.

*Step*2: Update a new x from.

$$x_{k+1} = x_k + \Delta x_{k+1} \tag{5.12}$$

*Step*3: Check a convergence criterion as follows:

$$|\Delta x_{k+1}| < \epsilon \tag{5.13}$$

ϵ is tolerance for stopping loop. If a result of Equation (5.11) is not satisfied, return to step 1 again.

5.1.2 Three-dimensional-positioning using an iterative method

The self-localization of a mobile robot capable of searching out an obstacle over its own position is realized as shown in Figure 5.7. The mobile robot can identify the object position in X-Y-Z coordinates. The ultrasonic three-dimensional system proposed in this navigation of this mobile robot is shown in Figure 5.8. The devices displayed under the designed system mainly consist of an ultrasonic speaker and three microphones. A transmitted signal exciting to the speaker uses a pair of two LPM signals. An echo signal from the object is incident on microphones and converted to a digital signal by three 7^{th} order delta-sigma modulators. On other hand, a reference signal utilizes a digital comparator as a signal converter. Next, both digital signals from these devices are performed together to compute TOF by means of the cross-correlation function. One-bit signal processing plays a vital role in saving computational-time cost. In the case of non-Doppler effect, TOF of a received LPM signal is typically estimated from the maximum peak time in the cross-correlation function. Based on Euclidean geometry, as Fig. 5.8, equations made up of referring to the relationship between the object, speaker, and microphone locations, and TOF are

$$f_1 = \sqrt{(x - x_1)^2 + y^2 + z^2} + \sqrt{x^2 + y^2 + z^2} - v_0 \cdot TOF_x = 0 \tag{5.14}$$

$$f_2 = \sqrt{x^2 + (y - y_2)^2 + z^2} + \sqrt{x^2 + y^2 + z^2} - v_0 \cdot TOF_y = 0 \tag{5.15}$$

$$f_3 = \sqrt{x^2 + y^2 + (z - z_3)^2} + \sqrt{x^2 + y^2 + z^2} - v_0 \cdot TOF_z = 0 \tag{5.16}$$

where x, y, and z describe the unknown position of the object. We consider a three-dimensional scenario where the acoustic sensor are on X, Y, and Z axes: (x_1, 0, 0), (0, y_1, 0), and (0, 0, z_1), respectively. The position of the sound source is set as the origin (0, 0, 0). TOF_x, TOF_y, and TOF_z are time-of-flight in each microphone, and c is the sound velocity in air. Equation (5.14) expresses the time duration and the distance from the sound source to the object and returns to the microphone on X-axis. Equation (5.15) expresses the time duration and the distance from the sound source to the object and returns to the microphone on Y-axis. Finally, Equation (5.16) expresses the time duration and the distance from the sound source to the object and returns to the microphone on Z-axis. This can be considered as a complicated problem of non-linear systems because square and square root operations are overlapped mathematically. We can simply explain Equations (5.14)-(5.16) by a parabolic graph as shown in Figure 5.9. To satisfy this problem, Newton-Raphson method plays an important role in

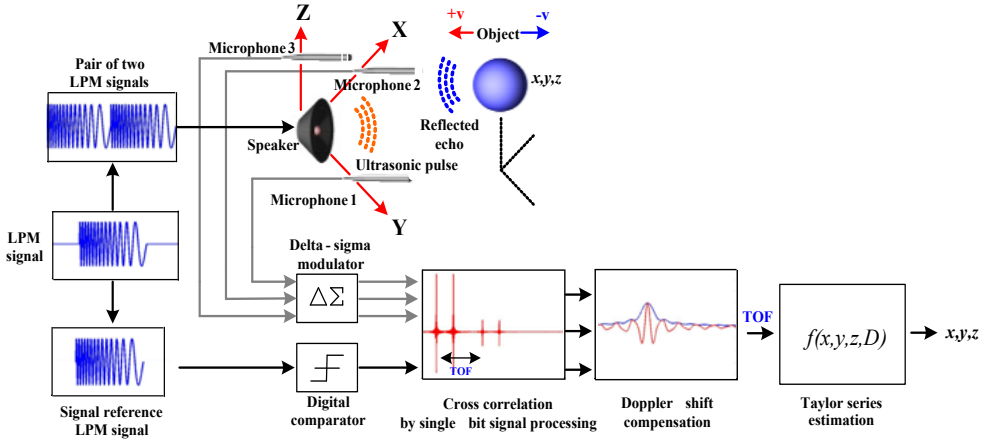

Figure 5.8 Proposed ultrasonic three-dimensional system inside the mobile robot s navigation.

the identification of the object position. The formula for three unknown parameters established is

$$\nabla \mathbf{F} \cdot \delta = -f \tag{5.17}$$

where

$$\nabla \mathbf{F} = \begin{bmatrix} \frac{\partial f_1}{\partial x} & \frac{\partial f_1}{\partial y} & \frac{\partial f_1}{\partial z} \\ \frac{\partial f_2}{\partial x} & \frac{\partial f_2}{\partial y} & \frac{\partial f_2}{\partial z} \\ \frac{\partial f_3}{\partial x} & \frac{\partial f_3}{\partial y} & \frac{\partial f_3}{\partial z} \end{bmatrix}, \delta = \begin{pmatrix} x - x_0 \\ y - y_0 \\ z - z_0 \end{pmatrix}, f = \begin{pmatrix} f_1 \\ f_2 \\ f_3 \end{pmatrix}$$

where x_0, y_0, and z_0 are initial values, and δ is update data. However, this iterative method has significant disadvantage, that is, the requirement of an initial guess [71, 76]. When carefully scrutinizing all TOFs measured from microphones, we enable them to be used as a starting point of routines. To do so, an initial distance (D_0) is averaged by the duration time, for progressing only one way from the speaker to the object, and thereafter with sound velocity.

$$D_0 = \frac{v_0 \cdot (TOF_x + TOF_y + TOF_z)}{2 \times 3} \tag{5.18}$$

Assume that x_0, y_0, and z_0 have the same values. We know that the distance D_0, which is connected to a co-ordinate x, y, and z, is

$$D_0 = \sqrt{x_0^2 + y_0^2 + z_0^2} \tag{5.19}$$

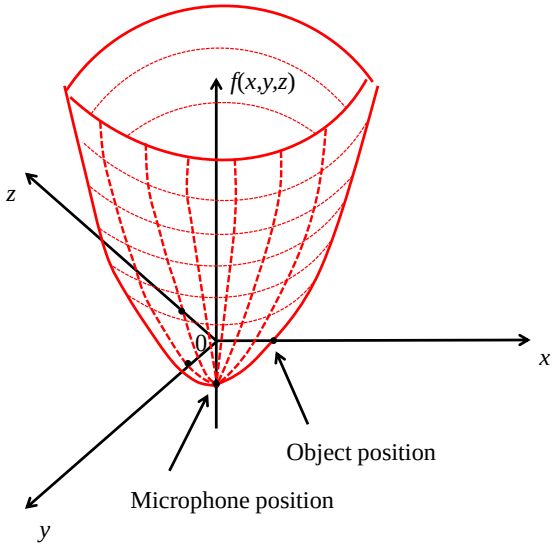

Figure 5.9 Parabolic graph due to Equations (5.14)-(5.16).

The initial object position can be determined easily, as below. Therefore, the obtained initial values are dependent on the TOF of the object.

$$x_0 = y_0 = z_0 = \frac{D_0}{\sqrt{3}} \tag{5.20}$$

In every time instance in which the update data are computed data are added with the old values for the new values.

$$\delta^k = -\left[\nabla \mathbf{F}^k\right]^{-1} \cdot f^k \tag{5.21}$$

After that, update and check the convergence criterion; stop when the difference is less than the tolerance, ε.

Newton-Raphson algorithm for unknown-parameters estimation, $\boldsymbol{u} = [x, y, z]^T$, can be summarized in the following steps:

*Step*1: Make an initial guess for the parameter vector $\boldsymbol{u}^0$ and $k = 0$ from Equation (5.20) (an upper case is iterative number).

*Step*2: Model $\boldsymbol{F} = [f_1, f_2, f_3]^T$. A quadratic approximation $\boldsymbol{F}$ can be obtained using the given twice continuously differentiable object function. The Taylor series expansion plays a vital role of $\boldsymbol{F}$ approximation about the current point $\boldsymbol{u}^k$, neglecting terms of order three and higher. We obtain $f_i(x^0 + \Delta x, y^0 + \Delta y, z^0 + \Delta z) \approxeq f_i(x^0, y^0, z^0) + \frac{\partial f_i}{\partial x}(x^1 - x^0) + \frac{\partial f_i}{\partial y}(y^1 - y^0) + \frac{\partial f_i}{\partial z}(z^1 - z^0)$, i =1, 2, and 3. Thus, a root of f_i can be estimated by using the iteration of $\boldsymbol{u}^k = [x^k, y^k, z^k]^T$.

*Step*3: Iterate the parameter vector $\boldsymbol{u}^{k+1} = \boldsymbol{u}^k + \delta^k$ by the update data from Equation (5.21).

*Step*4: Check convergence criterion $\| \boldsymbol{u}^{k+1} - \boldsymbol{u}^k \| < \varepsilon$, then stop.

*Step*5: Set $k \rightarrow k + 1$ and go to step 2.

5.1.3 Simulation results for three-dimensional-positioning using an iterative method

Simulation results are performed to confirm the proposed three-dimensional-positioning method. First, we will show that how it works by assuming that an object position is x=80 cm, y=65 cm, and z = 25 cm and the microphone positions are (10 cm, 0 cm, 0 cm), (0 cm, 10 cm, 0 cm), and (0 cm, 0 cm, 10 cm). The object position estimation under an ultrasonic three-dimensional system determined by the proposed one-bit signal processing method was evaluated by MATLAB computer simulation. The period of the single LPM signal was swept linearly from 20 μs to 50 μs. The sampling frequency rate was 12.5 MHz. The LPM signal had the length equal to 3.278 ms. The propagation velocity of an ultrasonic wave in air was 345.1 m/s at 22.4 C^o. SNR was set at 10 dB compared with the echo signal The constant attenuation factor of the received signal was -2.107 dB/m degraded from that of the original signal. Table 5.1 shows steps of update data from an origin to a final point when tolerance was 0.5 mm. The received signals and the normalized cross-correlation functions obtained by one-bit signal processing are illustrated in Figure 5.10. The received signals were changed into the single-bit delta-sigma modulated signal by the 7^{th}-order delta-sigma modulator. The one-bit signal of the received echo was correlated together with the one-bit signal of the reference, which was the transmitted LPM signal converted into

Iterations	x position (cm)	y position (cm)	z position (cm)
Initial valuea	59.801	59.801	59.801
First time	84.037	69.257	30.822
Second time	80.152	65.079	24.777
Third time	80.010	65.023	24.911
Fourth time	80.010	65.023	24.990
Fifth time	80.010	65.023	24.990

Table 5.1 Iteration for three dimensional position measurement.

the one-bit digital signal by a digital comparator. The cross-correlation function of the one-bit received signal and the one-bit reference signal was obtained directly from the recursive cross-correlation operation of one-bit signal processing and the smoothing operation accomplished by the triangular weighted moving average filter. Signal had 399 zero-cross points. Accordingly, the computational cost of the recursive cross-correlation operation was the integration and 401 summations of one-bit samples. For the smoothing operation, the length of the triangular weighted moving average filter, which consists of a pair of 55-tap moving average filters, was 109 taps. The position error by the noise included in the received echoes was evaluated by MATLAB computer simulation. In the simulation, the SNR of the reflected echo was converted by including normal distribution of random noises, or white noise, to the received echoes. In the case of each SNR, the position of the estimation was evaluated from 100 simulations. To confirm this situation, the probability distributions of the estimated position are determined from 100 estimation and illustrated in Figure 5.11.

5.2 Velocity measurement using vector projection

In this case, the velocity can be estimated from the signal length of the echo, which is reflected from the target. The signal length difference is in proportional to the velocity of the object as previously said in Chapter 3. We use this idea for the basis of three dimensional velocity vector measurement.

5.2.1 Three dimensional velocity vector measurement

The velocities measured by pulse compression of the two-cycle LPM signals are the vector component, in Figure 5.12, of the ultrasonic propagation direction. Next, the moving-object velocity is estimated using data of the relative velocities at each micro-

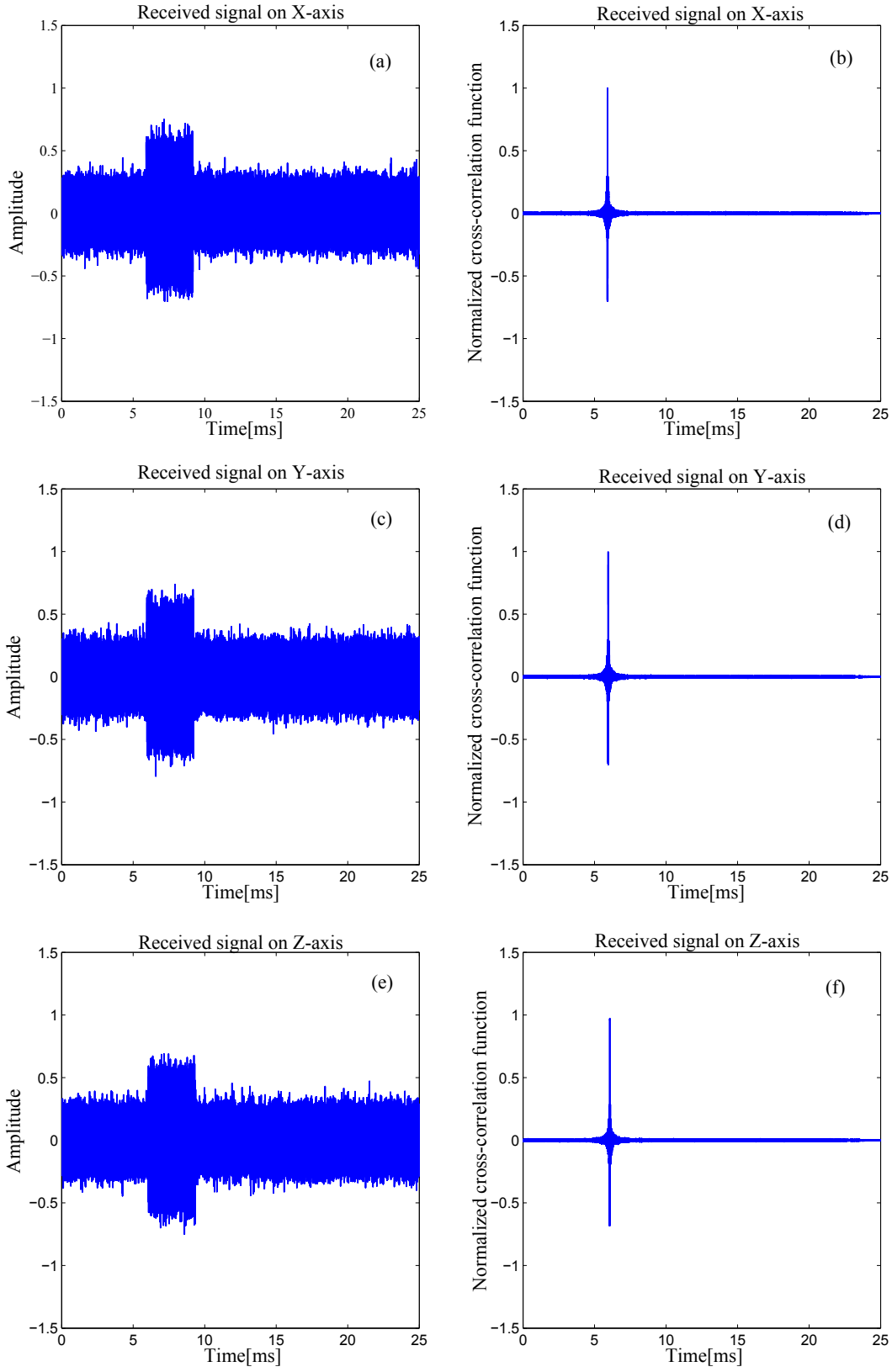

Figure 5.10 The received signals and the cross-correlation functions obtained by single-bit signal processing in the simulations at the position x = 80 cm, y = 65, and z = 25 cm.

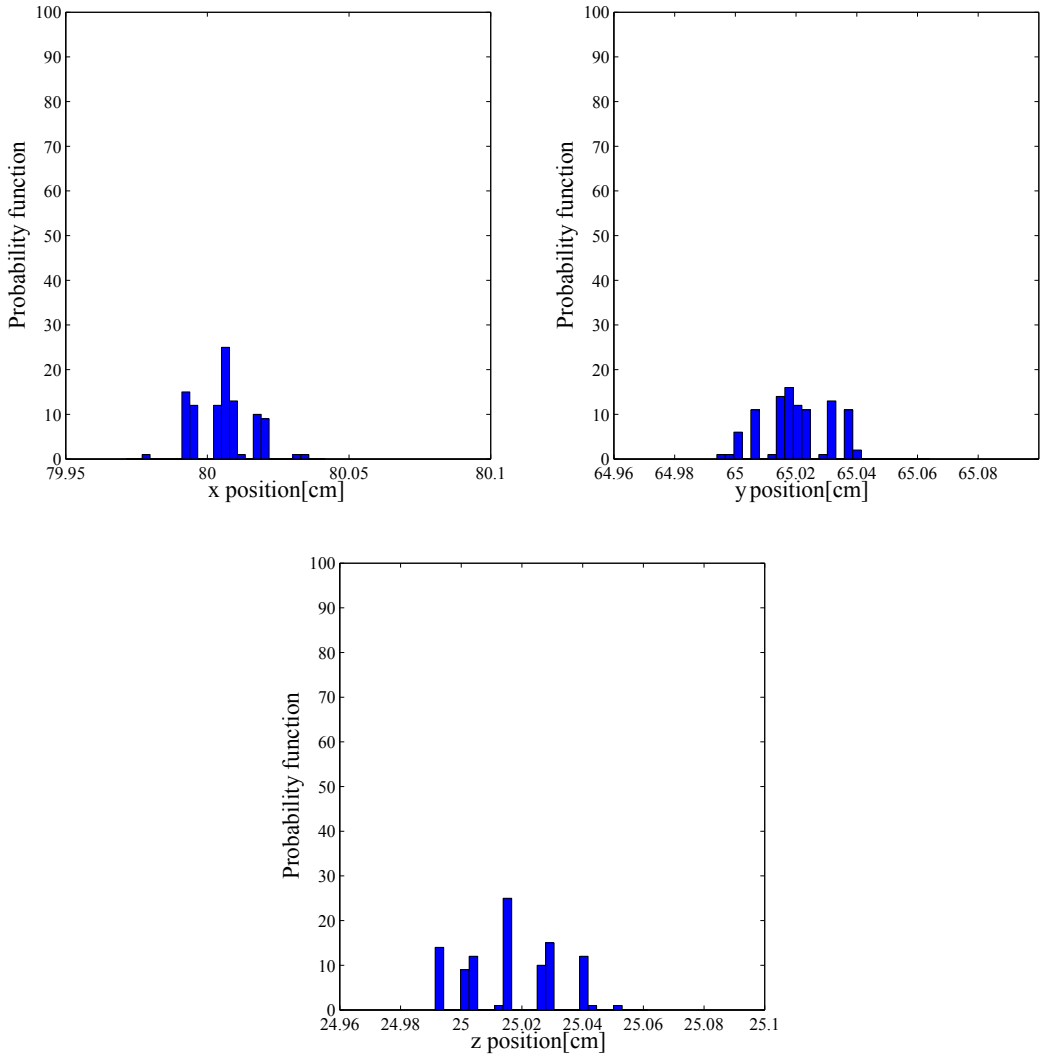

Figure 5.11 The probability distributions of the estimated distance in the simulations at the position x = 80 cm, y = 65 cm, and z = 25 cm.

-phone, that is,v_{dx} on x-axis, v_{dy} on y-axis, and v_{dz} on z-axis, the instantaneous position of the moving object, computed in 5.1.2., and microphone positions. On the basis of the simple fundamentals of the vector theory, vector projection can be considered as the dot product between two vectors as shown as Figure 5.12. Hence, the results of vector projection between the Doppler-shifted velocity estimation at each microphone,

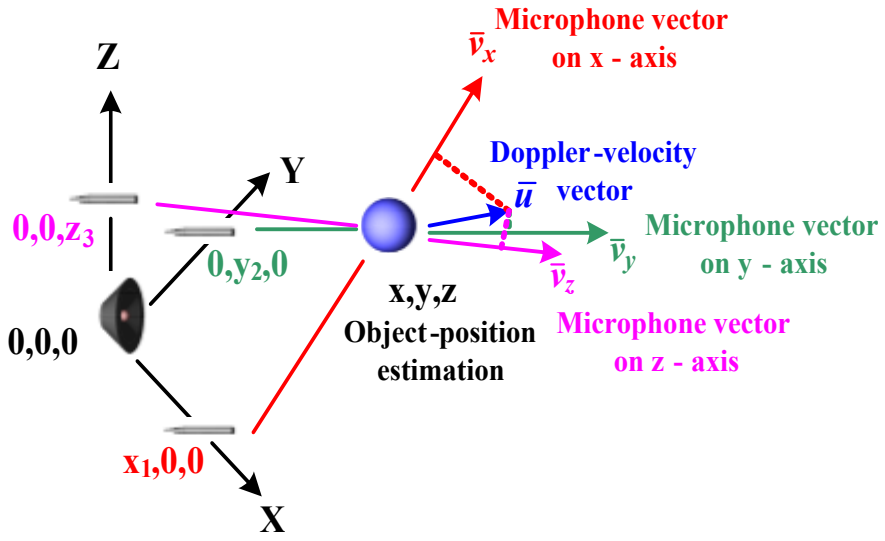

Figure 5.12 Object-velocity vector configuration

depicted as

$$\begin{pmatrix} v_{dx} \\ v_{dy} \\ v_{dz} \end{pmatrix} = \boldsymbol{u} \cdot \begin{pmatrix} \frac{\boldsymbol{v}_x}{|\boldsymbol{v}_x|} \\ \frac{\boldsymbol{v}_y}{|\boldsymbol{v}_y|} \\ \frac{\boldsymbol{v}_z}{|\boldsymbol{v}_z|} \end{pmatrix} \tag{5.22}$$

$\boldsymbol{u}$ is the unknown object-velocity vector. $\boldsymbol{v}_x$,$\boldsymbol{v}_y$, and $\boldsymbol{v}_z$ are the microphone vectors, where

$$\boldsymbol{u} = \begin{pmatrix} u_x \\ u_y \\ u_z \end{pmatrix}; \boldsymbol{v}_x = \begin{pmatrix} x - x_1 \\ y \\ z \end{pmatrix}; \boldsymbol{v}_y = \begin{pmatrix} x \\ y - y_2 \\ z \end{pmatrix};$$

and

$$\boldsymbol{v}_z = \begin{pmatrix} x \\ y \\ z - z_3 \end{pmatrix} \tag{5.23}$$

Substitute Equation (5.23) into Equation (5.22) and rearrange again.

$$\begin{pmatrix} u_x \\ u_y \\ u_z \end{pmatrix} = \begin{bmatrix} x - x_1 & y & z \\ x & y - y_2 & z \\ x & y & z - z_3 \end{bmatrix}^{-1} \cdot \begin{pmatrix} v_{dx} \cdot |\vec{v}_x| \\ v_{dy} \cdot |\vec{v}_y| \\ v_{dz} \cdot |\vec{v}_z| \end{pmatrix} \tag{5.24}$$

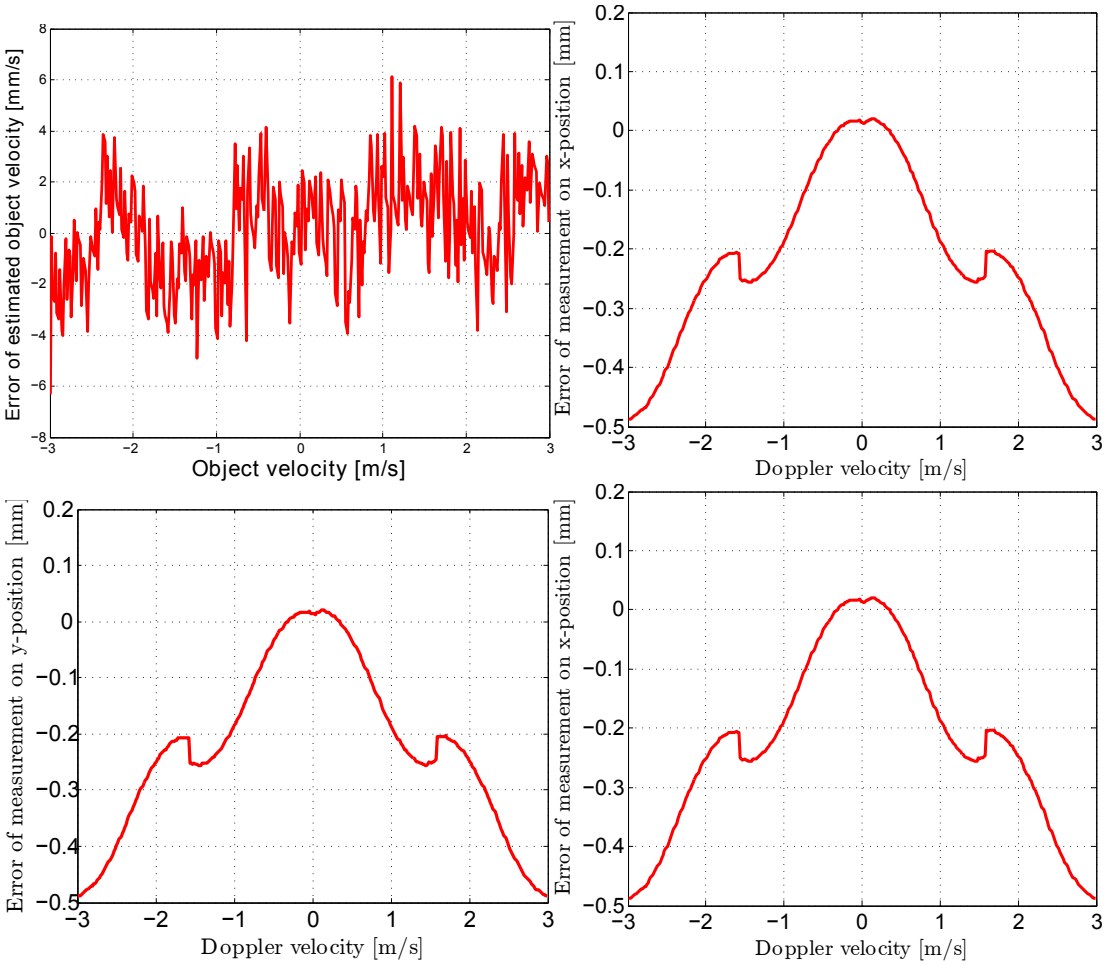

Figure 5.13 Errors of object position and velocity measurements at an instantaneous position x=y=z=1 m.

By plugging a solution of Equation (5.23) back into Equation (5.24), the object-velocity vector $\boldsymbol{u}$ can easily be determined. In addition, the magnitude of the object-velocity can be defined as

$$|\boldsymbol{u}| = \sqrt{{u_x}^2 + {u_y}^2 + {u_y}^2} \tag{5.25}$$

This equation can estimate the object-velocity of the moving object in three dimensional velocity vector measurement by means of the simple fundamental of projection.

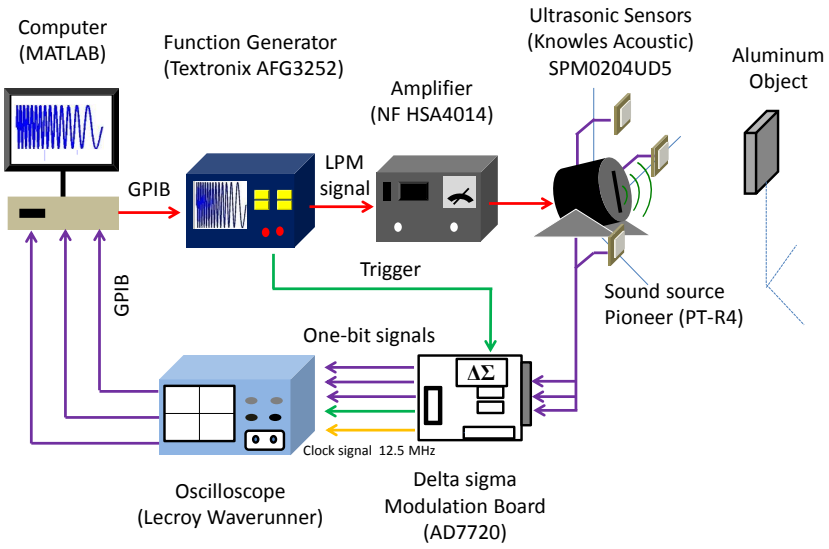

Figure 5.14 Experimental setup of the proposed three dimensional positioning method using Newton-Raphson algorithm.

5.2.2 Simulation results for three dimensional velocity vector measurement

The Doppler velocity and object position from the earlier measurements were used to determine the object velocity on the basis of vector theory. To confirm our idea, the moving object position and velocity were evaluated by MATLAB computer simulation. In simulation, the velocity of the moving object was varied from -3 m/s to 3 m/s. For each velocity, the position of the moving object was evaluated by 100 simulations. The probability distributions of the estimated object position, under the assumption that there constantly was an instantaneous position, were set up at $x = y = z = 1$ m. The moving-object-position errors varying with the object velocity are displayed in the top and bottom onto left side of Figure.5.13. The graphs are not smooth at about 1.5 m/s because the waveform of the cross-correlation function, based on Doppler shift, is inverted at those points. The errors due to Doppler-shift compensation are sharper in such case. In the bottom right of Figure.5.13, it shows the deviation of object-velocity estimation when the object was continuously moving at a the velocity from -3 to 3 m/s.

5.3 Optimal microphone position of the iterative method

Three microphone positions located on x-y-z axes plays a vital role for the determination of nonlinear functions because the distance from the loudspeaker is obtained for equation creation. Each microphone position is directly proportional to the convergence of Newton-Raphson method to achieve the target. In this section, adjusting the microphone position is studied for the lowest error of object measurement at the optimal microphone position. The microphone position was varied from 0.005 to 0.5 cm in one axis, and at other axes the microphone position was fixed. It is observed in Figure 15 that the microphones on all axes is concurrently varying from 0.005 to 0.5 cm. The errors about 0.2 mm oscillates up and down in the first time during 0 - 10 cm of a distance from the speaker and after that they are going to a constant level at approximately 0.05 mm. We can conclude from this observation that the optimal microphone position corresponding the proposed mathematical model of Newton-Raphson-based method is at coordinates more than (10, 0, 0), (0, 10, 0), and (0, 0, 10) cm.

5.4 Experimental results

The experimental setup of the three-dimensional ultrasonic positioning system proposed in this chapter is depicted in Figure 5.14. A transmitted signal was used as an LPM signal. The frequency of this signal was swept from 50 kHz to 20 kHz. The length of the transmitted LPM signal was 3.274 ms. The LPM signal was generated by a function generator and enlarged 20 times by a power amplifier. The sound source was adjusted by raising the elevation angle 5 degree. A hand held telecommunication device was embedded in a signal processing board. An echo was measured by the acoustical receivers. In addition, the acoustic receivers had frequency responses over the range 10-100 kHz. The pre-amplifier and the low pass filter were 20 dB and a frequency cut off of 100 kHz, respectively. Then, the response was converted to a one-bit signal using a 7^{th}-order delta-sigma modulation board at a 12.5 MHz sampling frequency. A reference signal, which was generated using MATLAB, utilizes a digital comparator as a one-bit signal converter. The length of the weighted moving average filter for smoothing the cross correlation signal was 141 taps. The microphone positions were located at (18, 0, 0), (0, 18, 0) and (0, 0, 18) cm on the X,Y, and Z axes, respectively. The reason why the microphones were not positioned on (10, 0, 0), (0, 10, 0) and (0, 0, 10) cm as the optimal microphone position because these positions had the strong direct sound, and they directly affected to the reflected echo. To compromise this point, the microphones

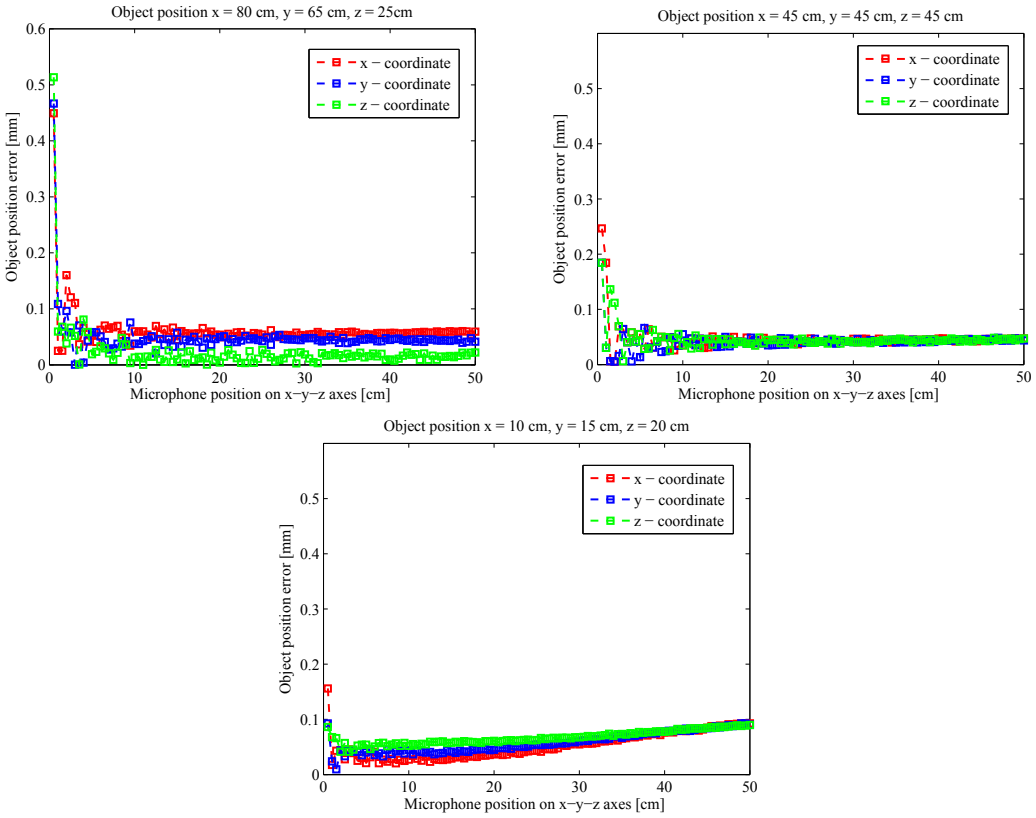

Figure 5.15 Object position error when varying the microphone position.

were shifted from 10 to 18 cm. In this experiment, a flat aluminum object with a width, height, and thickness of 13, 17, and 4 cm, respectively, was used. The propagation velocity of the ultrasonic wave in air was approximately 345 m/s at a temperature of 25 C^o and 35% RH.

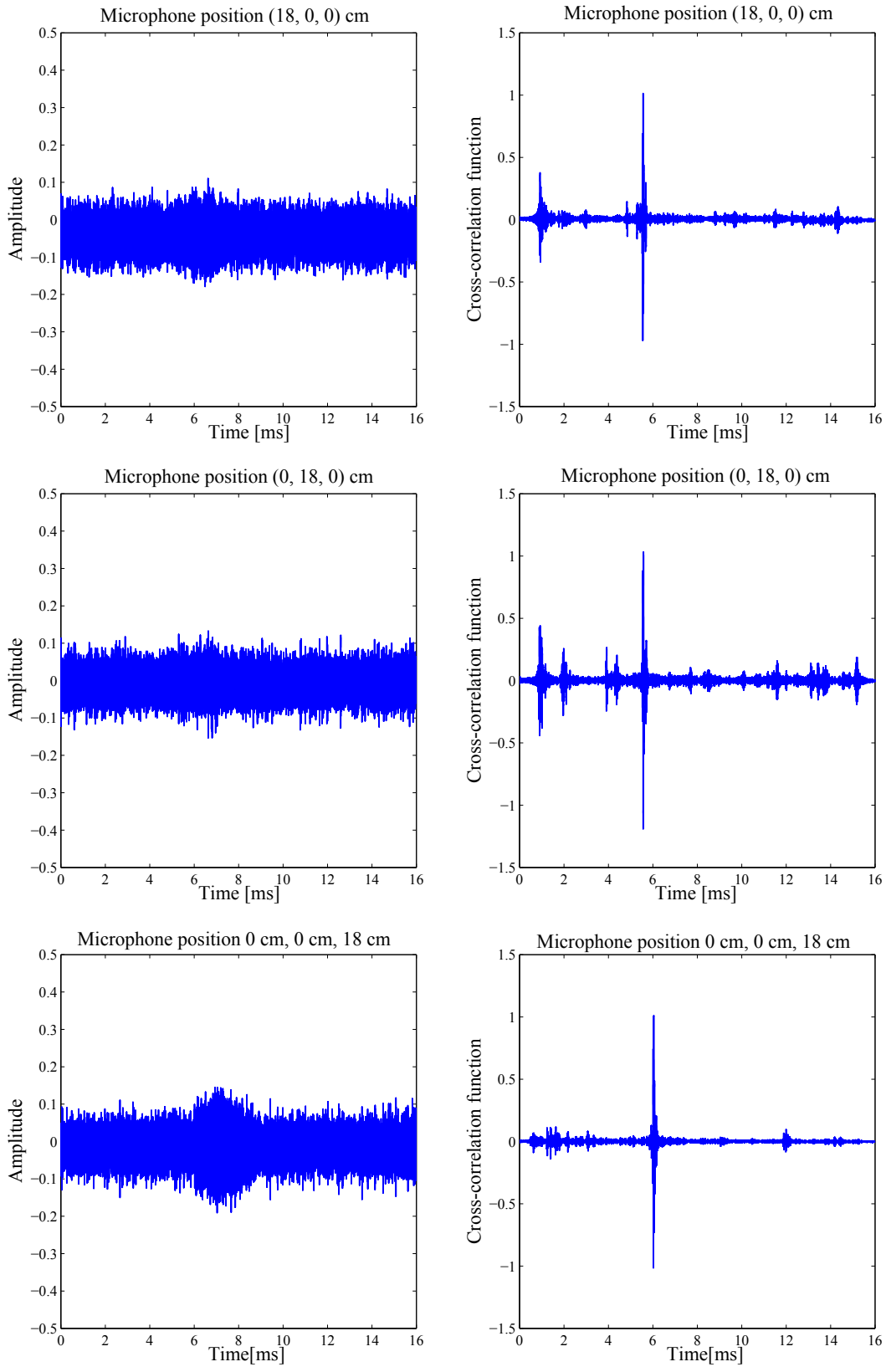

Figure 5.16 Echo and cross-correlation function at the object position (65 cm, 65 cm,50 cm).

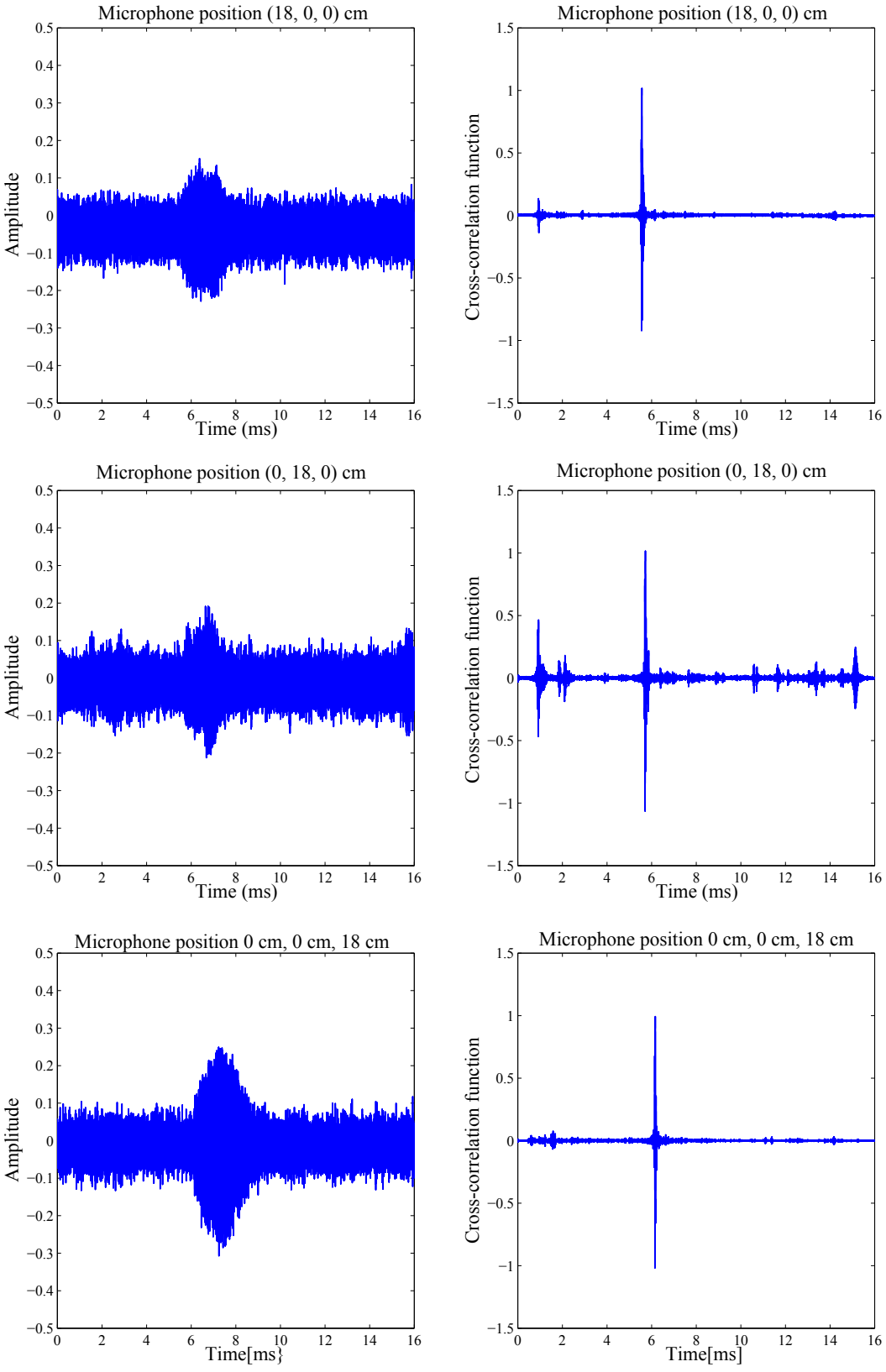

Figure 5.17 Echo and cross-correlation function at the object position (80 cm,65 cm,25 cm)

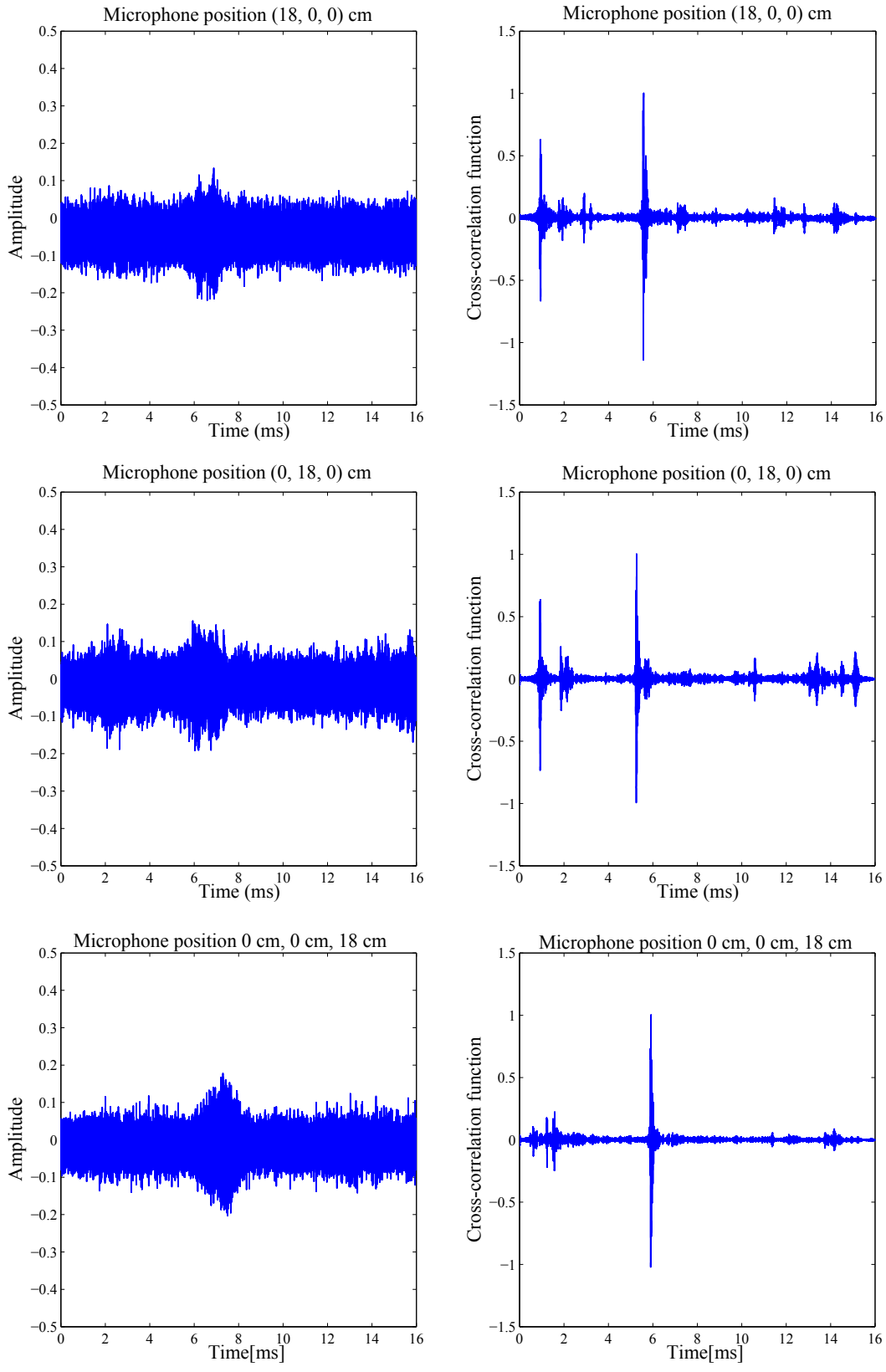

Figure 5.18 Echo and cross-correlation function at the object position (55 cm, 85 cm,35 cm)

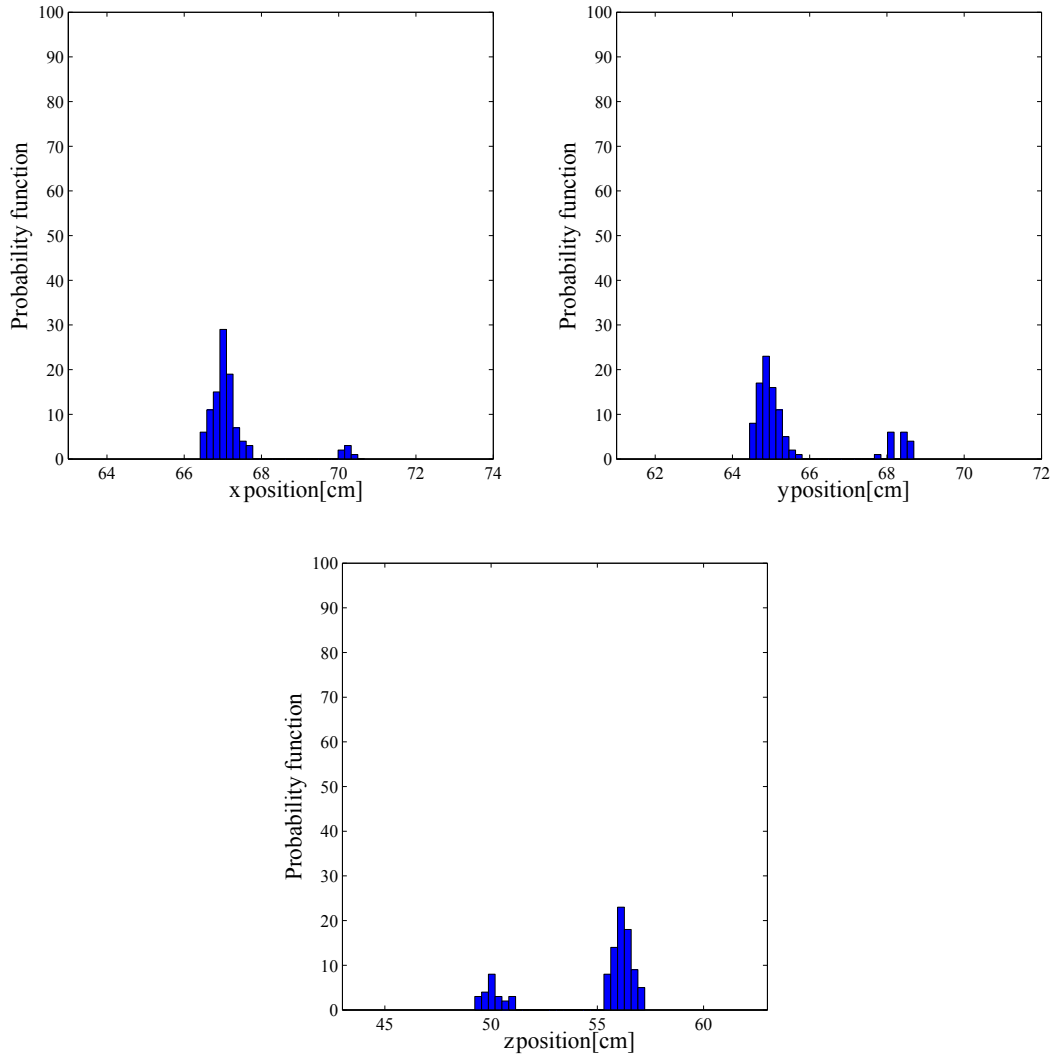

Figure 5.19 Repeatability of the object position measurements x = 65 cm, y = 65 cm, and z = 50 cm.

For the first position, we assume that the object was located at x=65 cm, y=65 cm, and z=50 cm. This position was on an approximately diagonal line from the sound source to the object. Echoes and the cross correlation based on one-bit signal of this position was sensed by microphones as shown in Figure 5.16. For the second position, we tried to move the object closer to the X-axis: x=80 cm, y=65 cm, z=25 cm. Finally, the third position was x=55 cm, y=85 cm, and z=35 cm, which is closer to the Y-axis. To confirm these conditions, the repeatability of the measurements was determined

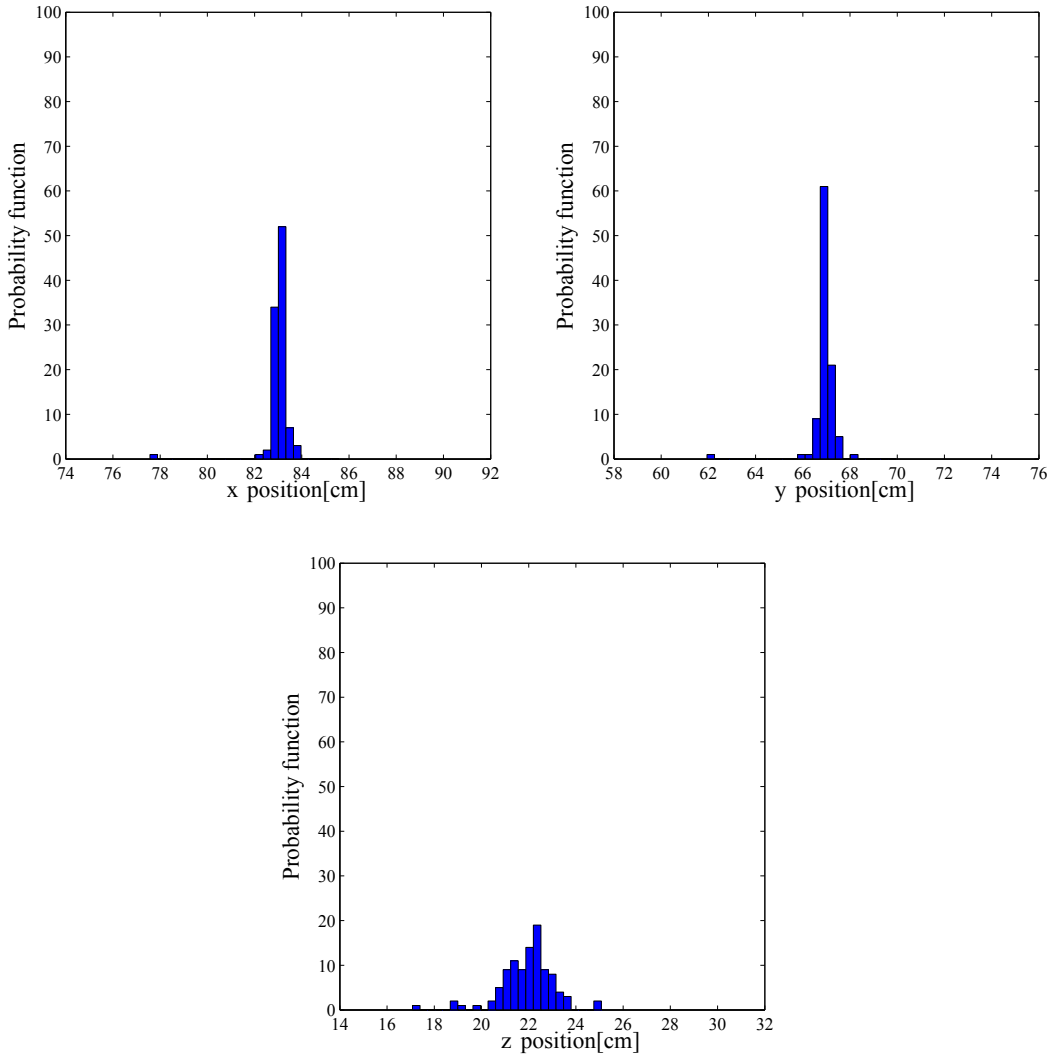

Figure 5.20 Repeatability of the object position measurements x = 80 cm, y = 65 cm, and z = 25 cm.

from 100 measurements. The first position is indicated in Figure 5.19, the second position is shown in Figure 5.20, and the third position is depicted in Figure 5.21. The mean and standard deviation values were determined via statistical evaluation of Figure 5.19, Figure 5.20, and Figure 5.21, respectively, and are listed in Table 5.2. Cumulative density function is available for the position-error analysis. This function is used to determine the lowest error, the highest error, and variance from 100 measurements, as shown in Figure 5.22. In the proposed system, we employed an iterative method to

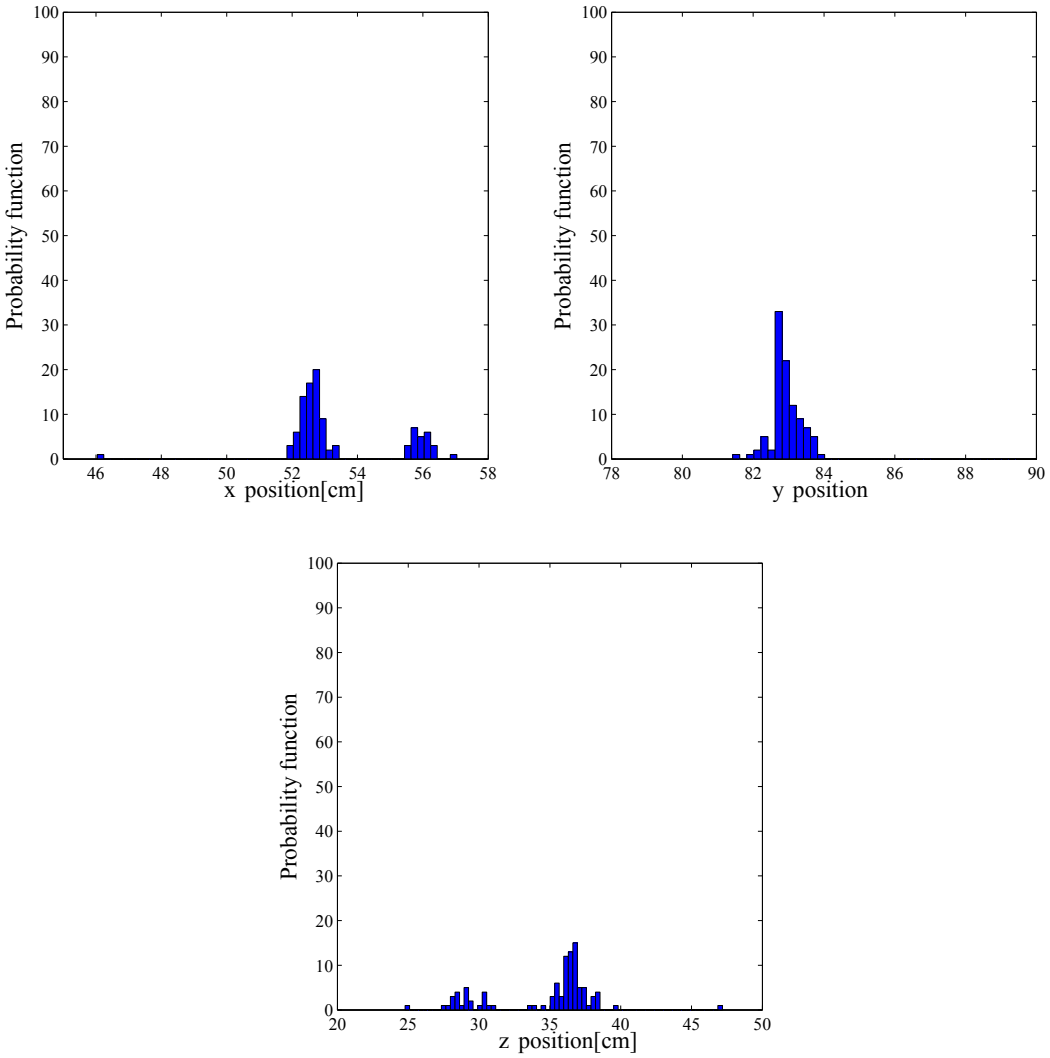

Figure 5.21 Repeatability of the object position measurements x = 55 cm, y = 85 cm, and z = 35 cm.

solve the object-position problem in three-dimensional space. The number of iterations is very important for real-time applications. The convergence from the initial point to the target took less than four iterations. Because Equation (5.14) to (5.16) is a high-slope parabolic curve as shown in Figure 5.9, it requires a few cycles to determine the tendency. The tolerance for stopping the iterations was 0.001. We used a rectangular object in this experiment. The sound that was incident on the object propagated from many points, which resulted in many different TOFs at the same receivers. It is

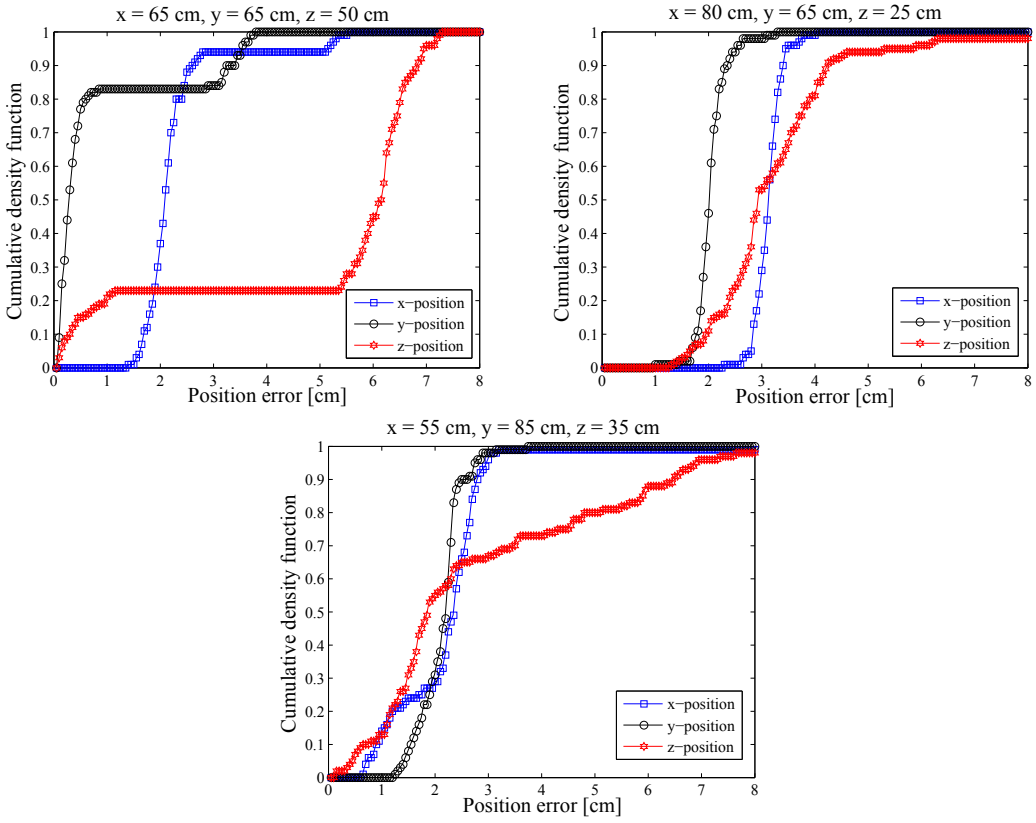

Figure 5.22 Cumulative density function of position error at different positions

The object position	average value (cm)	standard deviation (mm)
First position		
x-position	67.208458	8.12859
y-position	65.510344	13.08260
z-position	54.799311	26.37833
Second position		
x-position	83.021071	6.16193
y-position	66.923571	5.79461
z-position	22.153814	25.23126
Third position		
x-position	53.378771	16.92404
y-position	82.923429	4.03455
z-position	34.781123	37.23870

Table 5.2 Statistical evaluation for the object-position measurements.

dependent on the efficiency of the sound propagation of the sound source. In addition, the z position had greater variance than the x and y positions. However, it shows that this method has the ability to estimate the position in three-dimensional space.

5.5 Summary

An ultrasonic three-dimensional system for moving object position and velocity estimation using a pair of LPM was proposed. The design method comprises, one-bit signal processing, object-velocity-measurement and Newton Raphson method. We employed three microphones to detect the reflected echo from the moving object. Time-of-flight and the relative velocity were computed with low-cost time. Newton-Raphson played a vital role as object-position estimator. Finally, the Doppler velocity and object position from the earlier measurements were used to determine the object velocity on the basis of vector velocity theory. To firstly confirm proposed idea, the moving-object position and velocity were evaluated by MATLAB computer simulation. The simulation results confirmed the validity of the proposed method. To satisfy the experimental results, an object in three-dimensional space is based on TOF measurements form silicon microphones for hand held telecommunication devices. The object was considered to be in Euclidean space. The three receivers were positioned on three different axes, which were perpendicular to each other. The location of the sound source was set as the origin. The TOF was computed using a one-bot cross correlation to allow for real-time applications. The experiment results guarantee that the proposed method can converge. The validity of the estimation is determined through 100 measurements and statistical tests. The optimal microphone position from simulations was located at 10 cm on x-y-z axes.

6

Ultrasonic position and velocity measurement by a Direction-of-Arrival method (Second method)

6.1 Position measurement using an Direction-of-Arrival method

In the previous chapter, a method for three-dimensional-positioning by means of an iterative method of numerical methods has been described. This method can achieve the object positions when an object is assumed as an aluminum flat plate hanged on three dimensional spaces. The boundary of the proposed three dimensional spaces is assumed that the object appears in 90^o perpendicular axes of x-y-z co-ordinates. When deeming this situation, the object cannot be detected in a few critical areas outside readability of the assigned spaces, as shown in Figure 6.1. The improved detectability can cover an area from +X axis to -X axis and from +Z down to -Z. This is a full-range vision in front of mobile robots when their own position is walking on the floor. To satisfy this condition, the microphone positions used for echo recorder should be rearranged to fully cover such an detection area. Moreover, Newton-Raphson method, which is performed to estimate the required position, is not convenient for real-time applications because iterations, which are the unique basis of numerical methods, inevitably require the computational repeatability. An improve method for three-dimensional-positioning

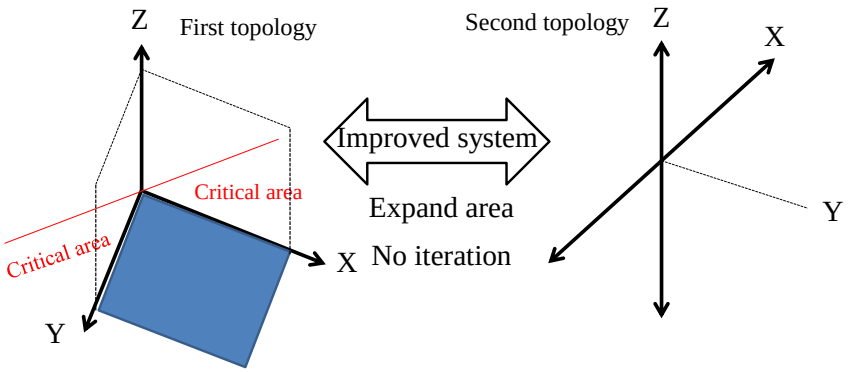

Figure 6.1 Improved readability of second topology

should be realized. Thus, Direction-of-Arrival method, which is well known in a field of sound-sources localization, is fascinating to be technically applied for three-dimensional ultrasonic position measurement.

6.1.1 Direction-of-Arrival method

Direction-of-Arrival (DOA) method (direction finding) essentially involves with the measurement of direction finding of signal sources, either in the form radio or acoustic waves, directly incident on a sensor array. DOA method corresponds to the requirements of tracking and finding signals from the original source in areas of civilian and military applications, such as sonar, seismology, and wireless 911 emergency call location [77]. An overview for DOA method in this chapter is described. In general, DOA techniques can be broadly grouped into traditional beamforming techniques, maximum likelihood techniques, and subspace-based techniques. To more study about DOA estimations, an excellent doctoral dissertation on array signal processing has been contributed [78]. Now we consider a uniform linear array, which composes of N omnidirectional elements, are aligned on a two-dimensional arrays. This array can estimate the angles in both azimuth and elevation of a source, as shown in Figure 6.2. Similarly,

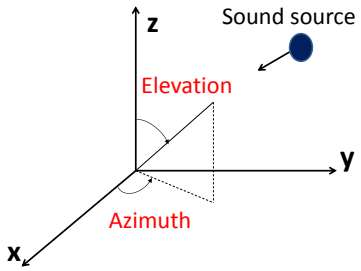

Figure 6.2 Definition of azimuth and elevation angles.

we can improve a concept of sound direction into applications involving with echolocations. In the next chapter, the microphone alignment and a method-based DOA for echolocations is expressed.

6.1.2 Three-dimensional-positioning using a Direction-of-Arrival method

According to Figure 6.3, The proposed method can detect the object on ranging measurements from -X to +X and from -Z to +Z. The object appears in front of the sound source in +Y axis. This method provides more ranging measurements than the previous method four times. In Figure 6.3, Four microphones are located onto +X, -X, +Z, and -Z, and their own position are $(m, 0, 0), (-m, 0, 0), (0, 0, +n)$, and $(0, 0, -n)$, respectively. We assume that the object has a unknown position on (x, y, z). The object position can be viewed between X-Y plane and Z-axis as Figure 6.4. d is a distance from the sound source to object, θ is the angle of elevation on X-Y plane, and r is a distance between microphone 3 and 4 equal to $2n$. Firstly, we have to decide that the object is on +Z or -Z axis by checking TOF_3 and TOF_4. If TOF_3 is greater than TOF_4, that means the object on +Z axis. On the other hand, the object appears on -Z axis. Then, if we assume that d has much more length than r, $d >> r$, we can deduce the first triangle to be a secant in Figure 6.5. In this secant, it consists of two known sides $2n$ and time-of-flight difference between microphone 3 and 4, multiplied to sound velocity v_0, which is $(TOF_4 - TOF_3) \cdot v_0$. There are two unknown parameters A and γ in this situation. The relationship between A and γ relates to Equation (6.1) via the first triangle as

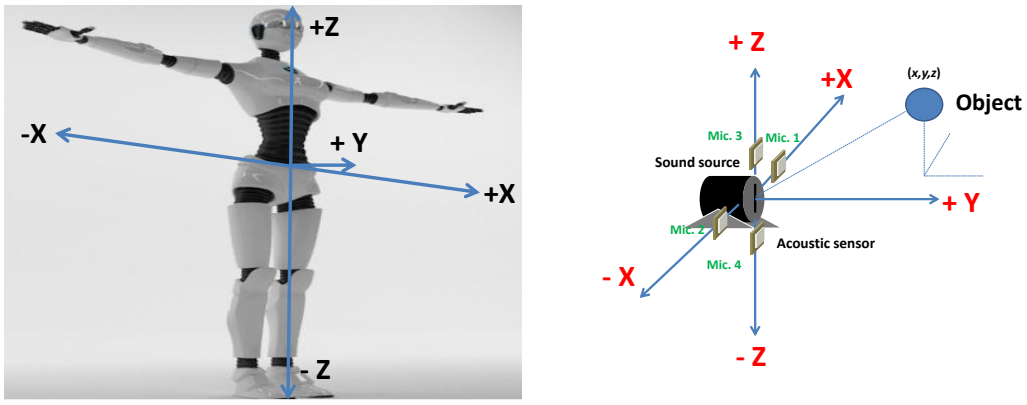

Figure 6.3 Improvement of the three-dimensional-positioning method.

$$A = 2n\cos\gamma. \tag{6.1}$$

Because of cosine law, Equation (6.2) can link the TOF difference, A, γ , and $2n$ of the first triangle following to

$$(TOF_4 - TOF_3)^2 v_0^2 = 4n^2 + A^2 - 2(2n)A\cos\gamma. \tag{6.2}$$

Insert Equation (6.1) into Equation (6.2) and reform Equation.

$$(TOF_4 - TOF_3)^2 v_0^2 = 4n^2 + 4n^2\cos^2\gamma - 8n^2\cos^2\gamma. \tag{6.3}$$

$$(TOF_4 - TOF_3)^2 v_0^2 = 4n^2(1 - \cos^2\gamma) \tag{6.4}$$

$$\cos^2\gamma = 1 - \left[\frac{(TOF_4 - TOF_3)v_0}{2n}\right]^2 \tag{6.5}$$

$$\gamma = \cos^{-1}\sqrt{1 - \left[\frac{(TOF_4 - TOF_3)v_0}{2n}\right]^2} \tag{6.6}$$

If we look at the second triangle at the same condition $d >> r$, θ is approximately equal to γ. Finally, we can know the angle of elevation of the object on X-Y plane from Equation (6.7).

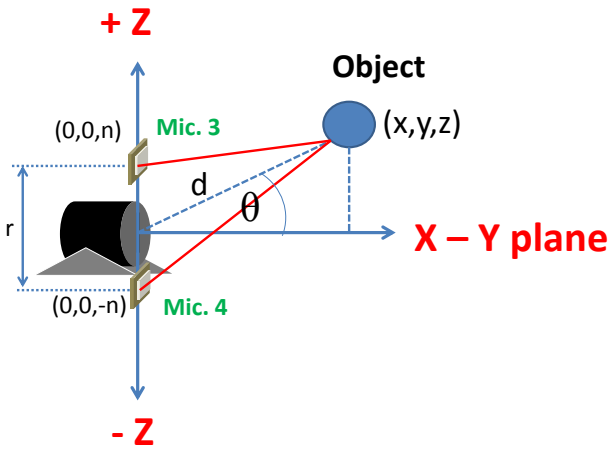

Figure 6.4 The object position on X-Y plane and Z-axis.

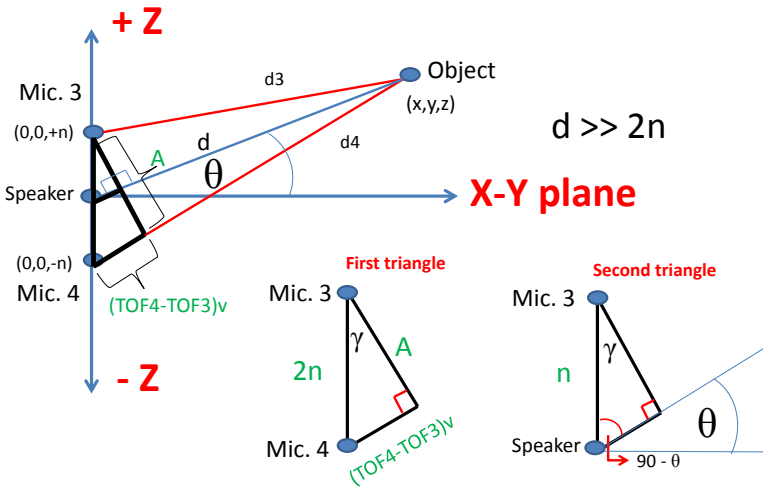

Figure 6.5 The case of the object on +Z axis.

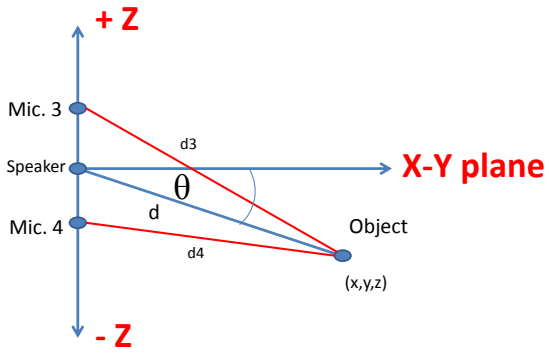

Figure 6.6 The case of the object on -Z axis.

$$\theta \approx \cos^{-1}\sqrt{1-\left[\frac{(TOF_4 - TOF_3)v_0}{2n}\right]^2} \tag{6.7}$$

Reform Equation (6.8);

$$d^2 + 2n\sin\theta d + \left(n^2 - d_4^2\right) = 0 \tag{6.8}$$

We solve above equation for determining parameter d. In the next step, we tried to solve the parameter d. Looking back to Figure 6.5 again, we can create an obtuse triangle at Mic 4, speaker, and object points. Cosine law is used to make the relationship between d, d_4, and θ as Equation (6.8).

$$d_4^2 = d^2 + n^2 - 2dn\cos(90^o + \theta). \tag{6.9}$$

When $d = TOF_4 v_0 - d_4$, put back into Equation (6.9) again. We can get d_4.

$$d_4 = \frac{\left(TOF_4 v_0\right)^2 + n^2 + 2nTOF_4 v_0 \sin\theta}{2TOF_4 v_0 + 2n\sin\theta} \tag{6.10}$$

We solve above equation for determining parameter d.

$$d = -n\sin\theta + \sqrt{n^2\sin^2\theta - \left(n^2 - d_4^2\right)} \tag{6.11}$$

Otherwise, if TOF_4 is less than TOF_3, the object is on -Z axis shown as Figure 6.6.

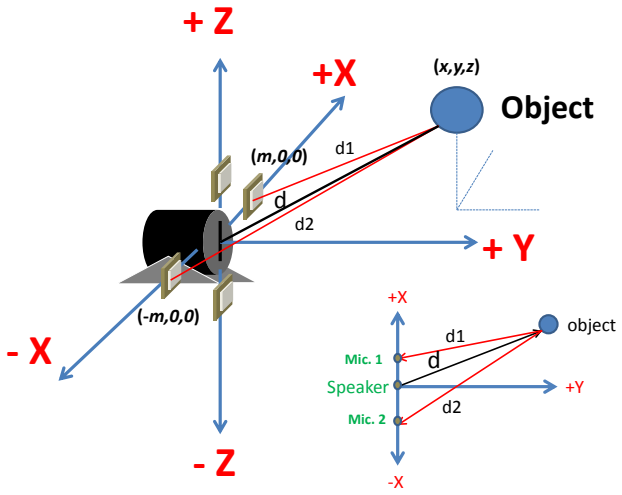

Figure 6.7 The object on X-Y plane.

We still compute θ in Equation (6.7), but d is different to Equation (6.11). It can be expressed in Equation (6.13).

$$d_3 = \frac{(TOF_3 v_0)^2 + n^2 + 2nTOF_3 v_0 \sin\theta}{2TOF_3 v_0 + 2n\sin\theta} \tag{6.12}$$

$$d = -n\sin\theta + \sqrt{n^2\sin^2\theta - \left(n^2 - d_3^2\right)} \tag{6.13}$$

Now, we absolutely know a parameter z by d and θ in Equation (6.14).

$$z = d\sin\theta \tag{6.14}$$

We consider the unknown parameters x and y in Figure 6.7. The distance between the sound source, the object, and the microphone 1 is equal to $d + d_1 = TOF_1 v$. We revise this relationship again with the parameters x, y, and z in Equation (6.15).

$$d + \sqrt{(x-m)^2 + y^2 + z^2} = TOF_1 v_0 \tag{6.15}$$

Reform it for keeping the parameter y on the left hand side.

$$y^2 = -x^2 - z^2 + 2mx - m^2 + (TOF_1 v_0)^2 - 2dTOF_1 v_0 + d^2 \tag{6.16}$$

Consider on the microphone 2, $d + d_2 = TOF_2 v_0$. We get Equation (6.17).

$$y^2 = -x^2 - z^2 - 2mx - m^2 + (TOF_2 v_0)^2 - 2dTOF_2 v_0 + d^2 \tag{6.17}$$

Subtract Equation (6.16) by Equation (6.17)

$$4mx + \left(TOF_1^2 - TOF_2^2\right) v^2 + 2dv_0(TOF_2 - TOF_1) = 0 \tag{6.18}$$

Now, we have only an unknown parameter x alone.

$$x = \frac{2dv_0(TOF_1 - TOF_2) + \left(TOF_2^2 - TOF_1^2\right) v_0^2}{4m} \tag{6.19}$$

Finally, it is not difficult task for unknown parameter y.

$$y = \sqrt{d^2 - x^2 - z^2} \tag{6.20}$$

Sometimes, it might not be comfortable for designating the object position on Cartesian coordinates because the object will be seen as a small point. In practical, the object for testing is rigid body. It cannot be considered to be the small point. Thus, it is better if the object position is provided by the meaning of Direction of Arrival on Spherical coordinates. This system consists of the distance (d), the elevation angle (α) of +Z axis, and the azimuth angle (ϕ) of +X axis. The parameters d is already known and we can define α by $90^o - \theta$. In Figure 6.2, the azimuth angle can be linked to x parameter of Cartesian coordinate, $x = d\sin\alpha\cos\phi$. The azimuth angle is

$$\phi = \cos^{-1}\frac{2dv_0(TOF_1 - TOF_2) + \left(TOF_2^2 - TOF_1^2\right) v_0^2}{4dm\sin\alpha}. \tag{6.21}$$

We can summarize this method again step by step:
***Step*1.** Estimate the angle of elevation θ.

$$\theta \cong \cos^{-1}\sqrt{1 - \left[\frac{(TOF_4 - TOF_3)v_0}{2n}\right]^2}$$

or

$$\theta \cong \sin^{-1}\frac{(TOF_4 - TOF_3)v_0}{2n}$$

***Step*2.** Evaluate the object on +Z or -Z
if $TOF_4 > TOF_3$, the object onto +Z area.

$$d_4 = \frac{(TOF_4 v_0)^2 + n^2 + 2nTOF_4 v_0 sin\theta}{2TOF_4 v_0 + 2n\sin\theta}$$

$$d = -n\sin\theta + \sqrt{n^2\sin^2\theta - \left(n^2 - d_4^2\right)}$$

$$z = d\sin\theta$$

if $TOF_3 > TOF_4$, the object onto -Z area.

$$d_3 = \frac{(TOF_3 v_0)^2 + n^2 + 2nTOF_3 v_0 \sin\theta}{2TOF_3 v_0 + 2n\sin\theta}$$

$$d = -n\sin\theta + \sqrt{n^2\sin^2\theta - \left(n^2 - d_3^2\right)}$$

$$z = -d\sin\theta$$

***Step*3.** Compute the parameter x and y for rectangular coordinates

$$x = \frac{2dv_0(TOF_1 - TOF_2) + \left(TOF_2^2 - TOF_1^2\right) v_0^2}{4m}$$

$$y = \sqrt{d^2 - x^2 - z^2}$$

***Step*4.** For Spherical coordinates d, α, and ϕ.
if $TOF_4 > TOF_3$, the object onto +Z area.

$$\alpha = 90^o - \theta$$

if $TOF_3 > TOF_4$, the object onto -Z area.

$$\alpha = 90^o + \theta$$

$$\phi = \cos^{-1}\frac{2dv_0(TOF_1 - TOF_2) + \left(TOF_2^2 - TOF_1^2\right) v_0^2}{4dm\sin\alpha}.$$

6.1.3 Simulation results for three-dimensional-positioning using a Direction-of-Arrival method

Simulation results are performed to represent the proposed three-dimensional-positioning method by a Direction-of-Arrival method. We will show that how it works by assuming that an object position is d=80 cm, α=75^o, and $\phi = 120^o$ and the microphone positions

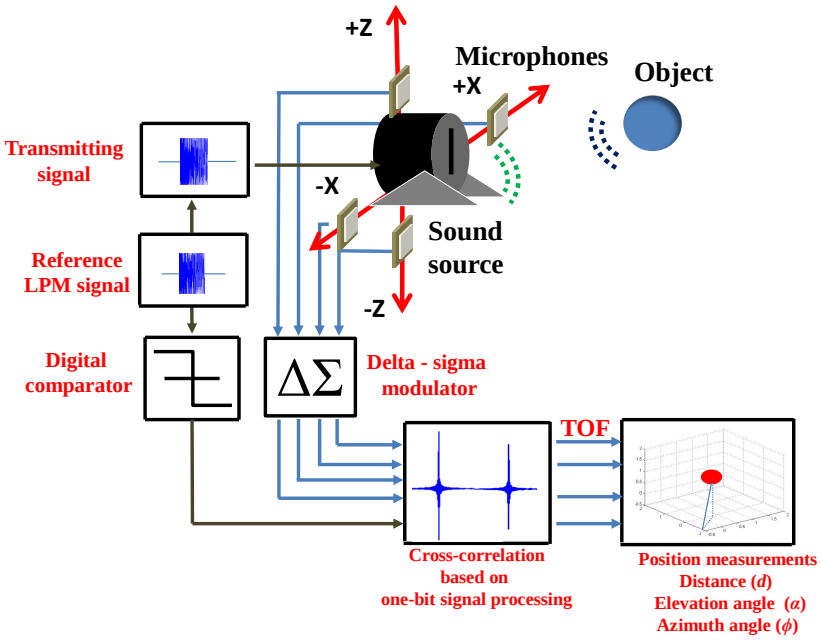

Figure 6.8 Proposed three-dimensional positional position measurement based on a Directional-of-Arrival.

are (10 cm, 0 cm, 0 cm), (-10 cm, 0 cm, 0 cm), (0 cm, 0 cm, 10 cm) and (0 cm, 0 cm, -10 cm). The object position estimation under an ultrasonic three-dimensional system determined by the proposed one-bit signal processing method was evaluated by MATLAB computer simulation. The period of the single LPM signal was swept linearly from 20 μs to 50 μs. The sampling frequency rate was 12.5 MHz. The LPM signal had the length equal to 3.278 ms. The propagation velocity of an ultrasonic wave in air was 345.1 m/s at 22.4 C^o. SNR was set at 0 dB compared with the echo signal. The constant attenuation factor of the received signal was -2.107 dB/m degraded from that of the original signal. The received signals and the normalized cross-correlation functions obtained by one-bit signal processing are illustrated in Figure 6.8. The received signals were changed into the single-bit delta-sigma modulated signal by the 7^{th}-order delta-sigma modulator. The one-bit signal of the received echo was correlated together with the one-bit signal of the reference, which was the transmitted LPM signal converted into the one-bit digital signal by a digital comparator. The cross-correlation function of

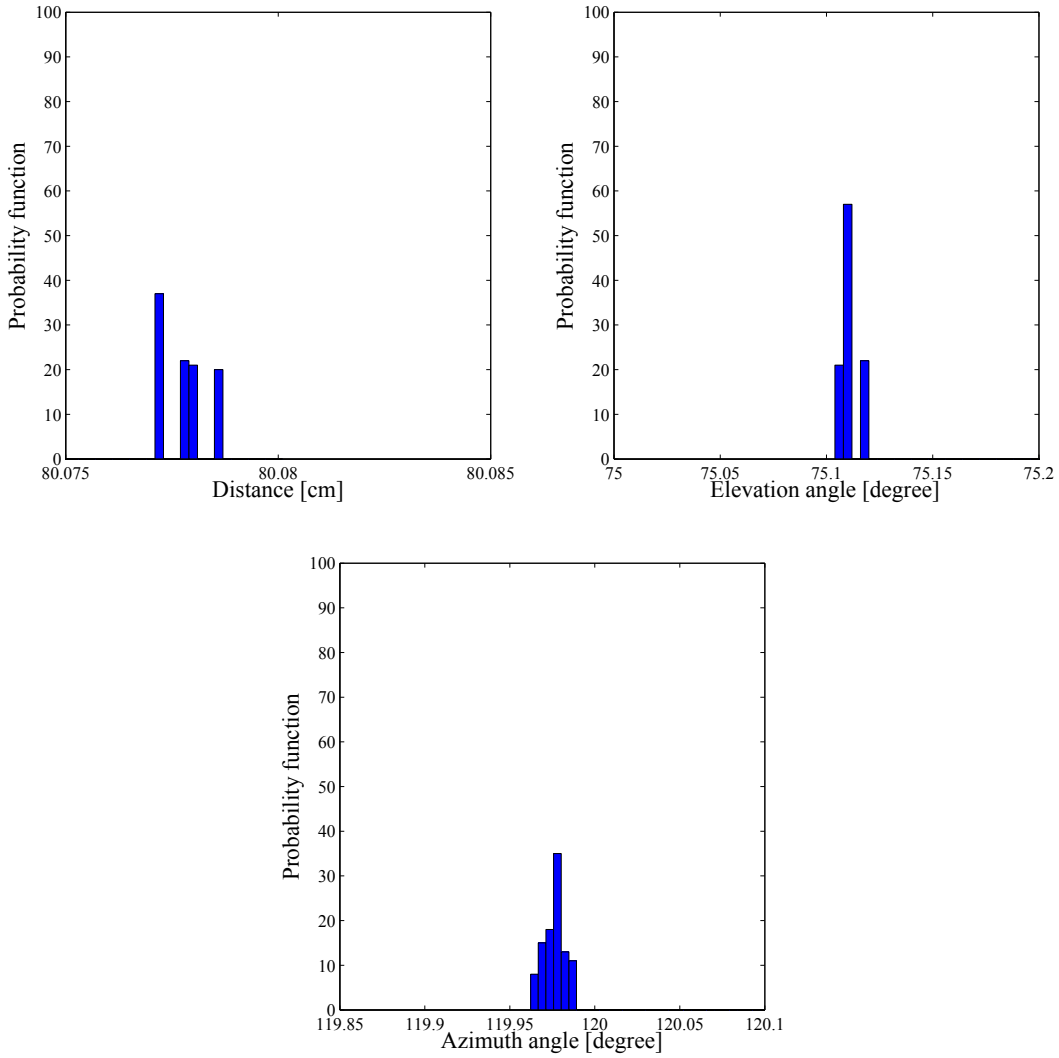

Figure 6.9 The probability distributions of simulations at the position: distance = 80 cm, elevation angle = 75 degree, and azimuth angle = 120 degree.

the one-bit received signal and the one-bit reference signal was obtained directly from the recursive cross-correlation operation of one-bit signal processing and the smoothing operation accomplished by the triangular weighted moving average filter. Signal had 399 zero-cross points. Accordingly, the computational cost of the recursive cross-correlation operation was the integration and 401 summations of one-bit samples. For the smoothing operation, the length of the triangular weighted moving average filter, which consists of a pair of 55-tap moving average filters, was 109 taps. The position

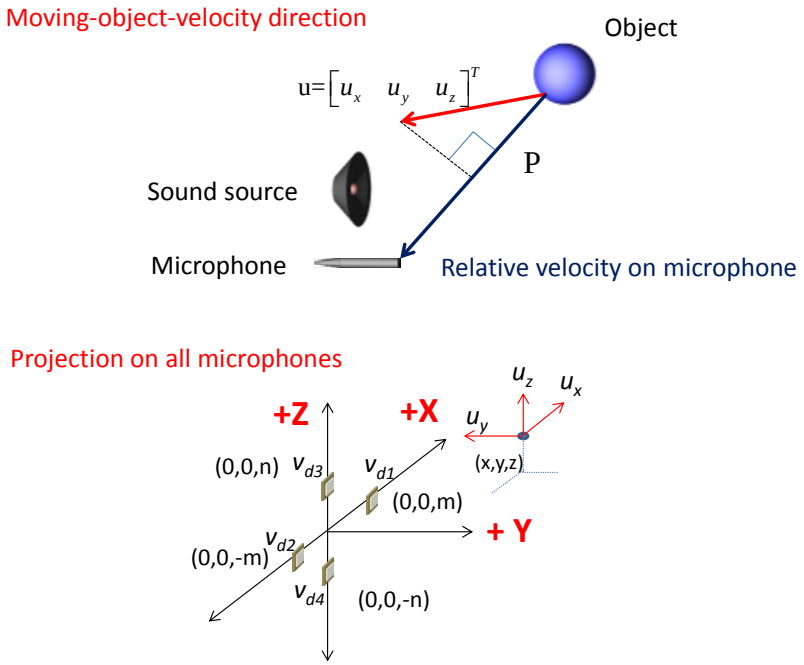

Figure 6.10 Object-velocity vector configuration based on a Directional-of-Arrival.

error by the noise included in the received echoes was evaluated by MATLAB computer simulation. In the simulation, the SNR (0 dB) of the reflected echo was converted by including normal distribution of random noises, or white noise, to the received echoes. In the case of each SNR, the position of the estimation was evaluated from 100 simulations. The probability distributions of the estimated position are determined from 100 estimation and illustrated in Figure 6.9. The simulation results was observed that the distance is between 80.075 to 80.08 cm, the elevation angle is between 75.1 to 75.15 degree, and the azimuth angle is 119.95 to 120 degree.

6.2 Velocity measurement using vector projection

The moving-object velocity is estimated using data of the relative velocities at each microphone, that is,v_{d1} on the first microphone, v_{d2} on the second microphone, v_{d3} on the third microphone and v_{d4} on the fourth microphone, the instantaneous position

of the moving object, computed in 5.1.2., and microphone positions. On the basis of the simple fundamentals of the vector theory, vector projection can be considered as the dot product between two vectors as shown as Figure 6.10. Hence, the results of vector projection between the relative velocity estimation at each microphone, $\boldsymbol{u}$ is the unknown object-velocity vector, and $\boldsymbol{v_d}$ is the microphone vector. If the unknown velocity vector of the moving object $\boldsymbol{u} = [u_x, u_y, u_z]^T$ is projected onto the microphone vectors, the result of the projection is the relative velocity measured by the microphones. Thus, the velocity of the moving object can be estimated using the measurements from the relative velocity of each microphone, the instantaneous object position of the moving object, and the microphone positions. We use the relative-velocity measurements $\boldsymbol{v_d} = [v_{d1}, v_{d2}, v_{d3}, v_{d4}]^T$ of microphone 1, 2, 3 and 4, respectively. The projection of the unknown vector $\boldsymbol{u}$ on a microphone vector is

$$\boldsymbol{v_d} = \boldsymbol{u}^T \boldsymbol{Q} \tag{6.22}$$

where $\boldsymbol{Q} = [\frac{\boldsymbol{p_1}}{\|\boldsymbol{p_1}\|} \frac{\boldsymbol{p_2}}{\|\boldsymbol{p_2}\|} \frac{\boldsymbol{p_3}}{\|\boldsymbol{p_3}\|} \frac{\boldsymbol{p_4}}{\|\boldsymbol{p_4}\|}]^T$. Assume that a point (x, y, z) is the instantaneous position of the moving object when the wave is incident on the surface of the object. The microphone vectors $\boldsymbol{p_1} = -[x-n, y, z]^T$,$\boldsymbol{p_2} = -[x+n, y, z]^T$, $\boldsymbol{p_3} = -[x, y, z-m]^T$, and $\boldsymbol{p_4} = -[x, y, z+m]^T$ have a magnitude of the form $\|\boldsymbol{p}\| = \sqrt{\boldsymbol{p}^T \boldsymbol{p}}$. Now, our system has four equations and only three unknown variables. In general, $\boldsymbol{v_d}$ can be projected onto the column space of a 4 by 3 matrix. Therefore, $\boldsymbol{u}$ can be estimated by means of linear-least-squares approach [79].

$$\boldsymbol{u} = (\boldsymbol{H}^T \boldsymbol{H})^{-1} \boldsymbol{H}^T \boldsymbol{W} \boldsymbol{v} \tag{6.23}$$

where

$$\boldsymbol{H} = -\begin{bmatrix} x-n & y & z \\ x+n & y & z \\ x & y & z-m \\ x & y & z+m \end{bmatrix}$$

$$\boldsymbol{W} = \frac{1}{4}\begin{bmatrix} 1 & 1 & 1 & 1 \\ 1 & 1 & 1 & 1 \\ 1 & 1 & 1 & 1 \\ 1 & 1 & 1 & 1 \end{bmatrix}$$

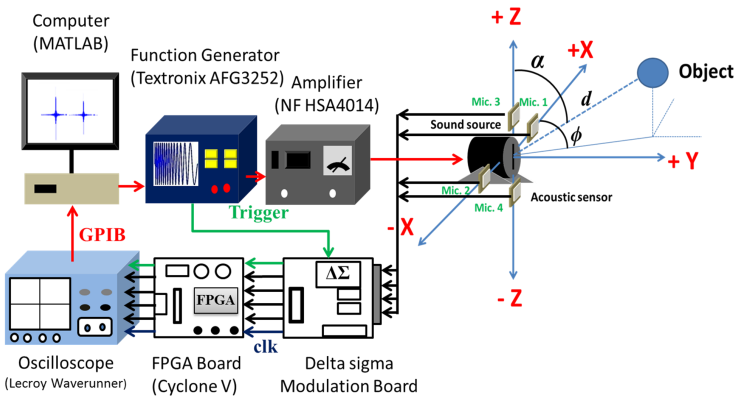

Figure 6.11 Three-dimensional-positioning system based on a Directional-of-Arrival.

and

$$\boldsymbol{v} = \begin{bmatrix} v_{d1}\|\boldsymbol{p_1}\| \\ v_{d2}\|\boldsymbol{p_2}\| \\ v_{d3}\|\boldsymbol{p_3}\| \\ v_{d4}\|\boldsymbol{p_4}\| \end{bmatrix}$$

H is an observation matrix, and **W** is a weighted averaging matrix.

6.3 Experimental results

6.3.1 Non-moving-object case

The experimental setup for the airborne ultrasonic three-dimensional positioning system is shown in Figure 6.11. In the experiment, the frequency of the transmitted LPM signal was swept from 50 kHz to 20 kHz. The length of the transmitted LPM signal was 3.274 ms. The driving voltage of the function generator was 4 Vp-p. The LPM signal was generated from the function generator and enlarged 10 times with an amplifier. The loudspeaker transmitted the LPM signal, and the spherical object, having a diameter of 10 cm, was sensed by the four silicon MEMS microphones based on a device for hand-held telecommunication instruments (Knowles SPM0204UD5). This model has sufficient sensitivity to detect sound pressure omnidirectionally. Frequencies are allowed to pass through it from 10 kHz to 100 kHz. A silicon microphone is em-

bedded on a signal processing board containing a low-pass frequency circuit with 60 kHz frequency cutoff and a pre-amplifier with 20 decibels (dB). Sensitivity achieves a minimum level of - 47 dB at a humidity not over 70 RH. The loudspeaker, which has been accepted for use in a variety of studies, was a Pioneer company model PT-R4. It was of the direct-radiator type as is often used in small address systems. A satisfactory response over a comparatively wide frequency range was achieved. The distance from the loudspeaker to the microphones on the X-axis was 10 cm and that on the Z-axis was 11 cm. The propagation velocity of an ultrasonic wave in the air was approximately 345 m/s at a temperature of $20 - 25^o$ C and humidity of 50 RH. The signals obtained using the acoustical receivers were converted into one-bit signals by a 7^{th} -order delta-sigma modulator (Analog Devices AD7720). The sampling frequency of the delta-sigma modulator was 12.5 MHz. The cross correlation and smoothing operation for 141 taps of a weighted moving average filter was designed and programmed on a FPGA board model cyclone V 5CGXFC5C6F27C7. The logic utilization of the FPGA board for the cross correlation based on one-bit signal processing involved 2602 logic elements, the total number of registers was 5777, and the total block memory was 175,948 bits. To evaluate the ability of the sound beam radiation to cover a possible object position, the target was located on the left- and right-hand sides of the top and bottom areas away from the sound-beam radiation source.

The position of the object was estimated from 50 experiments. The probability distributions of the estimated position are presented. The repeatability of measurements was defined using averages and standard deviations. The resolution of the system was approximately 14 μm at a sampling rate of 12.5 MHz when the sound velocity was assumed to be 345 m/s. The object position was considered in the case when the loudspeaker position was not rotated. Rotating the loudspeaker position enables the shift of the sound beam from the original position of the sound source to scan the object outside the beam. In the first case, the object was positioned in four locations with the three-dimensional space under a sound beam that the speaker can radiate. The loudspeaker has an area of sound-beam radiation with approximately $\pm\ 20^o$ above the Z-Y plane and $\pm\ 45^o$ to either side of the X-Y plane when a reference of a sound source was in the original point shown in Figure 4.16. Therefore, the object position was estimated within the area of the sound beam. The object-position measurements are shown by the different color bars for 50 repeated measurements. The probability distributions are illustrated in Figure 6.12. Average and standard deviations of the object positions are given in Table 6.1. We note that the standard deviation of the object position at distance = 77 cm, elevation angle = 85^o, and azimuth angle = 104^o had

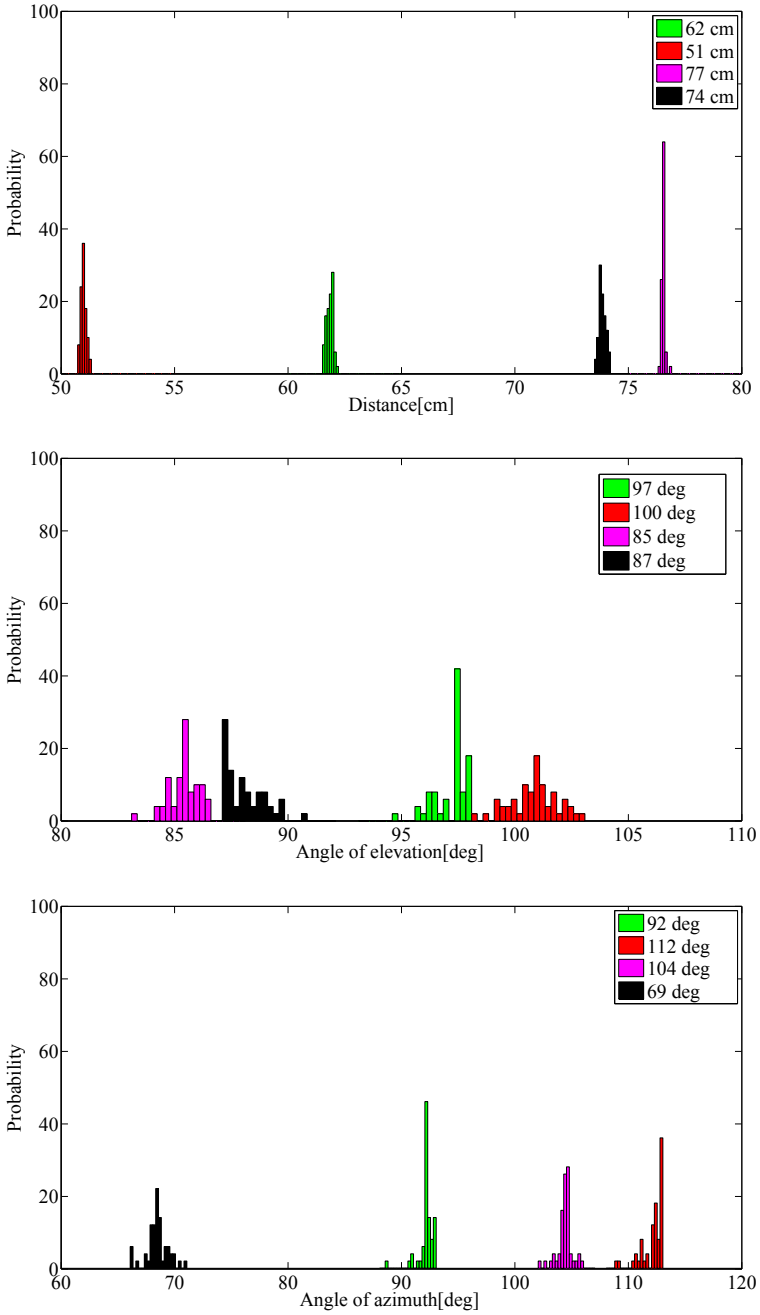

Figure 6.12 Probability of the position measurement in the case of no rotating speaker position: distance measurement, elevation-angle measurement, and azimuth-angle measurement.

Object position	average value	standard deviation
First position (black)		
Distance d (cm)	73.8241	0.1334
Elevation angle α (deg)	88.2003	0.7122
Azimuth angle ϕ (deg)	69.3104	0.6833
Second position (red)		
Distance d (cm)	51.0007	0.1227
Elevation angle α (deg)	100.8642	1.0295
Azimuth angle ϕ (deg)	112.4113	1.1168
Third position (pink)		
Distance d (cm)	76.5783	0.0738
Elevation angle α (deg)	85.4192	0.7095
Azimuth angle ϕ (deg)	104.4730	0.6688
Fourth position (green)		
Distance d (cm)	61.8941	0.1429
Elevation angle α (deg)	97.3282	0.9057
Azimuth angle ϕ (deg)	92.3034	0.7886

Table 6.1 Averages and standard deviations of positions determined in the case of no rotating speaker position

minimum variance compared with the other measurements. The reason is that this position was set up at a location near the central line of the +Y-axis of sound radiation in Figure 4.16(b). The sound pressure was moved toward the object and then returned to the microphones at an intense and constant sound level. The repeatability of the point of contact on the object was high. On the other hand, when the object position was at distance = 74 cm, elevation angle = 87^o, and azimuth angle = 69^o, the greatest dispersion of standard deviations was observed. This was a location comparatively far away from the main sound beam. Accordingly, the repeatability of contact at the same point was less likely.

In order to scan the area of detection, the sound beam was shifted up + 10^o and down 10^o in the Z-axis by manually lifting the loudspeaker, as shown in Figure 6.13. Then, the position determined was located outside the area of the first case. The probability distributions of the loudspeaker positions are shown in Figure 6.14. Averages and standard deviations of the locations are listed in Table 6.2. With the object positioned at distance = 88 cm, elevation angle = 72^o, and azimuth angle = 90^o, this position is on the +Y-axis and results in the minimum standard deviation because the main

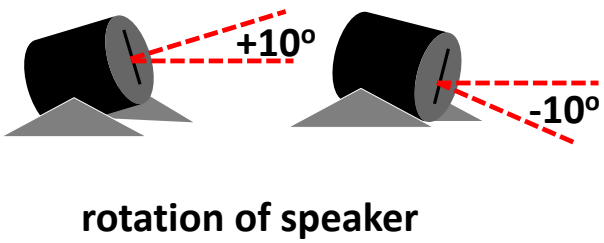

Figure 6.13 Sound beam scanning by rotating speaker position.

sound beam from the loudspeaker was directly incident on the same point on the object surface over repeated measurements. In other cases in which the positions had more oblique contact with the main beam, the sound pressure moving toward the object was not constant for each pulse of sound. Repeatability of these conditions thus had a larger variance over many measurements. In addition, the object in the experiments was a rigid body, but in the proposed method, we assumed that the object was a small point. A measurement point can be estimated from many points on a surface because we do not know the exact reference point on the rigid body on which the sound was incident. For this reason, some deviation between the reference point and the measurement point was observed. Therefore, fluctuations in measurements depend on the direction of the sound propagation from the sound source to the target and the shape of the object.

6.3.2 Moving-object case

The experimental setup for the three-dimensional position and velocity measurements is pictured in Figure 6.15. In this experiment, the frequency of the transmitted LPM signal swept from 50 kHz to 20 kHz. The length of the transmitted LPM signal was 3.274 ms. A pair of LPM signals was generated from a function generator at 4 V_{p-p} and enlarged by a factor of 10 with an amplifier. A loudspeaker radiated the LPM signal to a tested spherical object with a 10 cm diameter. The echoed signals were sensed by the four silicon MEMS of SPM0204UD5 acoustical receivers. This model

Object position	average value	standard deviation
First position (pink)		
Distance d (cm)	88.2245	0.1433
Elevation angle α (deg)	72.4113	0.7122
Azimuth angle ϕ (deg)	91.9296	0.3839
Second position (green)		
Distance d (cm)	106.7000	0.2534
Elevation angle α (deg)	75.8840	1.3724
Azimuth angle ϕ (deg)	72.7489	0.8176
Third position (yellow)		
Distance d (cm)	71.5283	0.2534
Elevation angle α (deg)	114.9014	1.0215
Azimuth angle ϕ (deg)	128.2738	0.4027
Fourth position (black)		
Distance d (cm)	77.0861	0.1413
Elevation angle α (deg)	79.9812	1.3728
Azimuth angle ϕ (deg)	124.3327	0.3844
Fifth position (red)		
Distance d (cm)	55.2843	0.0784
Elevation angle α (deg)	108.1178	0.8263
Azimuth angle ϕ (deg)	54.8733	1.4468

Table 6.2 Averages and standard deviations of positions determined in the case of rotating speaker position

has the ability to sense sound pressure or particle velocity in all directions (i.e., it is omnidirectional). The allowed frequencies range from 10 kHz to 100 kHz. As such, the sensor is embedded into a signal processing board with a low-pass frequency circuit with a 60 kHz frequency cutoff and a preamplifier of 20 dB. The minimum sensitivity level of the sensor is -47 dB when the humidity does not exceed 70 R.H. The distance from the Pioneer PT-R4 loudspeaker to the microphones on the X-axis was 10 cm. On the other hand, the distance to the microphones on the Z-axis was 11 cm. The propagation velocity of the ultrasonic wave in the air was approximately 345 m/s at the temperatures from $20-25^o$ C and a humidity of 50 R.H. The signals obtained using the acoustical receivers were converted into one-bit signals by an AD7720 delta-sigma modulator. The sampling frequency of the delta-sigma modulator was 12.5 MHz. The length of the weighted moving average filter for smoothing the cross-correlation

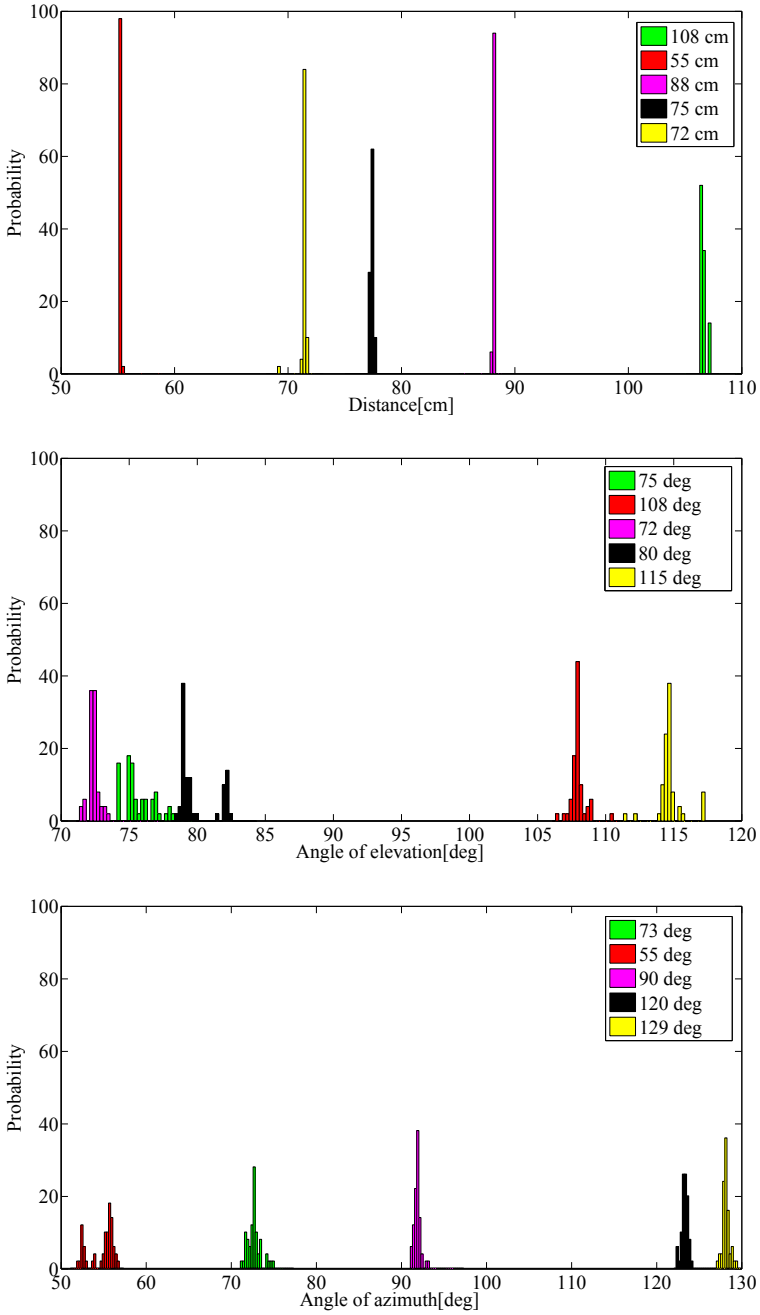

Figure 6.14 Probability of the position measurement in the case of rotating speaker position: distance measurement, elevation-angle measurement, and azimuth-angle measurement.

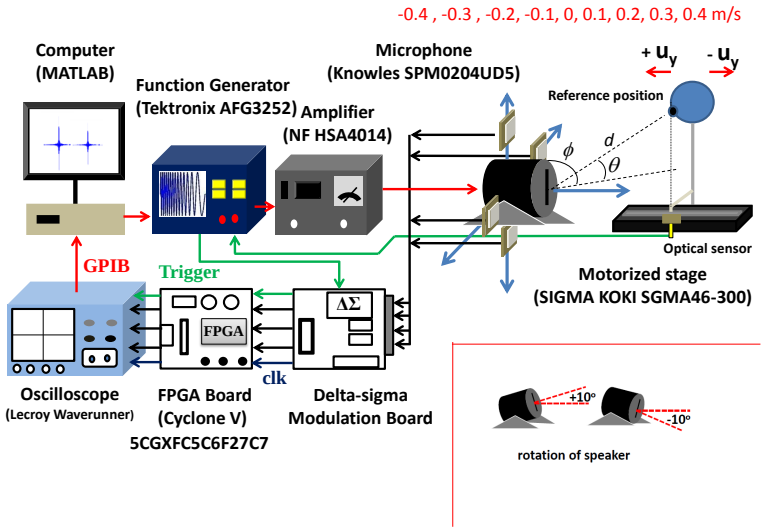

Figure 6.15 Experimental setup for three-dimensional ultrasonic position and velocity measurements.

function was 141 taps. The cross-correlation function for one-bit signal processing was programmed into a Cyclone V 5CGXFC5C6F27C7 FPGA board. The logic utilization specifications for the one-bit cross-correlation function programmed into the FPGA board were 2602 logic elements, 5777 total registers, 175,948 bits of total block memory and 10 total pins. The moving object was driven using a SIGMA KOKI SGMA46-300 motorized stage, which can drive a moving object in only the +Y and -Y direction with maximum and minimum velocities of ± 0.4 m/s; the velocities could be adjusted in ± 0.1 m/s steps. The resolution of the proposed system was approximately 14 μm at a sampling rate of 12.5 MHz with the sound velocity assumed to be 345 m/s.

The distance to the object was repeated continuously in 50 experiments. The cumulative density function of the estimated position at the various velocities are illustrated in Figure 6.16 - 6.18. The first position was located using a soundbeam radiation of the speaker at a fixed position. The range of sound radiation was ± 10^o in the vertical direction and ± 45^o in the horizontal direction. The first position was at distance (d) = 96 cm, elevation angle $(\alpha) = 85^o$ and azimuth angle $(\phi) = 78^o$. The cumulative density function for the first position is shown in Figure 6.16. Averages for the distance, the elevation angle, and the azimuth angle in the first position were 95.7 cm, 4.2^o and 77.3^o, respectively. The maximum standard deviations for the distance, the elevation angle, and the azimuth angle in the first position were 0.037 cm, 0.412^o and 0.392^o,

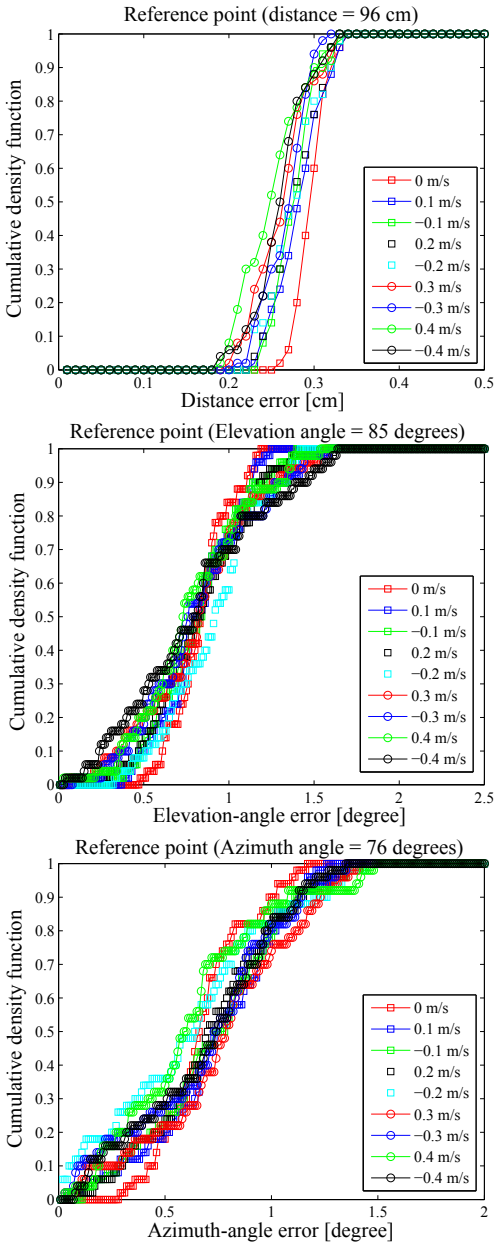

Figure 6.16 The cumulative density function of the first position measurement : distance error, elevation-angle error, and azimuth-angle error.

respectively. For the second position, the tested object was still in the same X-Y quadrant as the first position, but the object was shifted to a positive direction in +Z direction. The object was now outside the range of the main sound beam radiation of

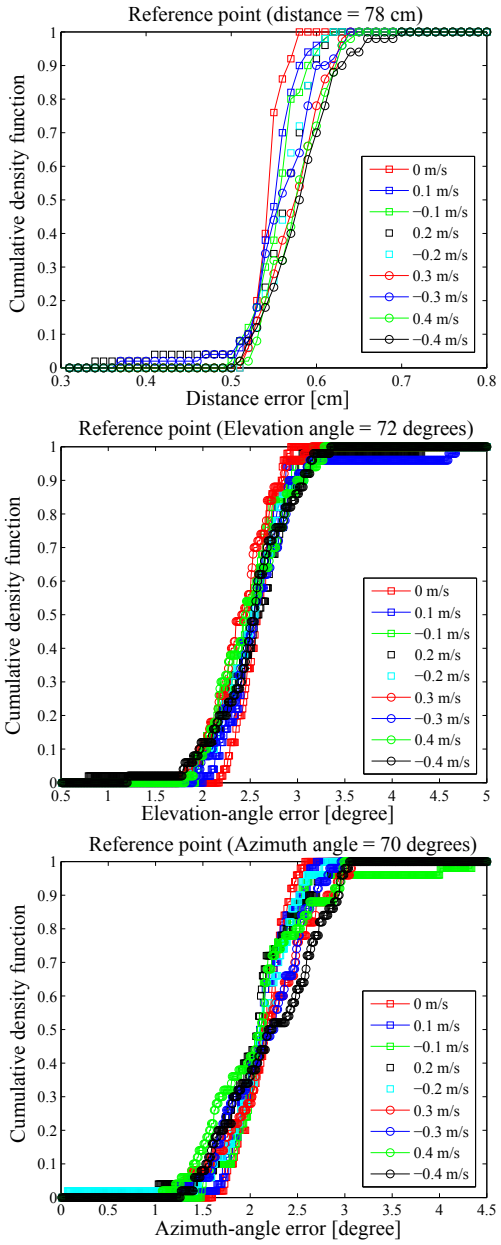

Figure 6.17 The cumulative density function of the second position measurement : distance error, elevation-angle error, and azimuth-angle error.

the speaker. The sound beam in this case had a weaker intensity than the previous case. For the second position, distance $d = 78$ cm, elevation angle $(\alpha) = 72^o$ and azimuth angle $(\phi) = 70^o$. The cumulative density function for the second position is shown in

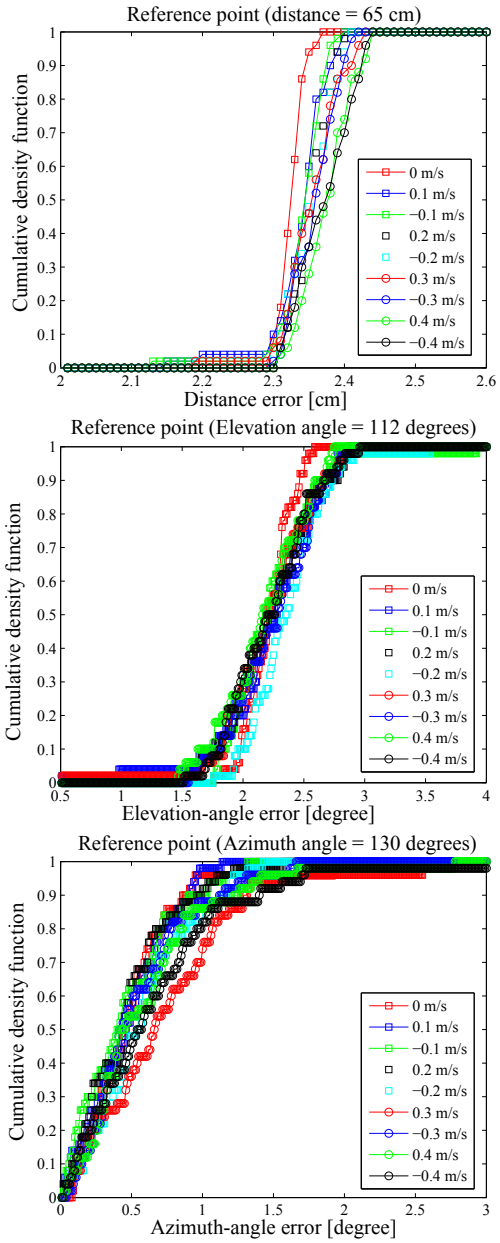

Figure 6.18 The cumulative density function of the third position measurement : distance error, elevation-angle error, and azimuth-angle error.

Figure 6.17. Averages of the distance, the elevation angle, and the azimuth angle for the second position were 76.6 cm, 69.5^o and 72.1^o, respectively. The maximum standard deviations of the distance, the elevation angle, and the azimuth angle for the second

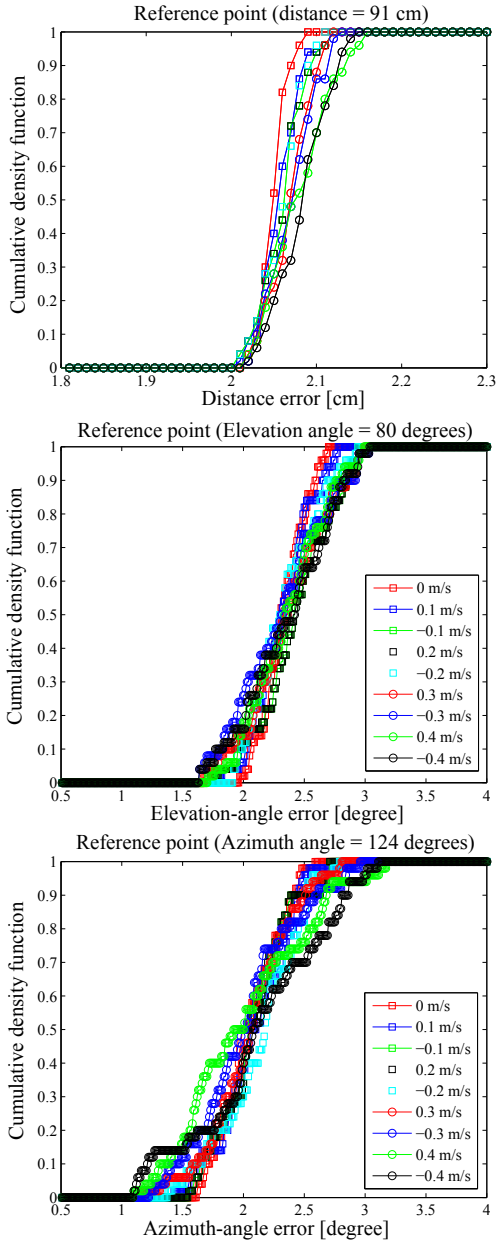

Figure 6.19 The cumulative density function of the fourth position measurement : distance error, elevation-angle error, and azimuth-angle error.

position were 0.0472 cm, 0.515^o, and 0.507^o, respectively. The object position in the third case was assumed to move to the right-hand side of the speaker in the -Z direction. This position also belonged outside of the main sound beam. The third position was

distance (d) = 65 cm, elevation angle (α) = 122^o and azimuth angle (ϕ) = 130^o. The cumulative density function for the third position is depicted in Figure 6.18. The averages of the distance, the elevation angle, and the azimuth angle for the third position were 67.3 cm, -119.7^o and 130.4^o, respectively. The maximum standard deviations of the distance, the elevation angle, and the azimuth angle for the third position were 0.043 cm, 0.765^o and 0.439^o, respectively. Finally, the fourth position was distance (d) = 91 cm, elevation angle (α) = 80^o and azimuth angle (ϕ)= 124^o. The cumulative density function for the fourth position is depicted in Figure 6.19. Averages of the distance, the elevation angle, and the azimuth angle for the fourth position were 93.4 cm, 78.6^o, and 121.9^o, respectively. The maximum standard deviations of the distance, the elevation angle, and the azimuth angle for the fourth position were 0.033 cm, 0.377^o and 0.547^o, respectively.

The object in the experiments was a rigid body, but for the proposed method, we assumed that the object was a point. A measurement point can be estimated from many points on the surface because we do not know the exact reference point on the rigid body that the sound was incident. The exact reference point was unpredictable on the rigid body. For this reason, there were deviations between the reference point and the measurement point. Therefore, fluctuations of measurements are dependent on the direction of the sound propagation from the sound source to the target and the body shape of the object. From the experimental results for the four object positions, we noticed that the distance (d) had the relatively smallest variance when compared with the elevation angle (α) and the azimuth angle (ϕ). The reason is that the computations from TOFs for the α and ϕ parameters are more sensitive than those for the d parameter. For the case when the tested object was outside the main sound beam, we could expand the range of measurements by altering the position of the speaker. The sound beam was shifted up $+10^o$ and down -10^o from the Z-axis by manually lifting the loudspeaker position, as shown in Figure 6.13. The variance of these conditions was not different from the case when the object was inside the main sound beam. In addition, when we increased the velocity of the moving object, a greater variance of position measurements was produced. This is likely due to vibrations in the moving object because the motorized stage for driving the object was controlled by an automatic system for repeated evaluations.

For the velocity measurements, the velocity of the moving object measured by four microphones was estimated using three-dimensional velocity vector measurements. The velocity estimation was composed of X, Y, and Z components, which are represented by u_x, u_y, and u_z. In our experiment, the moving object could be controlled by a motor-

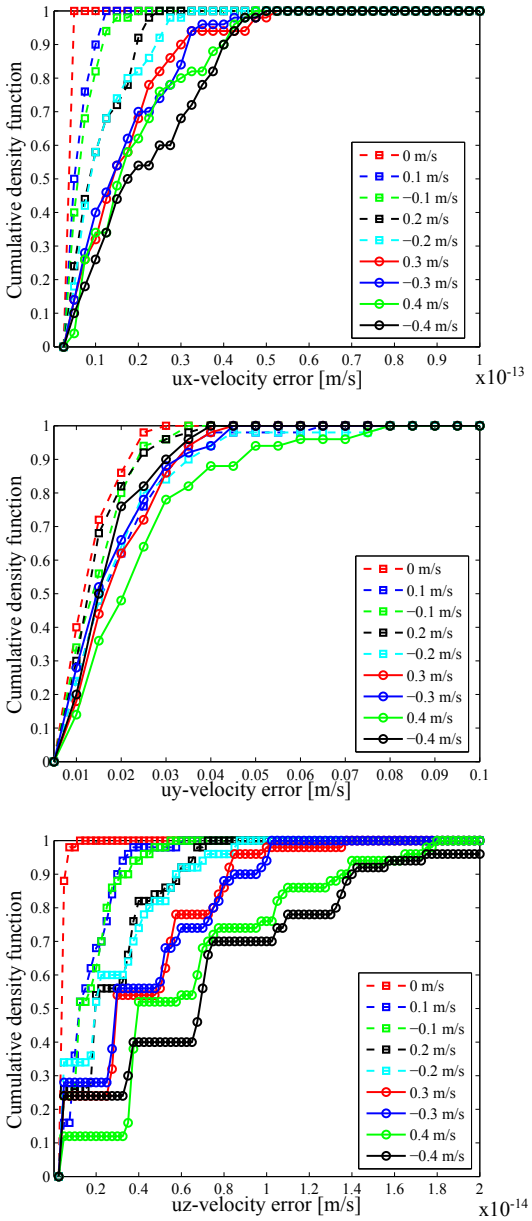

Figure 6.20 The cumulative density function of the velocity measurement at distance (d) = 96 cm, elevation angle (α) = 85^o and azimuth angle (ϕ) = 78^o : u_x velocity error, u_y velocity error, and u_z velocity error.

-ized stage, which could move only along the Y-axis. Therefore, a reference velocity was setup only for the u_y component, and u_x and u_z were assumed to be zero. The velocity measurement results for the first position are shown as Figure 6.20. The u_y

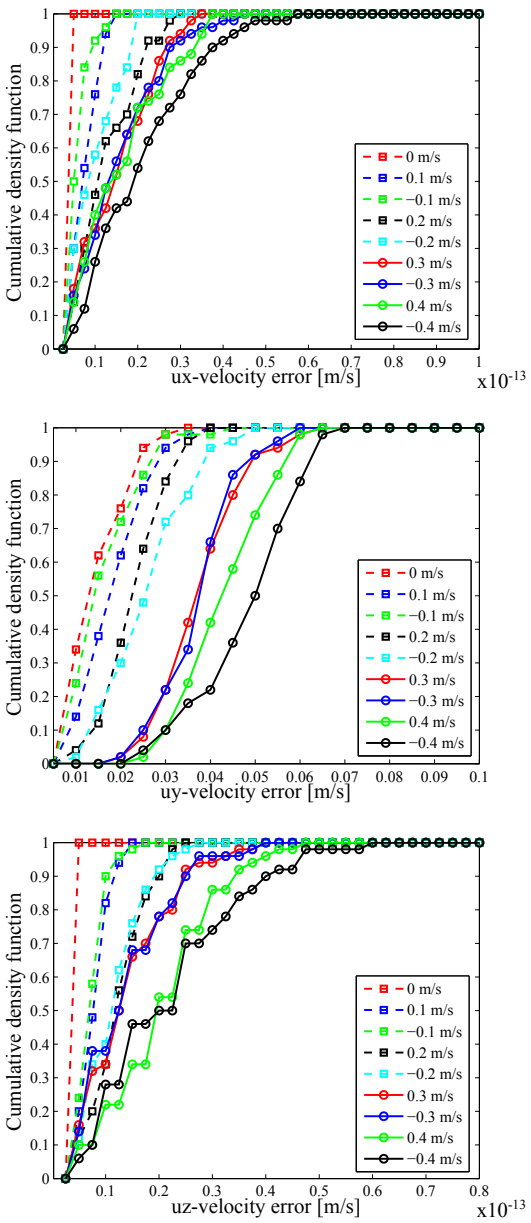

Figure 6.21 The cumulative density function of the velocity measurement at distance (d) = 78 cm, elevation angle (α) = 72^o and azimuth angle (ϕ) = 70^o : u_x velocity error, u_y velocity error, and u_z velocity error.

velocity component for the first case agreed with the reference. The u_x and u_z velocity components for the first case were between -0.1 to 0.1 m/s and -0.04 to 0.04 m/s, respectively. The velocity measurement results for the second case are shown as Figure

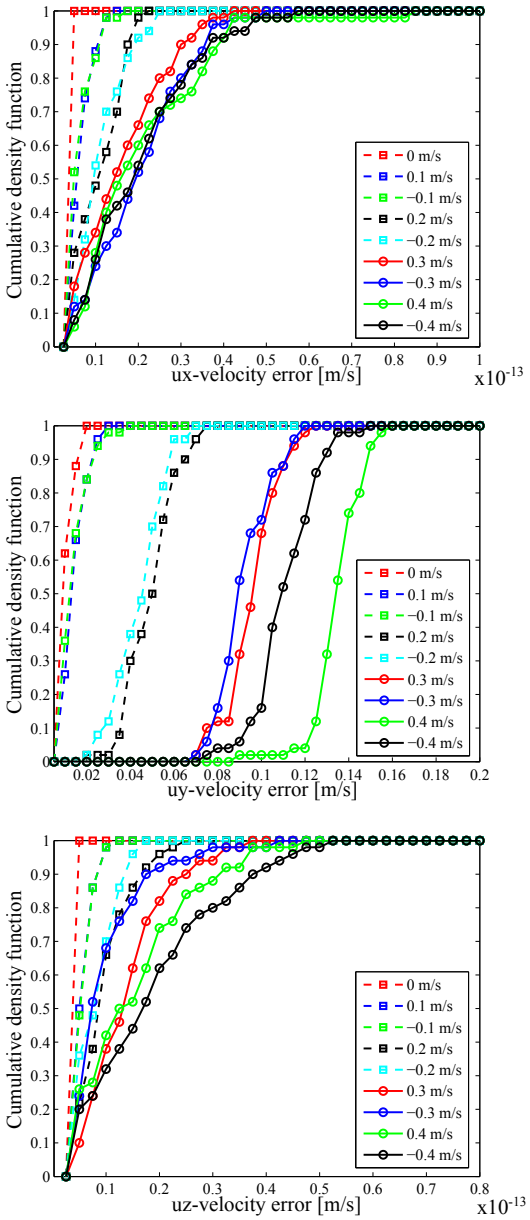

Figure 6.22 The cumulative density function of the velocity measurement at distance (d) = 65 cm, elevation angle (α) = 122^o and azimuth angle (ϕ) = 130^o : u_x velocity error, u_y velocity error, and u_z velocity error.

6.21. The u_y velocity component for the second case was higher than the reference by about ± 0.05 m/s for the higher velocity ± 0.4 m/s. The velocity measurement results for the third case are shown as Figure 6.22. The u_y velocity component for the third

case was smaller than the reference by about ± 0.02 m/s for the higher velocity.

6.4 Optimal microphone position of the Direction-of-Arrival method

Consider in Figure 6.5, accuracy of the object position is assumed that the distance (d) is much more than a duration ($2n$) of the distance between the microphone 3 and 4 located on Z-axis. The elevation angle is determined directly from TOFs of those microphones, and then the distance (d) is computed. In the first case, we will study the duration of varying the microphone position 3 and 4 affecting to accuracy of the object position. The distance between the microphone 3 and 4 was varied from 0.5 to 50 cm, and we fixed the microphone position 1 and 2 located X-axis equal to 10 cm. Simulation results under SNR of 0 dB in Figure 6.23 show that the more distance between the microphone 3 and 4, the more position error. In the next study, the microphone position 3 and 4 is fixed, and the microphone 1 and 2 was varied from 0.5 to 50 cm. In Figure 6.24, it is observed that the more distance between the microphone 1 and 2 is less proportional to the accuracy of the object position. However, in the case of the azimuth-angle error at distance between the microphone 1 and 2 smaller than 10 cm is the most variance, and has the largest error. Finally, we concurrently change every position of microphones in their own position, for example, the microphone 1 in +X direction, the microphone 2 in -X direction, the microphone 3 in +Z, and the microphone in -Z. Simulation results in Figure 6.25 are observed that the optimal microphone positions providing the minimum error are approximately located on 7 cm in each axis when the object position was assumed at distance (d) = 80 cm, elevation angle (α) = 75^o and azimuth angle (ϕ) = 120^o. Next, If the object was shifted closer to the speaker position at distance (d) = 80 cm, elevation angle (α) = 75^o and azimuth angle (ϕ) = 120^o, simulation results show the optimal microphone position at 5 cm, as shown in Figure 6.26.

6.5 Summary

A three-dimensional position and velocity measurement based on an oversampling signal processing method using an LPM ultrasonic signal was demonstrated. The velocity measurements were computed based on the three-dimensional velocity vector measurements. The object position was estimated using spherical coordinates (i.e., the distance from the sound source to the target, the angle of elevation, and the azimuth angle).

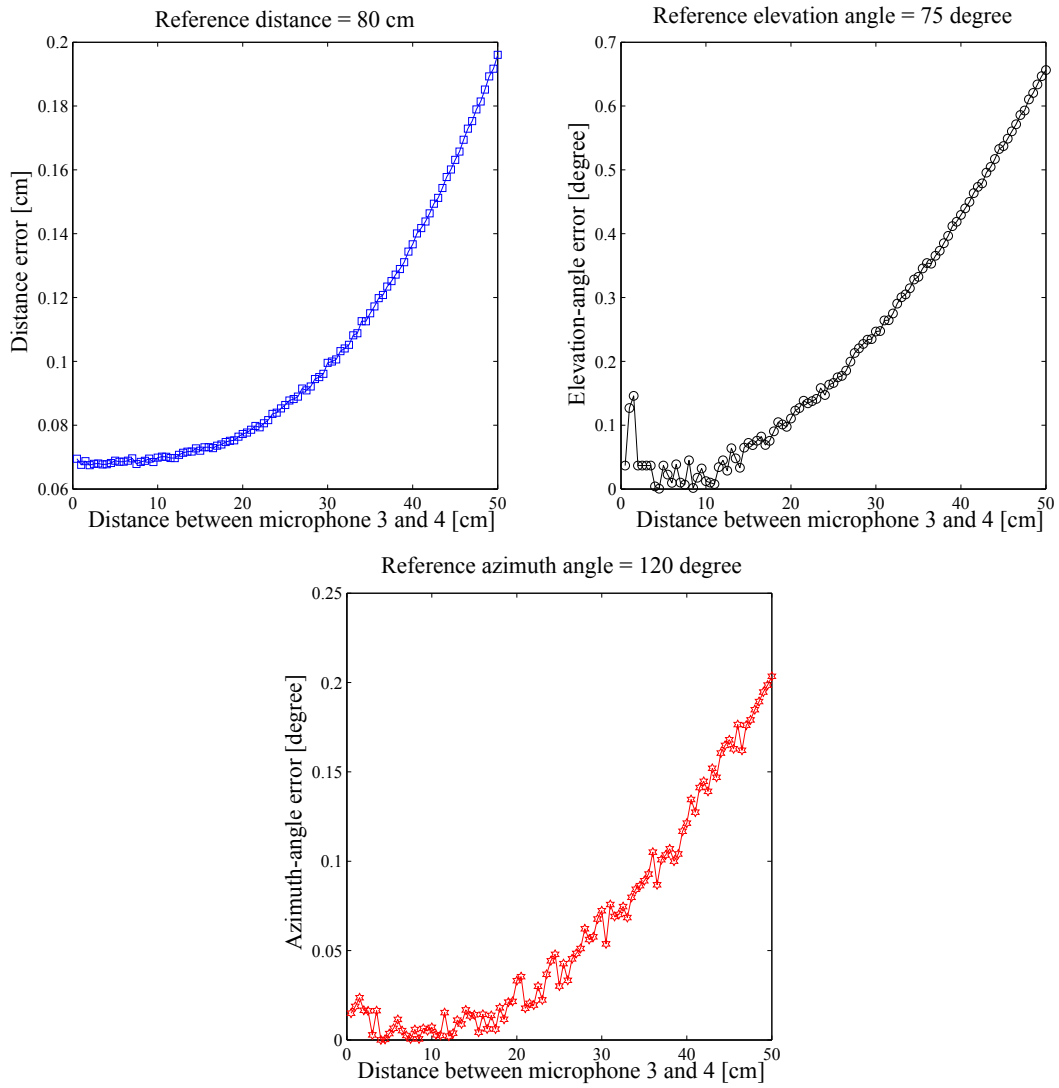

Figure 6.23 The object position error when varying distance between the microphone 3 and 4 and fixing the microphone 1 and 2 at 10 cm: distance (d) = 80 cm, elevation angle (α) = 75^o and azimuth angle (ϕ) = 120^o.

Positions determined in the proposed system were evaluated by experiments using ultrasonic position measurements. The object position can be sensed by the sound beam propagated by a loudspeaker. Rotating the loudspeaker can expand the range of measurements to a wider area. Accuracy of the proposed method for position measurements was expressed as the probability distributions for 50 trials. Averages and standard deviations were used to determine the reliability of the measurements. The resolution of

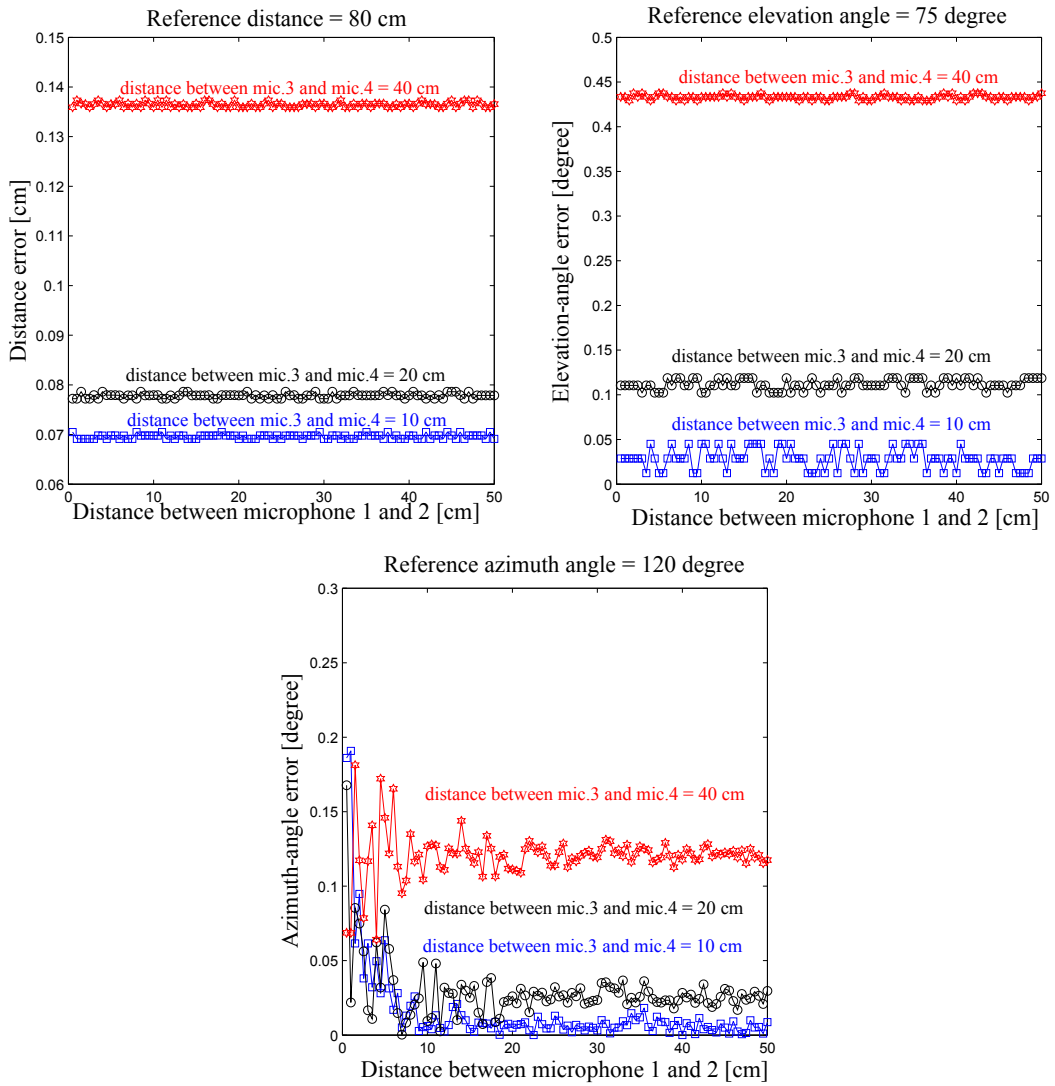

Figure 6.24 The object position error when varying distance between the microphone 1 and 2 and fixing the microphone 3 and 4 at 5, 10, 20 cm: distance (d) = 80 cm, elevation angle (α) = 75^o and azimuth angle (ϕ) = 120^o.

the proposed system was approximately 14 μm for a sound velocity of 345 m/s and a sampling rate of 12.5 MHz. The deviation of the actual results is for a point, but the target was a spherical ball. We do not know exactly where the reference point was located on the target object. Therefore, the reference of the object position was fixed to the center on the surface of the ball. The sound wave from the loudspeaker might

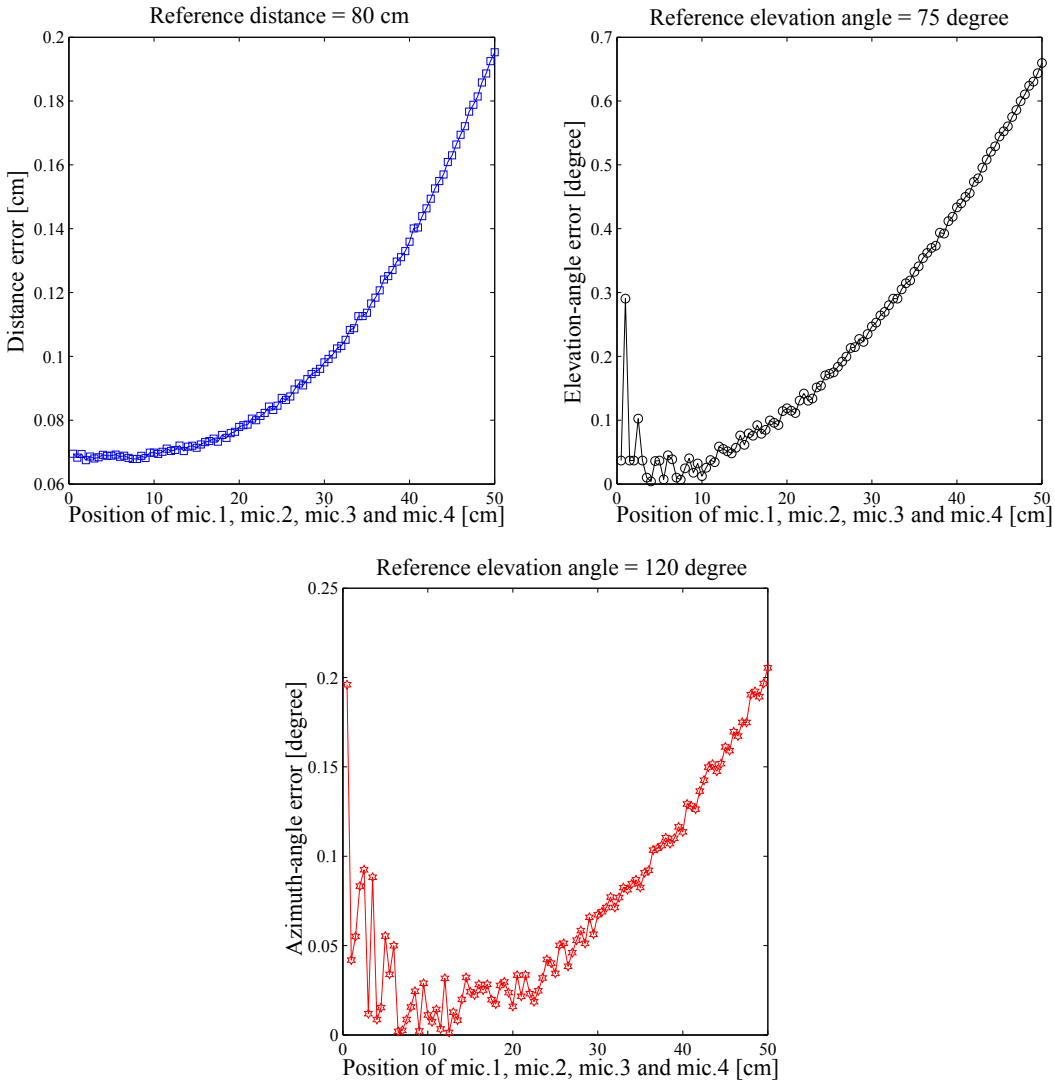

Figure 6.25 The optimal microphone position providing the minimum error at distance $(d) = 80$ cm, elevation angle $(\alpha) = 75^o$ and azimuth angle $(\phi) = 120^o$.

not have been incident to the reference point that we had assumed. It is thus difficult to compare the experimental results with the true value. The velocity estimation was made up of components in the X, Y, and Z directions. The proposed method can estimate the moving object in only the Y direction. The velocity measurements of the X and Z components were completely zero.

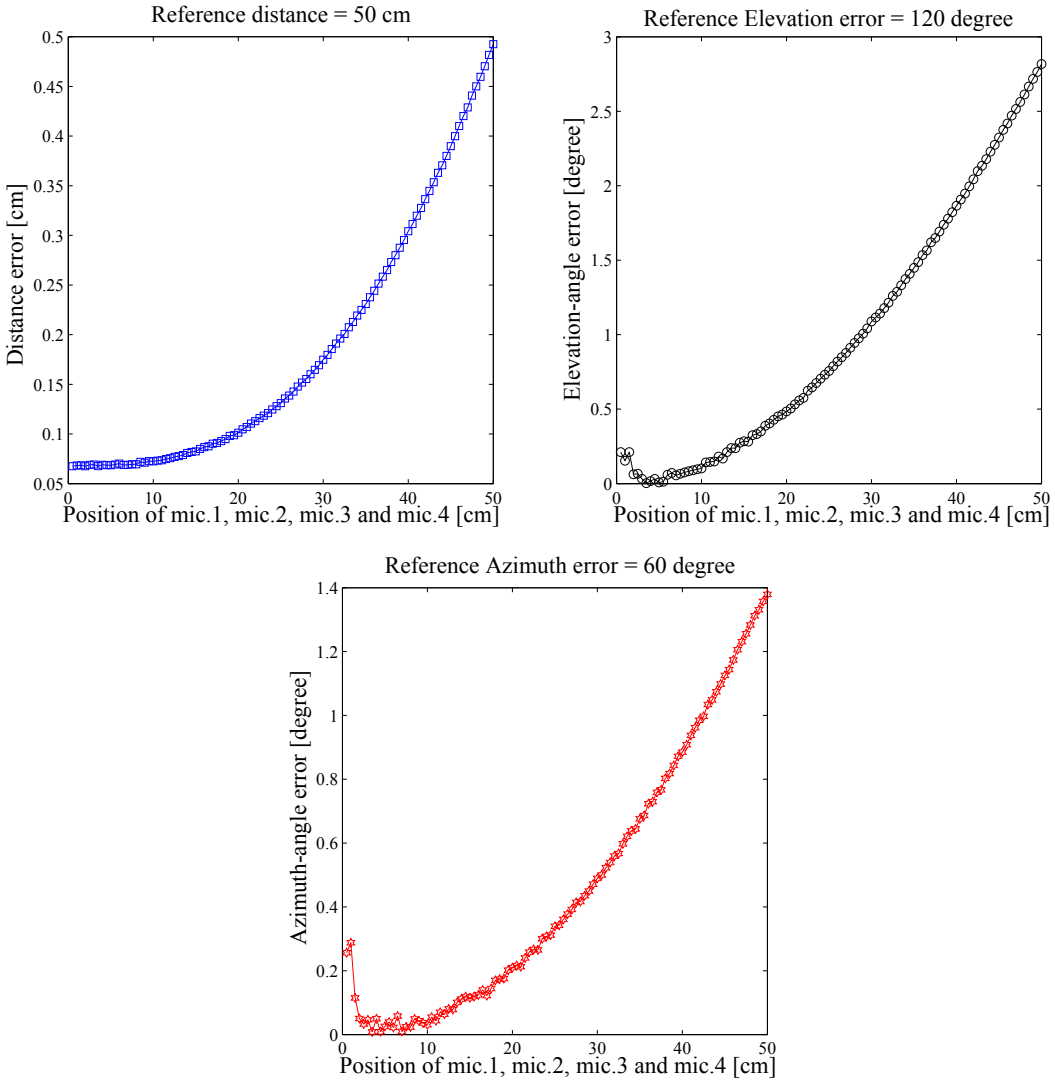

Figure 6.26 The optimal microphone position providing the minimum error at distance $(d) = 50$ cm, elevation angle $(\alpha) = 120^o$ and azimuth angle $(\phi) = 60^o$.

7

Ultrasonic position and velocity measurement by a linearization-based method (Third method)

7.1 Position measurement using a linearization-based method

In the previous method relied on an Direction-of-Arrival method, the four microphone positions have to be located X and Z axes for the object location achievement. Sometimes, this arrangement is not flexible when the microphone positions are required to be positioned in somewhere over X and Z axes. In addition, carefully scrutinizing in three dimensional spaces, although the original mathematics is written in three non-linear equations, the number of unknown variables equals three. We can redesign the microphone position to satisfy three unknowns by using three microphones, and convert equations from linearity into non-linearity. In this chapter, we propose a method based on only linear equations for position and velocity measurement.

7.1.1 Introduction to linear algebra

This chapter begins with the warmth up of linear algebra: solving linear equations. The most significant case, and the simplest, is when the number of unknowns equals

the number of equations. We have n equations in n unknowns, for example:

$$\begin{aligned} 1x + 2y &= 3 \\ 2x + 2y &= 4 \end{aligned} \tag{7.1}$$

The unknowns are x and y. Elimination method and determinants method are described to solve these equations. Certainly, x and y are determined from only the numbers 1,2,3 and 4 to solve the system.

1) Elimination method is subtraction the first equation from the second equation. This eliminate x from the second equation, and it leaves one equation for y:

$$\begin{aligned} &\text{(equation 2)-2(equation 1)} \\ &-2y = -2. \end{aligned} \tag{7.2}$$

Now, we know y=1. Then x comes form the first or the second equation by back-substitution x=1.

2) Determinants method is a ratio of determinants and written down for solution directly:

$$y = \frac{\begin{bmatrix} 1 & 3 \\ 2 & 4 \end{bmatrix}}{\begin{bmatrix} 1 & 2 \\ 2 & 2 \end{bmatrix}} = \frac{1 \cdot 4 - 2 \cdot 3}{1 \cdot 2 - 2 \cdot 2} = \frac{-2}{-2} = 1. \tag{7.3}$$

$$x = \frac{\begin{bmatrix} 3 & 2 \\ 4 & 2 \end{bmatrix}}{\begin{bmatrix} 1 & 2 \\ 2 & 2 \end{bmatrix}} = \frac{3 \cdot 2 - 4 \cdot 2}{1 \cdot 2 - 2 \cdot 2} = \frac{-2}{-2} = 1. \tag{7.4}$$

Linear equations lead to geometry of planes. Practically, it is not simple to visualize in many dimensional planes in several dimensional spaces, for example, ten equations. It is more difficult to see ten of those planes, intersecting at the solution to ten equations. The simple example has two lines in Figure 7.1, meeting at the point $(x, y) = (-1, 2)$. This is used for representing linear algebra into ten dimensions, where the intuition has to imagine the geometry. Next, we move to matrix notation, writing the n unknowns as a vector x and the n equations as $Ax = b$. A is multiplied by elimination matrices

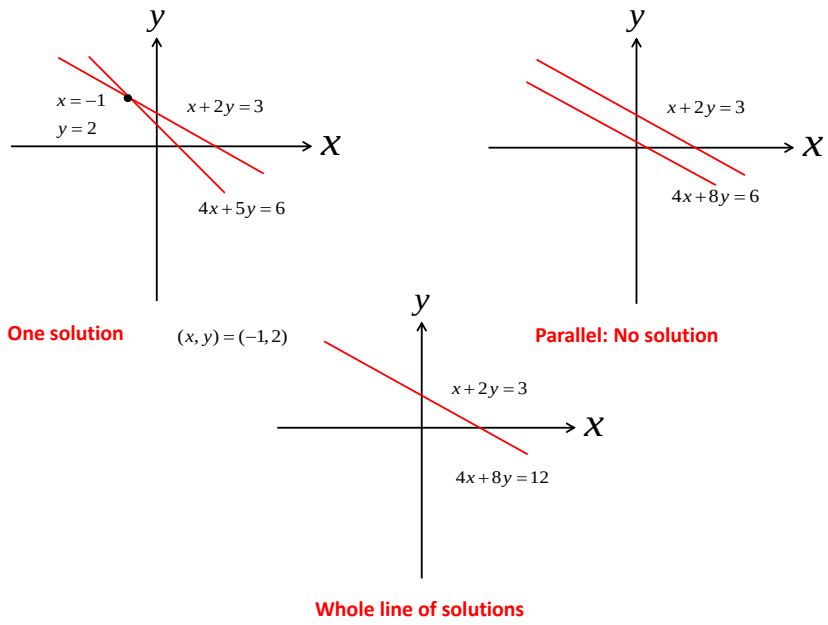

Figure 7.1 The example has one solution. Singular cases have none or too many.

to achieve an upper triangular matrix U. Those procedures factor A into L times U, where L is lower triangular. A and its factors are explained:

$$\text{Factorization} A = \begin{bmatrix} 1 & 2 \\ 4 & 5 \end{bmatrix} = \begin{bmatrix} 1 & 0 \\ 4 & 1 \end{bmatrix} \begin{bmatrix} 1 & 2 \\ 0 & -3 \end{bmatrix} = L \text{times} U. \tag{7.5}$$

First we introduce matrices and vectors and the rules for multiplication. Every matrix obtains a transpose A^T, and also has an inverse A^{-1}. In most cases elimination moves forward without difficulties. The matrix has an inverse and the system $Ax = b$ provides one solution. In exceptional cases the method will break down-either the equations were written in the wrong order, which is easily fixed by converting them, or the equations do not have a unique solution.This singular case has no solution. Other singular cases have infinitely many solutions. In this chapter, we will use this definition to find every possible solution for position measurement in three dimensional space.

7.1.2 Three-dimensional-positioning using a linearization-based method

In Figure 7.2, the designed system can detect the object on ranging measurements from -X to +X axis and from -Z to +Z axis. The object appears in front of the loudspeaker

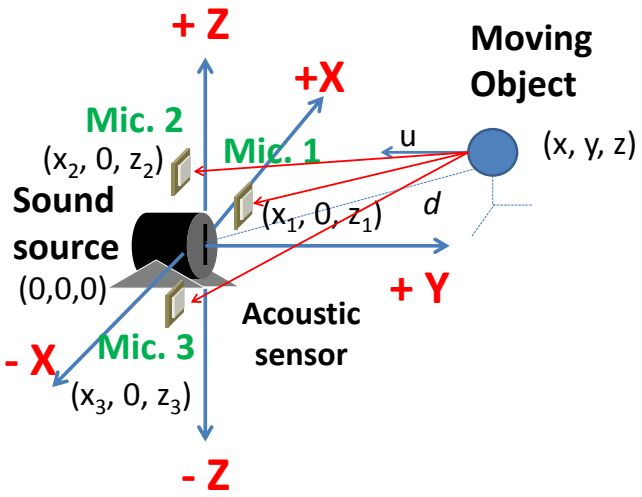

Figure 7.2 Design of microphone position for linear system support.

in +Y axis. We assume that the position of three microphones can freely be placed on X-Z plane. Their position are $(x_1, 0, z_1)$, $(x_2, 0, z_2)$, and $(x_3, 0, z_3)$, and the object has an unknown position as a small point on (x, y, z). d is a distance between an original point and the object. A simple equation of the microphone position, the object position, and the TOF is

$$d + \sqrt{(x - x_i)^2 + y^2 + (z - z_i)^2} = TOF_i \cdot v_0, \tag{7.6}$$

where i is 1,2, and 3. Because Equation (7.6) is a nonlinear form, it has to be rewritten as a linear form as

$$\left(\sqrt{(x - x_i)^2 + y^2 + (z - z_i)^2}\right)^2 = \left(TOF_i \cdot v_0 - d\right)^2, \tag{7.7}$$

$$x^2 - 2x \cdot x_i + x_i^2 + y^2 + z^2 - 2z \cdot z_i + z_i^2 = \left(TOF_i \cdot v_0\right)^2 - 2TOF_i \cdot v_0 \cdot d + d^2 \tag{7.8}$$

$$-2x_i \cdot x - 2z_i \cdot z + 2TOF_i \cdot v_0 \cdot d = \left(TOF_i \cdot v_0\right)^2 - x_i^2 - z_i^2 \tag{7.9}$$

Now, we already have three unknown parameters x, y, and d. x and y are the object position and d is a distance from an original point to a target. We can write this equation into a matrix.

$$2 \cdot \boldsymbol{A} \cdot \boldsymbol{b} = \boldsymbol{c}, \tag{7.10}$$

where

$$\boldsymbol{A} = \begin{bmatrix} -x_1 & -z_1 & TOF_1 \cdot v_0 \\ -x_2 & -z_2 & TOF_2 \cdot v_0 \\ -x_3 & -z_3 & TOF_3 \cdot v_0 \end{bmatrix}, \boldsymbol{b} = \begin{bmatrix} x \\ z \\ d \end{bmatrix},$$

and

$$\boldsymbol{c} = \begin{bmatrix} TOF_1^2 \cdot v_0^2 - x_1^2 - z_1^2 \\ TOF_2^2 \cdot v_0^2 - x_2^2 - z_2^2 \\ TOF_3^2 \cdot v_0^2 - x_3^2 - z_3^2 \end{bmatrix}.$$

$\boldsymbol{b}$ is unknown parameters. A matrix $\boldsymbol{A}$ consists of any locations of the microphone position and the TOFs. In practical, the matrix $\boldsymbol{A}$ might be a deficient matrix from these values if the determinant is zero. Thus, this system should be designed to avoid the singular-matrix problem due to det.$(\boldsymbol{A}) = 0$. For det.$\boldsymbol{A}$,

$$\text{det.}\boldsymbol{A} = (x_2 \cdot z_3 - x_3 \cdot z_2) \cdot TOF_1 \cdot v_0 + (x_3 \cdot z_1 - x_1 \cdot z_3) \cdot TOF_2$$

$$\cdot v_0 + (x_1 \cdot z_2 - x_2 \cdot z_1) \cdot TOF_3 \cdot v_0 \neq 0. \tag{7.11}$$

Look at Equation (7.11), TOF_1, TOF_2 and TOF_3 are definitely positive in every situation. We can only consider in some terms of Equation (7.11) that are $(x_2 \cdot z_3 - x_3 \cdot z_2)$, $(x_3 \cdot z_1 - x_1 \cdot z_3)$, and $(x_1 \cdot z_2 - x_2 \cdot z_1)$. These terms are designed freely from the microphone location. To guarantee that the design of the microphone position does not make the matrix $\boldsymbol{A}$ singular, the microphone locations have to satisfy Equation (7.11) when $(x_2 \cdot z_3 - x_3 \cdot z_2) > 0$, $(x_3 \cdot z_1 - x_1 \cdot z_3) > 0$, and $(x_1 \cdot z_2 - x_2 \cdot z_1) > 0$ This condition can make det.$\boldsymbol{A}$ only positive and impossible for zero value.

In the next step, the unknown parameters in Equation (7.10) will be solved by the row echelon form of $\boldsymbol{A}$ and $\boldsymbol{c}$. Assume that $a_1 = \frac{x_2}{x_1}$ multiplies to the first row of the matrices $\boldsymbol{A}$ and $\boldsymbol{c}$ and then subtracted from the second row of $\boldsymbol{A}$ and $\boldsymbol{c}$, we have new

forms $\boldsymbol{A'}$ and $\boldsymbol{c'}$ as

$$\boldsymbol{A'} = \begin{bmatrix} -x_1 & -z_1 & TOF_1 \cdot v_0 \\ 0 & -z_2 + a_1 \cdot z_1 & TOF_2 \cdot v_0 - a_1 \cdot TOF_1 \cdot v_0 \\ -x_3 & -z_3 & TOF_3 \cdot v_0 \end{bmatrix} \tag{7.12}$$

and

$$\boldsymbol{c'} = \begin{bmatrix} c(1,1) \\ c(2,1) - a_1 \cdot c(1,1) \\ c(3,1) \end{bmatrix}.$$

where $c(1,1) = TOF_1^2 \cdot v_0^2 - x_1^2 - z_1^2$, $c(2,1) = TOF_2^2 \cdot v_0^2 - x_2^2 - z_2^2$, and $c(3,1) = TOF_3^2 \cdot v_0^2 - x_3^2 - z_3^2$ Next, $a_2 = \frac{x_3}{x_1}$ times the first row of the matrix $\boldsymbol{A'}$ and $\boldsymbol{c'}$ and subtracted from the third row. We can get

$$\boldsymbol{A''} = \begin{bmatrix} -x_1 & -z_1 & TOF_1 \cdot v \\ 0 & -z_2 + a_1 \cdot z_1 & TOF_2 \cdot v_0 - a_1 \cdot TOF_1 \cdot v_0 \\ 0 & -z_3 + a_2 \cdot z_1 & TOF_3 \cdot v_0 - a_2 \cdot TOF_1 \cdot v_0 \end{bmatrix}. \tag{7.13}$$

and

$$\boldsymbol{c''} = \begin{bmatrix} c(1,1) \\ c(2,1) - a_1 \cdot c(1,1) \\ c(3,1) - a_2 \cdot c(1,1) \end{bmatrix}.$$

from the third row. Therefore, $\boldsymbol{A'''}$ and $\boldsymbol{c'''}$ are

$$\boldsymbol{A'''} = \begin{bmatrix} -x_1 & -z_1 & TOF_1 \cdot v \\ 0 & -z_2 + a_1 \cdot z_1 & \Big(TOF_2 - a_1 \cdot TOF_1\Big) \cdot v_0 \\ 0 & 0 & \Big(TOF_3 - a_2 \cdot TOF_1\Big) \cdot v_0 - \Big(TOF_2 - a_1 \cdot TOF_1\Big) \cdot v_0 \cdot a_3 \end{bmatrix} \tag{7.14}$$

and

$$\boldsymbol{c'''} = \begin{bmatrix} c(1,1) \\ c(2,1) - a_1 \cdot c(1,1) \\ c(3,1) + (a_1 \cdot a_3 - a_2) \cdot c(1,1) - a_3 \cdot c(2,1) \end{bmatrix}.$$

We call $\boldsymbol{A'''}$ the upper-traingular matrix of $\boldsymbol{A}$. The determinant of $\boldsymbol{A'''}$ is same as

$\boldsymbol{A}$. In addition, when we look at $\boldsymbol{A'''}$, the first pivot,$-x_1$, must not be zero. The first microphone position has to satisfy this condition. As for other terms in diagonal line of $\boldsymbol{A'''}$, they are not zero if the microphone position is designed according to Equation (7.11). Then, we can find out the unknown parameter, $\boldsymbol{b}$, using Equation (7.15)

$$2 \cdot \boldsymbol{A'''} \cdot \boldsymbol{b} = \boldsymbol{c'''}. \tag{7.15}$$

$$2 \cdot \begin{bmatrix} -x_1 & -z_1 & TOF_1 \cdot v_0 \\ 0 & -z_2 + a_1 \cdot z_1 & \Big(TOF_2 - a_1 \cdot TOF_1\Big) \cdot v_0 \\ 0 & 0 & \Big(TOF_3 - a_2 \cdot TOF_1\Big) \cdot v_0 - \Big(TOF_2 - a_1 \cdot TOF_1\Big) \cdot v_0 \cdot a_3 \end{bmatrix} \cdot \begin{bmatrix} x \\ z \\ d \end{bmatrix}$$

$$= \begin{bmatrix} c(1,1) \\ c(2,1) - a_1 \cdot c(1,1) \\ c(3,1) + (a_1 \cdot a_3 - a_2) \cdot c(1,1) - a_3 \cdot c(2,1) \end{bmatrix}.$$

Therefore, the object position is

$$d = \frac{0.5 \cdot \boldsymbol{c'''}(3,1)}{\Big((a_1 \cdot a_3 - a_2) \cdot TOF_1 - a_3 \cdot TOF_2 + TOF_3\Big) \cdot v_0} \tag{7.16}$$

$$z = \frac{0.5 \cdot \boldsymbol{c'''}(2,1) - (TOF_2 - a_1 \cdot TOF_1) \cdot v_0 \cdot d}{a_1 \cdot z_1 - z_2} \tag{7.17}$$

$$x = \frac{TOF_1 \cdot v_0 \cdot d - 0.5 \cdot \boldsymbol{c'''}(1,1) - z_1 \cdot z}{x_1} \tag{7.18}$$

$$y = \sqrt{d^2 - z^2 - x^2} \tag{7.19}$$

7.1.3 Simulation results for three-dimensional-positioning using a Direction-of-Arrival method

Simulation results are performed to represent the proposed three-dimensional-positioning method by a linearization-based method. We will show that how it works by assuming that an object position is x=80 cm, y=75 cm, z=60 cm and the microphone positions are (10 cm, 0 cm, -10 cm), (0 cm, 0 cm, 10 cm), and (-10 cm, 0 cm, -10 cm). The

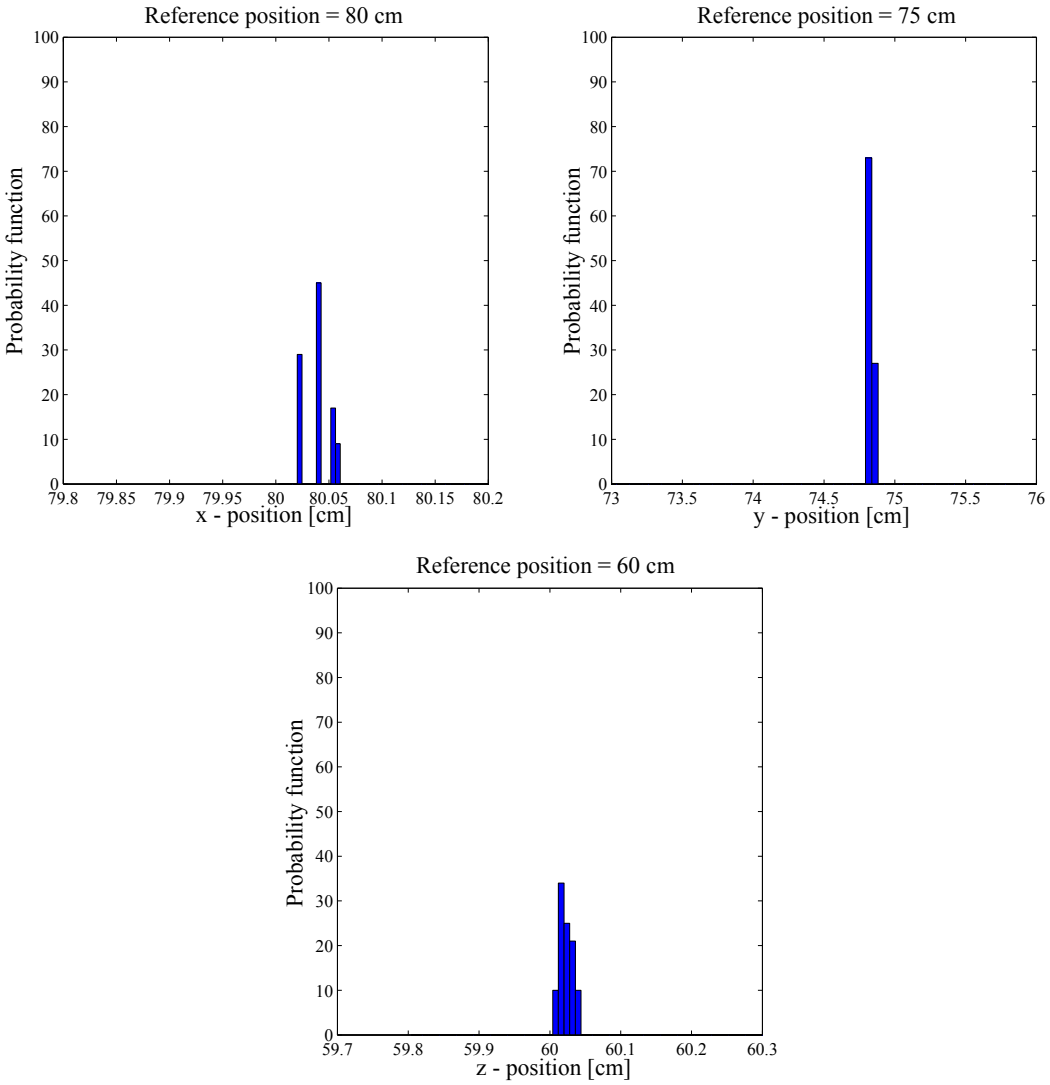

Figure 7.3 The probability distributions of simulations at the position: x = 80 cm, y = 75 cm, and z = 60 cm.

object position estimation under an ultrasonic three-dimensional system determined by the proposed one-bit signal processing method was evaluated by MATLAB computer simulation. The period of the single LPM signal was swept linearly from 20 μs to 50 μs. The sampling frequency rate was 12.5 MHz. The LPM signal had the length equal to 3.278 ms. The propagation velocity of an ultrasonic wave in air was 345.1 m/s at 22.4 C^o. SNR was set at 0 dB compared with the echo signal. The constant attenuation factor of the received signal was -2.107 dB/m degraded from that of the original signal.

The received signals and the normalized cross-correlation functions are obtained by one-bit signal processing. The received signals were changed into the single-bit delta-sigma modulated signal by the 7^{th}-order delta-sigma modulator. The one-bit signal of the received echo was correlated together with the one-bit signal of the reference, which was the transmitted LPM signal converted into the one-bit digital signal by a digital comparator. The cross-correlation function of the one-bit received signal and the one-bit reference signal was obtained directly from the recursive cross-correlation operation of one-bit signal processing and the smoothing operation accomplished by the triangular weighted moving average filter. Signal had 399 zero-cross points. Accordingly, the computational cost of the recursive cross-correlation operation was the integration and 401 summations of one-bit samples. For the smoothing operation, the length of the triangular weighted moving average filter, which consists of a pair of 55-tap moving average filters, was 109 taps. The position error by the noise included in the received echoes was evaluated by MATLAB computer simulation. In the simulation, the SNR (0 dB) of the reflected echo was converted by including normal distribution of random noises, or white noise, to the received echoes. In the case of each SNR, the position of the estimation was evaluated from 100 simulations. The probability distributions of the estimated position are determined from 100 estimation and illustrated in Figure 7.3. The simulation results was observed that the x-position is approximately 80.5 cm, the y-position is between 74.8 to 74.9 cm, and the z-position is 60 to 60.05 cm.

7.1.4 Comparison with the Cramer-Rao Lower Bound

In general, any unknown parameter estimators should be unbiased on the average, and the variance is smaller than that of the other estimators. The Cramer-Rao Lower Bound (CRLB) is the lowest possible variance that an unbiased estimator can obtain. First, we have to consider a model of the proposed method. A object in a three-dimension scenario used to determine the position is $\mathbf{p} = [x, y, z]^T$, and the microphone position $\mathbf{s_i} = [x_i, 0, y_i]^T$ $i = 1$, 2, and 3 is assumed known, as shown Figure 7.2. As proposed in Equation (7.6), we have three unknown parameter $\mathbf{b} = [x, z, d]^T$ to be estimated and can consider a linear model of Equation (7.6) as

$$r_i = |\mathbf{p} - \mathbf{s_i}| + d = \sqrt{(\mathbf{p} - \mathbf{s_i})^T(\mathbf{p} - \mathbf{s_i})} + d, \tag{7.20}$$

where r_i is the distance between the speaker, object, and the microphone i. We will

assume that the TOF measurements can be expressed by the additive noise model as

$$\mathbf{r} = r_i + \Delta r_i \tag{7.21}$$

where $\mathbf{r} = [r_1, r_2, r_3]^T$, and is noise from TOF_i. It is zero mean and has covariance matrix $\mathbf{Q}$.

$$\mathbf{Q} = \begin{bmatrix} \sigma_1^2 & 0 & 0 \\ 0 & \sigma_2^2 & 0 \\ 0 & 0 & \sigma_3^2 \end{bmatrix} \tag{7.22}$$

In the presence of TOF noise, noisy values result in the equation error vector from Equation (7.6).

$$\varepsilon = \mathbf{c} - \mathbf{A}\mathbf{b} \tag{7.23}$$

The least square (LS) solution of $\mathbf{b}$ that minimize ε is

$$\mathbf{b} = (\mathbf{A}^T\mathbf{A})^{-1}\mathbf{A}^T\mathbf{c} \tag{7.24}$$

The Probability Density Function (PDF) is viewed as a function of the unknown parameters as

$$p_i(r_i; \mathbf{b}) = \prod_{n=0}^{N-1} \frac{1}{\sqrt{2\pi\sigma^2}} \exp\Big(-\frac{1}{2\sigma^2}\Big[r_i[n] - \sqrt{(\mathbf{p}-\mathbf{s_i})^T(\mathbf{p}-\mathbf{s_i})} - d\Big]^2\Big) \tag{7.25}$$

Next, in the presence of noise, the variances cannot be less than those expressed by the CRLB. CRLB is equal to the inverse of the Fisher matrix defined as

$$\mathbf{J} = -E\Big[\Big(\frac{\partial \ln p(\mathbf{r};\mathbf{b})}{\partial \mathbf{b}}\Big)^T\Big(\frac{\partial \ln p(\mathbf{r};\mathbf{b})}{\partial \mathbf{b}}\Big)\Big] \tag{7.26}$$

After taking natural logarithm and then differentiating this function, the CRLB for the underlying problem can be reduced to [80]

$$\begin{aligned} \mathrm{CRLB}(\mathbf{b}) &= \mathbf{J}^{-1} \\ &= \Big[\Big(\frac{\partial \mathbf{r}(\mathbf{b})}{\partial \mathbf{b}}\Big)^T \mathbf{Q}^{-1}\Big(\frac{\partial \mathbf{r}(\mathbf{b})}{\partial \mathbf{b}}\Big)\Big]^{-1} \end{aligned} \tag{7.27}$$

The terms along the diagonal of inverse Fisher information matrix result in the CRLB

bounds on the variances:

$$\mathrm{var}(\hat{x}) \geq \frac{\sigma^2}{\det(\mathbf{J})N}[9 + 6A_1 - 4A_2^2] \tag{7.28}$$

$$\mathrm{var}(\hat{z}) \geq \frac{\sigma^2}{\det(\mathbf{J})N}[9 + 6B_1 - 4B_2^2] \tag{7.29}$$

$$\mathrm{var}(\hat{d}) \geq \frac{\sigma^2}{\det(\mathbf{J})N}[4A_1B_1 - 6(B_1 + A_1 + 2C_1) - C_1^2] \tag{7.30}$$

where N is all trials and

$$A_1 = \frac{(z - z_1)^2}{\sqrt{(\mathbf{p} - \mathbf{s_1})^T(\mathbf{p} - \mathbf{s_1})}} + \frac{(z - z_2)^2}{\sqrt{(\mathbf{p} - \mathbf{s_2})^T(\mathbf{p} - \mathbf{s_2})}} + \frac{(z - z_3)^2}{\sqrt{(\mathbf{p} - \mathbf{s_3})^T(\mathbf{p} - \mathbf{s_3})}}$$

$$A_2 = \frac{(z - z_1)}{\sqrt{(\mathbf{p} - \mathbf{s_1})^T(\mathbf{p} - \mathbf{s_1})}} + \frac{(z - z_2)}{\sqrt{(\mathbf{p} - \mathbf{s_2})^T(\mathbf{p} - \mathbf{s_2})}} + \frac{(z - z_3)}{\sqrt{(\mathbf{p} - \mathbf{s_3})^T(\mathbf{p} - \mathbf{s_3})}}$$

$$B_1 = \frac{(x - x_1)^2}{\sqrt{(\mathbf{p} - \mathbf{s_1})^T(\mathbf{p} - \mathbf{s_1})}} + \frac{(x - x_2)^2}{\sqrt{(\mathbf{p} - \mathbf{s_2})^T(\mathbf{p} - \mathbf{s_2})}} + \frac{(z - z_3)^2}{\sqrt{(\mathbf{p} - \mathbf{s_3})^T(\mathbf{p} - \mathbf{s_3})}}$$

$$B_2 = \frac{(x - x_1)}{\sqrt{(\mathbf{p} - \mathbf{s_1})^T(\mathbf{p} - \mathbf{s_1})}} + \frac{(x - x_2)}{\sqrt{(\mathbf{p} - \mathbf{s_2})^T(\mathbf{p} - \mathbf{s_2})}} + \frac{(x - x_3)}{\sqrt{(\mathbf{p} - \mathbf{s_3})^T(\mathbf{p} - \mathbf{s_3})}}$$

$$C_1 = \frac{(z - z_1)(x - x_1)}{\sqrt{(\mathbf{p} - \mathbf{s_1})^T(\mathbf{p} - \mathbf{s_1})}} + \frac{(z - z_2)(x - x_2)}{\sqrt{(\mathbf{p} - \mathbf{s_2})^T(\mathbf{p} - \mathbf{s_2})}} + \frac{(z - z_3)(x - x_3)}{\sqrt{(\mathbf{p} - \mathbf{s_3})^T(\mathbf{p} - \mathbf{s_3})}}$$

To perform estimation, we used a Monte-Carlo simulation to achieve the means and the variances against the CRLB. A position x= 50 cm, y = 50 cm, z = 50 cm and d = 86.6025 cm was simulated. A zero mean WGN process with the variance is included to the LPM signal. The means and variance are tabulated in Table 7.1 with SNR of 10, 0 and -10 dB. The Cramer Rao bounds, computed using Equations (7.28) to (7.30) are obtained under the variance for comparison. The result can be observed that the means closely achieve the assumed position, and the variance can reach the CRLB for SNR as low as 0 dB, as shown in Table 7.1.

	x-position (cm)	y-position (cm)	z-position (cm)
	50 cm	50 cm	86.6025
10-dB SNR			
Mean	50.0311	50.0456	86.6712
Variance	$0.73231x10^{-3}$	$0.92723x10^{-3}$	$0.13606x10^{-3}$
CRLB	$0.72180x10^{-3}$	$1.20002x10^{-3}$	$0.14998x10^{-3}$
0-dB SNR			
Mean	50.0392	50.0445	86.6711
Variance	$0.898697x10^{-3}$	$2.0567x10^{-3}$	$0.21002x10^{-3}$
CRLB	$0.76897x10^{-3}$	$1.50044x10^{-3}$	$0.179619x10^{-3}$
-10-dB SNR			
Mean	51.8095	49.4945	86.5692
Variance	0.05256	0.16008	0.02557
CRLB	0.02919	0.07425	$0.55801x10^{-3}$

Table 7.1 Comparison of the CRLB and the variances for SNRs 100 trials - MONTE CARLO simulation

7.2 Velocity measurement using vector projection

The moving-object velocity is estimated using data of the relative velocities at each microphone, that is,v_{d1} on the first microphone, v_{d2} on the second microphone, and v_{d3} on the third microphone, the instantaneous position of the moving object, computed in 5.1.2., and microphone positions. On the basis of the simple fundamentals of the vector theory, vector projection can be considered as the dot product between two vectors as shown as Figure 7.2. Hence, the results of vector projection between the relative velocity estimation at each microphone, $\boldsymbol{u}$ is the unknown object-velocity vector, and $\boldsymbol{v_d}$ is the microphone vector. If the unknown velocity vector of the moving object $\boldsymbol{u} = [u_x, u_y, u_z]^T$ is projected onto the microphone vectors, the result of the projection is the relative velocity measured by the microphones. Thus, the velocity of the moving object can be estimated using the measurements from the relative velocity of each microphone, the instantaneous object position of the moving object, and the microphone positions. We use the relative-velocity measurements $\boldsymbol{v_d} = [v_{d1}, v_{d2}, v_{d3}]^T$ of microphone 1, 2, and 3 respectively. Based on the fundamentals of three-dimensional Doppler velocimetry, vector projection can be thought of as the dot product between the two vectors, then, the projection is expressed as:

$$\boldsymbol{v_d} = [\frac{\boldsymbol{u}^T\boldsymbol{p}_1}{\|\boldsymbol{p}_1\|}, \frac{\boldsymbol{u}^T\boldsymbol{p}_2}{\|\boldsymbol{p}_2\|}, \frac{\boldsymbol{u}^T\boldsymbol{p}_3}{\|\boldsymbol{p}_3\|}]^T \tag{7.31}$$

where $\boldsymbol{p}_i$ at i = 1,2, and 3 is a vector $[x_i - x, -y, z_i - z]^T$, that has a direction from the object position to the microphone position, and Therefore, the unknown vector $\mathbf{u}$ can be expressed as:

$$\boldsymbol{u} = \boldsymbol{H}^{-1}\boldsymbol{W}\boldsymbol{g} \tag{7.32}$$

where

$$\boldsymbol{H} = -\begin{bmatrix} x - x_1 & -y & z_1 - z \\ x - x_2 & -y & z_2 - z \\ x - x_3 & -y & z_3 - z \end{bmatrix}$$

$$\boldsymbol{W} = \frac{1}{3}\begin{bmatrix} 1 & 1 & 1 \\ 1 & 1 & 1 \\ 1 & 1 & 1 \end{bmatrix}$$

and

$$\boldsymbol{g} = \begin{bmatrix} v_{d1}\|\boldsymbol{p_1}\| \\ v_{d2}\|\boldsymbol{p_2}\| \\ v_{d3}\|\boldsymbol{p_3}\| \end{bmatrix}$$

$\mathbf{H}$ is an observation matrix, and $\mathbf{W}$ is inserted to reduce the variance of the relative velocity measurements between all microphones.

7.3 Experimental results

The experimental setup for the three-dimensional positioning system is proposed in Figure 7.4. In the experiment, the frequency of the transmitted LPM signal was swept from 50 kHz to 20 kHz. The length of the transmitted LPM signal was 3.274 ms, and the length of two cycles of the LPM signal was 6.548 ms. The driving voltage of the function generator was 4 Vp-p. The LPM signal was distributed from the function generator and enlarged 10 times with an amplifier. The loudspeaker transmitted the LPM signal, and then echoes were sensed by the silicon MEMS microphone based on a development of hand held telecommunication instruments using Knowles Acoustic model SPM0204UD5. A stainless ball with a diameter 10 cm was used as a test object. According to the calculations, the first microphone was located at x_1=10 cm, y_1 = 0 cm, z_1 = -10 cm, the second microphone was located at x_2 =0 cm, y_2 = 0 cm, z_2 =10 cm, the third microphone was located at x_3 = -10 cm, y_3= 0 cm, z_3 = -10 cm. The propagation velocity of an ultrasonic wave in the air was approximately 345 m/s at

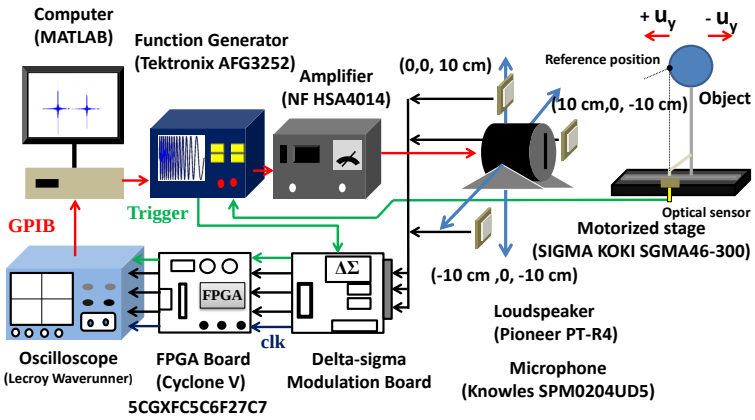

Figure 7.4 Experimental setup for three-dimensional ultrasonic position and velocity measurements.

a temperature of $20^o - 25^o$ C and a humidity of 40 - 50 R.H. The signals measured by the acoustical receivers were converted into one-bit signal by 7th order delta-sigma modulators AD7720. The sampling frequency of the delta-sigma modulator was 12.5 MHz. The cross correlation and the smoothing operation performed by 141 taps of weighted moving average filter were designed and embedded on an FPGA board model cyclone V 5CGXFC5C6F27C7. The logic utilization for the cross correlation using one-bit signal, programmed into the FPGA board were 2602 logic elements; the number of total registers was 5777; and the total block of memory used included 175,948 bits. The moving object was driven using SIGMA KOKI SGMA46-300 motorized stage, which can drive a moving object in only the +Y and Y direction with maximum and minimum velocities of ± 0.4 m/s; velocities could be adjusted in ± 0.1 m/s steps. A reference point of the object position is set up on the object surface and synchronized with the acoustic transmitter by using an optical sensor shown in Figure 7.4. When the moving object passed through the reference point, instantaneously the speaker was trigged to generate the LPM signals.

The three-dimensional position determined by the proposed method was evaluated by the experimental results. In the experiments, the velocity of the motorized stage was adjusted from -0.4 m/s to +0.4 m/s. The velocity of the motorized stage was determined by 50 experiments per position of the moving object. The cumulative

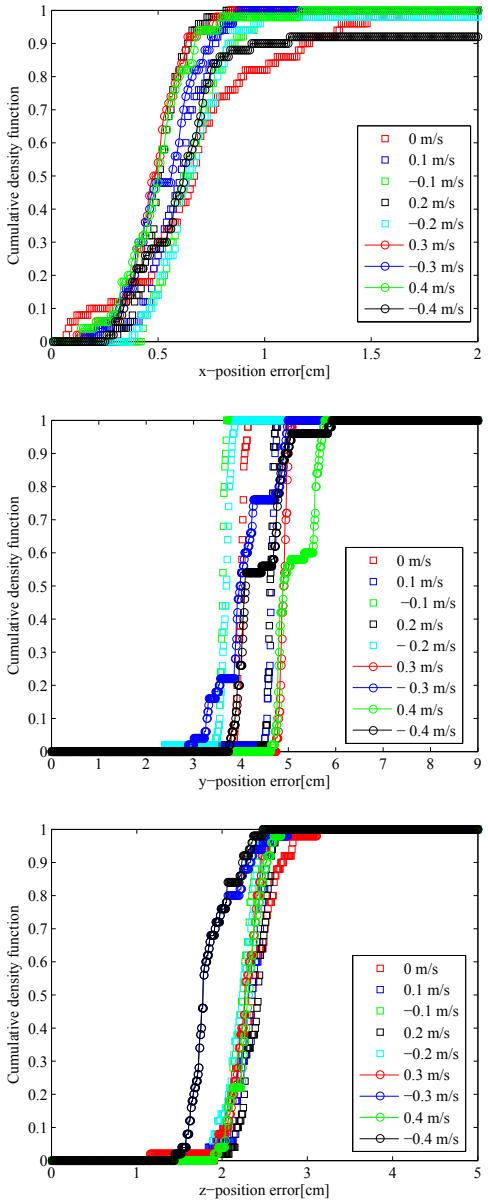

Figure 7.5 The cumulative density function of the first position measurement: x=19, y=92, z=7 cm

density functions (CDFs) of the positions are illustrated in Figure 7.5 - 7.8. The examples of the determined positions in the proposed system are assumed to be located at four positions. To ensure that the real moving object positions were covered in every quadrant of detection, the position was assumed to be on the +X, -X, +Z, -Z, and +Y

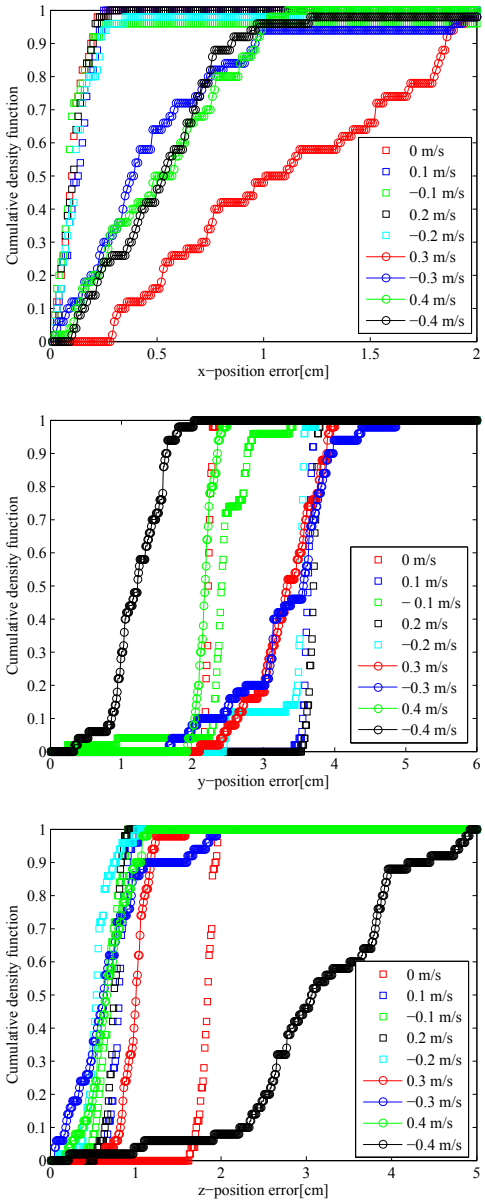

Figure 7.6 The cumulative density function of the second position measurement: x=25, y=70, z=-25 cm

axes. The first position was (19, 94, 7) cm, the second was (25, 70, -25) cm, the third was (-50, 75, 0) cm, and the fourth was (-40, 60, -20) cm. The velocities determined by the proposed method of Doppler velocity estimation and Doppler-shift compensation are illustrated in Figure 7.10 - 7.13. The velocity and position of the moving object

can

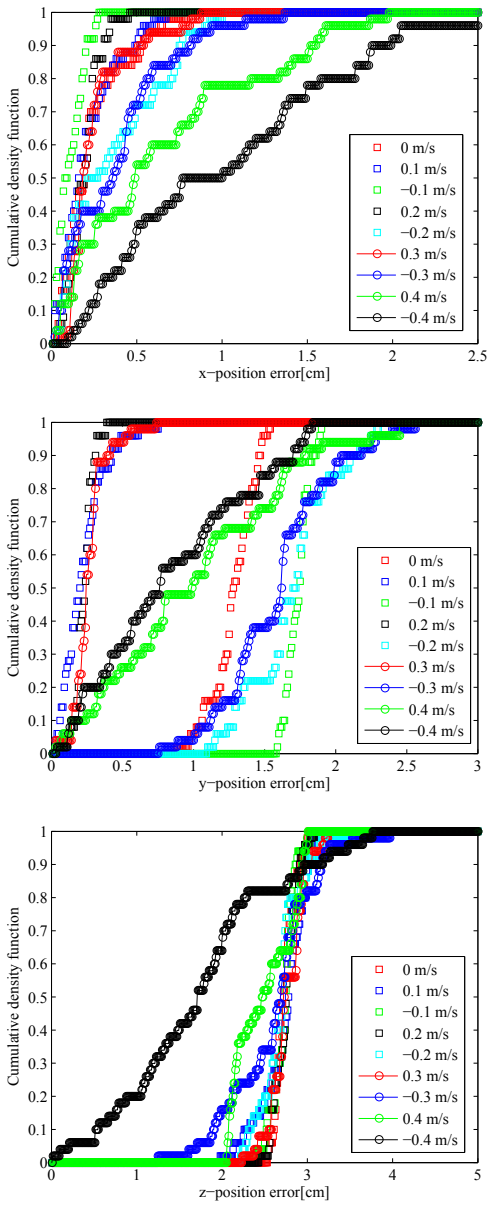

Figure 7.7 The cumulative density function of the third position measurement: x=-50, y=75, z=0 cm

be concurrently determined by the proposed ultrasonic system based on one-bit signal processing. In the experiment, deviations between the real position and reference positions were found; this was likely caused by the spherical object used in this paper,

which had a diameter of 10 cm, while the proposed three-dimensions-positioning mea-

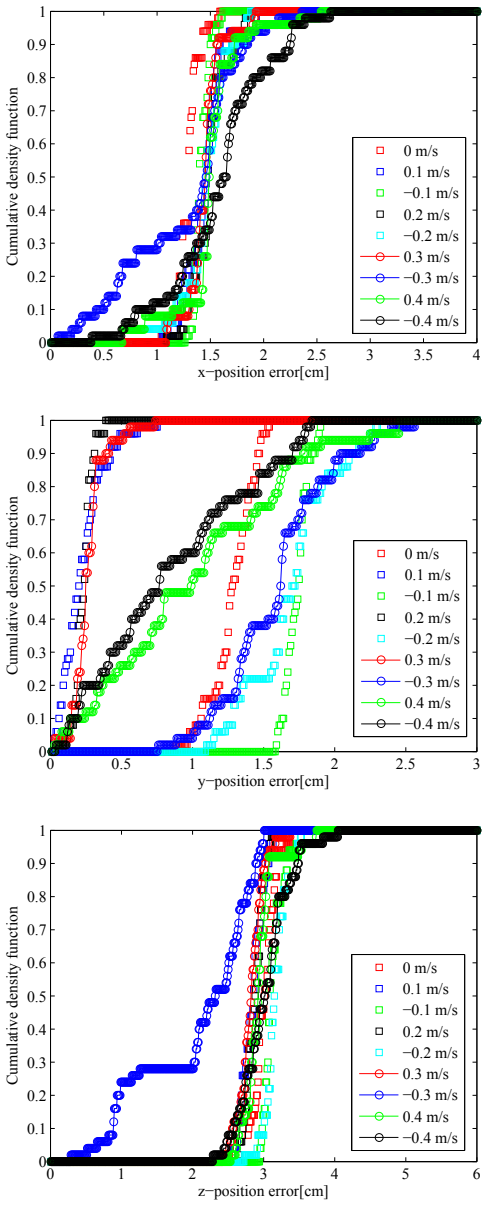

Figure 7.8 The cumulative density function of the fourth position measurement: x=-40, y=60, z=-20 cm

-surement assumed that the object was a small point. Therefore, the sound that was incident on the object propagated from many points, which resulted in many different TOFs at the same acoustical receivers. This affected the efficiency from the echoed-

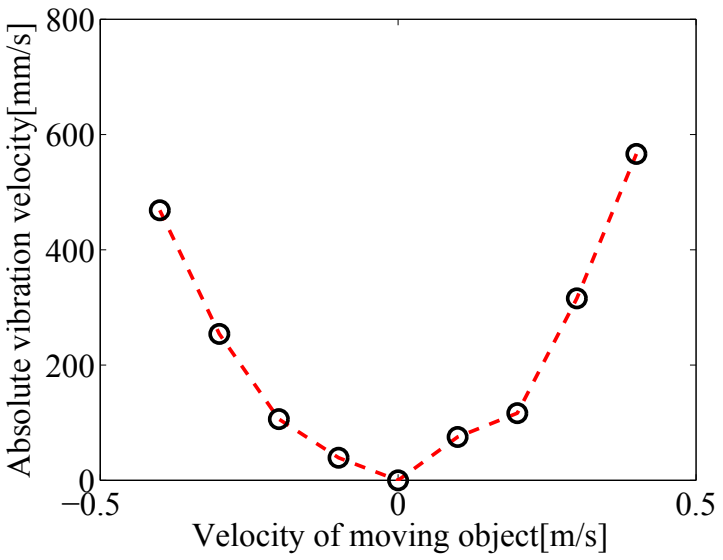

Figure 7.9 Vibration velocity of the moving object at given velocities.

sound propagation of the object, producing an error due to variance of the position and velocity measurements used in the proposed system. The experimental results at a reference point $x = 19$ cm in Figure 7.5 show that the x-position error measurement at -0.4 to 0.4 m/s is approximately a ranging performance from 0.5 to 1.5 cm while the 10 % x-position error at -0.4 m/s provides higher than 2 cm. At a reference point $y = 92$ cm in Figure 7.5 , the errors vary from 3 to 5 cm but the 40 % y-position error is more than 5 cm at the velocity 4 m/s. In Figure 7.5, the CDF of the y - position errors has a narrow bandwidth interval 1.5 - 2.5 cm. In the second position (25, 70, -25) cm of Figure 7.6, the x-position errors are less than 0.25 cm at the velocity range -0.2 to 0.2 m/s while the rest of the x-position errors varies from 0 to 2 cm, the y-position errors are approximately in a range measurement 0 to 4.5 cm, the z-position errors swing from 0 to 2 cm but at the error range (0 to 5 cm) of the velocity -0.4 m/s the CDF is wider distribution than other velocities. The errors of the third position (-50, 75, 0) cm have deviation from x = 0 to 2 cm, y = 0 to 2.5 cm, and z = 0 to 3 cm as shown in Figure 7.7. In the fourth position (-40, 60, -20), the x-y-z position errors are determined as the interval 0 to 2 cm, 0 to 2.5 cm , and 0 to 4 cm, respectively, as shown in Figure 7.8. In addition, ranging performances of Figure 7.7 and 7.8 above 0.3 and below -0.3 m/s are less satisfactory with regard to standard deviation with an assumed position at (-50, 75, 0) and (-90, 60, -20) cm; this is likely due to the vibration of the moving object. The motorized stage for driving the object was controlled by an automatic

system to evaluate repeatability. Then, a rod was connected between the object and the motorized stage. When the moving object was accelerated to a high velocity in each turn, the object did not completely stop because the rod swung with higher vibration. The object assumed as a rigid body thus was not at a static condition during the next measurements. We can explain this condition by experimentally measuring vibration velocity versus various velocities. This effect was evaluated by a Polytech OFV-302 vibrometer during vibration testing. Relatability to high velocity measurements of a moving part in the Surface Acoustic Wave (SAW) motor [81] was found along with vibration velocity of the titanium-based hydrothermal lead zirconate titanate thick film transducer. The vibrometer was placed 50 cm away from a measurement point. At that point, the object was accelerated to -0.4, -0.3, -0.2, -0.1, 0, 0.1, 0.2, 0.3 and 0.4 m/s, and the rod, that was connected to the moving object and the motorized stage, had a length 40 cm. Experiment results regarding the vibration effect of the moving object is shown in Figure 7.9; higher velocities tend to show higher vibration velocities. Regarding object position at 0, 0.1, 0.2, -0.1, and -0.2 m/s, they are shown to have satisfactory repeatability. A moving object had a lower vibration than the objects moving at 0.3, 0.4, -0.3, and -0.4 m/s.

In Figure 7.10-7.13, the determined velocity measurement in the ±Y direction was presented alone. The component u_y was analyzed because it is in the same direction as the motorized stage movement. The component vectors of u_x and u_z were estimated to be nearly zero. At the first position in Figure 7.10, the velocity errors have more satisfaction than other positions and 10 % of the velocity errors over 0.05 m/s. The velocity-measurement range, from -0.2 to 0.2 m/s, of the position (x=25, y= 70, z=-25) cm provides the velocity errors smaller than 0.04 m/s but for other velocities 10 % of their results have error at nearly 0.07 m/s, as shown in Figure 7.11. In Figure 7.12 , the velocity errors are less than 0.03 m/s at the velocity measurement from -0.1 to 0.1 m/s, and the velocity errors of -0.4, -0.3, 0.3, and 0.4 m/s have the interval from 0 to 0.08 m/s. In Figure 7.13, the most velocity error varies in the range of 0 to 0.045 m/s, except -0.4, -0.3, and 0.4 m/s the results are inside the error range of 0.02 to 0.065 m/s. Measurement was shown to have the highest error and dispersion at velocities of 0.3, 0.4, -0.3, and -0.4 m/s, which was likely because three-dimensional velocity vector measurement relied on the position computation and thus directly varied according to the accuracy of the determined position.

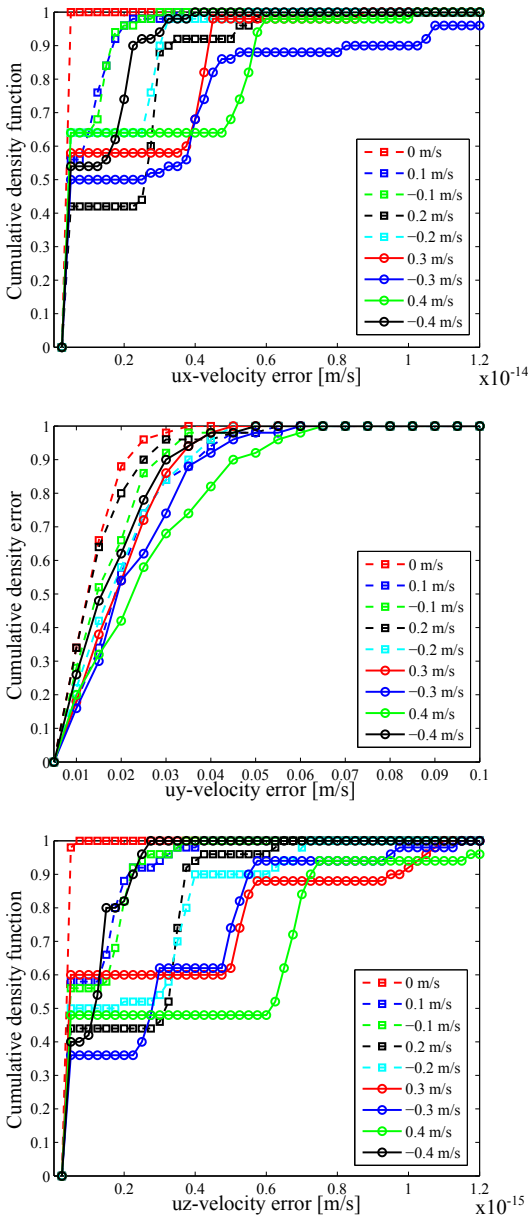

Figure 7.10 The cumulative density function of the first position measurement for velocity measurement: x=19, y=92, z=7 cm

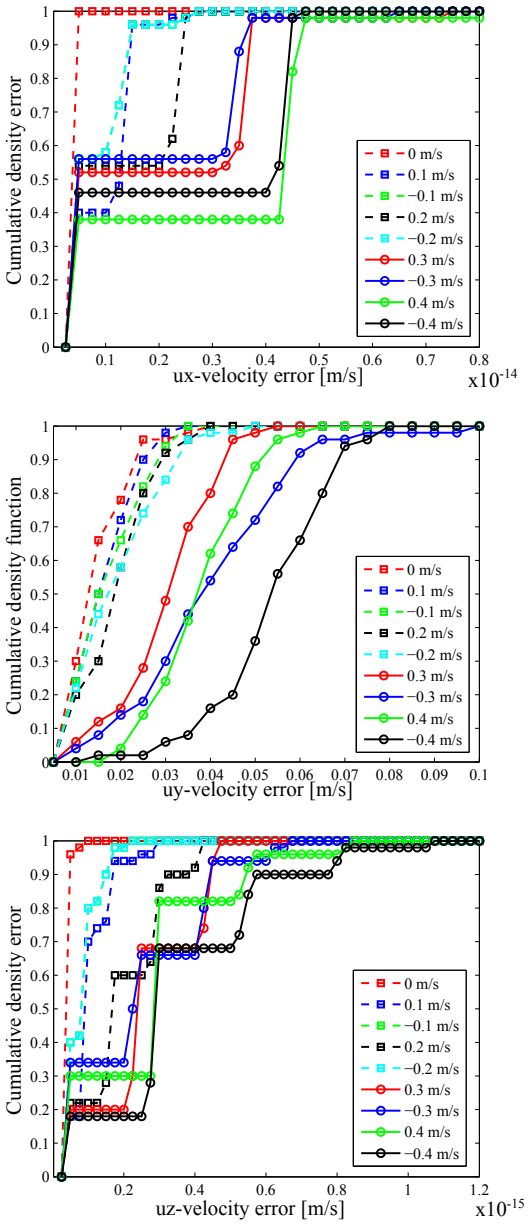

Figure 7.11 The cumulative density function of the second position measurement for velocity measurement: x=25, y=70, z=-25 cm

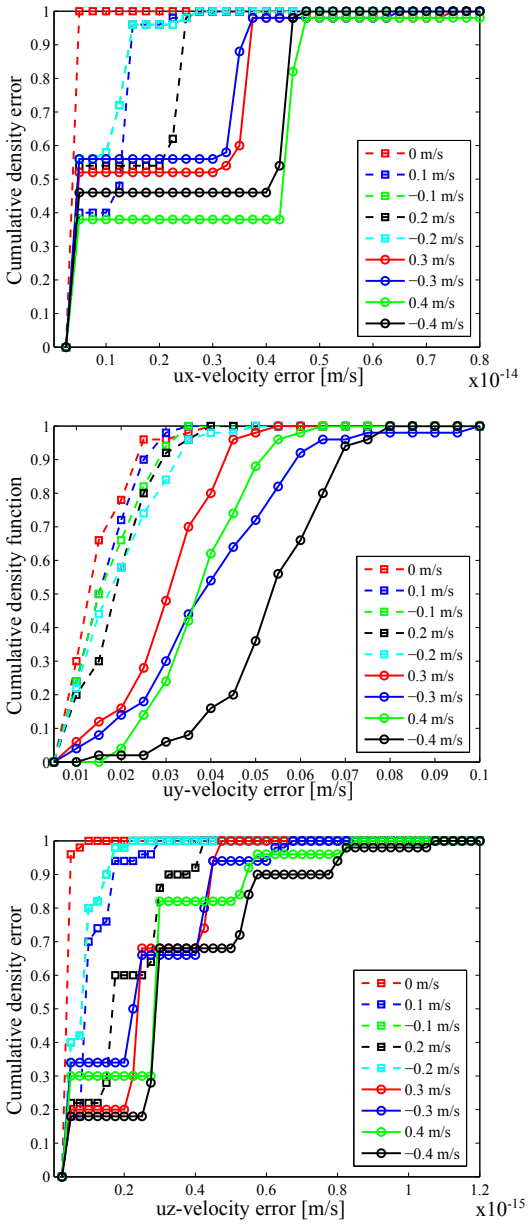

Figure 7.12 The cumulative density function of the third position measurement for velocity measurement: x=-50, y=75, z=0 cm

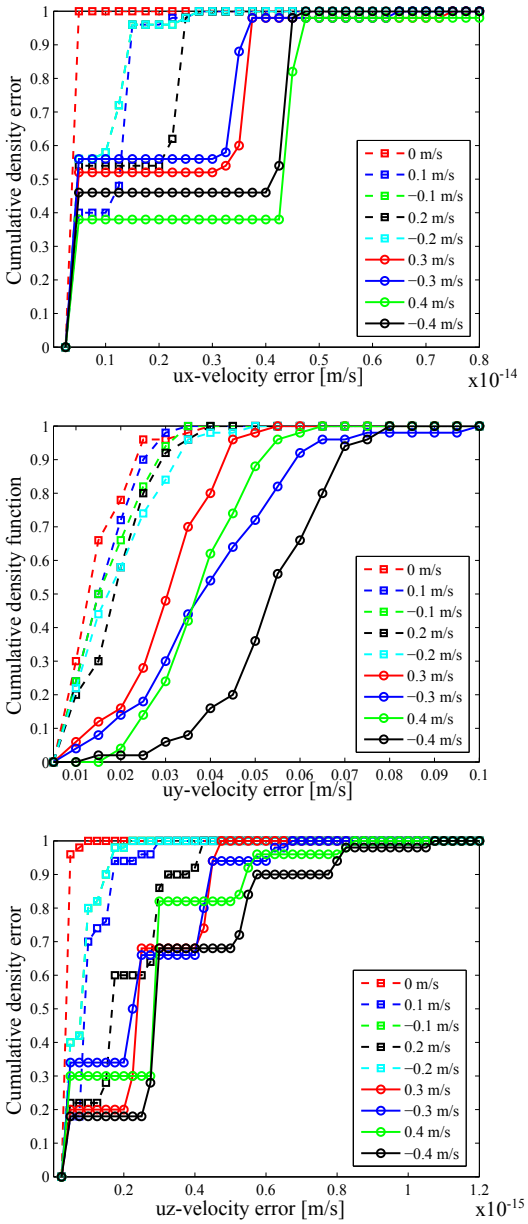

Figure 7.13 The cumulative density function of the fourth position measurement for velocity measurement: x=-40, y=60, z=-20 cm

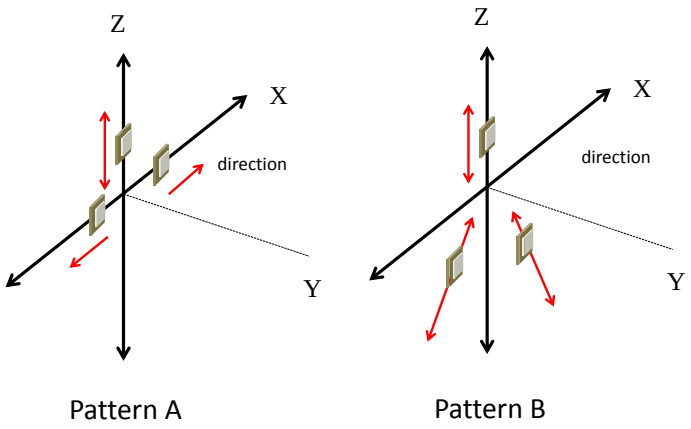

Figure 7.14 Microphone-arrangement patterns

7.4 Optimal microphone position of the linearization-based method

7.4.1 Arbitrary microphone positions

Basically, the object position is a ratio of distances from the speaker position to the target and returning to each microphone. This condition has to be determined on non-linearity. In general, non-linear equations can be solved using numerical methods requiring an initial point and routines, as previously expressed in chapter 5. In this chapter, we try to improve non-linear forms into linear forms. The microphone position plays a significant role to control accuracy of the object position. This section is to express the optimal microphone position when directly adjusting the microphone positions for the minimum error. The microphone position of the linearization-based method can freely be located on X-Z plane. First, we adjust the microphone position in the pattern A according to Figure 7.14 that the microphones are moving on only X and Z axes. Simulation results under SNR of 0 dB are observed that, in the pattern A, the optimal microphone position providing the minimum error is at the first microphone of (0,0,3) cm, the second microphone of (3,0,0) cm, and the third microphone of (-3,0,0) cm. The minimum error is approximately 0.2 cm. For other microphone positions, the maximum error in x, y, and z co-ordinate is not over 0.5 cm. This error is not a big problem for echolocation because this application does not require high precision of

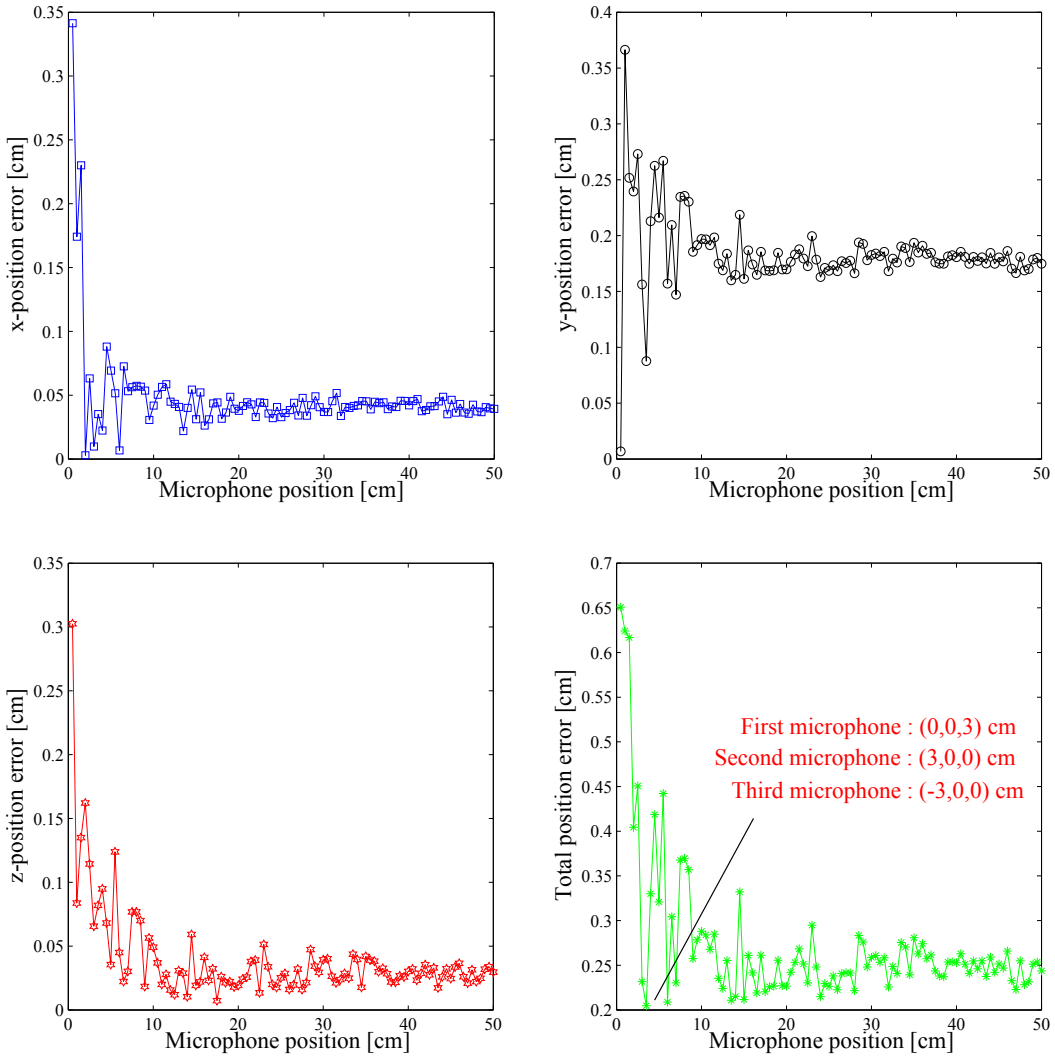

Figure 7.15 The optimal microphone position of the pattern A at an object position: x=80, y=75, z=60 cm

measurements. In the next simulation, the pattern B is performed to achieve the minimum error. Simulation results under SNR of 0 dB are observed that, in the pattern B, the optimal microphone position providing the minimum error is at the first microphone of (0,0,3) cm, the second microphone of (3,0,-3) cm, and the third microphone of (-3,0,-3) cm. The minimum error is approximately 0.1 cm.

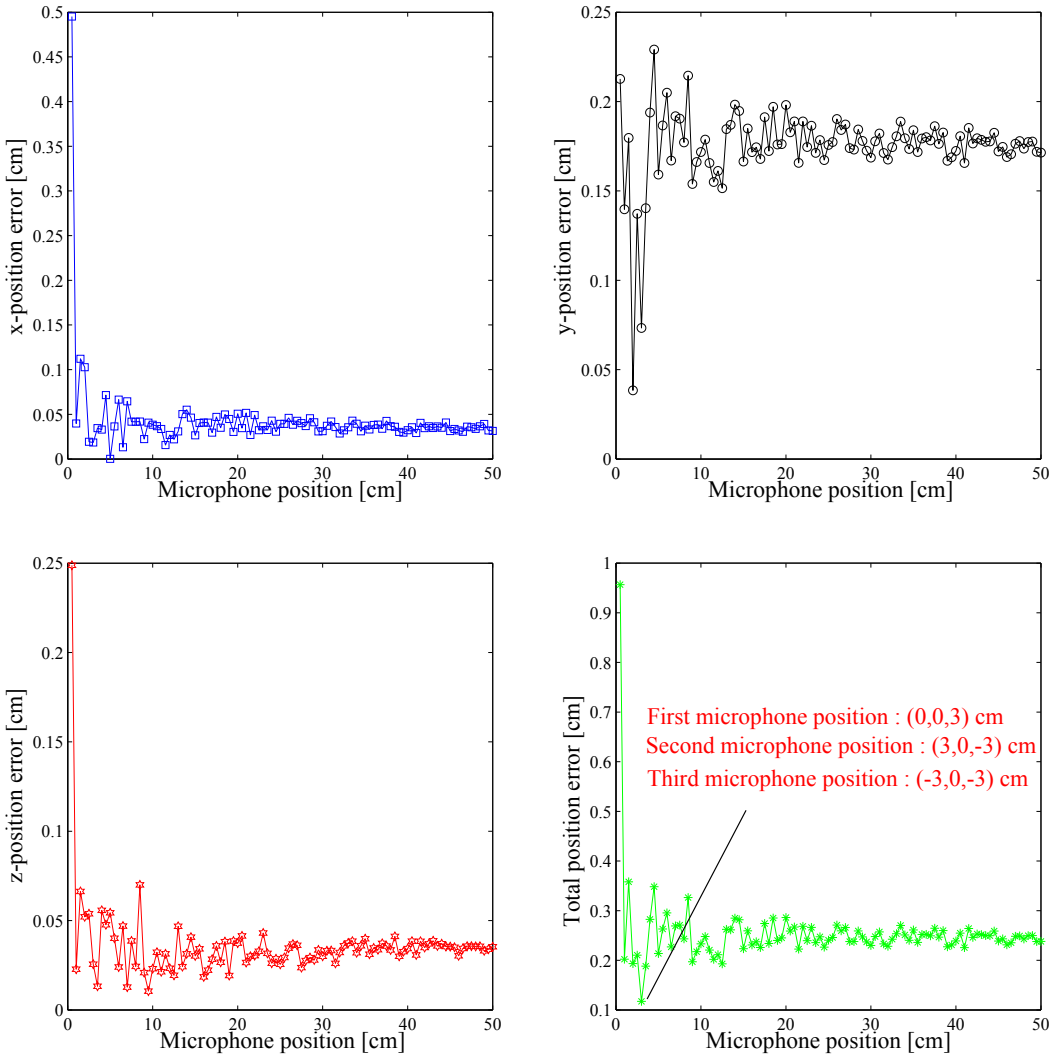

Figure 7.16 The optimal microphone position of the pattern B at an object position: x=80, y=75, z=60 cm

7.4.2 Critical microphone positions

In addition, some cases of the microphone arrangement cannot determine the object position because these cases occur no solution. Such patterns make singular matrix of microphone beacons. A singularity of the matrix A in Equation (7.10) will not be produced as long as the three microphones do not lie on a line. These conditions are pictured in Figure 7.17. Therefore, position measurement using a linearization-based

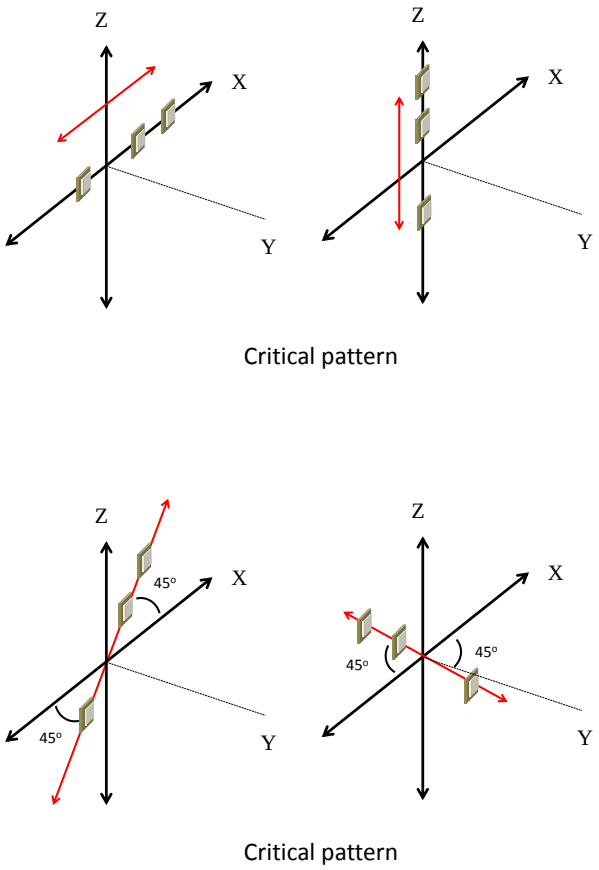

Figure 7.17 Critical microphone position

method has avoid the microphone positions providing singular matrix.

7.5 Summary

The proposed system by redesigning the receiver arrangement uses cross-correlation one-bit signal processing technology, low-computation-cost Doppler-shift compensation, and low-cost devices. This is the development from the previous space measurement of one-bit signal processing to simultaneously measure position and velocity in three-dimensional space. Through Monte-Carlo computer simulation of 100 trials, the variances of estimated parameters can achieve the analytical CRLB for SNR as low as 0 dB. Accuracy of the proposed method was tested by the additional White Gaussian

Noise. The results can provide accuracy less than 0.1 mm at a SNR of 0 dB. Since the position-measurement model is a form of nonlinear systems, it is then improved into a linear model.

In this method, three-dimensionalpositioning measurement was determined by three acoustical receivers and one sound source. We proposed a method to design the optimal receivers-positions. The velocity of the moving object was calculated using the concept of vector projection. In the experiments, four-example positions in each area were evaluated with velocities between -0.4 m/s and +0.4 m/s by in steps of 0.1 m/s. The repeatability of the proposed system was determined via 50 measurements at each position and velocity. From the experimental results, it is observed that accuracy of the position measurement compared with a reference point can be achieved between 0.2 to 5 cm, and accuracy of the velocity measurement is between 0.02 to 0.07 m/s. Moreover, we notice that the moving-objects position showed the most variance at high velocities due to the vibration velocity on the object surface.

8

Performance evaluation, testing, and comparisons

8.1 Mathematical modeling of noise

As mentioned in chapter 5, 6, and 7, the proposed models for object positioning to be described using White Gaussian Noise (WGN) can also be tested for other noises. The mathematical modeling of observation noise bases heavily on random process theory. All the noise models are assumed to have known probability density functions (PDFs). When the noise model has a PDF with unknown parameter, the estimation from field data for subsequent algorithm development can become exceedingly difficult. Similarly, the required parameter for estimation is a demanding task. This chapter is useful for evaluating the performance of the proposed method in other situations of noises.

8.1.1 White Gaussian noise

WGN can be described that each sample in the data set $w[0], w[1], w[2], ..., w[N-1]$ has the same PDF (identically distributed) and the PDF is Gaussian, as given by

$$p_W(w) = \frac{1}{\sqrt{2\pi\sigma^2}} \exp\Big(-\frac{1}{2\sigma^2} w^2\Big) \tag{8.1}$$

σ^2 is variance of random signal. Each noise sample is independent of every other noise sample. It is implied that we cannot predict any sample relied on observing the others. We might say that this random process is very "noise-like". An example is shown in Figure 8.1 for σ^2=3.

As a result of the properties that $w[n]$ is consisted of identically distributed samples,

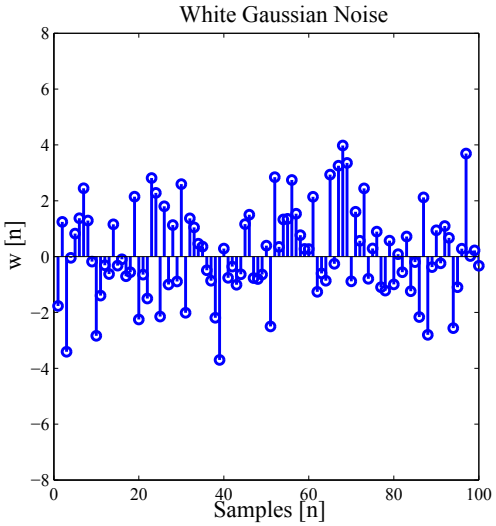

Figure 8.1 Realization of WGN with $\sigma^2 = 3$.

the PSD is flat with

$$P_w(f) = \sigma^2. \tag{8.2}$$

The WGN random process is generally employed in communications to model observation noise. In addition, it is used in radar/sonar to model the ambient noise and for virtually any signal processing system subject to electronic noise.

8.1.2 Colored Gaussian noise

Clutter in radar [82] and reverberation in sonar [83] both have power signal density (PSD) that are nonflat in the band of interest. That PSD can be categorized as a low PSD, whereby most of its power is below about f=0.1. A particularly useful model for a nonflat PSD is the autoregressive (AR) model. It takes the mathematical form

$$P_w(f) = \frac{\sigma^2}{|1 + a[1]\exp(-j2\pi f) + ... + a[p]\exp(-j2\pi fp)|^2} \tag{8.3}$$

We usually include the model order in the description by referring to it as an AR(p) PSD model. Its usefulness is based on PSD as long as the model order p is chosen large

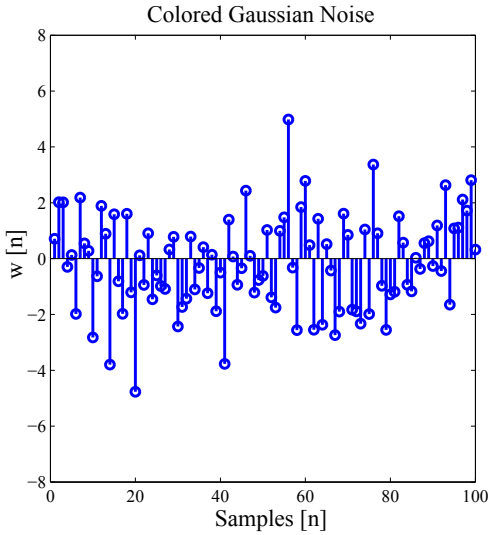

Figure 8.2 Realization of Colored Gaussian noise with AR(1) model: a[1]=-0.5 and σ^2 =3.

enough. As an example, consider the AR(1) model given by

$$P_w(f) = \frac{\sigma^2}{|1 + a[1]\exp(-j2\pi f)|^2} \tag{8.4}$$

For a[1]=-0.5 and σ^2 =3, the PSD is shown in Figure 8.2. Once the value of a[1] has been chosen to specify the bandwidth, the value of σ^2 can be used to specify the total average power, which is given by $\frac{\sigma^2}{1-a^2[1]}$.

8.1.3 General Gaussian noise

In previous two noises, Gaussian noise models for stationary noise data is presented. The definition of stationary is ability to define a PSD. Nonstationary Gaussian random process can occur in practice due to abrupt changes in the characteristics of the random process and gradual changes. In the case of abrupt changes it may still be possible to use a stationary random process model if we use two different models, one prior to the change and the other after the change. For example, the model actually used to create

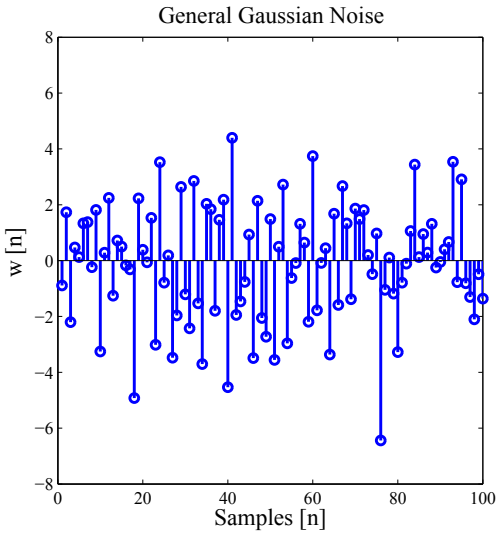

Figure 8.3 Realization of General Gaussian noise with AR(1) model: $a[1,n] = -0.9 + \frac{n}{N}$ and σ^2 =3.

this signal is

$$\begin{aligned} w[n] &= w_1[n] \Rightarrow n = 0, 1, ..., M-1 \\ &= 2w_1[n] \Rightarrow n = M, M+1, ..., N-1 \end{aligned} \tag{8.5}$$

where $w_1[n]$ is WGN with variance σ^2 =1 and $M = 100$. To use this model, knowledge of transition time $n = M$.

The second type of nonstationarity is exhibited by data with a more gradual change in characteristics. This type of nonstationary random process is referred to as locally stationary, in that over a small enough time interval we can assume the realization could have been generated by a stationary random process. To model a locally stationary random process we can modify the AR (1) model of the previous section to allow for temporal variation in the filter and/or excitation noise parameters. Therefore, we have

$$w[n] = -a[1,n]w[n-1] + w[n] \tag{8.6}$$

$a[1,n]$ is a time-varying filter parameter and $u[n]$ is zero mean Gaussian noise but with a variance at time n of $\sigma_u^2[n]$. This model is performed to generate the realization of General Gaussian noise. In particular, we have chosen $\sigma_u^2[n] = \sigma_u^2 = 3$ so that the $u[n]$

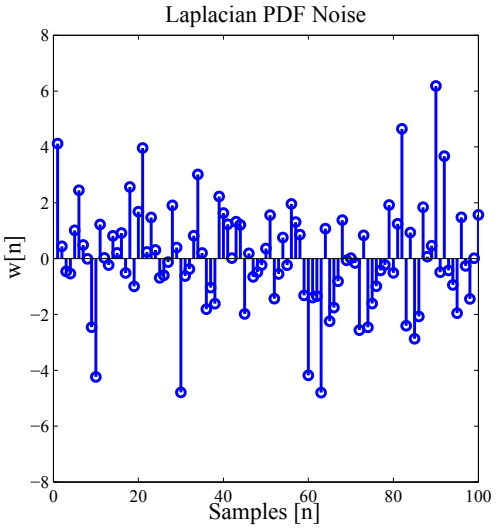

Figure 8.4 Realization of Laplacian PDF noise: σ^2 =3.

is WGN (a stationary random process), but a time-varying filter parameter given by

$$a[1,n] = -0.9 + \frac{n}{N} \tag{8.7}$$

to yield a nonstationary AR process shown in Figure 8.3.

8.1.4 Laplacian PDF Noise

In this subsection, we consider noise that a nonGaussian PDF. This means that the normal rule of the amplitude being less than or equal to three standard deviations or $-3\sigma < w[n] < 3\sigma$ no longer applies. As a result, for a fixed average noise power σ^2 the noise samples might exhibit large spikes. In particular, nonGaussian noise PDF used to produce the realization of noise samples is the Laplacian PDF given by

$$p_W(w) = \frac{1}{\sqrt{2\pi\sigma^2}} \exp\left(-\sqrt{\frac{2}{\sigma^2}}|w|\right) \tag{8.8}$$

It is seen that there are no Gaussian noise samples that exceed $\pm 3\sigma = \pm 3$ but many nonGaussian noise samples that do so. This is because the probability of exceeding 3σ, which can be computed from

$$P[w[n] > 3\sigma] = \int_{3\sigma}^{\infty} p_W(w)dw \tag{8.9}$$

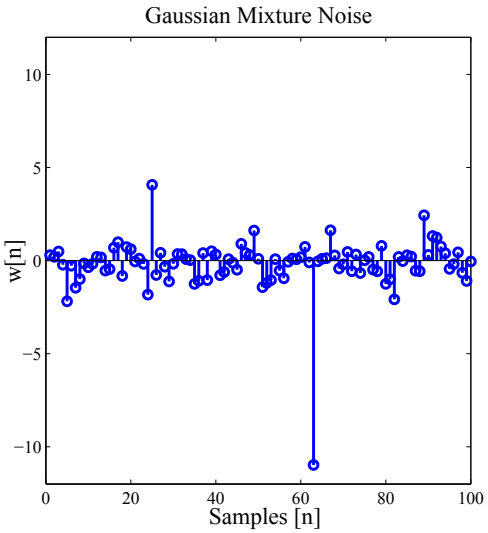

Figure 8.5 Realization of Gaussian mixture noise: σ_1^2 =0.5, σ_2^2 =50, and $\varepsilon = 0.01$

is larger for the Laplacian PDF than for the Gaussian PDF. It is said that the area in the tails of the PDF is larger, shown in Figure 8.4. Large noise spikes are indicative as man-made noise [84], acoustic transients [85], and geomagnetic noise [86].

8.1.5 Gaussian Mixture Noise

A second type of nonGaussian PDF that is available in practice is the Gaussian mixture PDF. It is simply generated if uniform and Gaussian random number generators are available. Also, it can be extended to the generation of multivariate Gaussian mixture PDFs, useful in classification problems [87]. A simple example is

$$p_W(w) = (1-\varepsilon)\frac{1}{\sqrt{2\pi\sigma_1^2}}\exp\Big(-\frac{1}{2\sigma_1^2}w^2\Big) + \varepsilon\frac{1}{\sqrt{2\pi\sigma_2^2}}\exp\Big(-\frac{1}{2\sigma_2^2}w^2\Big). \tag{8.10}$$

It mixes two Gaussian PDFs with variances σ_1^2 and σ_2^2, and with probabilities $1-\varepsilon$ and ε, respectively. Typically, σ_2^2 is large relative to σ_1^2. Therefore, the outcome will potentially be large in magnitude due to the large value of σ_2^2. A large level amplitude $|w| > \sigma_2$ will occur with probability of about 0.32ε. The PDF parameters are $\sigma_1^2 = 1/2, \sigma_2^2 = 50$, and $\varepsilon = 0.01$. Note that the average power or variance can be

expressed to be

$$\sigma^2 = (1-\varepsilon)\sigma_1^2 + \varepsilon\sigma_2^2 \tag{8.11}$$

which for this example is $\sigma^2 \approx 1$. Many spikes with amplitude $|w| > \sigma_2 \approx 7$ are viewed. The probability of observing a spike is the probability that it exceed σ_2 in magnitude, as shown in Figure 8.15.

8.2 Accuracy testing due to different kinds of noise

8.2.1 Accuracy testing due to different kinds of noise

In the previous section, we describe different types of noise from many applications. Next, we will assume that the proposed methods is tested in different situations of those noises. Simulation results are performed to confirm the three proposed three-dimensional-positioning method. We will show that how many SNR they can attain by assuming that an object position is x=30 cm, y=50 cm, and z = 30 cm. In the first method, we used the microphone positions,which have the minimum error as expressed in chapter 5, that are (10 cm, 0 cm, 0 cm), (0 cm, 10 cm, 0 cm), and (0 cm, 0 cm, 10 cm). We assume that the microphone positions are located at 3 cm on +X axis, -3 cm on -X axis, 3 cm on Z axis, and 3 cm on -Z axis for the second method. In the final method, they are positioned at (0 cm, 0 cm, 3 cm), (-3 cm, 0 cm, -3 cm), and (3 cm, 0 cm, -3 cm). The object position estimation under an ultrasonic three-dimensional system determined by the proposed one-bit signal processing method was evaluated by MATLAB computer simulation. The period of the single LPM signal was swept linearly from 20 μs to 50 μs. The sampling frequency rate was 12.5 MHz. The LPM signal had the length equal to 3.278 ms. The propagation velocity of an ultrasonic wave in air was 345.1 m/s at 22.4 C^o. SNR was set at 10 dB compared with the echo signal The constant attenuation factor of the received signal was -2.107 dB/m degraded from that of the original signal. The received signals were changed into the single-bit delta-sigma modulated signal by the 7^{th}-order delta-sigma modulator. The one-bit signal of the received echo was correlated together with the one-bit signal of the reference, which was the transmitted LPM signal converted into the one-bit digital signal by a digital comparator. The cross-correlation function of the one-bit received signal and the one-bit reference signal was obtained directly from the recursive cross-correlation operation of one-bit signal processing and the smoothing operation accomplished by the triang-

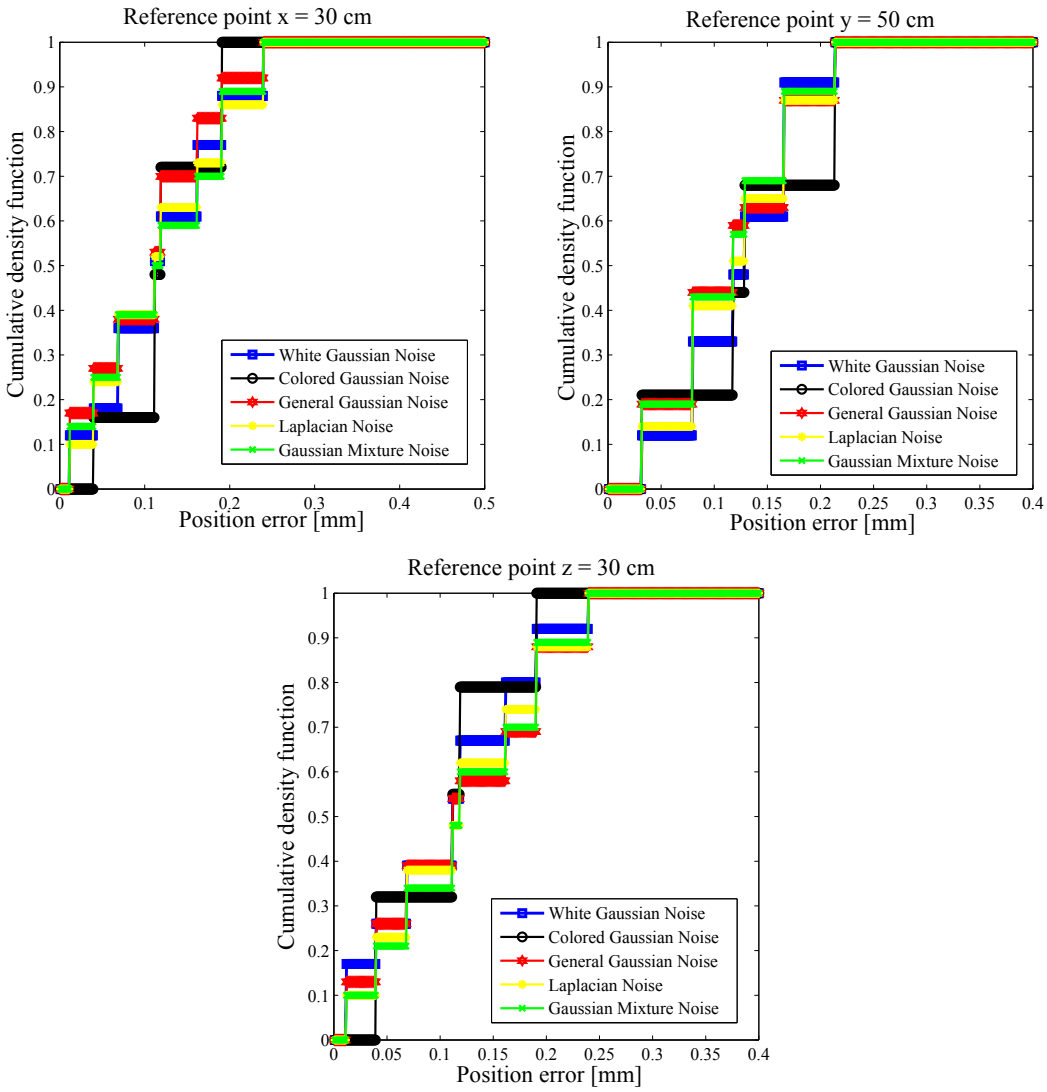

Figure 8.6 Position error of the first method from different noises at SNR = 10 dB.

-ular weighted moving average filter. Signal had 399 zero-cross points. Accordingly, the computational cost of the recursive cross-correlation operation was the integration and 401 summations of one-bit samples. For the smoothing operation, the length of the triangular weighted moving average filter, which consists of a pair of 55-tap moving average filters, was 109 taps. The position error by the noises included in the received echoes was evaluated by MATLAB computer simulation. In the simulation, the SNR of the reflected echo was converted by including five different types of noise : White Gaussian Noise, Colored Gaussian Noise, General Gaussian Noise, Laplacian

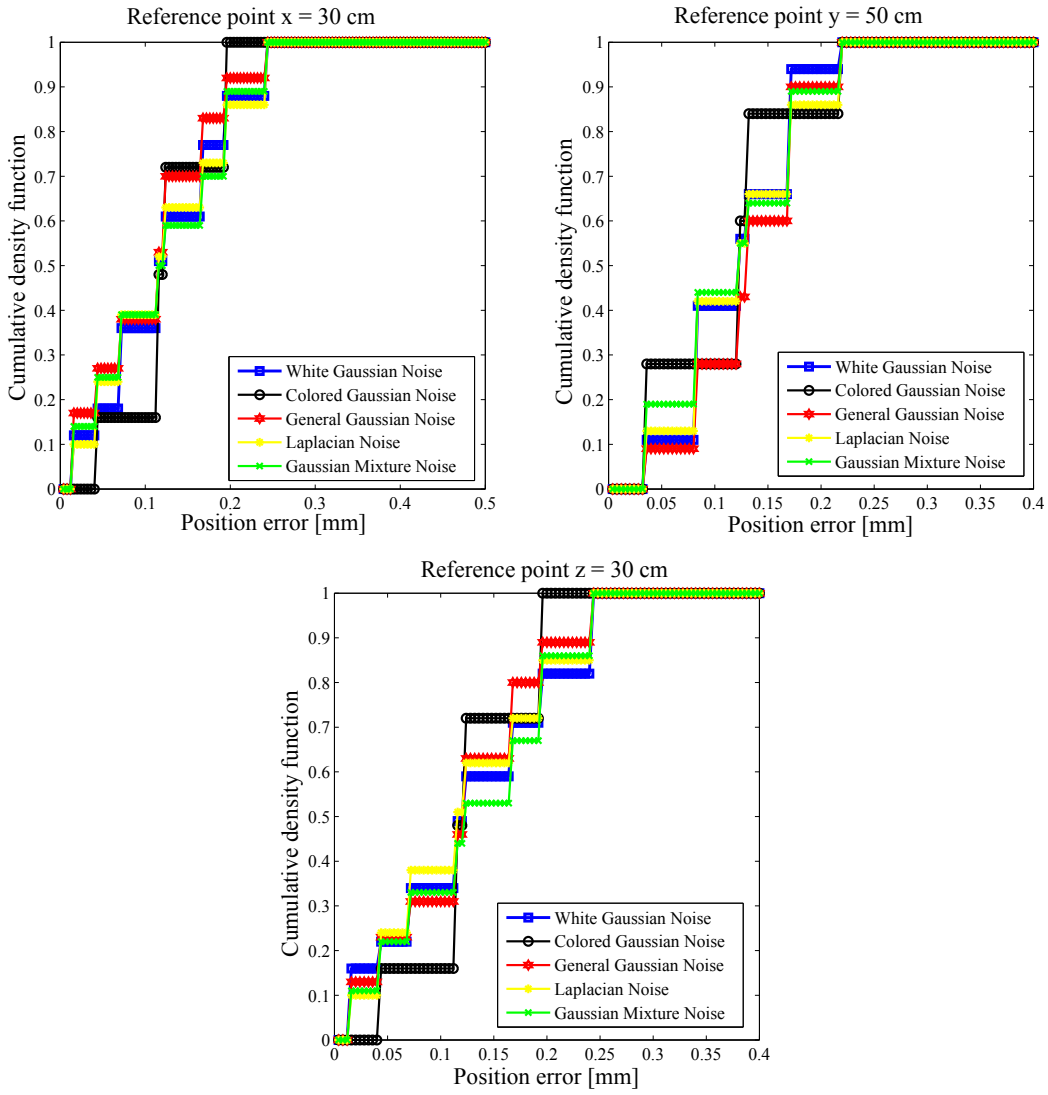

Figure 8.7 Position error of the first method from different noises at SNR = 0 dB.

PDF Noise, and Gaussian Mixture Noise, to the received echoes. In the case of each SNR: 10 dB, 0 dB, and -10 dB, the position of the estimation was evaluated from 100 simulations. To evaluate these situations, the cumulative density distributions of the estimated position are determined from 100 estimation and illustrated in Figure 8.6 to 8.14. In Figure 8.6 to 8.8, they are observed that the first method can attain errors as high as 0.5 mm at SNRs of 10 dB and 0 dB, but for SNR of -10 dB, it has error more than 100 mm. This is robustness for responding all types of noise. Next, we reproduce the same procedure but the second method was rather than the first method. Accuracy

of the second method has the maximum error at 1 mm at SNR 0 dB in Figure 8.9 and

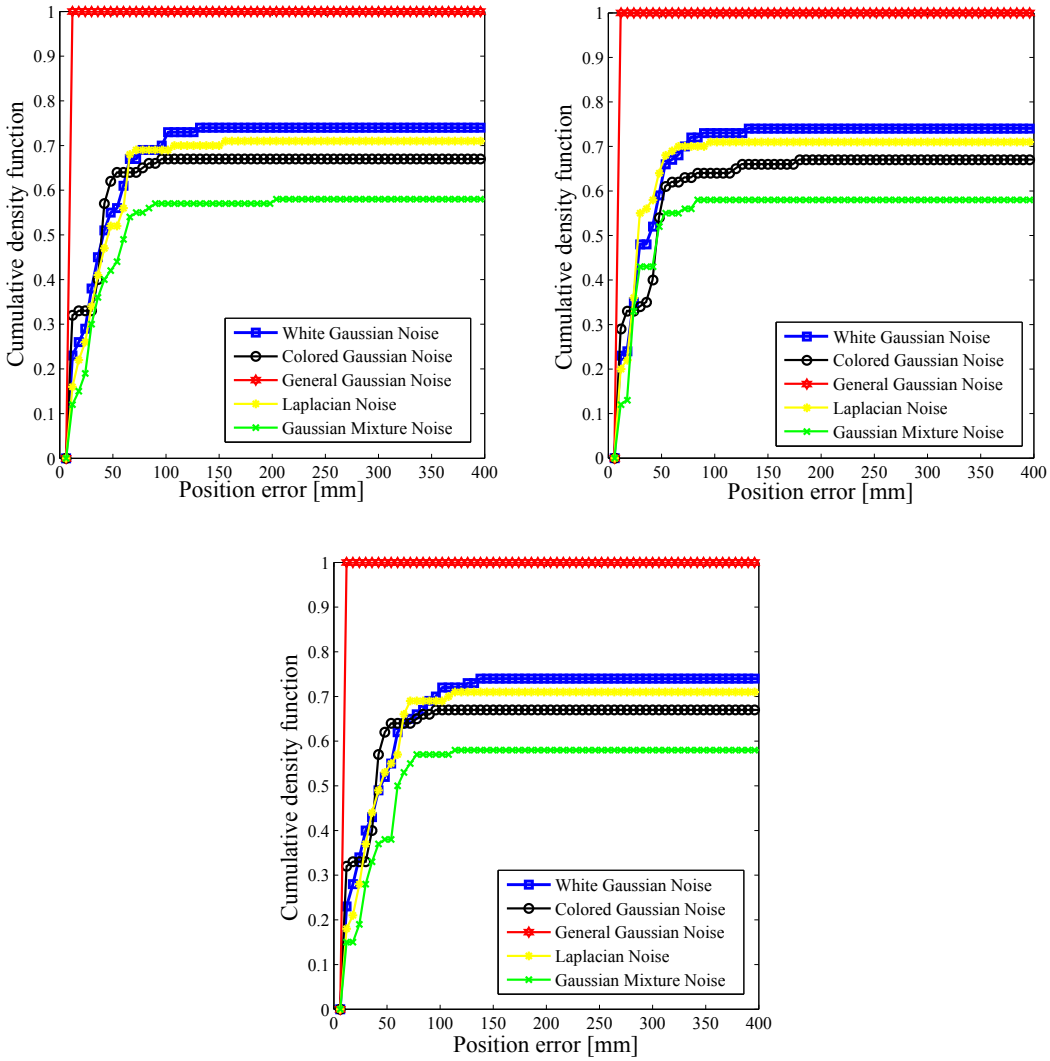

Figure 8.8 Position error of the first method from different noises at SNR = -10 dB.

8.10. However, when the SNR was adjusted as low as possible at -7 dB for the second method, simulation results can get accuracy smaller than 1 mm at only General Gaussian Noise. In other noises, the second method cannot guarantee the results because position errors are more than 100 mm, as shown in Figure 8.11. Finally, the third method was tested at different noises as same as the previous methods with SNRs of 10, 0, and -10 dB. In Figure 8.12, the third method has the maximum error about

approximately 1.5 mm. In Figure 8.13, the third method still keep accuracy not more

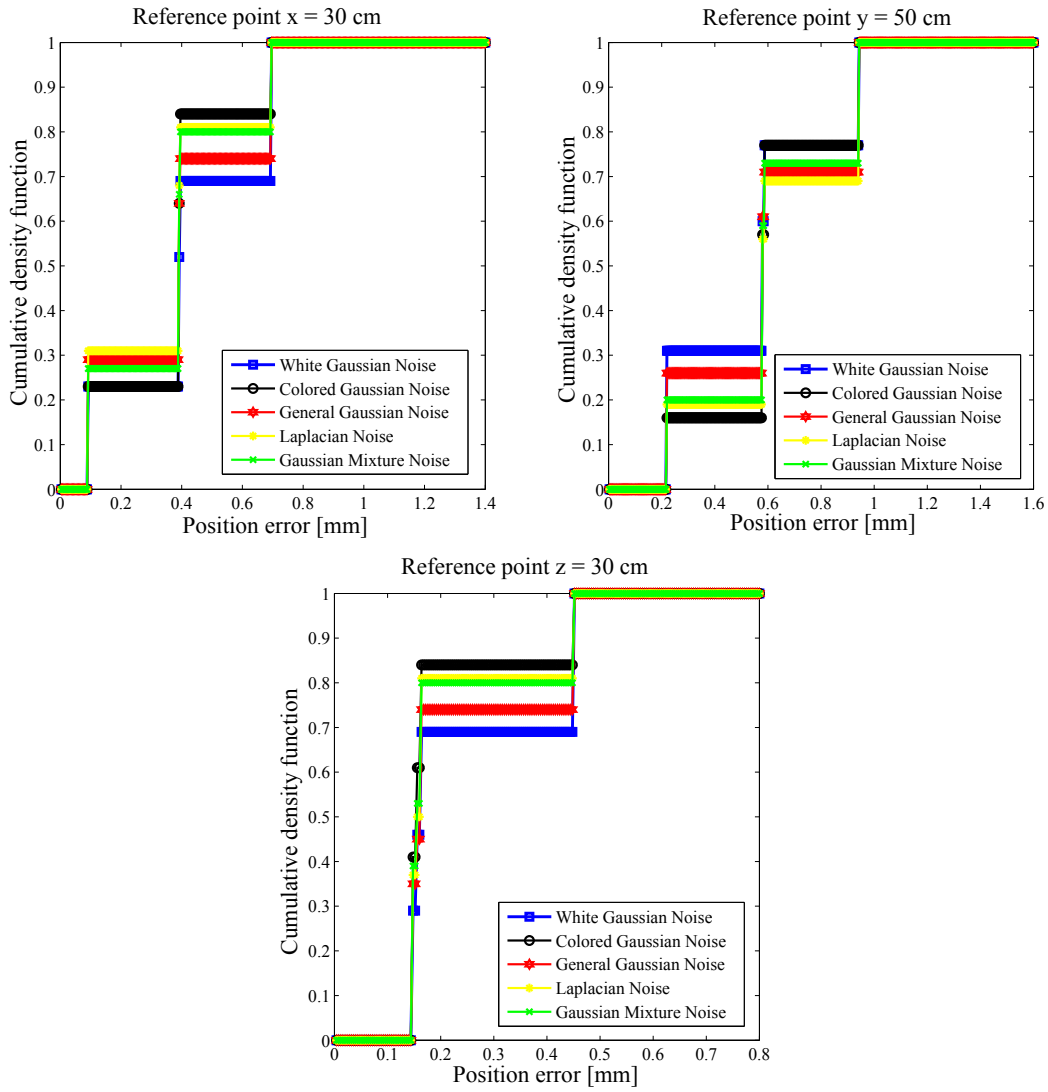

Figure 8.9 Position error of the second method from different noises at SNR = 10 dB.

than 1.6 mm. In case of SNR at -10 dB, simulation results of the third method are similar to the second method in that it is strong to General Gaussian Noise as low as -10 dB. If, however, other noises was included directly, simulation results cannot attain and have errors higher than 100 mm. We can conclude that the first method (an iterative method) is the most robustness when relatively compared with others as low as -10 dB. In case of the second method (an Direction-of-Arrival method), this

method can achieve the minimum SNR at 0 dB and, at SNR of -7 dB, it corresponds

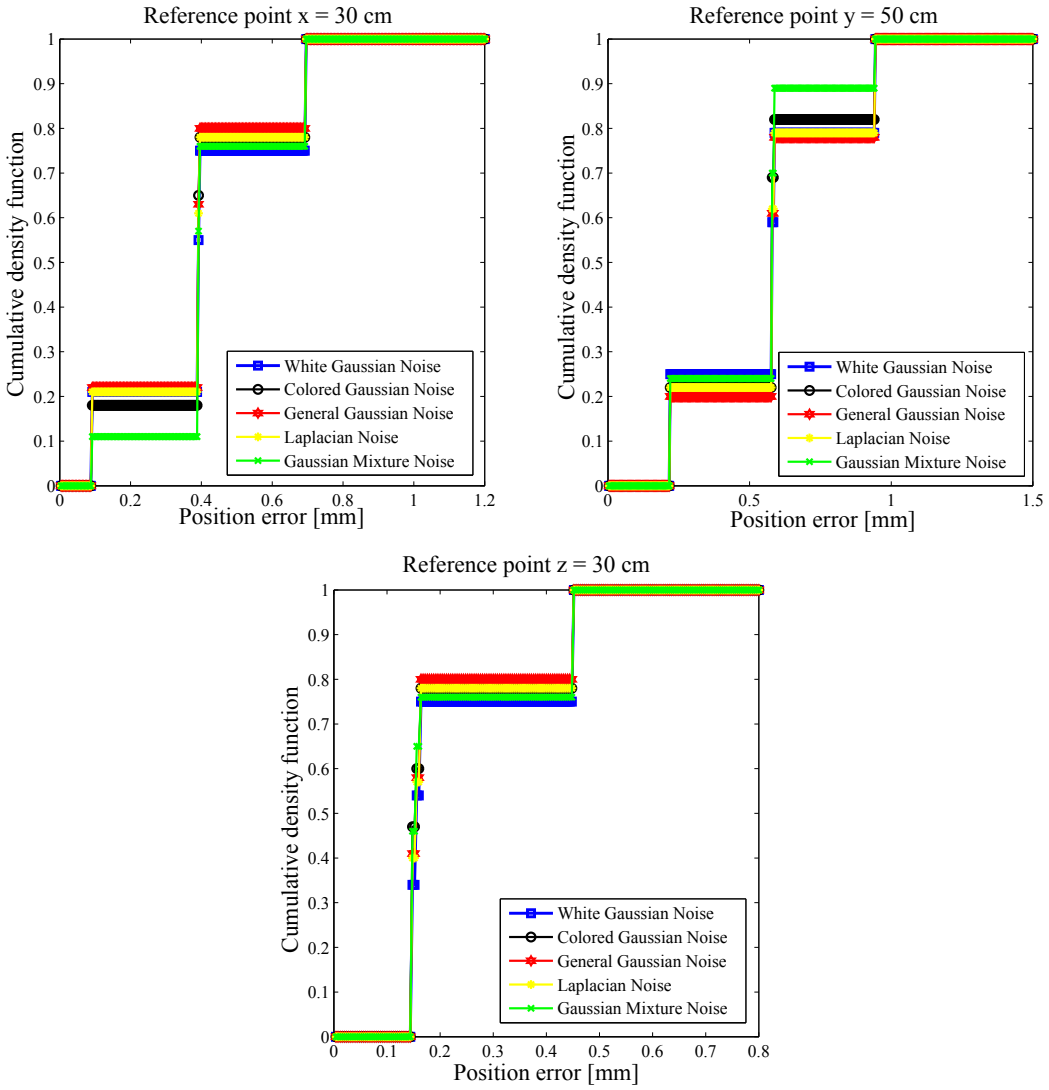

Figure 8.10 Position error of the second method from different noises at SNR = 0 dB.

only at General Gaussian Noise. Similarly, the third method (an linearization-based method) has the SNR as low as 0 dB, and at SNR of -10 dB, the third method is only strong to General Gaussian Noise.

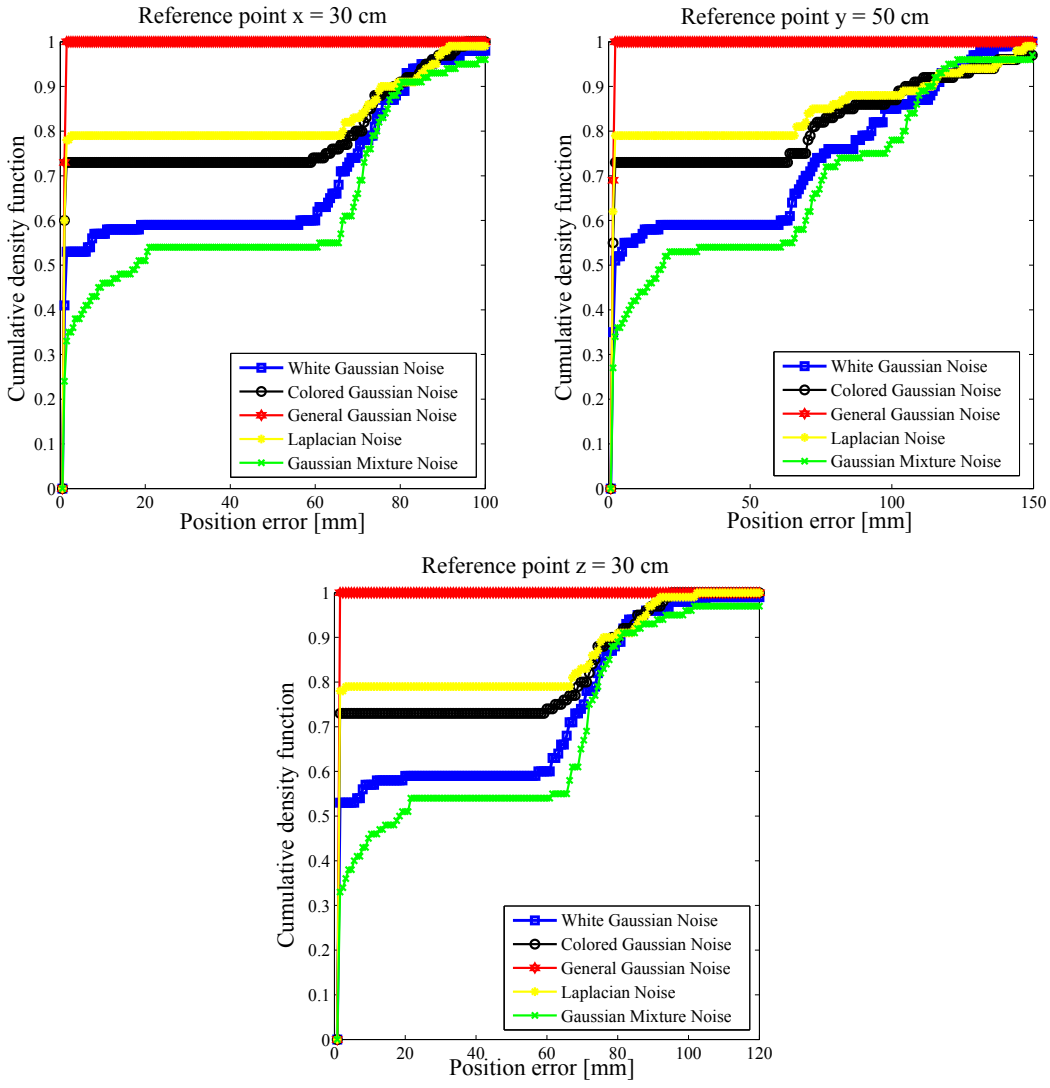

Figure 8.11 Position error of the second method from different noises at SNR = -7 dB.

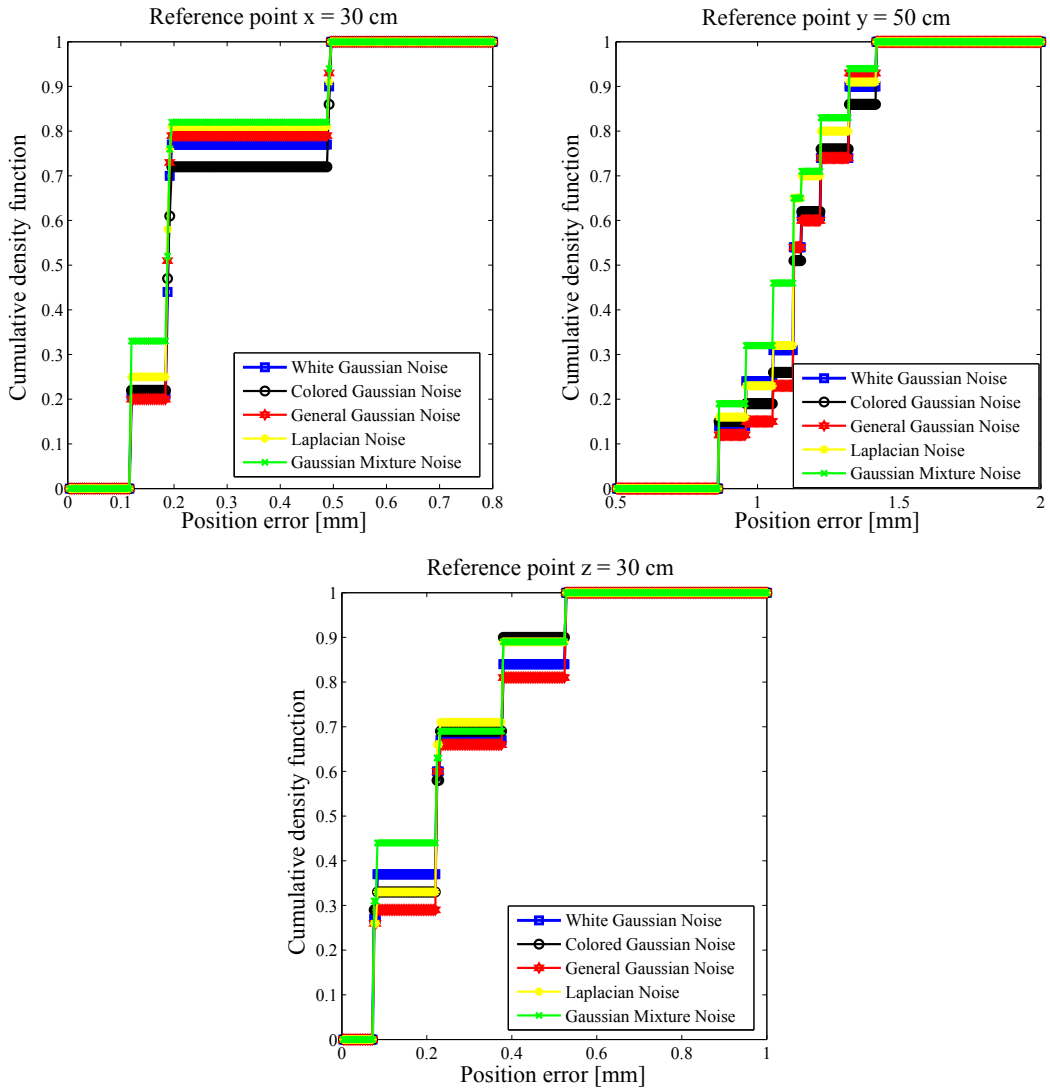

Figure 8.12 Position error of the third method from different noises at SNR = 10 dB.

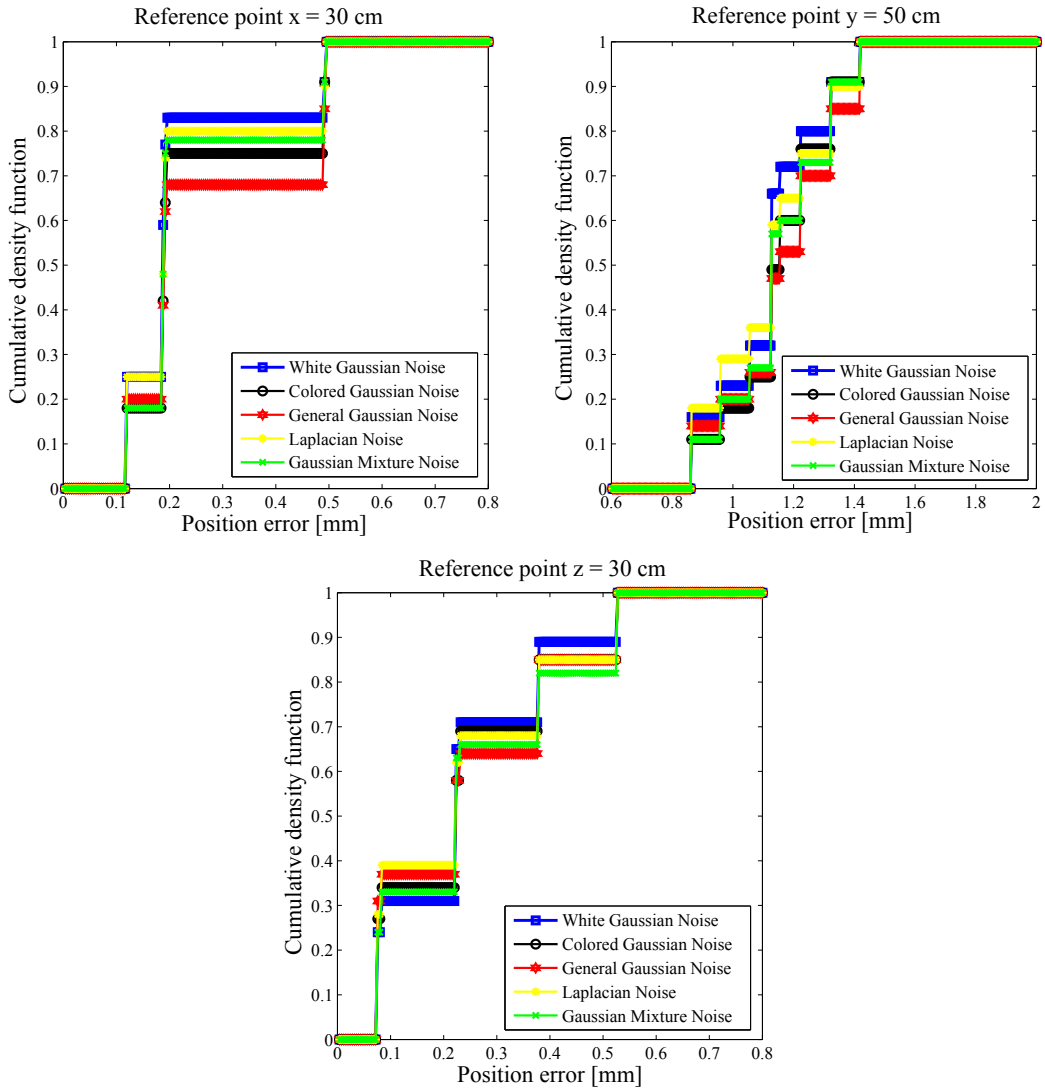

Figure 8.13 Position error of the third method from different noises at SNR = 0 dB.

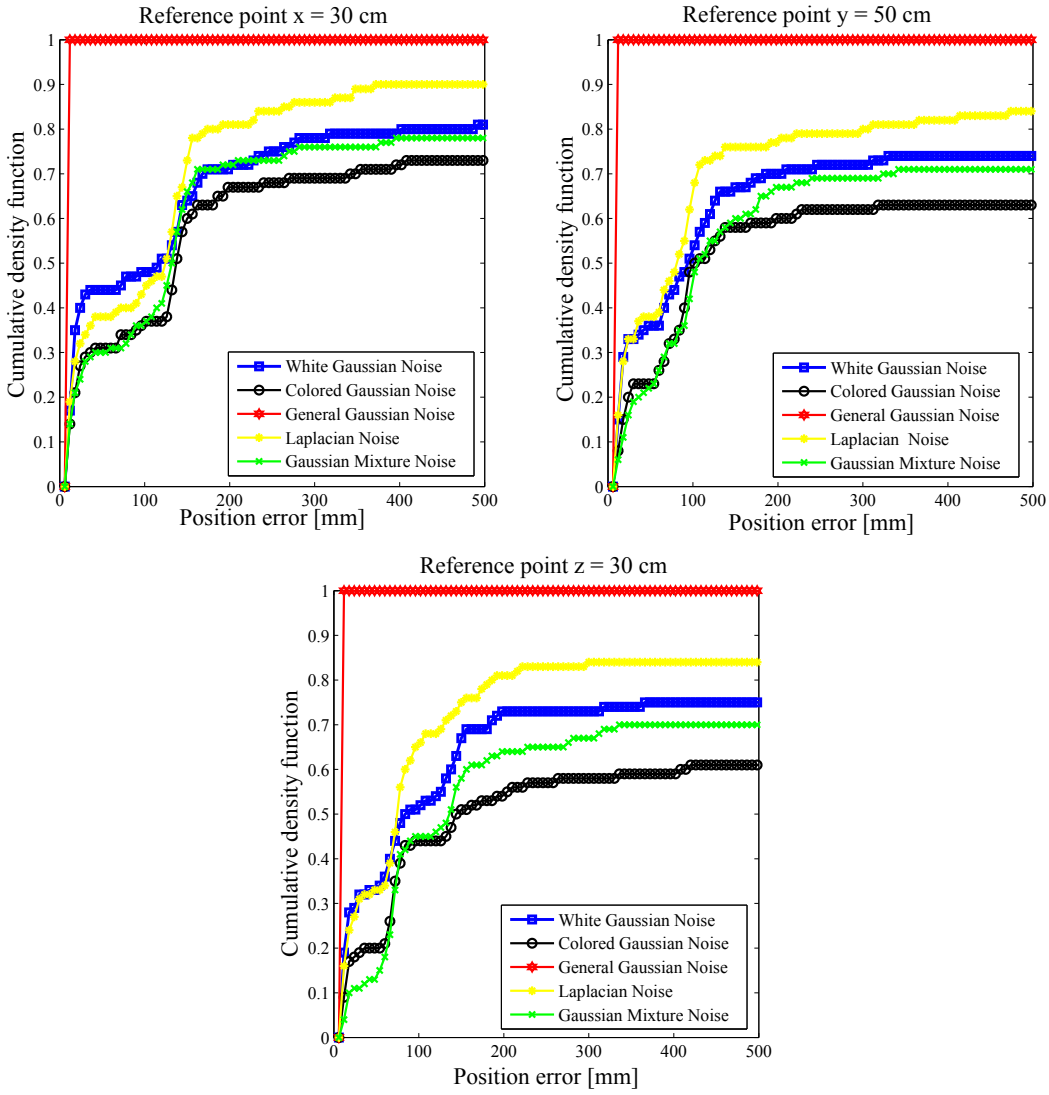

Figure 8.14 Position error of the third method from different noises at SNR = -10 dB.

8.2.2 Comparisons

In this subsection, accuracy from proposed methods is directly compared with the reference line. Distance due to simulation was varied from 1 cm up to 1 m and enlarged a distance especially in a range 24 cm to 25 cm as shown in Figure 8.15. In comparison, it is observed that the first method (an iterative method) provides the most accuracy when relatively compared with the second method (an Directional-of-Arrival) and the third method (an linearization-based method). Error from measurement of the first method is about 0.2 mm. For the second method, measurement is deviated from the reference from 0.8 mm. The worst case is the third method. It expresses error from the reference around 1 mm. The important reason why the the first method has the highest accuracy because a mathematical model of the object position, in fact, comes form a nonlinear model. The first method directly solves this task using an iterative method relied on the nonlinear solution. In contrast, the second method and the third method are transformed from the nonlinear model to reduce complexity, or called indirect methods. It effectively makes lower accuracy in the second method and the third method.

8.3 Summary

In this chapter we describe Gaussian as well as nonGaussian noise model, stationary as well as some nonstationary models. In the most case, we assume that the proposed method is proceeded under White Gaussian Noise. Thus, to evaluate the proposed method in other conditions, ultrasonic LPM signal including Colored Gaussian Noise, General Gaussian Noise, Laplacian PDF Noise, and Gaussian Mixture Noise is performed. Simulation results were observed that the first method has robustness as low as SNR of -10 dB. The second method and the third method can just achieve robustness as low as SNR of 0 dB. In the case of accuracy comparisons, error from measurement of the first method is approximately 0.2 mm. For the second method, measurement is deviated from the reference from 0.8 mm. The worst case expresses error from the reference around 1 mm that is the third method.

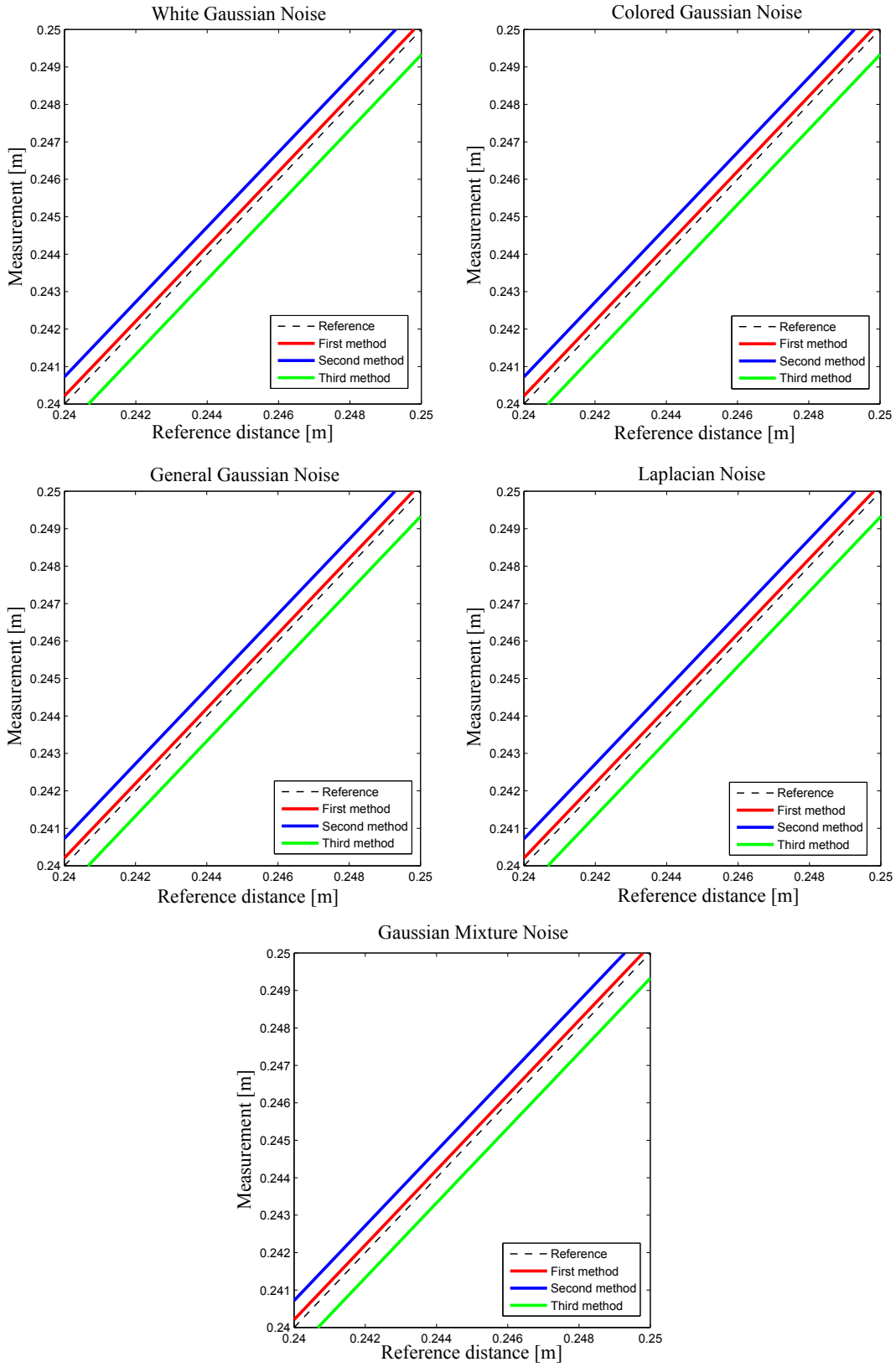

Figure 8.15 Accuracy comparison from each proposed methods in different noises.

9

Conclusions

Chapter 1: This chapter describes various technologies enabling position identification: laser, camera, millimeter wave, and ultrasonic. In general, ultrasonic considered a distance less than 5 m is very attractive when compared with others for the mobile-robot applications due to simple hardwares, small size, and low cost.

Chapter 2: Many methods involving with the ultrasonic system for autonomous mobile robots are described in this chapter. The most important points for enabling autonomous mobile robots real-time signal processing are low computational time, reliability and low cost. Although the most of proposed ultrasonic systems can provide high accuracy of the position measurement, they may use the complex devices, which require a long computational time and a high price. In addition, they have only the ability of measuring the position without the knowledge of the velocity measurement. A system capable of concurrently measuring the 3D position and the velocity measurements is proposed. This method, in which an ultrasonic transmitter is a moving target, can be applied in a special work. Nevertheless, the development of simultaneously measuring the 3D position and the velocity under ultrasonic echolocation system with low computational cost is far from complete.

Chapter 3: One-bit $\Delta\Sigma$ modulation signal rather than a multi-bit signal sampled by means of oversampling can obtain a high SNR. By means of oversampling, very high resolution is obtained. The cross-correlation using one-bit $\Delta\Sigma$ modulated signal processing is compared with the cross correlation of multibit digital signal. This technique can be performed to reduce the circuit scale. To support a real-time application, FPGA cyclone V is useful to calculate recursive cross correlation of one-bit signals.

Chapter 4: LPM ultrasonic wave, a period of which is linearly swept with time, was proposed for Doppler-effect compensation. This wave is directly generated by means of PT-R4 pioneer speaker from a sound source to a target. The loudspeaker of Pioneer model PT-R4 has a rectangular plane surface source. It can radiate ultrasonic wave from area X to +X and from area Z to +Z when the object appears in front of the loudspeaker in the +Y area. Moreover, a low-cost silicon MEMS microphone based on a development for hand-held telecommunication instruments is presented. It can extremely reduce the cost more than 100 times when relatively compared with the previous microphone of B&K and ACO.

Chapter 5: An ultrasonic three-dimensional system for moving object position and velocity estimation using a pair of LPM was proposed. The design method comprises, one-bit signal processing, object-velocity-measurement and Newton Raphson method. We employed three microphones to detect the reflected echo from the moving object. Time-of-flight and the relative velocity were computed with low-cost time. Newton-Raphson played a vital role as object-position estimator. Finally, the Doppler velocity and object position from the earlier measurements were used to determine the object velocity on the basis of vector velocity theory.

Chapter 6: A three-dimensional position and velocity measurement based on an oversampling signal processing method using an LPM ultrasonic signal was demonstrated. The velocity measurements were computed based on the three-dimensional velocity vector measurements. The object position was estimated using spherical coordinates (i.e., the distance from the sound source to the target, the angle of elevation, and the azimuth angle). Positions determined in the proposed system were evaluated by experiments using ultrasonic position measurements. The object position can be sensed by the sound beam propagated by a loudspeaker. Rotating the loudspeaker can expand the range of measurements to a wider area.

Chapter 7: The proposed system by redesigning the receiver arrangement uses cross-correlation one-bit signal processing technology, low-computation-cost Doppler-shift compensation, and low-cost devices. This is the development from the previous space measurement of one-bit signal processing to simultaneously measure position and velocity in three-dimensional space. Through Monte-Carlo computer simulation of 100 trials, the variances of estimated parameters can achieve the analytical CRLB for SNR

as low as 0 dB. Accuracy of the proposed method was tested by the additional White Gaussian Noise. The results can provide accuracy less than 0.1 mm at a SNR of 0 dB. Since the position-measurement model is a form of nonlinear systems, it is then improved into a linear model.

Chapter 8: In this chapter we describe Gaussian as well as nonGaussian noise model, stationary as well as some nonstationary models. In the most case, we assume that the proposed method is proceeded under White Gaussian Noise. Thus, to evaluate the proposed method in other conditions, ultrasonic LPM signal including Colored Gaussian Noise, General Gaussian Noise, Laplacian PDF Noise, and Gaussian Mixture Noise is performed. Simulation results were observed that the first method has robustness as low as SNR of -10 dB. The second method and the third method can just achieve robustness as low as SNR of 0 dB. In the case of accuracy comparisons, error from measurement of the first method is approximately 0.2 mm. For the second method, measurement is deviated from the reference from 0.8 mm. The worst case expresses error from the reference around 1 mm that is the third method.

References

[1] http:// www.jara.jp/data/dl/kndo.pdf

[2] K. Saito, S. Takahama, S. Yamasaki, M. Takato, Y. Sekine, and F. Uchikoba, IC chip of pulse-type hardware neural networks for hexapod walking MEMS micro robot, Proc. of The 2013 International Joint Conference on Neural Networks, pp. 1-6, Dallas, USA, Aug. 4-9, 2013.

[3] T. Kato, T. Izui, Y. Murakawa, K. Okabayashi, M. Ueki, Y. Tsuchiya, and M. Narita, Research and development environments for robot services and its implementation Proc. of 2011 IEEE/SICE International Symposium on System Integration, pp. 306-311, Kyoto, Japan, Dec. 20-22, 2011.

[4] http:// www.sony.jp/products/Consumer/aibo/index.html

[5] http:// www.honda.co.jp/ASIMO/

[6] Shinnosuke Hirata A method of ultrasonic distance and velocity measurement using a pair of chirp signals by single-bit signal processing, Ph.D Thesis, Tokyo Institute of Technology, 2009. (In Japanese)

[7] http:// www.acuitylaser.com/support/measurement-principles

[8] J. Smit, R. Kleihorst, A. Abbo, J. Meuleman, and G. van Willigenburg,Real time depth mapping performed on an autonomous stereo vision module pp. 306-310.
[9] http://www.mitsubishielectric.com/bu/automotive/$advanced_technology/pdf/vol94_tr5.pdf$

[10] http://www2.cscamm.umd.edu/programs/trb10/presentations/$LDV.pdf$

[11] http://www.tasco-japan.co.jp/bushnell digitalspeedgun.html

[12] S. Hirata, M. K. Kurosawa, and T. Katagiri, Cross-correlation by Single-bit Signal Processing for Ultrasonic Distance Measurement, IEICE Trans. Fundamentals, vol. E91-A, no. 4, pp.1031-1037, 2008.

[13] S. Hirata, M. K. Kurosawa, and T. Katagiri, Accuracy and Resolution of Ultrasonic Distance Measurement with High - time - resolution Cross - correlation Function Obtained by Single - bit Signal Processing, Acoust. Sci. Technol., vol. 30, no. 6, pp.429 - 438, 2009.

[14] S. Hirata and M. K. Kurosawa, Ultrasonic Distance and Velocity Measurement using a Pair of LPM Signals for Cross - correlation Method - Improvement of Doppler - Shift Compensation of Doppler Velocity Estimation, Ultrasonics, vol. 52, no. 7, pp.873 - 879, 2012

[15] S. Saito, M. K. Kurosawa, Y. Orino, and S. Hirata, Airborne Ultrasonic Position and Velocity Measurement Using Two Cycles of Linear-Period-Modulated Signal, Proc. of 12th Conference Towards Autonomous Robotic System, Sheffield Hallam University, City Campus, Sheffield, UK, pp. 46-53, Aug. 31-Sep. 2, 2011.

[16] D. Marioli, E. Sardini, and A. Taroni, Ultrasonic distance measurement for linear and angular position control, IEEE Trans. Instrumentation and Measurement, vol. 37, no. 4, pp. 578-581, Dec., 1988.

[17] M. S. Yuan and X. D. Ming, Measurement of three-dimensional coordinates by ultrasonic multi- phase difference method, Journal of Precision Measurements, vol. 52, no. 2, pp.332 - 337, 1986. (In Japanese)

[18] X. D. Ming and M. S. Yuan, Measurement of three-dimensional coordinate with multiple phase difference of intermittent ultrasound, Journal of Precision Measurements, vol. 53, no. 9, pp.1408 1413, 1987. (In Japanese)

[19] S. Chow, P. M. Schultheiss, Delay estimation using narrow-band processes, IEEE Trans. Acoustics, Speech and Signal Processing, vol. 29, no. 3, pp. 478-484, June,

1981. [20] D. Marioli, C. Narduzzi, C. Offelli, D. Petri, E. Sardini, and A. Taroni, Digital time-of flight measurement for ultrasonic sensors, IEEE Trans. Instrumentation and Measurement, vol. 41, no. 1, pp. 93-97, Feb., 1992.

[21] K. W. Jorg, M. Berg, Sophisticated mobile robot sonar sensing with pseudo-random codes, Robotics and Autonomous Systems, vol. 25, no. 3, pp. 241-251, Nov., 1998.

[22] M. Pollakowski, H. Ermert, Chirp Signal Matching and Signal Power Optimization in Pulse-Echo Mode Ultrasonic Nondestructive Testing, IEEE Trans. Ultrasonics, Ferroelectrics, and Frequency Control, vol. 41, no. 5, pp. 655-659, Sep., 1994.

[23] Y. Wang, T. Siginouchi, M. Hashimoto, and H. Hachiya, Development of ultrasonic multiple access method based on M-sequence code, Jpn. J. Appl. Phys. vol. 46 pp. 4490-4496, 2007.

[24] H. Matsuo, T. Yamaguchi, and H. Hachiya, Target Detectability Using Coded Acoustic Signal in Indoor Environments, Jpn. J. Appl. Phys. vol. 47 pp. 4325-4328, 2008.

[25] H. Wang and P. Chu, Voice Source Localization for Automatic Camera Pointing System in Videoconferencing, IEEE Acoustics, Speech, and Signal Processing, vol.1 pp.187-190, 1997.

[26] G.C. Carter, Coherence and time delay estimation: an applied tutorial for research, development, test, and evaluation engineering, Piscataway, NJ: IEEE Press, 1993.

[27] S. Bedard, B. Champagne, and A. Stephenne, Effects of Room Reverberation on Time-Delay Estimation Performance, IEEE Trans. Acoustics, Speech, and Signal Processing, vol.2, pp. 261-264, 1994.

[28] Q. Y. Zou and ZH. P. Lin, Measurement Time Requirement for Generalized Cross-correlation Based Time-Delay Estimation, IEEE Trans. Circuits and Systems, vol.3 pp. 492-495, 2002.

[29] J.P. Ianniello, Time Delay Estimation Via Cross-correlation in The Presence of Large Estimation Errors, IEEE Trans. Acoustics, Speech, and Signal Processing, vol.30,

no. 6 pp. 998-1003, 1982.

[30] M.V.Nageswara Rao and K.Raja Rajeswari,Target Detection with Cross Ambiguity Function using Binary Sequences with high Discrimination, International Journal of Computer Applications vol.16, no.4, pp 8-12, 2011. [31] Christopher L. Yatrakis Computing the Cross Ambiguity Function A Review Master Thesis, Binghamton University, State University of New York, 2001.

[32] J. C. Jackson, R. Summan, G. I. Dobie, S. M. Whiteley, S. G. Pierce, and G. Hayward, Time-of-Fight Measurement Techniques for Airborne Ultrasonic Ranging, IEEE Trans. Ultrasonics, Ferroelectrics, and Frequency Control, vol. 60, no. 2, pp. 343-355, Feb., 2013.

[33] S. Satomura and Z. Kaneko, Ultrasonic blood rheograph, Proc. of the 3rd International Conference on Medical Electronics, pp. 254-258, 1960.

[34] D. W. Baker, Pulsed ultrasonic Doppler blood-flow sensing, IEEE Trans. Sonics and Ultrasonics, vol. 17, no. 3, pp. 170-184, 1970.

[35] W. D. Barber, J. W. Eberhard, and S. G. Karr, A new time domain technique for velocity measurements using Doppler ultrasound, IEEE Trans. Biomedical Engineering, vol. BME-32, no. 3, pp. 213-229, 1985.

[36] P. Atkinson, An ultrasonic fluctuation velocimeter, Ultrasonics, vol. 13, no. 6, pp. 275-278, Nov., 1975.

[37] T. Asakura and N. Takai,Dynamic laser speckles and their application to velocity measurements of the diffuse object, Appl. Phys., vol. 25, no. 3, pp. 179-194, July, 1981.

[38] S. Shoval and J. Borenstein, Measuring The Relative Position And Orientation Between Two Mobile Robots With Binaural Sonar Proc. of 9th International Topical Meeting on Robotics and Remote Systems, Seattle, Washington, March 4- 8, 2001.

[39] C. C. Hsu, H. C. Chen, and C. Y. Lai, An Improved Ultrasonic-Based Localization Using Reflection Method, Proc. of International Asia Conference on Informatics in Control, Automation and Robotics, Bangkok, Thailand, pp. 437-440, Feb. 1-2, 2009.

[40] H. Nonaka and D. Tsutomu, Ultrasonic position measurement and its applications to human interface, IEEE Trans on Instrumentation and Measurement, vol. 44, no. 3, pp. 771-774, 1995.

[41] J. H. Ko, W. J. Kim, and M. J. Chung, A method of acoustic landmark extraction for mobile robot navigation IEEE Trans on Robotic and Automation, vol. 12, no. 3, pp. 478-485, 1996.

[42] L. S. Yin, and Y. K. Sheng, Developing a blind robot: Study on 2D mapping, Proc. of 2008 IEEE Conference on Innovative Technologies in Intelligent Systems and Industrial Applications, Cyberjaya, pp. 12-14, Jul. 12-13, 2008.

[43] Sv. Noykov and Ch. Roumenin, Calibration and interface of a polaroid ultrasonic sensor for mobile robots, Sensors and Actuators A: Physical, vol. 135, pp. 169-178, 2007.

[44] J.M. Matin Abreu, R. Ceres, L. Calderon, M. A. Jimenez, and P. Gonzalez-de-Santos, Measuring the 3D position of a walking vehicle using ultrasonic and electromagnetic waves, Sensors and Actuators A: Physical, vol. 75, pp. 131-138, 1999.

[45] O. Bischoff, N. Heidmann, J. Rust, and S. Paul, Design and Implementation of an Ultrasonic Localization System for Wireless Sensor Networks using Angle-of-Arrival and Distance Measurement, Procedia Engineering, vol. 47, pp. 953-956, 2012.

[46] J.M. Martin, A.R. Jimenez, F. Seco, L. Calderon, J.L. Pons, and R. Ceres, Estimating the 3D position analysis and a new processing algorithm, Sensors and Actuators A: Physical, vol. 101, pp. 311-321, 2002.

[47] J. D. Bjerknes,W. Liu, A. Winfield and C. Melhuish, Low Cost Ultrasonic Positioning System for Mobile Robots, Proc. of 7th Conference Towards Autonomous Robotic System, University of Wales Aberystwyth, UK, 8 pages, Sep. 3-5, 2007.

[48] V. Auer, M.M. Maes, M.J.C. Bonfim, M.M. Wanderley & M.V. Lamar, 3D Positioning Acquisition System with Application in Real-Time Processing, Proc. of 7th International Conference on Signal Processing Application and Technology, Santa Clara

Convention Center, CA, USA, pp. 505-509, Oct. 28-31, 1996.

[49] S. Nakamura, T. Sato, M. Sugimoto, and H. Hashizume, An Accurate Technique for Simultaneous Measurement of 3D Position and Velocity of a Moving Object Using a Single Ultrasonic Receiver Unit, Proc. of International Conference on Indoor Positioning and Indoor Navigation, Zurich, Switzerland, 7 pages, Sep. 15-17, 2010.

[50] Super Audio CD Production Using Direct Stream Digital Technology, Electronics and Sony Corporation copyright, 2000 and 2001. [online] http://www.canadapromedia.com.

[51] H. Inose, Y. Yasuda, and J. Murakami, A telemetering system by code modulation-$\Delta - \Sigma$ modulation, IRE Trans. Space Electron. Telemetry, vol. SET-8, pp. 204-209, Sept., 1962.

[52] H. Inose, Y. Yasuda, A unity bit coding method by negative feedback, Proc. of the IEEE, vol. 51, no. 11, pp. 1524-1535, Nov., 1963.

[53] R. Schreier and G. C. Temes, Understanding Delta-Sigma Data Converters, (IEEE Press, Piscataway, 2005).

[54] Analog Devices, Inc., AD7720, http://www.analog.com/en/analog-todigital-converters/ad-converters/ad7720/products/product.html

[55] Masahiko Kawakami, Brushless DC motor control using one -bit digital signal processing, Master's thesis, Tokyo Institute of Technology, 2001. (In Japanese)

[56] S. Hirata, M. K. Kurosawa, and T. Katagiri, Cross-correlation by single-bit signal processing for ultrasonic distance measurements IEICE Trans. Fundamentals vol. E91-A, no. 4, pp.1031-1037, 2008.

[57] S. Hirata, M. K. Kurosawa, and T. Katagiri Accuracy and resolution of ultrasonic distance measurement with high-time-resolution cross-correlation function obtained by single-bit signal processing Acoust. Sci. & Tech. vol. 30, no. 6, pp. 429-438, 2009.

[58] http://www.terasic.com.tw/cgibin/page/archive.pl?Language=English&Category No=167&No=830

[59] J. J. Kroszczynski, Pulse compression by means of linear-period modulation, Proc. of the IEEE, vol. 57, no. 7, pp. 1260-1266, July, 1969.

[60] R. A. Altes, D. P. Skinner, Sonar-velocity resolution with a linear-period-modulated pulse, J. Acoust. Soc. Am. , vol. 61, no. 4, pp.1019-1030, 1977.

[61] J. E. Wilhjelm, P. C. Pedersen, Target velocity estimation with FM and PW echo ranging Doppler systems I. Signal analysis, IEEE Trans. Ultrasonics, Ferroelectrics and Frequency Control. vol. 40, no. 4, pp. 366-372, July, 1993.

[62] J. E. Wilhjelm, P. C. Pedersen, Target velocity estimation with FM and PW echo ranging Doppler systems II. Systems analysis, IEEE Trans. Ultrasonics, Ferroelectrics and Frequency Control. vol. 40, no. 4, pp. 373-380, July, 1993.

[63] S. Hirata and M. K. Kurosawa, Ultrasonic distance and velocity measurement using a pair of LPM signals for cross-correlation method improvement of Doppler-shift compensation of Doppler velocity estimation, Ultrasonics, vol. 52, pp 873-879, February 2012.

[64] L. L. Beranek, Acoustics Acoustic Laboratory, Massachusetts Institute of Technology, Acoustical Society of America, New York, 1996.

[65] D. Royer and E. Dieulesaint, (Translated by D. P. Morgan), Elastic Waves in Solids I Spring-Verlag Berlin Heidelberg, 2000.

[66] K. B. Ocheltree, Sound Field Calculation for Rectangular Sources, IEEE Trans. Ultrasonics, Ferroelectrics and Frequency Control. vol. 36, no. 2, pp. 242-248, March, 1989.

[67] http://pioneer.jp/support/purpose/manual-catalog/manualdl/manual-pdf.php

[68] B&K application note

[69] http://www.aco-japan.co.jp/eng/profile.html

[70] K. Muzutani, T. Ito, M. Sugimoto, and H. Hashisume, TSaT-MUSIC: a novel algorithm for rapid and accurate ultrasonic 3D localization, EURASIP Journal on Advances in Signal Processing 2011: 101, 2011.

[71] W. H. Foy, Position-location solutions by Taylor-series estimation IEEE Transaction on Aerospace, Electronic, and System, AES-12, pp. 187-193, 1976. [72]. E. K. Chong and S. H. Zak, An Introduction to Optimization 2rd Edition, John Wiley & Sons, Inc, Canada, 2001.

[73] Pramote Dechaumphai and Nipon Wanasopak, Numerical Methods in Engineering CUBOOK, Bangkok, 2010. (In Thai)

[74] E. Acha, B. Kazemtabrizi, L.M. Castro, A New VSC-HVDC Model for Power Flows Using the Newton-Raphson Method IEEE Transaction on Power Systems, vol. 28, no. 3, pp. 2602-2612, 2013.

[75] R. Mitsuoka, T. Mifune, T. Matsuo, C. Kaido, A Vector Play Model for Finite-Element Eddy-Current Analysis Using the Newton-Raphson Method IEEE Transaction on Magnetics, vol. 49, no. 5, pp. 1689-1692, 2013.

[76] K. Yu, Y. J. Guo and I. Oppermann, Modified Taylor Series Expansion Based Positioning Algorithms, Proc. of IEEE Vehicle and Technology, pp. 2656-2660, 2008.

[77] Zhizhang Chen, Gopal Gokeda, and Yiqiang Yu, Introduction Direction-of-Arrival Estimation, Artech House, 2010.

[78] M. Haardt, Efficient One-, Two-, and Multidimensional High-Resolution Array Signal Processing, New York: Shaker Verlag, 1997.

[79] S. M. Kay, Fundamentals of Statistic Signal Processing (Prentic Hall, New Jercy, 1993) p. 225.

[80] K. C. Ho and W. Xu, An accurate algebraic solution for moving source location using TDOA and FDOA measurements IEEE Trans. Signal Processing, vol. 52, no. 9, pp. 2453 2463, September, 2004.

[81] T. Shigematsu and M. K. Kurosawa, Friction Drive of an SAW Motor. Part I: Measurements IEEE Trans. Ultras. Ferro. Freq. Contr. vol. 55, no. 9, pp. 2005-2015, September. 2008.

[82] F. E. Nathanson, Radar Design Principles SciTech Pubs., NJ, 1999.

[83] W. S. Burdic, Underwater Acoustic Systems Analysis, Prentice-Hall, Englewood Cliffs, NJ, 1984.

[84] D. Middleton, Man-made noise in urban environment and transportation systems: models and measurements IEEE Trans. on Communications, vol. 21., pp. 1232-1241, Nov. 1973.

[85] R. Dwyer, A technique for improving detection and estimation of signals contaminated by under ice noise, Journal Acoustical Society of America, vol. 74, Issue 1, pp. 124-130, July 1983.

[86] J. Schweiger, Evaluation of geomagnetic activity in the MAD frequency band (0.04 to 0.6 Hz), Master Thesis, Naval Postgraduate School, Oct. 1982.

[87] R. O. Duda, P. E. Hart, and D.G. Stork, Pattern Classification, Second Ed., J. Wiley, NY, 2001.

Acknowledgment

At this moment, I would like to express my dearest gratitude to my academic supervisor, Prof. Minoru Kurosawa for his kindness and encouragement throughout the course of my study. I would also like to express my sincerest thanks to Prof. Hiroyuki Hachiya, Prof. Kentaro Nakamura, Prof. Nobuhiko Sugino, and Prof. Marie Tabaru, who together with my supervisor, constitute my thesis committees, for their invaluable comments and suggestions. Moreover, I would like to thank Prof. Aoyama at University of Electro-Communications for guiding me to Prof. Kurosawa. If without his help, I could have not studied in Japan.

I would like to give my cordial thanks to Dr. Shinnosuke Hirata and Mr. Yuichiro Orino for their supportive assistance to my research. My gratitude also goes to all Kurosawa laboratory members for their warmest regards, constant supports and tireless efforts. Moreover, I kindly thank to Prof. Jirasak and Dr. Danucha at King Mongkut's University of Technology North Bangkok for their suggestions and invaluable helps in assembling A/D converter circuits. This research will not be successfully finished without the great-hearted support from staffs at Thai Embassy.

For fulfilling my life in Japan, I heartily appreciate to Dr. Tanya for her small talks almost everyday that give me strength to continue my research, to Ms. Chonnipa for her helps in my first year, and to Thai friends in Tokyo Institute of Technology.

Finally, I would like to thank my father and mother who were being a part of my life, support, and encouragement so far.

Natee Thong-un

Department of Information Processing
Interdisciplinary Graduate School of Science and Engineering
Tokyo Institute of Technology
2015

List of Papers

Journal papers

[1] Natee Thong-un, Shinosuke Hirata, Minoru Kurosawa, and Yuichiro Orino, "Three-Dimensional Position and Velocity Measurements using A Pair of Linear-Period-Modulated Ultrasonic Wave", Acoustical and Science Technology, vol. 34, no. 3, pp. 233-236, 2013.

[2] Natee Thong-un and Minoru Kurosawa, "Doppler Velocity Estimation of Overlapping Linear-Period-Modulated Ultrasonic Waves Based on an Expectation-Maximization Algorithm", Advances in Acoustics and Vibration, vol. 2014, Article ID 921876, 7 pages, 2014.

[3] Natee Thong-un, Shinosuke Hirata, and Minoru Kurosawa, "Three-Dimensional Positioning based on echolocation using a simple iterative method", International Journal of Electronics and Communications, Elsevier, vol. 69, no. 3, pp. 680-684, 2015.

[4] Natee Thong-un, Shinosuke Hirata,and Minoru Kurosawa, "Improvement in airborne position measurements based an ultrasonic linear-period-modulated wave by 1-bit signal processing", Japanese Journal of Applied Physics, vol. 54, no. 7S1, 07HC06, 6 pages, 2015.

[5] Natee Thong-un, Shinosuke Hirata, Y. Orino and Minoru Kurosawa, "A linearization-based method of simultaneous position and velocity measurement using ultrasonic waves", Sensors & Actuators A: Physical, Elsevier, vol. 233, pp. 480-499, 2015.

Proceedings

[1] N. Thong-un, M. K. Kurosawa, and S. Hirata, "A simple method for 3-D ultrasonic position and velocity measurement using echolocation," 2013 Spring Meeting Acoustical Society of Japan, pp. 1457-1458, 3-5 March, Tokyo, Japan, 2013.

[2] N. Thong-un, M. K. Kurosawa, Y. Orino, and S. Hirata, "Three-dimensional-positioning measurements based on echolocation using linear-period-modulated ultrasonic signal" 2014 IEEE International Ultrasonics Symposium Proceedings, pp. 2478-2481, 3-6 September, Chicago, USA, 2014.

[3] N. Thong-un, M. K. Kurosawa, and S. Hirata, "Examination of three-dimensional airborne ultrasonic position real-time measurement using chirp wave" Proceedings of Symposium on Ultrasonic Electronics, vol.35, pp. 239-240, 3-5 December, Tokyo, Japan, 2014.